Revised Manuscript (Text Unmarked) Click here to view linked References

Journal of Molecular Graphics and Modelling, Volume 122, July 2023, Article number 108485
DOI: 10.1016/j.jmgm.2023.108485

Computational Insights into bis-N,N-dimethylaniline based D-π-A Photosensitizers Bearing Divergent-Type of π-Linkers for DSSCs

Harun NALÇAKAN[1], Gülbin KURTAY[2,*], Kübra SARIKAVAK[2], Nilgün ŞEN[3,4], Fatma SEVİN[2]

[1]Department of Chemistry, Faculty of Science, Ankara University, 06100, Ankara, Turkey
[2]Department of Chemistry, Faculty of Science, Hacettepe University, 06800, Ankara, Turkey
[3]Turkish National Police Academy, Institute of Forensic Sciences, 06580, Ankara, Turkey
[4]Centre for Defence Chemistry, Cranfield University, Shrivenham, SN6 8LA, United Kingdom
corresponding author: gulbinkurtay@hacettepe.edu.tr

Authors

Harun NALÇAKAN
e-mail: hnalcakan@ankara.edu.tr
ORCID: https://orcid.org/0000-0003-3821-8681

Gülbin KURTAY *(corresponding author)*
e-mail: gulbinkurtay@hacettepe.edu.tr
ORCID: https://orcid.org/0000-0003-0920-8409

Kübra SARIKAVAK
e-mail: kubra.sarikavak@hacettepe.edu.tr
ORCID: https://orcid.org/0000-0001-9900-4463

Nilgün ŞEN
e-mail: nilgun.sen@cranfield.ac.uk
ORCID: https://orcid.org/0000-0002-1997-1312

Fatma SEVİN
e-mail: sevin@hacettepe.edu.tr
ORCID: https://orcid.org/0000-0001-9977-1291

Published by Elsevier. This is the Author Accepted Manuscript issued with: Creative Commons Attribution Non-Commercial No Derivatives License (CC:BY:NC:ND 4.0).
The final published version (version of record) is available online at DOI:10.1016/j.jmgm.2023.108485. Please refer to any applicable publisher terms of use.

Abstract

In this study, theoretically designed D-π-A derivatives containing different π-subunits as linkers were investigated to enlighten their potential applicability in photovoltaic applications. For this aim, we first focused on clarifying the effect of tailored π-linker scaffolds on the frontier orbital energies of the investigated photosensitizers. In the concomitant step, global descriptors, TiO_2 adsorption, maximum absorbance wavelength, light-harvesting efficiency (LHE), energy conversion efficiency (η), short circuit current density (J_{SC}), open circuit photovoltage (V_{OC}), fill factor (FF), and reorganization energy (λ_e, λ_h, λ_T) values, electron density differentiation maps (EDDM), transition density matrices (TDM), fragmental contributions on electron-hole overlap were investigated in detail. Based on the trend of the calculated properties, 2,3-dimethylthieno[3,4-b]pyrazine (D-$Ɛ_3$-δ_n-A; n=1-3) and 5-isobutyl-10,11-dimethyl-10,11-dihydro-5H-pyrrolo[3,4-e]thieno[2',3':4,5]pyrrolo[3,2-g]thieno[3,2-b]indole (D-$Ɛ_6$-δ_n-A; n=1-3) bearing molecules were identified as the best-suited and improved dye candidates for DSSC applications. Following the prediction of photovoltaic properties for the pristine dye molecules, our consecutive efforts have contributed to a similar calculation protocol comprising DFT and subsequent TD-DFT computations for the D-$Ɛ_n$-δ_n-A@Ti_5O_{10} clusters to elucidate the interaction of the investigated photosensitizers with the semiconductor layer (TiO_2).

Keywords: bis-N,N-dimethylaniline, Thienothiophene; Dithienothiophene, D-π-A, DSSC; DFT, TD-DFT.

1. Introduction

Massive usage of fossil fuels as an energy source has increased the accumulation of carbon dioxide in the atmosphere leading to energy and environmental crisis in human civilization [1–3]. Therefore, creating clean solar energy has become a common goal of humanity to deal with increasingly severe global climate change and energy shortages [4,5]. Since the publication of the development of a p-n junction silicon-based photovoltaic device in 1954, significant breakthroughs have been made in the science and technology of these precious materials [6–8]. In 1991, a low-cost and environmentally friendly dye-sensitized solar cell was developed by Grätzel and O'Regan as an alternative to silicon-based solar cells [9]. These novel metal-free organic dye-sensitized solar cells are sought-after compounds for their comparable power conversion effect to conventional ruthenium cells and their requirement for economical raw materials [10,11]. The structural configuration of the donor-π-*bridge*-acceptor (D-π-A) with an electron donor group (D), an electron-rich bridge (π) system, and an electron acceptor (A) (*or anchoring*) fragment has generally been embraced by the frequently investigated organic photosensitizers, displaying various benefits over conventional ruthenium dyes in terms of significant molar extinction coefficients, low cost of development, and remarkable diversity [12,13].

Concisely, a representative DSSC device is composed of several parts: the photo-anode (fluorine-doped tin-oxide, FTO or indium-doped tin-oxide, ITO), redox couple electrolyte solution (typically I^-/I_3^- ion pair) in which oxidized dye is regenerated in the electrolyte, sensitizer layer (consisted of organic or inorganic photosensitizers) and the counter electrode (typically, Pt- or C-coated indium-tin-oxide or fluorine tin-oxide-coated glass/PET) [14]. The sensitizer layer is essential for light harvesting via electron excitation and subsequent injection of an electron into the semiconductor layer's conduction band. The semiconductor must be transparent to allow light to enter the dye sensitizers to affect light harvesting. The network must have an enormous surface area to absorb adequate dye molecules [15–19]. To be more authentic, a DSSC is constructed from a thin layer of organic or inorganic dye molecule anchored to a thin layer of TiO_2 semiconductor [20]. After the absorption of sunlight, the photosensitizer adsorbed on the TiO_2 surface absorbs photons and gets excited. Energy is propagated when an electron released from the valence band of the dye molecule is quickly inserted into the conduction band of the TiO_2. The dye molecule gains electrons from the electrolyte solution (I^-/I_3^-). The electron injection process from the dye molecules to the

semiconductor layer creates a highly rapid interfacial electron transfer operation [5,21–24]. It is a well-known fact that to obtain a prosperous state of separation of charge and injection of an electron from dye to the conduction band of the semiconductor, the highest occupied molecular orbitals (HOMOs) should primarily locate on the part of the donor while the lowest unoccupied molecular orbitals (LUMOs) are on the acceptor (*or* preferably anchoring) subunit. The electron transfer occurs between the HOMO and LUMO of dyes and the conduction band of TiO_2 [18,25,26].

This protocol has two critical proposals for producing an ultrafast interfacial electron transfer and an efficient photovoltaic response. First of all, the photosensitizer's LUMO energy should be higher than the conduction band of the TiO_2 semiconductor (-4.04 *vs. in vacuum*) [27]. Furthermore, the HOMO energy of the photosensitizer should lie below the oxidation/reduction potential of the I^-/I_3^- (-4.85 eV *vs. in vacuum*) ion pair [28]. The dye molecule is regenerated quicker in these two primary phases, which prevents the expelled electrons from recombining back into the photosensitizers [29–31]. In recent years, studies on the theoretical characteristics of these innovative photosensitizers to construct a practical model of empirically manufactured DSSCs have grown in popularity [32,33]. These results indicate that an intramolecular charge transfer (ICT) from the donor fragment to the acceptor fragment occurred after the dyes were photoexcited, which creates the required electron-hole separation for retro-injection of an electron into the conduction band of the studied semiconductor. The ICT process usually occurs in the photoexcited state, where a molecule achieves this when it absorbs light of the required wavelength. As a result, organic dyes may be improved by their adjustable redox and absorption characteristics, allowing for a rational and planned chemical enhancement and the ability to customize the structural properties of the donor, spacer, and acceptor units [34–36]. Extending the π-bridge by adding extra electron-donating or electron-withdrawing groups (EDG and EWG, respectively) is the most extensively used and approved approach for widening the light absorption wavelength range of specified organic dye molecules [37–41].

In this theoretical study, we focused on twenty newly created photosensitizers to highlight the link between photoelectric characteristics and molecular structures based on the model dye validated by Patil et al., in which they manifested the DSSC performance is directly correlated to the β_0 and γ values of the sensitizers. They demonstrated that the most efficient photosensitizer among the four candidate dye molecules is the compound with a bis-dimethylaniline donor unit connected to the thiophene as a π-bridge, which we used as the

model dye (D-δ_1-A) [42]. In this context, we have mainly separated our dye molecules into three series, each of which contains thiophene (δ_1), thieno[3,2-b]thiophene (δ_2), or dithieno[3,2-b:2',3'-d]thiophene (δ_3) functional groups, tied to the benzo[c][1,2,5]thiadiazole (ε_1), 5-methyl-4H-thieno[3,4-c]pyrrole-4,6(5H)-dione (ε_2), 2,3-dimethylthieno[3,4-b]pyrazine (ε_3), 3a,6a-dihydrothiazolo[5,4-d]thiazole (ε_4), 2-isobutyl-2H-dithieno[3',2':3,4;2'',3'':5,6]benzo[1,2-d][1,2,3]triazole (ε_5) or 5-isobutyl-10,11-dimethyl-10,11-dihydro-5H-pyrrolo[3,4-e]thieno[2',3':4,5]pyrrolo[3,2-g]thieno[3,2-b]indole (ε_6) fragments (**Figure 1**).

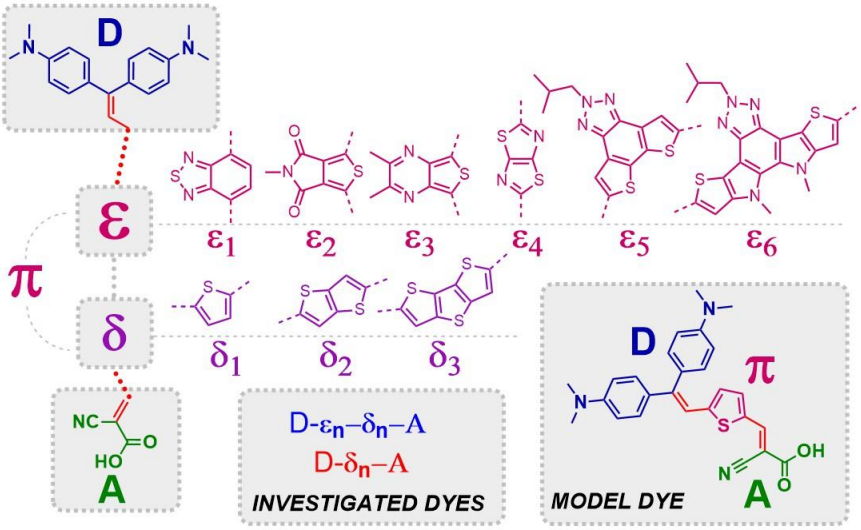


Figure 1. Structure of the model dye and the chemical scheme of the investigated D-π-A photosensitizers.

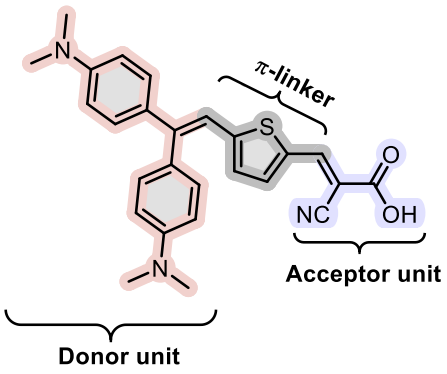
2. Computational Details

All reported quantum chemical calculations were carried out using density functional theory (DFT) and time-dependent density functional theory (TD-DFT) by Gaussian 09 [43]. To this aim, investigated photosensitizers were constructed by GaussView (v5.0.8) software [44], and their initial geometries were predicted with a potential energy surface (PES) scan utilizing the PM6 method. In the subsequent step, our objective was to identify the most suitable computational method and basis set for the model dye (D-δ_1-A) by considering its experimentally determined UV-vis absorption data. To achieve this, we evaluated a range of well-established density functional theory (DFT) methods, including B3LYP, CAM-B3LYP, LC-wPBE, M06L, M06-2X, and PBEPBE, in conjunction with the 6-31G(d,p) basis set (**Table 1**). These functionals were specifically chosen due to their proven performance in accurately predicting electronic and optical properties of various molecular systems, particularly those relevant to photovoltaic applications. Each of the selected functionals possesses distinct characteristics that influence their accuracy in predicting the properties of interest. For instance,

B3LYP is a widely used hybrid functional that often provides reliable results for diverse molecular systems [45], while CAM-B3LYP is a range-separated hybrid functional specifically designed to improve the description of long-range electron correlation effects [46]. On the other hand, LC-wPBE is a long-range corrected functional that aims to provide an accurate description of charge-transfer excitations [47]. M06L is a local functional, M06-2X is a hybrid functional, and PBEPBE is a generalized gradient approximation functional, all of which are members of the Minnesota family of functionals and have demonstrated good performance for a broad range of chemical systems [48–50].

In our study, B3LYP, CAM-B3LYP, M06L, and PBEPBE functionals were found to overestimate the absorption energy, while LC-wPBE underestimated it. Despite these discrepancies, a remarkable agreement was observed between the experimental and theoretical absorption wavelengths when utilizing the M06-2X/6-31G(d,p) method. This functional has been widely acknowledged for its superior performance in predicting charge transfer excitations and optical properties, primarily due to its balanced treatment of both short- and long-range electron correlation effects [51,52]. By adopting the M06-2X/6-31G(d,p) method, we were able to achieve a comprehensive understanding of the electronic structure and optical properties of the investigated D-π-A derivatives, ultimately facilitating the identification of promising candidates for photovoltaic applications.

Table 1. TD-DFT calculation methods applied to the model dye (D-δ_1-A)



Structure of the model dye (experimental λ_{max}: 469 nm) [42]

Computational method	**Calculated λ_{max} (nm)**	**$\Delta\lambda_{max}$ |Calc.-Exp.|(nm)**
B3LYP / 6-31G(d,p)	605	136
CAM-B3LYP / 6-31G(d,p)	526	57
LC-wPBE / 6-31G(d,p)	390	79
M06L / 6-31G(d,p)	622	153
M06-2X / 6-31G(d,p)	481	**12**
PBEPBE / 6-31G(d,p)	681	212

From these initial outputs, the ground-state geometries of target molecules were predicted *in vacuo* with no symmetry constraints at density functional theory (DFT) with M06-2X level of theory and 6-31g(d,p) as the basis set [53]. After this stage, the local minima were verified, and required vibrational frequency calculations were executed to identify the convergence to a real minimum. Consequently, the absence of imaginary values demonstrated that the geometry optimization processes were completed successfully. As previously indicated, the optimization and frequency calculations were initially carried out in the gas phase. To reveal the solvent effect based on these parameters, self-consistent reaction field theory was also integrated using the conductor-like polarizable continuum model (CPCM) by using the dielectric constant value of ethyl alcohol (Ɛ=24.55). The solvent was selected to be consistent with the experimental conditions applied to determine the model dye's (D-δ_1-A) UV-*vis* spectra. The investigations mentioned above were also applied to the photosensitizer@Ti_5O_{10} clusters utilizing the same computational approach.

The localized-orbital locator (LOL) plots of the twenty studied photosensitizers were visualized by using Multiwfn (v.3.8) software [54] and depicted with their corresponding optimized geometries in the electronic supplementary information (ESI†; **Table S1**). Accordingly, the resultant Cartesian coordinates of the photosensitizers and dye@Ti_5O_{10} complexes are also provided in **Table SC1-28**. Subsequently, the highest occupied molecular orbital ($Ɛ_{HOMO}$) and lowest unoccupied molecular orbital ($Ɛ_{LUMO}$) energies, as well as associated bandgap ($Ɛ_{gap}$) energies, were predicted. Additionally, Koopmans' theorem was used to evaluate a variety of global descriptors, specifically, ionization potential (I), electron affinity (A), hardness (η), hyper-hardness (Γ), chemical potential (μ), electronegativity (χ), electrophilicity (ω), electron-accepting power (ω^+), and electron-donating power (ω^-). The determination of the ionization potential (IP) and electron affinity (EA) values in this study was also achieved through the delta-self-consistent field (delta-SCF) calculations [55], and the requisite single-point energy calculations for both the cationic and anionic species of the studied molecules were carried out using the same computational methodology and basis set. Furthermore, the optimized geometries were also calculated for the various charged states (anionic, cationic) to calculate the corresponding reorganization energies (λ_e, λ_h, λ_T) to enlighten the hole and electron transport [56]. As indicated before, the present study aimed to elucidate the underlying patterns of the relative efficiencies of the investigated compounds as dyes in dye-sensitized solar cells (DSSCs). To achieve this goal, a thorough analysis of the electron and hole contributions, as well as electron-hole overlaps, was performed for each respective atom and fragment within

the molecule. The electron density on the anchoring segments was specifically focused on. Transition density matrices (TDM) were utilized to investigate the extent of charge transfer (CT) during excitations by providing information about the departure of each electron from its corresponding hole. In this regard, the charge separation distance (Δr) between the electron and its corresponding hole, as well as the degree of electron-hole overlap (Λ), were examined [56] by using Multiwfn (v.3.8). In the following subsection, the first six vertical excitations were calculated using the time-dependent DFT (TD-DFT) method. The solvent effect was added at the CPCM/TD-M06-2X/6-31G(d,p) stage, similar to the geometry optimization studies. We have also focused on interpreting the properties of the electronic absorption of the investigated photosensitizers. Consequently, we have predicted the light-harvesting efficiency (LHE), the maximum wavelength of absorbance (λ_{max}), oscillator strength (*f*), the lifetime of the excited state (τ), the oxidation potential of the excited dye (ε^*_{dye}), the driving force (ΔG^{inject}) of the electron injection, reorganization energy (ΔG^{regen}) and open-circuit potential (V_{oc}). In addition, we have established the electron density differentiation maps (EDDMs) to comprehend the impact of π-bridge scaffolds on the photovoltaic efficiency of the photosensitizer. GaussSum (v3.0) software [57] was utilized to calculate the partial contributions of subunits on the frontier molecular orbitals and develop their EDDM maps, which included the UV–*vis* absorption values and the accompanying transition characteristics. According to the studies mentioned above, we identified the best candidate photosensitizer from each $\mathcal{E}_n$-δ_n fragment. The photovoltaic outputs of these photosensitizers were then investigated using simulations of their dye@Ti_5O_{10} clusters using corresponding DFT and TD-DFT calculations, which mimic the semiconductor layer in contact with the dye layer that has been adsorbed.

3. Results and Discussion

3.1. Structural Properties

The conjugated degree of the investigated sensitizers is a common geometrical component that substantially impacts charge transport efficiency [58]. To characterize π-linkers and enhance the harvesting range of the dye molecules, we have maintained the same donor (bis-dimethylaniline) and the acceptor (cyanoacrylic acid) units, and the bond lengths, bond angles, and dihedral angle values between these different components were theoretically studied. The systematic quantification of photosensitizers, including the measurements of carbon-carbon bonds (d_{1-3}) between two neighboring motifs, as well as their bond angle and dihedral angle values, are shown in the ESI† (**Table S2**). It is general knowledge that the above-mentioned

structural findings have a considerable impact on the photophysical characteristics of the candidate sensitizers. It is also crucial to state that π-π dye aggregation is a phenomenon resulting in the quenching of molecular excited states and unfavorable back electron transfer, which has a significant impact on electron injection efficiency and, as a result, reduces device efficiency [59]. In this scope, the calculated dihedral angle values demonstrate that a twisted structure is observed due to the steric effect between the donor and π-bridge fragments. Thus, the designated candidate sensitizers have a considerable potential to eliminate the above-mentioned undesirable π-π dye aggregation. On the other hand, the values of bond length (d_{1-3}) between two adjacent fragments are determined as 1.54 Å (*std.* C-C *single bond length*) > d_{1-3} > 1.34 Å (*std.* C=C *double bond length*), which stands for the bonds that are moderately conjugated throughout the structure. In this regard, the presented localized-orbital locator (LOL, η(r)) plots (**Table S1**) achieve high values (>0.5) in subunits where the electron density is dominated by electron localization, revealing the fragments of molecular space where the probability of finding an electron pair is significant. The overall findings demonstrate that the geometry of each of the target molecules is suitable for the process of charge transfer from the donor to the anchoring group.

3.2. Global Reactivity Descriptors (GRD)

In this study, several global reactivity descriptors (GRDs) that are mainly based on Koopmans' theorem have been evaluated. To this aim, frontier molecular orbitals (FMOs), ionization potential (I), electron affinity (A), reorganization energies (λ_e, λ_h, λ_T), hardness (η), hyper-hardness (Γ), chemical potential (μ), electronegativity (χ), electrophilicity (ω), electron-accepting power (ω^+), and electron-donating power (ω^-) were calculated to propose the interrelationship between the photovoltaic efficiency and investigated candidate photosensitizers. In addition, the I and A values derived using the delta-SCF method are also provided for comparison. In order to achieve clarity, we have included the calculations for various global reactivity descriptors in the ESI, and as such, **Table S4** showcases the resultant data obtained from these calculations.

3.2.1. Frontier Molecular Orbitals (FMOs)

Investigation of frontier molecular orbitals (FMOs) is pivotal to determining the reactivity pattern of a compound, including its optical and electrical properties. Furthermore, the capacity to donate and accept an electron is also described by the HOMO and LUMO characteristics, respectively. The difference between the LUMO and HOMO energies is defined as bandgap

energy ($\varepsilon_{gap}=\varepsilon_{LUMO}-\varepsilon_{HOMO}$), and the gathered ε_{HOMO}, ε_{LUMO}, and ε_{gap} values are visualized in **Figure 2**. It is particularly significant to underline that smaller bandgap energy is favorable for DSSCs, and it has several benefits in terms of boosting light-harvesting efficiency. The ε_{gap} of dyes is essential for broadening the absorption range of the dyes, which improves their photocurrent performance. Furthermore, the chemical and optical polarizability of a compound is determined by the ε_{gap} energy. Simultaneously, a low ε_{gap} value helps generate excitations and improves photoexcitation performance [60,61].

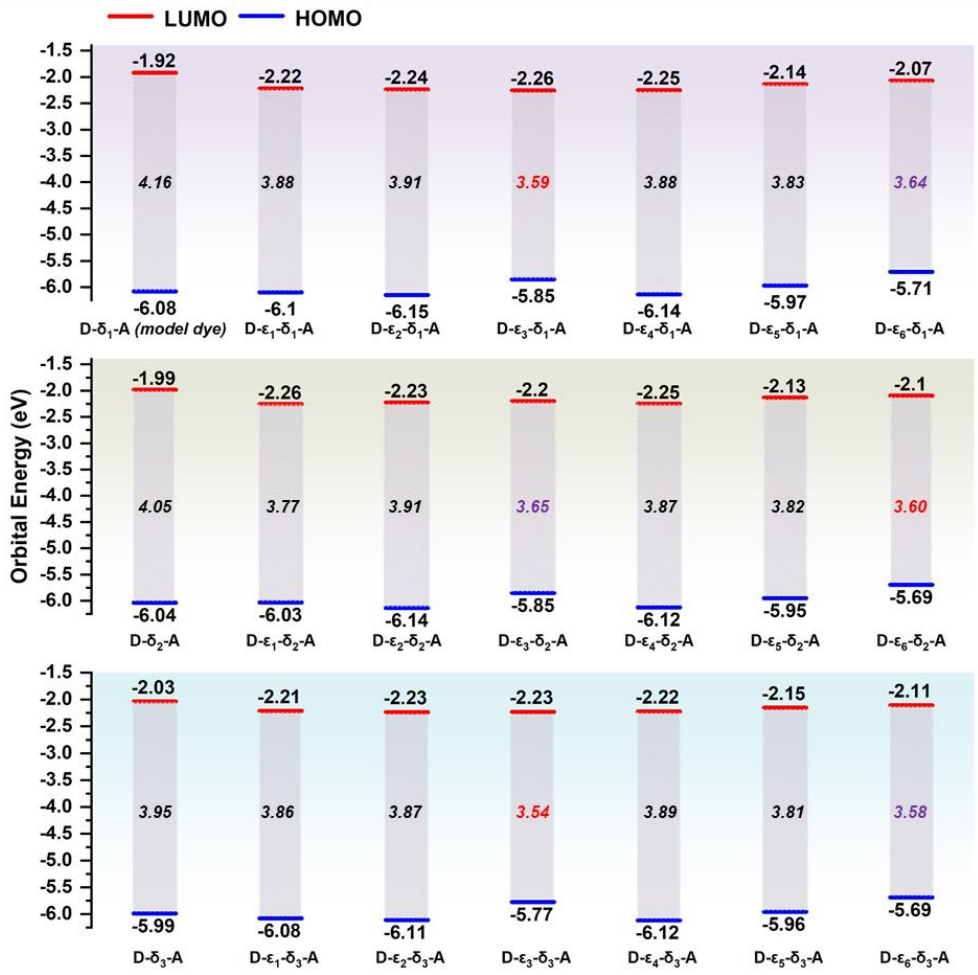


Figure 2. Computed HOMO, LUMO, and bandgap energies of the D-π-A photosensitizers [M06-2X/6-31G(d,p) solvent model: CPCM, $\varepsilon_{ethanol}$ = 24.55].

The operating concept of DSSCs dictates that organic dyes must have adequate energy levels for electron injection and dye regeneration. As can be seen from the obtained data, compared to the D-δ_1-A model dye, the inclusion of additional π-linker subunits in the D-ε_n-δ_n-A backbone has a significant impact on reducing the ε_{LUMO} energies. On the other hand, the presence of ε_n units particularly increases the ε_{HOMO} energies of D-ε_3-δ_n-A and D-ε_6-δ_n-A dyes.

These observations represent the destabilization of HOMO and stabilization of LUMO, resulting in the observed decrease in the associated ε_{gap} values. Furthermore, the ε_{HOMO} values of all investigated D-ε_n-δ_n-A molecules lie sufficiently below the redox potential of I^-/I_3^- (-4.85 eV *vs. in vacuum*), indicating that oxidized dye could be restored by getting electrons from the electrolyte. On a comparable basis, the ε_{LUMO} values of all the photosensitizers are calculated above the conduction band energy level of TiO_2 (-4.04 *vs. in vacuum*). Hence, electrons can be injected from the semiconductor layer into the dye.

A representative diagram for the energy levels of HOMO-4 to LUMO+4 orbitals of all studied photosensitizers is provided in **Figure S1**, in comparison with the redox potential of the ITO, TiO_2, and I^-/I_3^- ion pairs. Due to the fact that the driving force for dye regeneration can influence the back electron transfer kinetics between the injected electrons in the conduction band with the oxidized dye and I^-/I_3^-, it is essential to have an optimal driving force for dye regeneration to ensure the efficient operation of DSSC. In general, the narrower the bandgap, the more it impacts and facilitates electron transport from HOMO to LUMO by absorbing light energy of a relevant wavelength. Our findings demonstrate lower ε_{gap} values for D-ε_3-δ_n-A and D-ε_6-δ_n-A series than other investigated systems.

The representative contour plots of molecular orbitals for D-δ_1-A (*model dye*), D-ε_3-δ_n-A, and D-ε_6-δ_n-A are then depicted in **Figure 3** (other contour plots are provided in **Table S5** for the sake of clarity). To achieve an effective charge-separated state by photo-absorption, the HOMO should be localized on the donor moiety and the LUMO on the anchoring group moiety. It could be seen that in the case of model dye, HOMO's electron density is spread entirely over the molecule, howbeit for the tailored D-ε_g-δ_n-A molecules, HOMO orbitals are mainly localized on donor and π-linker parts. On this basis, when LUMO orbitals are investigated, the electron density lies on the δ-linker and is primarily localized on the anchoring (cyanoacrylic acid) unit, as expected. These observations reveal that the electron separation between the HOMO and LUMO orbitals is favorable for intramolecular charge transfer (ICT) transitions in target photosensitizers.

Furthermore, in order to explore the interfacial electronic properties and the band edge shift, the density of states (DOS) and projected density of states (PDOS) curves of the photosensitizers were generated using a Gaussian function with a standard deviation (s = 0.50 eV), as described in **Table S9**.

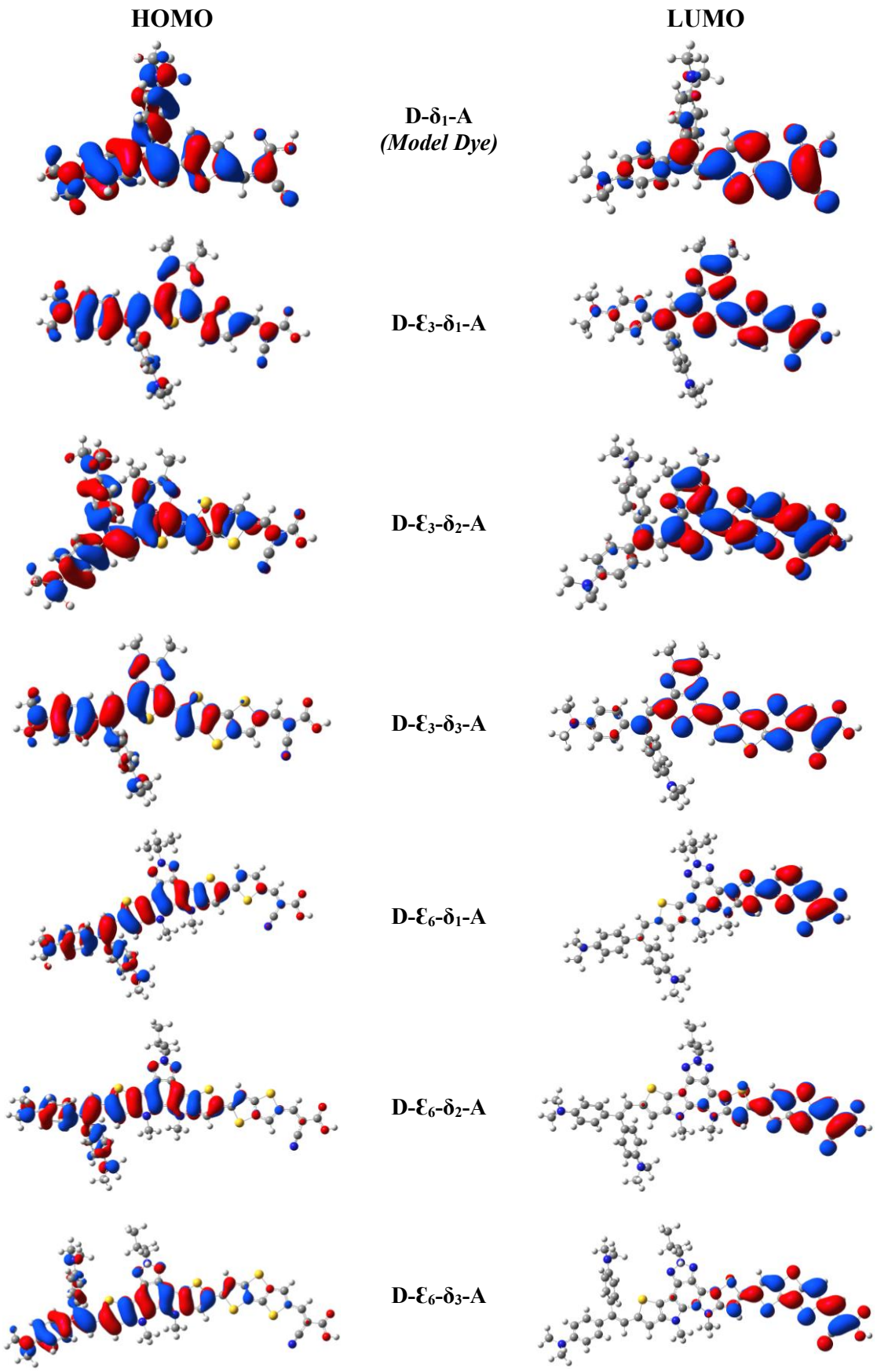


Figure 3. HOMO and LUMO contour plots of the investigated D-$Ɛ_3$-$δ_n$-A and D-$Ɛ_6$-$δ_n$-A systems. The threshold of contours is ±0.02 au [M06-2X/6-31G(d,p) solvent model: CPCM, $Ɛ_{ethanol}$ = 24.55].

3.2.2. Ionization potential (I), electron affinity (A), reorganization energies (λ_e, λ_h, λ_T)

Ionization potential (I) and electron affinity (A): The fundamental parameters for determining the analyzed systems' relative electron injection and hole generation kinetics are dependent on the I and A values. Generally, dyes with exceptional DSSC performance should have superior charge transfer and injection capacity. On this basis, the formation of holes is much more supported in the presence of lower values of I, and the emission of electrons from the excited dye molecules to the conduction band of semiconductors occurs faster if the A values are higher. In this study, we applied two divergent methods (vertical excitations using the geometry of the neutral molecules or adiabatic excitations by using the optimized structure for both the charged and neutral molecules) to determine the investigated dye molecules' corresponding I and A values. Firstly, according to Koopmans' theorem, these parameters are preceded by taking the negative values of the HOMO ($I=-\varepsilon_{HOMO}$) and LUMO ($A=-\varepsilon_{LUMO}$) energies. Accordingly, the calculated first vertical ionization potential and electron affinity values are provided in **Table S6**. As an alternative methodology, the energy barrier for hole and electron injection, which is described by the I and, A, were calculated using the following equations (**Equation 1**), also known as the delta-SCF method using the adiabatic excitations:

$$I = \varepsilon_{cation} - \varepsilon_{neutral} \qquad A = \varepsilon_{neutral} - \varepsilon_{anion} \qquad \textbf{Equation 1}$$

where ε_{cation}, ε_{anion}, and $\varepsilon_{neutral}$ represent the charged (cationic-anionic) and neutral states' SCF energies of the optimized photosensitizers, respectively. The corresponding ionization potential and electron affinity values are also compatibly tabulated in **Table S6**.

It should be emphasized that a similar ascending/descending trend of ionization potential/electron affinity values was observed in both of the calculation methods. To be clearer, the ionization potential of D-δ_1-A was found to be 5.267 (*6.083-Koopman*) eV, whereas especially for the D-Ɛ_3-δ_n-A and D-Ɛ_6-δ_n-A systems, ionization potential values were found lower than the model dye. This output indicates that the hole generation should be easier for 2,3-dimethylthieno[3,4-b]pyrazine (Ɛ_3) and especially 5-isobutyl-10,11-dimethyl-10,11-dihydro-5H-pyrrolo[3,4-e]thieno[2',3':4,5]pyrrolo[3,2-g]thieno[3,2-b]indole (Ɛ_6) bearing dye molecules. On the other hand, the electron affinity value of D-δ_1-A was detected as 2.794 (*1.918-Koopman*) eV. The overall assessment revealed that the tailored dye molecules' electron affinity values were all higher than the D-δ_1-A system, which makes them more suitable for quicker emission of electrons.

In order to achieve a qualitative description of the electron-accepting and electron-donating capabilities of the investigated molecules, a full-electron donor-acceptor map (FEDAM) was also prepared (**Figure 4**). According to obtained data, D-Ɛ$_3$-δ$_n$-A and D-Ɛ$_6$-δ$_n$-A systems are found to be positioned in quadrant IV (in the good acceptor-good donor region) (except D-Ɛ$_6$-δ$_1$-A which belongs to quadrant III howbeit, it is very close to the quadrant IV). Therefore, it could be concluded that these designated photosensitizers have low I and high A values. Moreover, the findings were found consistent with the frontier orbitals' energy trends and could explain the promoted electron-acceptor and hole-creation abilities of these molecules.

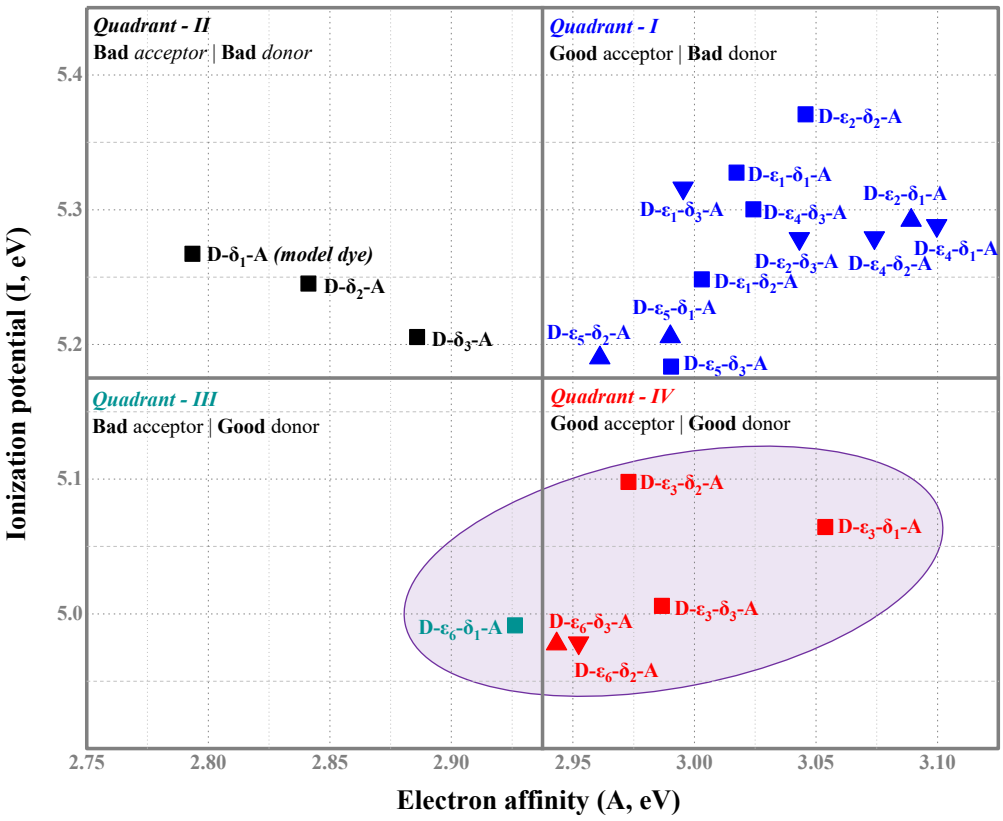


Figure 4. Full-electron-donor-acceptor map of the investigated photosensitizers (I and A values predicted via *delta-SCF* method) [M06-2X//6-31G(d,p) solvent model: CPCM, $\varepsilon_{ethanol} = 24.55$].

Reorganization energies (λ_e, λ_h, λ_T): The reorganization energy could influence the kinetics of electron injection, according to Marcus' theory of electron transfer rate (**Equation 2**).

$$K = A.\exp(-\frac{\lambda}{4k_bT}) \qquad \textbf{Equation 2}$$

where A is a pre-exponential factor, λ is the reorganization energy, k_b is the Boltzmann constant, and T is the absolute temperature. Because the other components in the preceding equation are constant, the rate constant for charge transfer is mostly determined by λ. Consequently, λ is

defined as a measure of the energy cost caused by the alteration of the geometry and the surrounding medium during the charge transfer step. On this premise, λ could be subdivided into two subparts, namely external (λ_{ext}) and internal (λ_{int}) reorganization energies. The λ_{ext} indicates the influence of the solvent medium on charge transfer, while λ_{int} is the outcome of the structural changement between neutral and ionic (cationic/anionic) species. In order to determine the reorganization energies, we focus solely on λ_{int} of the isolated organic photosensitizers and disregard the solvent relaxation for the ab-initio calculation to underline the charge carrier mobility. As a result, the projected total reorganization energy (λ_T) should be identified as the sum of the hole (λ_h) and electron (λ_e) reorganization energies (**Equation 3** and **Equation 4**, respectively).

$$\lambda_h = \lambda_1 + \lambda_2 = [E^+(dye_0) - E^+(dye_+)] + [E^0(dye_+) - E^0(dye_0)] \quad \textbf{Equation 3}$$

$$\lambda_e = \lambda_3 + \lambda_4 = [E^-(dye_0) - E^-(dye_-)] + [E^0(dye_-) - E^0(dye_0)] \quad \textbf{Equation 4}$$

where $E^0(dye_0)$ represents the energy of the neutral dye at its ground state, $E^{\pm}(dye_0)$ defines the energy of the positively or negatively charged dye molecule calculated based on the optimized geometry of the neutral dye, $E^{\pm}(dye_{\pm})$ is the energy of the corresponding cationic or anionic state of dye molecules determined through the optimized geometry of cation/anion form of the dye, and lastly, $E^0(dye_{\pm})$ is the energy of the neutral dye calculated at its cationic or anionic state.

Accordingly, the smaller λ_T values would be better for the electron injection from the excited photosensitizers to the conduction band (CB) of the semiconductor TiO_2 and hence provide to gather desirable short-circuit current density (J_{SC}) values. On this behalf, the calculated reorganization energy (λ_e, λ_h, λ_T) values for all studied molecules are provided in **Figure 5**. As could be presumed from the obtained data, the dye series containing $\mathcal{E}_2$ and $\mathcal{E}_4$ subunits showed the lowest λ_T values varying between 0.643 to 0.742 eV. Interestingly, the shorter π-bridge possessing dye molecules (D-δ_n-A) displayed considerably better performance (λ_T: 0.680-0.773 eV) when compared to the molecules with $\mathcal{E}_3$ and $\mathcal{E}_6$ fragments (λ_T: 0.827-0.968 eV). It should be pointed out that smaller (and ideal) λ_T values could be related to the decreased λ_h values, indicating that especially $\mathcal{E}_2$ and $\mathcal{E}_4$ fragmentations possessing sensitizers are having better hole transport ability.

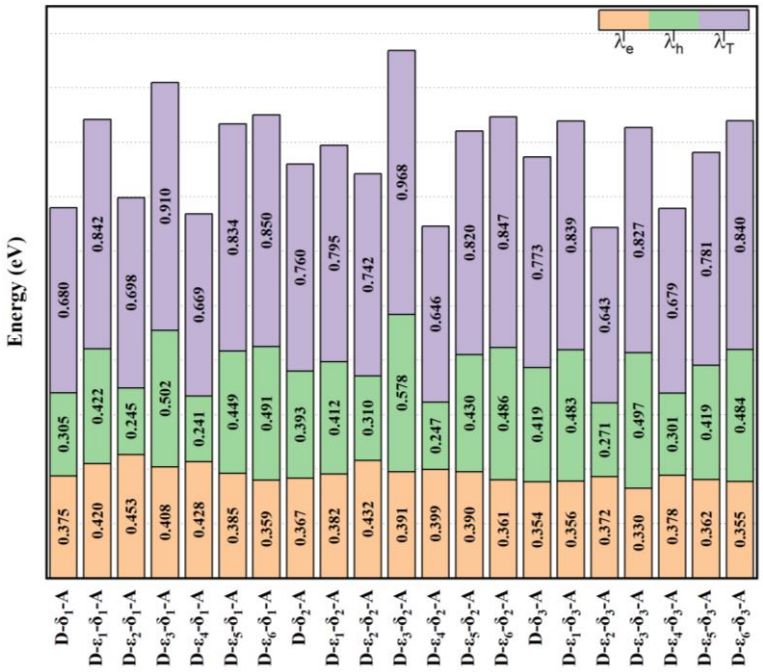


Figure 5. Calculated reorganization energies (λ_e, λ_h, λ_T) [M06-2X//6-31G(d,p)].

3.3. TD-DFT Studies

This study section aims to investigate the excited-state geometries and optical properties of our model sensitizers, building on the previously described DFT investigations. **Table S8** contains the detailed outputs of predicted electronic transitions.

On this basis, dyes containing the ε_3 functional group exhibit higher absorption maxima ranging between 574 (D-ε_3-δ_2-A) – 593 nm (D-ε_3-δ_1-A) when compared to the other photosensitizers. Specifically, the model dye shows an absorption maximum of approximately 481 nm.

Based on the obtained results, the subsequent stage of the study employed the maximum computed absorption and oscillator strength values to predict the photosensitizer properties of the investigated dye molecules in more detail. Accordingly, several parameters were calculated, including the light-harvesting efficiency (LHE, eV), the oxidation potential of the excited dye (ε^*_{dye}, eV), the driving force of the electron injection (ΔG^{inject}, eV), dye regeneration (ΔG^{regen}, eV), excited-state lifetime (τ, ns), and open circuit potential (V_{oc}, eV), in order to gain a comprehensive understanding of the photosensitizer properties of the dyes. The obtained results are presented in **Table 2**.

Light-harvesting efficiency is mathematically related to the oscillator strength (*f*) of dye molecules and can be defined by **Equation 5**.

$$LHE = 1\text{-}10^{-f} \quad \textbf{Equation 5}$$

where f is oscillator strength, as mentioned above. The LHE value of the model dye is calculated as 0.9420 eV. In order to maximize the response of photocurrent, the LHE values of the investigated photosensitizers must be as high as possible while ensuring the greatest short current density (J_{sc}) values. Several examined photosensitizers had LHE values that were higher than the model dye and corresponding values varying between 0.8617 (D-ε_1-δ_1-A) - 0.9970 (D-ε_6-δ_3-A) eV. It can be concluded that upon analyzing the computed maximum absorption and oscillator strength values, it is observed that the ε_6 series exhibited higher light-harvesting efficiency (LHE) values compared to other investigated dye molecules. The enhanced LHE of the ε_6 series could be attributed to the favorable electronic structure of the anchoring unit that promotes efficient charge transfer from the excited dye to the TiO_2 semiconductor.

Charge injection (ΔG^{inject}) and dye regeneration (ΔG^{regen})

To elucidate the influence of the different functional groups on electron injection efficiency and dye regeneration kinetics, Koopmans' theorem was employed to predict the charge injection (ΔG^{inject}) and dye regeneration (ΔG^{regen}) values. At first glance, the calculated ground state oxidation potential energy, represented as ε_{dye}, was determined by the negative value of the ε_{HOMO}, and subsequently, the ε^*_{dye} was computed using **Equation 6**.

$$\varepsilon^*_{dye} = \varepsilon_{dye} - \lambda_{max} \quad \textbf{Equation 6}$$

The corresponding ΔG^{inject} can be described as **Equation 7**.

$$\Delta G^{inject} = \varepsilon^*_{dye} - \varepsilon_{CB} \quad \textbf{Equation 7}$$

Based on the computed values of ε^*_{dye}, all of the investigated systems were determined to have smaller values than the conduction band of titanium oxide (ε_{CB}=-4.04 eV *vs. in vacuum*), which suggests that electron injection is energetically favorable in all cases. As indicated in **Table 2**, the corresponding free energy changes (ΔG^{inject}) for each of the dye molecules were determined to be within the range of -0.282 (D-ε_3-δ_1-A) to -0.879 (D-ε_6-δ_3-A) eV. Hence, within the series of investigated molecules, D-ε_6-δ_3-A exhibited the lowest ΔG^{inject} value, indicating a faster electron injection rate.

The reorganization energy (ΔG^{regen}) plays a critical role in the efficiency of DSSC devices and is defined by **Equation 8** as the difference between the excited-state energy of the dye molecule ($\mathcal{E}^{*}_{dye}$) and the redox potential of the iodide/triiodide couple ($\mathcal{E}^{redox}_{I^-|I_3^-}$). To achieve faster electron transfer, a lower ΔG^{regen} value is desirable. The model dye's ΔG^{regen} value was determined to be 1.233 eV. The calculated ΔG^{regen} values ranged from 0.837 (D-$\mathcal{E}_6$-δ_3-A) to 1.300 (D-$\mathcal{E}_2$-δ_1-A) eV. The results indicate that the electron injection rate follows the order of $\mathcal{E}_2 > \mathcal{E}_4 > \mathcal{E}_1 > \mathcal{E}_5 > \mathcal{E}_3 > \mathcal{E}_6$, suggesting that the $\mathcal{E}_6$ functional group-containing dye molecules have the potential to achieve higher electron power conversion efficiency.

$$\Delta G^{regen} = \mathcal{E}^{*}_{dye} - \mathcal{E}^{redox}_{I^-|I_3^-} \qquad \textbf{Equation 8}$$

Excited-state lifetime (τ) is a crucial parameter for assessing the efficacy of charge transfer in dye-sensitized solar cells (DSSCs). The longer the lifetime of the excited state of a dye, the more conducive it is to charge transfer. To determine the excited-state lifetimes of the dye molecules, the optimized geometry of the molecules in the first excited singlet electronic state was utilized to evaluate the lowest excitation energy (ε) and the corresponding oscillator strength (*f*). The lifetime of the excited state in DSSCs can be determined using **Equation 9.**

$$\tau = 1.499/(f.\varepsilon^2) \qquad \textbf{Equation 9}$$

The excited-state lifetime (τ) values were calculated for the investigated dyes to assess their potential for facilitating charge transfer. The model dye displayed an excited-state lifetime of 2.809 ns, whereas the $\mathcal{E}_1$ and $\mathcal{E}_3$ subgroups showed longer lifetimes ranging from 3.097 (D-$\mathcal{E}_1$-δ_3-A) to 4.616 (D-$\mathcal{E}_1$-δ_1-A) ns. In contrast, the excited-state lifetime values of the other dyes were found to be generally shorter than the model dye, with lifetimes ranging from 1.429 to 2.725 ns. These results suggest that the $\mathcal{E}_1$ and $\mathcal{E}_3$ fragments containing dyes may be more efficient at facilitating charge transfer than the model dye and the other investigated dyes due to their longer excited-state lifetimes.

As part of this study, the value of Voc for all compounds was also evaluated. The maximum open circuit voltage (V_{oc}) of DSSCs can be approximately estimated by the energy difference between the lower unoccupied molecular orbital ($\mathcal{E}_{LUMO}$) of the dye and conduction band ($\mathcal{E}_{CB}$) of the semiconductor TiO_2, taking into account the energy lost during the photo-charge generation. The obtained values of V_{oc} for the investigated molecules were found between 1.782 (D-$\mathcal{E}_3$-δ_1-A) – 2.122 (D-δ_1-A, *model dye*) and sufficient for efficient electron injection.

Table 2. Calculated electronic properties, including maximum absorption wavelength (λ, nm), oscillator strength (*f*), light-harvesting efficiency (LHE, eV), the oxidation potential of the excited dye (ε_{dye}, eV), the electron injection driving force (ΔG^{inject}), regeneration of dye (ΔG^{regen}), the lifetime of the excited state (τ, ns) and open circuit potential (V_{oc}, eV) [M06-2X//6-31G(d,p) solvent model: CPCM, $\varepsilon_{ethanol}$ = 24.55]

Entry	λ_{max}(nm)	*f*	LHE	ε_{dye}* (eV)	ΔG^{inject}	ΔG^{regen}	τ (ns)	V_{oc}
D-δ$_1$-A (*model dye*)	481	1.2366	0.9420	3.507	-0.533	1.233	2.809	2.122
D-Ɛ$_1$-δ$_1$-A	514	0.8593	0.8617	3.689	-0.351	1.250	4.616	1.819
D-Ɛ$_2$-δ$_1$-A	490	1.1872	0.9350	3.621	-0.419	1.300	3.037	1.802
D-Ɛ$_3$-δ$_1$-A	593	1.3090	0.9509	3.758	-0.282	0.998	4.030	1.782
D-Ɛ$_4$-δ$_1$-A	483	1.5091	0.9690	3.572	-0.468	1.288	2.319	1.787
D-Ɛ$_5$-δ$_1$-A	477	1.8022	0.9842	3.367	-0.673	1.117	1.892	1.902
D-Ɛ$_6$-δ$_1$-A	506	1.9699	0.9893	3.261	-0.779	0.859	1.952	1.970
D-Ɛ$_2$-A	486	1.2972	0.9496	3.482	-0.558	1.185	2.725	2.054
D-Ɛ$_2$-δ$_2$-A	533	1.3165	0.9517	3.704	-0.336	1.180	3.236	1.783
D-Ɛ$_2$-δ$_2$-A	474	1.4327	0.9631	3.522	-0.518	1.286	2.354	1.814
D-Ɛ$_3$-δ$_2$-A	574	1.3448	0.9548	3.691	-0.349	1.001	3.673	1.839
D-Ɛ$_4$-δ$_2$-A	475	2.0469	0.9910	3.517	-0.523	1.275	1.656	1.788
D-Ɛ$_5$-δ$_2$-A	471	2.0336	0.9907	3.317	-0.723	1.099	1.636	1.907
D-Ɛ$_6$-δ$_2$-A	492	2.3670	0.9957	3.172	-0.868	0.844	1.530	1.943
D-δ$_3$-A	485	1.5523	0.9720	3.428	-0.612	1.137	2.269	2.005
D-Ɛ$_1$-δ$_3$-A	505	1.2361	0.9419	3.623	-0.417	1.226	3.097	1.827
D-Ɛ$_2$-δ$_3$-A	486	1.7473	0.9821	3.558	-0.482	1.257	2.029	1.806
D-Ɛ$_3$-δ$_3$-A	585	1.6048	0.9752	3.654	-0.386	0.922	3.202	1.813
D-Ɛ$_4$-δ$_3$-A	475	2.0462	0.9910	3.506	-0.534	1.267	1.652	1.818
D-Ɛ$_5$-δ$_3$-A	466	2.0854	0.9918	3.299	-0.741	1.107	1.564	1.889
D-Ɛ$_6$-δ$_3$-A	491	2.5268	0.9970	3.161	-0.879	0.837	1.429	1.935

3.4. Electron Density Differentiation Maps (EDDM)

The differentiation of electron densities in the investigated dye molecules before and after photoexcitation, as well as their electron-donating and electron-accepting properties, were explored through the execution of required calculations and preparation of electron density differentiation maps (EDDMs). To this end, each molecule was divided into four independent fragments, namely D (donor unit), Ɛ (first fraction - π-bridge), δ (second fraction - π-bridge), A (acceptor unit), and the corresponding density changes were calculated and provided with percent contributions information. Detailed data are provided in **Table S10**. The results indicate that the electron density values of all donor fragments decreased following photoexcitation, suggesting their successful electron-donating behaviors. After analyzing the data, it was observed that the δ_1-containing dyes had the highest percentage contribution change among the

donor fragments, ranging from 44 to 77%, indicating their efficient electron-donating properties compared to the other fragments in the studied dye molecules. Primarily, in the case of $\mathcal{E}_3$ and $\mathcal{E}_6$ bearing molecules, donor units were found to be less dominant to the electron donating pattern. The electron density cumulated on the acceptor fragment (anchoring unit) was found to be primarily influenced by the behavior of the δ subunits, and this effect was particularly prominent in the case of D-$\mathcal{E}_6$-δ_n-A dyes (**Table 3**).

3.5. Atom- and fragment-based electron-hole analysis

After disassembling each molecule into individual atoms to determine the concentration of excited electrons in the anchoring groups (see **Table S11** and **Table S12** for details), a detailed study was conducted to analyze the contribution of each fragment to electron-hole distribution. The results obtained from the electron-hole analysis revealed a similar trend to the EDDM analyses, with the acceptor fragment exhibiting the highest electron contributions. The electron density distribution analysis revealed that electrons were initially localized on the donor and π-spacer fragments and then became delocalized towards the acceptor fragments in all of the investigated compounds. The atom- and fragment-based electron-hole analysis of the model dye is depicted in **Figure 6**.

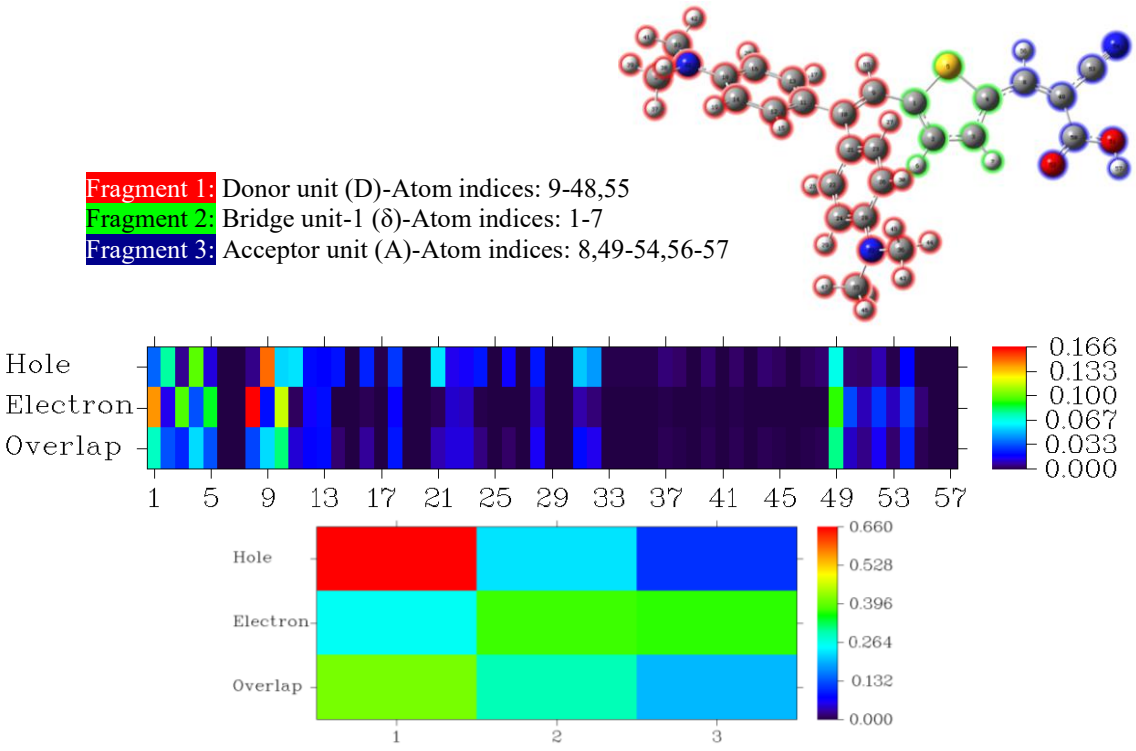
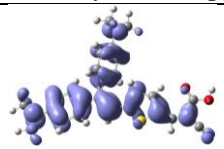
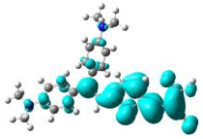
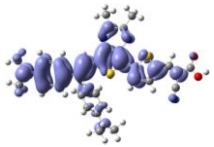
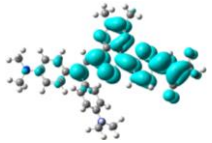
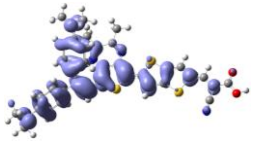
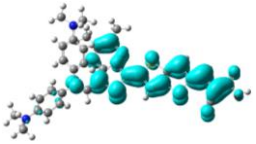
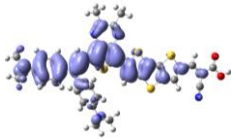
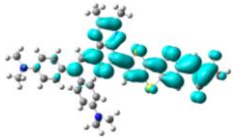
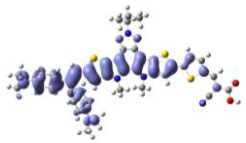
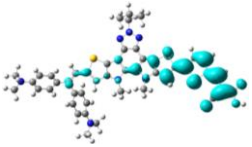
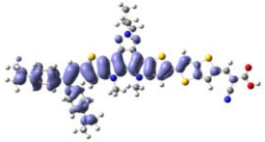
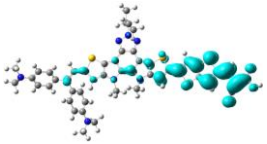
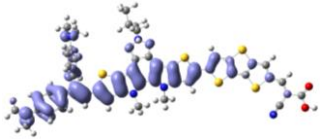
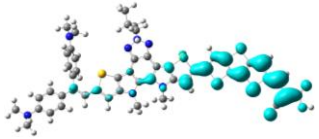


Figure 6. Atom- and fragment-based electron-hole distribution of *model dye* (D-δ_1-A)

Table 3. Electron density differentiation maps (EDDMs) and the corresponding percent contributions of the different fragments on the investigated D-$\mathcal{E}_3$-δ_n-A and D-$\mathcal{E}_6$-δ_n-A systems [M06-2x/6-31G(d,p) solvent model: CPCM, $\mathcal{E}_{ethanol}$ = 24.55].

Entry	absorption λ_{max}	*f*	change	contribution % D	ε	δ	A	EDDM BEFORE *(where the excited electron density is coming from)*	EDDM AFTER *(where the excited electron density is going to)*
D-δ_1-A (Model Dye)	481	1.24	**Before**	79	-	15	7		
			After	18	-	36	46		
			Net	**-61**	**-**	**21**	**39**		
D-$\mathcal{E}_3$-δ_1-A	593	1.30	**Before**	57	27	11	5		
			After	13	37	24	26		
			Net	**-44**	**10**	**13**	**21**		
D-$\mathcal{E}_3$-δ_2-A	574	1.34	**Before**	59	25	13	3		
			After	7	29	34	29		
			Net	**-52**	**24**	**21**	**26**		
D-$\mathcal{E}_3$-δ_3-A	585	1.60	**Before**	52	29	18	2		
			After	8	24	38	30		
			Net	**-44**	**-5**	**20**	**28**		
D-$\mathcal{E}_6$-δ_1-A	506	1.97	**Before**	42	53	3	1		
			After	1	21	36	43		
			Net	**-41**	**-32**	**33**	**42**		
D-$\mathcal{E}_6$-δ_2-A	492	2.37	**Before**	41	54	4	1		
			After	0	12	42	46		
			Net	**-41**	**-42**	**38**	**45**		
D-$\mathcal{E}_6$-δ_3-A	491	2.53	**Before**	39	55	5	1		
			After	0	9	48	43		
			Net	**-39**	**-46**	**43**	**42**		

3.6. Transition density and color correlation matrix analyses

The distribution and quantity of charge density in a simulated chemical system indicate the presence of different constituents. Therefore, employing a heat map to visualize the charge density is a valuable technique for analyzing the characteristics of various components during the charge transfer process. Distinct transitions play a crucial role in determining the mechanism of charge transfer, and the involvement of hydrogen in these transitions is relatively insignificant. The transition density matrix (TDM) and color correlation matrix of the investigated dye molecules were evaluated to gain insight into the excitation process. These matrices provide valuable information about the transitions that occur during the first excitation and help to elucidate the mechanisms of charge transfer. As can be seen in **Figure 7**, the studied dye molecule was segmented into three distinct fragments: the donor (D; fragment no. 1), the π-linker (fragment no. 2), and the acceptor (A; fragment no. 3). The color correlation matrix depicted in the central portion of the figure highlights the TDM contribution of each fragment.

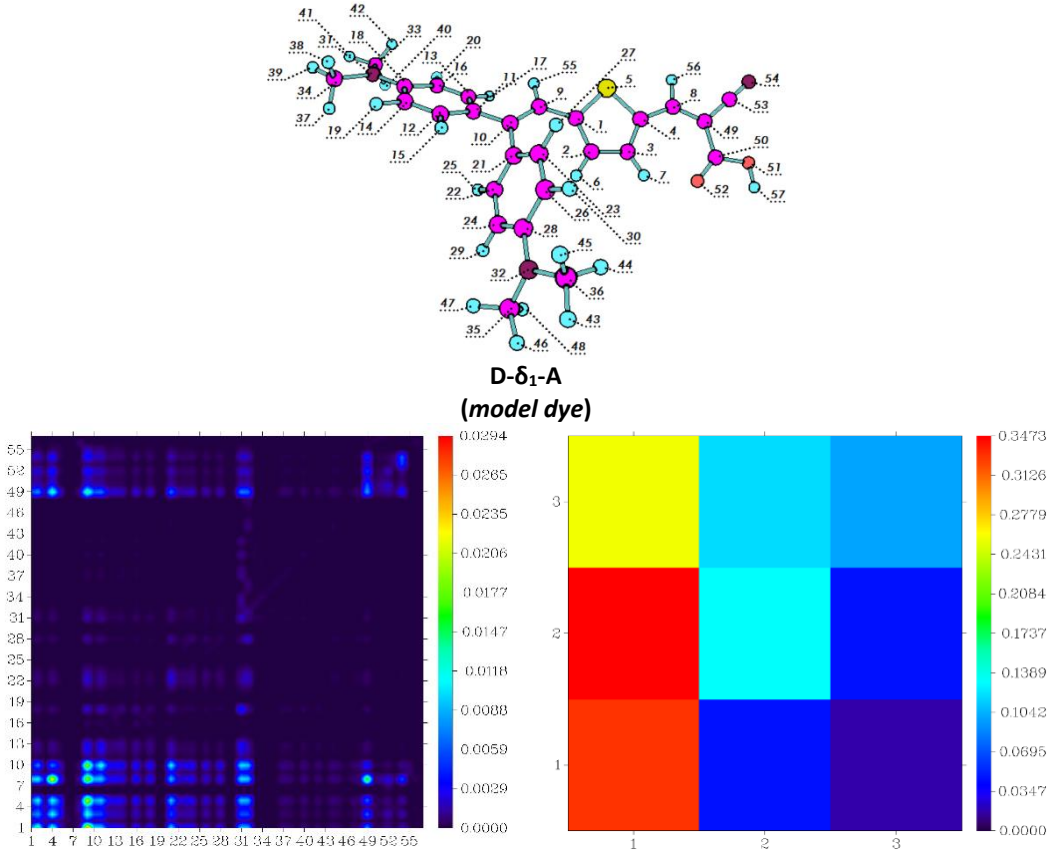


Figure 7. Atom- and fragment-based transition density and color correlation matrix (where the y-axis is the originating, and the x-axis is the receiving fragment for the excited electron) of the *model dye* [M06-2x/6-31G(d,p) solvent model: CPCM, $\varepsilon_{ethanol}$ = 24.55].

The color correlation matrix comprehensively depicts the TDM fragmental contribution correlation. This tool facilitates the assessment of the correlation between fragments throughout the investigated molecule. The observed color patterns in the matrix confirm that the donor unit (D or fragment no. 1) plays a significant role in the electron density distribution of the studied system. This is evidenced by the dominant red zone in the matrix. Furthermore, it is evident that electron density accumulates from the donor fragment toward the acceptor fragment. Corresponding plots for all studied dye molecules are provided in **Table S13**. The transition density matrix (TDM) is also a valuable tool for providing a spatial map that contains information about the length of charge transfer (Δr index) and the degree of electron–hole overlap (Λ) (**Table 4**). The charge-transfer lengths (Δr) measured by the transition density matrix (TDM) are significant in determining the distance between the electron and its corresponding hole. This chemical index is crucial in distinguishing between local excitations (LE) and charge transfer (CT). Specifically, if the Δr index value is less than or equal to 2 Å, it indicates local excitations, whereas a value greater than or equal to 2 Å suggests charge transfer. In our cases, because all the charge-transfer lengths (Δr) are greater than 2 Å, it would suggest that the excited states being analyzed involve charge transfer rather than local excitations.

Table 4. Calculated length of charge transfer (Δr index) and the degree of electron–hole overlap (Λ) for the investigated systems [M06-2x/6-31G(d,p) solvent model: CPCM, Ɛethanol = 24.55].

Entry	Δr index		Λ index	
	Overall (Å)	Predominating Orbital Pair' Contribution (Å)	Overall (Å)	Predominating Orbital Pair' Contribution (Å)
D-δ_1-A (*model dye*)	4.317	117→118 (4.063)	0.566	117→118 (0.500)
D-Ɛ$_1$-δ_1-A	6.614	151→152 (5.582)	0.446	151→152 (0.341)
D-Ɛ$_2$-δ_1-A	6.934	159→160 (6.017)	0.479	159→160 (0.331)
D-Ɛ$_3$-δ_1-A	4.436	159→160 (4.003)	0.634	159→160 (0.569)
D-Ɛ$_4$-δ_1-A	7.923	152→153 (6.729)	0.476	152→153 (0.302)
D-Ɛ$_5$-δ_1-A	8.843	191→192 (7.005)	0.451	191→192 (0.236)
D-Ɛ$_6$-δ_1-A	10.053	219→220 (7.734)	0.437	219→220 (0.256)
D-Ɛ$_2$-A	5.387	131→132 (5.019)	0.536	131→132 (0.448)
D-Ɛ$_2$-δ_2-A	6.701	165→166 (5.714)	0.514	165→166 (0.395)
D-Ɛ$_2$-δ_2-A	7.139	173→174 (6.148)	0.458	173→174 (0.249)
D-Ɛ$_3$-δ_2-A	5.561	173→174 (4.837)	0.572	173→174 (0.466)
D-Ɛ$_4$-δ_2-A	9.005	166→167 (7.173)	0.476	166→167 (0.248)
D-Ɛ$_5$-δ_2-A	9.342	205→206 (7.038)	0.455	205→206 (0.197)
D-Ɛ$_6$-δ_2-A	11.587	233→234 (8.508)	0.405	233→234 (0.192)
D-δ_3-A	6.602	145→146 (5.987)	0.507	145→146 (0.388)
D-Ɛ$_1$-δ_3-A	8.027	179→180 (6.041)	0.454	179→180 (0.256)
D-Ɛ$_2$-δ_3-A	7.912	187→188 (6.393)	0.500	187→188 (0.254)
D-Ɛ$_3$-δ_3-A	6.409	187→188 (5.422)	0.593	187→188 (0.460)
D-Ɛ$_4$-δ_3-A	8.868	180→181 (6.753)	0.495	180→181 (0.228)
D-Ɛ$_5$-δ_3-A	9.797	219→220 (6.666)	0.460	219→220 (0.150)
D-Ɛ$_6$-δ_3-A	12.363	247→248 (8.523)	0.406	247→248 (0.174)

3.7. Electron transfer and dye adsorption efficiency of D-$\mathcal{E}_n$-δ_n-A@Ti_5O_{10} clusters

This study section focuses on the realistic simulation of the investigated dye molecules to demonstrate their potential performance on DSSC devices. To achieve this, the optical and relative electronic properties of the model dye and six (D-$\mathcal{E}_3$-δ_n-A and D-$\mathcal{E}_6$-δ_n-A) of the best candidate sensitizers were calculated. The selected sensitizers were chosen based on their photovoltaic parameters, particularly their bandgap values, global descriptors, and EDDM studies. The full geometry optimization of D-$\mathcal{E}_3$-δ_n-A@Ti_5O_{10} and D-$\mathcal{E}_6$-δ_n-A@Ti_5O_{10} clusters was executed through the already submitted TD-DFT conditions for pristine dye molecules. The Ti_5O_{10} cluster was prepared by approximately cutting a TiO_2 rutile (110) film [62]. **Figure 8** illustrates the geometry-optimized structure of the studied clusters.

In order to gain insight into the charge distribution occurring in the D-$\mathcal{E}_{3or6}$-δ_n-A@Ti_5O_{10} systems, the corresponding electrostatic potential (ESP) maps were also generated and analyzed. As depicted in **Figure 9**, a similar pattern was observed for the model dye and D-$\mathcal{E}_{3or6}$-δ_n-A@Ti_5O_{10} clusters, where a homogeneously distributed charge delocalization was observed through the D-$\mathcal{E}_{3or6}$-δ_n-A system, with the anchoring groups acting as electron-acceptors. The charge distribution over their titanium clusters was also found to be in accordance, indicating the uniform charge delocalization properties of the model dye and investigated sensitizers bearing the $\mathcal{E}_3$ or $\mathcal{E}_6$ fragments.

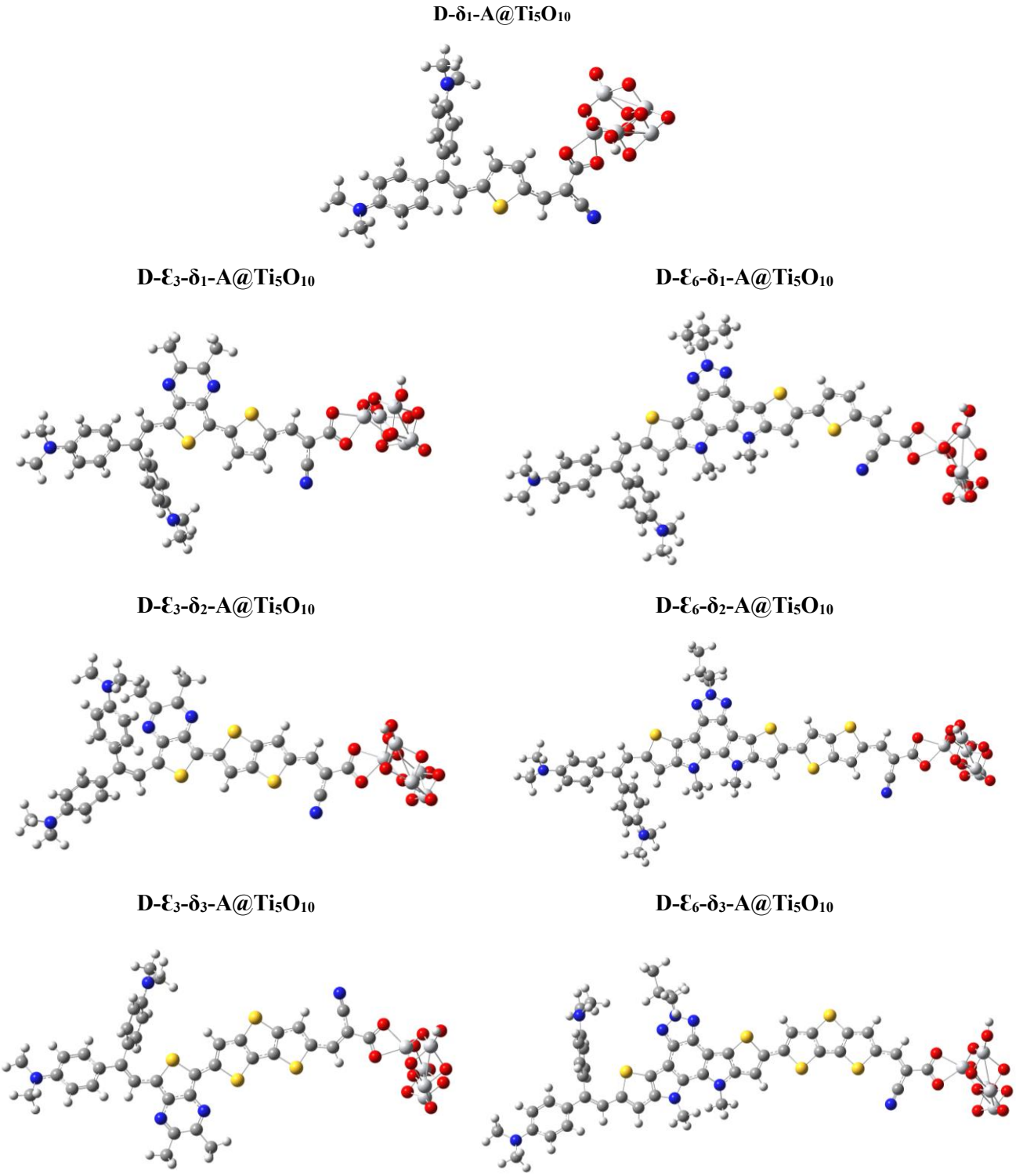


Figure 8. Geometry optimized molecular structures of the investigated dye@Ti_5O_{10} clusters [M06-2X//6-31G(d,p) solvent model: CPCM, $\varepsilon_{ethanol}$=24.55].

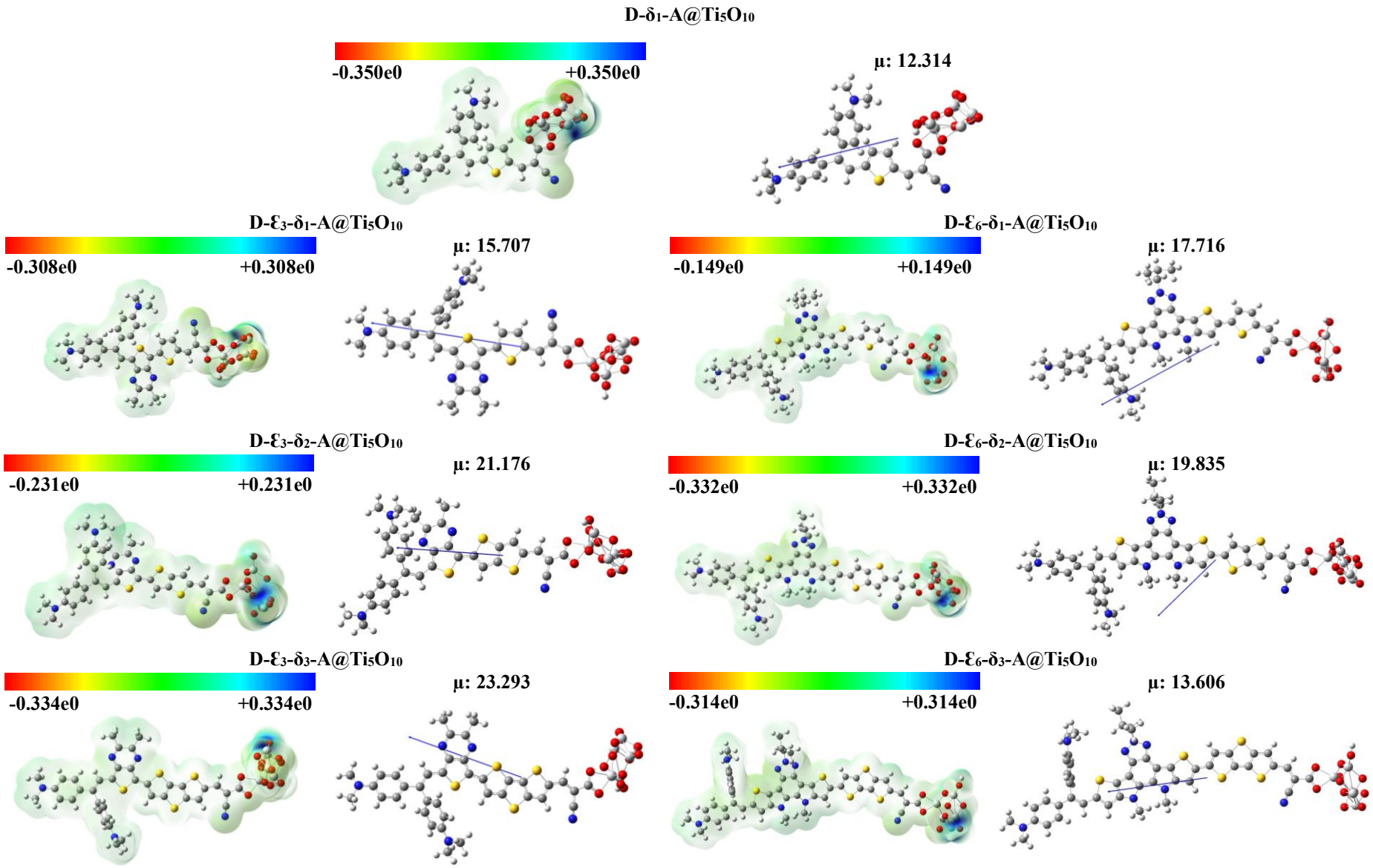


Figure 9. ESP maps and total dipole moment vectors of the investigated dye@Ti_5O_{10} clusters [M06-2X//6-31G(d,p) solvent model: CPCM, $\varepsilon_{ethanol}$ =24.55].

Representative contour plots of these molecular orbitals are shown in **Figure 10**, where it is observed that the HOMOs of the sensitizers are mostly localized on the D-$Ɛ_{3or6}$-δn fragments. In contrast, the LUMOs are primarily localized on the Ti_5O_{10} fragment, as expected. This result confirms the efficient electron injection from the sensitizers to the semiconductor layer. These findings support the potential use of these molecules for the development of high-performance DSSC devices.

The subsequent investigation of the TD-DFT calculated data illustrated that the first six vertical excitation states of the *model dye*@Ti_5O_{10} and D-$Ɛ_{3or6}$-δn-A@Ti_5O_{10} clusters were obtained and the outcomes are provided in **Table 6**. The data revealed that the HOMO→LUMO transition was the major contributor to the entire system's first vertical excitation states. Moreover, a substantial bathochromic shift of around 20 to 40 nm for all investigated dye@Ti_5O_{10} clusters, consistent with the expected behavior. It is noteworthy that all the measured wavelength values were found to be within the UV-vis region.

Table 6. Computed absorption wavelengths (λ, nm), oscillator strengths (*f*), and the orbitals involved in the transitions of dye@Ti_5O_{10} clusters [M06-2X//6-31G(d,p) solvent model: CPCM, $ε_{ethanol}$ =24.55]

Entry	λ	*f*	Transitions (%) *(only major contributions are indicated)*
D-$δ_1$-A@Ti_5O_{10}	521	1.25	HOMO→LUMO (91%)
	373	0.36	HOMO-1→LUMO (91%)
	316	0.11	HOMO-2→LUMO (83%)
D-$Ɛ_3$-$δ_1$-A@Ti_5O_{10}	631	1.53	HOMO→LUMO (90%)
	430	0.28	HOMO-1→LUMO (82%)
	413	0.16	HOMO-2→LUMO (11%), HOMO→LUMO+1 (74%)
D-$Ɛ_6$-$δ_1$-A@Ti_5O_{10}	540	2.00	HOMO-1→LUMO (20%), HOMO→LUMO (68%)
	399	0.36	HOMO-4→LUMO (11%), HOMO-1→LUMO (38%), HOMO→LUMO+3 (30%)
	379	0.73	HOMO-1→LUMO (16%), HOMO→LUMO (22%), HOMO→LUMO+3 (44%)
D-$Ɛ_3$-$δ_2$-A@Ti_5O_{10}	611	1.61	HOMO→LUMO (83%), HOMO→LUMO+1 (10%)
	439	0.51	HOMO-2→LUMO (25%), HOMO-1→LUMO (19%), HOMO→LUMO+1 (42%)
	407	0.13	HOMO-1→LUMO (44%), HOMO→LUMO+1 (33%)
D-$Ɛ_6$-$δ_2$-A@Ti_5O_{10}	526	2.43	HOMO-1→LUMO (19%), HOMO→LUMO (64%)
	402	0.22	HOMO-4→LUMO (13%), HOMO-1→LUMO (24%), HOMO→LUMO+3 (42%)
	387	0.89	HOMO-1→LUMO (21%), HOMO→LUMO (31%), HOMO→LUMO+3 (27%)
D-$Ɛ_3$-$δ_3$-A@Ti_5O_{10}	608	1.82	HOMO→LUMO (77%), HOMO→LUMO+1 (14%)
	448	0.24	HOMO-2→LUMO (12%), HOMO→LUMO+1 (71%)
	402	0.24	HOMO-2→LUMO (20%), HOMO-1→LUMO (51%), HOMO-1→LUMO+1 (15%)
D-$Ɛ_3$-$δ_3$-A@Ti_5O_{10}	511	2.49	HOMO-1→LUMO (20%), HOMO→LUMO (60%)
	400	0.23	HOMO-4→LUMO (21%), HOMO-1→LUMO (22%), HOMO→LUMO+3 (31%)
	388	1.16	HOMO-1→LUMO (11%), HOMO→LUMO (32%), HOMO→LUMO+3 (31%)

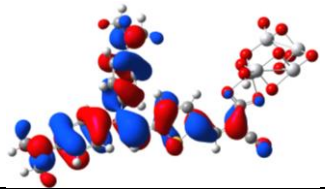
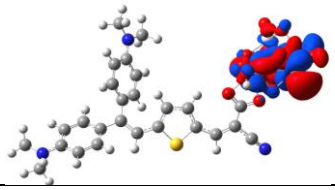
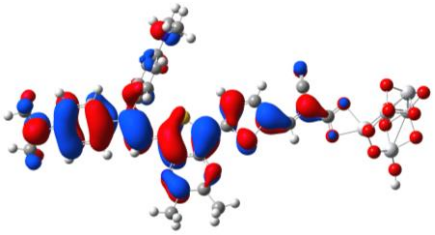
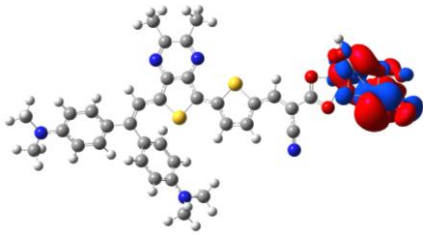
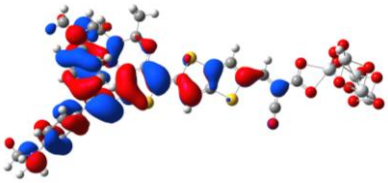
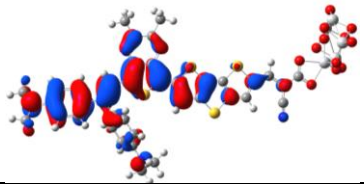
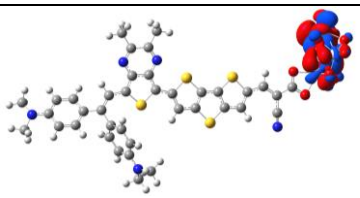
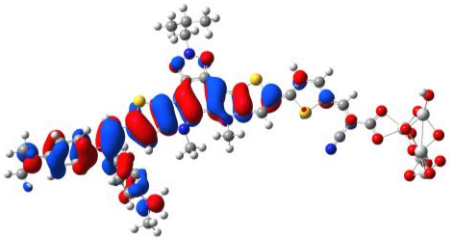
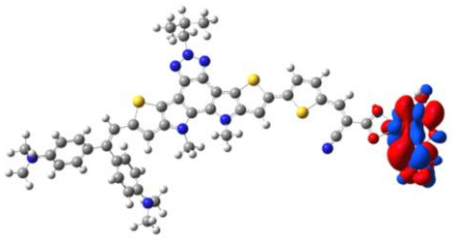
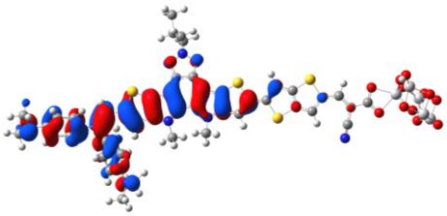
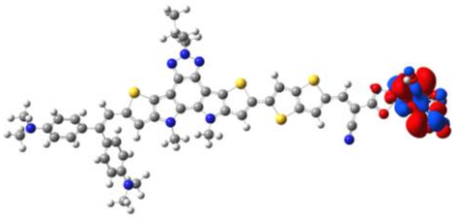
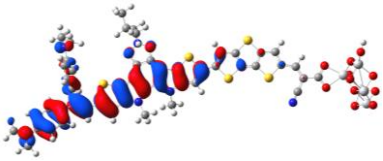
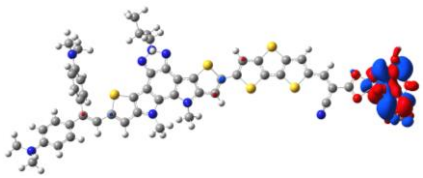
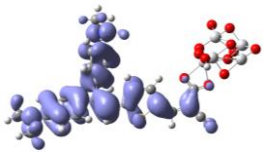
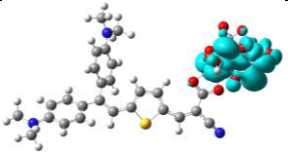
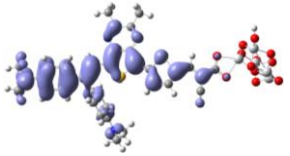
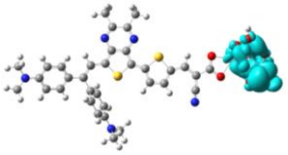
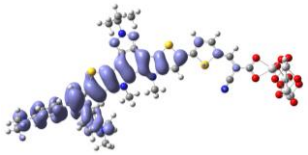
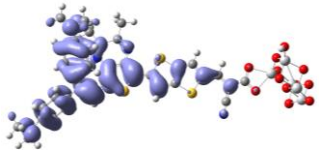
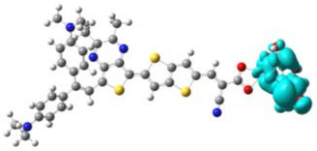
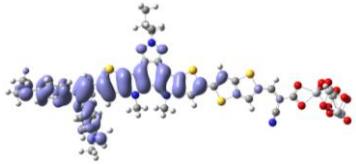
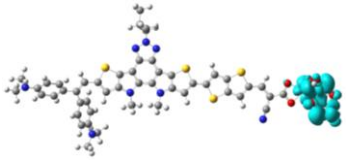
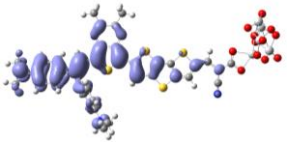
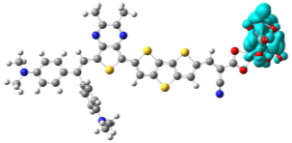
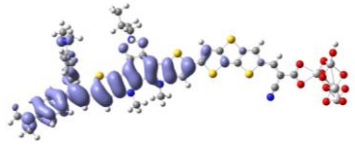
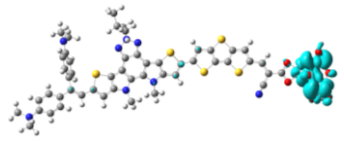
HOMO		LUMO
	**D-δ1-A@Ti5O10**	
	**D-Ɛ3-δ1-A@Ti5O10**	
	**D-Ɛ3-δ2-A@Ti5O10**	
	**D-Ɛ3-δ3-A@Ti5O10**	
	**D-Ɛ6-δ1-A@Ti5O10**	
	**D-Ɛ6-δ2-A@Ti5O10**	
	**D-Ɛ6-δ3-A@Ti5O10**	

Figure 10. Representative HOMO and LUMO contour plots of the investigated dye@Ti_5O_{10} clusters. The threshold of contours is ±0.02 au [M06-2X//6-31G(d,p) solvent model: CPCM, $\varepsilon_{ethanol}$ =24.55].

Table 7. Electron density differentiation maps (EDDMs) of the investigated dye@Ti_5O_{10} clusters [M06-2X//6-31G(d,p) solvent model: CPCM, $\varepsilon_{ethanol}$=24.55]

Entry	absorption λ_{max}	*f*	change	contribution % D	ε	δ	A	Ti_5O_{10}	EDDM BEFORE *(where the excited electron density is coming from)*	EDDM AFTER *(where the excited electron density is going to)*
D-δ_1-A@Ti_5O_{10}	521	1.25	**Before**	79	14	7	-	0		
			After	0	0	0	-	100		
			Net	*-79*	*-14*	*-7*	-	*100*		
D-ε_3-δ_1-A@Ti_5O_{10}	631	1.53	**Before**	58	26	10	5	0		
			After	0	0	0	0	100		
			Net	*-58*	*-26*	*-10*	*-5*	*100*		
D-ε_6-δ_1-A@Ti_5O_{10}	540	2.00	**Before**	44	51	3	2	0		
			After	0	0	0	0	100		
			Net	*-44*	*-51*	*-3*	*-2*	*100*		
D-ε_3-δ_2-A@Ti_5O_{10}	612	1.61	**Before**	59	25	12	3	0		
			After	0	0	0	0	100		
			Net	*-59*	*-25*	*-12*	*-3*	*100*		
D-ε_6-δ_2-A@Ti_5O_{10}	526	2.43	**Before**	42	53	4	1	0		
			After	0	0	0	0	100		
			Net	*-42*	*-53*	*-4*	*-1*	*100*		
D-ε_3-δ_3-A@Ti_5O_{10}	608	1.82	**Before**	52	28	17	2	0		
			After	0	0	0	0	100		
			Net	*-52*	*-28*	*-17*	*-2*	*100*		
D-ε_6-δ_3-A@Ti_5O_{10}	511	2.49	**Before**	40	55	5	1	0		
			After	0	0	0	0	100		
			Net	*-40*	*-55*	*-5*	*-1*	*100*		

The electron density cumulation on the Ti_5O_{10} fragment was highest for all investigated dye molecules (~100%), as revealed by the corresponding EDDM data in **Table 7**. This observation can be attributed to the efficient electron transfer from the excited sensitizers to the semiconductor layer. Therefore, the investigated dye molecules possess the potential to enhance electron transfer efficiency, which is a crucial factor in developing high-performance DSSC devices.

Conclusion

The present study investigated the potential of a series of D-Ɛ_n-δ_n-A as sensitizers in dye-sensitized solar cells (DSSCs). A range of theoretical methods was utilized to predict the photophysical properties of investigated dyes and charge transfer efficiency. In this regard, the structural and electronic properties of the dye molecules were evaluated using density functional theory (DFT) and time-dependent density functional theory (TD-DFT), respectively. Furthermore, global reactivity descriptors (GRDs) were employed to provide valuable insights into the electronic and photovoltaic properties of the candidate sensitizers.

The calculated results for the frontier molecular orbitals (FMOs) of D-Ɛ_n-δ_n-A@Ti_5O_{10} clusters showed that the LUMO energy levels of the target dyes were located in the conduction band of the TiO_2 semiconductor, indicating that these dyes could serve as efficient sensitizers for DSSCs. The HOMO-LUMO transition was the major contributor to the first six vertical excitation states of the dye@Ti_5O_{10} clusters, with a significant bathochromic shift observed for all the investigated systems. Moreover, various global reactivity descriptors (GRDs) were calculated to predict the photovoltaic efficiency of the candidate sensitizers. The results show that the investigated candidate sensitizers exhibit lower chemical hardness values, indicating a higher resistance to the transfer of intermolecular charge and, therefore, excellent conversion energy in DSSCs. Additionally, the D-ε_3-δ_n-A and D-ε_6-δ_n-A series were observed to be more reactive than the other studied molecules. The calculated dihedral angle values demonstrate that the designated candidate sensitizers can potentially eliminate undesirable π-π dye aggregation. The NBO analysis provided detailed information on the charge distribution and delocalization within the dye molecules. As anticipated, the acceptor units of all the investigated systems exhibited the highest negative charges. The obtained values indicate that the series of dyes with the thiophene (δ_1), thieno[3,2-b]thiophene (δ_2) fragments exhibit robust charge separation, suggesting the impact of the electron-withdrawing properties of the δ_1 and δ_2 units, which promote charge separation in the photosensitizer systems. It is worth noting that all candidates

demonstrated better charge separation than the *model dye* molecule. Furthermore, the FMOs were investigated, and it was found that the inclusion of additional π-linker subunits in the D-ε_n-δ_n-A backbone significantly reduces the LUMO energies. Overall, the gathered results provide a deeper understanding of the electronic structure and properties of the molecules under study, thereby shedding light on their potential applications in various chemical reactions.

Declaration of Competing Interest

The authors affirm that they do not have any financial interests or personal relationships that could have influenced the outcome or presentation of the work in this study.

Acknowledgments

The authors would like to express their gratitude to TUBITAK/ULAKBIM (High Performance and Grid Computing Center: TRUBA) for providing the computational resources utilized in this study.

References

[1] S. Collins, G. Bell, Phenotypic consequences of 1,000 generations of selection at elevated CO2 in a green alga, Nature. 431 (2004) 566–569. https://doi.org/10.1038/nature02945.

[2] J. Rogelj, M. den Elzen, N. Höhne, T. Fransen, H. Fekete, H. Winkler, R. Schaeffer, F. Sha, K. Riahi, M. Meinshausen, Paris Agreement climate proposals need a boost to keep warming well below 2 °C, Nature. 534 (2016) 631–639. https://doi.org/10.1038/nature18307.

[3] M. Freitag, J. Teuscher, Y. Saygili, X. Zhang, F. Giordano, P. Liska, J. Hua, S.M. Zakeeruddin, J.-E. Moser, M. Grätzel, A. Hagfeldt, Dye-sensitized solar cells for efficient power generation under ambient lighting, Nat. Photonics. 11 (2017) 372–378. https://doi.org/10.1038/nphoton.2017.60.

[4] H. Zhang, Z.-E. Chen, H.-R. Tian, Molecular engineering of metal-free organic sensitizers with polycyclic benzenoid hydrocarbon donor for DSSC applications: The effect of the conjugate mode, Sol. Energy. 198 (2020) 239–246. https://doi.org/10.1016/j.solener.2020.01.067.

[5] Y. Wu, W. Zhu, Organic sensitizers from D–π–A to D–A–π–A: effect of the internal electron-withdrawing units on molecular absorption, energy levels and photovoltaic performances, Chem. Soc. Rev. 42 (2013) 2039–2058. https://doi.org/10.1039/C2CS35346F.

[6] M.A. Green, Third generation photovoltaics: solar cells for 2020 and beyond, Phys. E Low-Dimensional Syst. Nanostructures. 14 (2002) 65–70. https://doi.org/10.1016/S1386-9477(02)00361-2.

[7] K.L. Chopra, P.D. Paulson, V. Dutta, Thin-film solar cells: an overview, Prog. Photovoltaics Res. Appl. 12 (2004) 69–92. https://doi.org/10.1002/pip.541.

[8] I. Repins, M.A. Contreras, B. Egaas, C. DeHart, J. Scharf, C.L. Perkins, B. To, R. Noufi, 19·9%-efficient ZnO/CdS/CuInGaSe 2 solar cell with 81·2% fill factor, Prog. Photovoltaics Res. Appl. 16 (2008) 235–239. https://doi.org/10.1002/pip.822.

[9] B. O'Regan, M. Grätzel, A low-cost, high-efficiency solar cell based on dye-sensitized colloidal TiO2 films, Nature. 353 (1991) 737–740. https://doi.org/10.1038/353737a0.

[10] N.-G. Park, Perovskite solar cells: an emerging photovoltaic technology, Mater. Today. 18 (2015) 65–72. https://doi.org/10.1016/j.mattod.2014.07.007.

[11] A. Mahmood, Triphenylamine based dyes for dye sensitized solar cells: A review, Sol. Energy. 123 (2016) 127–144. https://doi.org/10.1016/j.solener.2015.11.015.

[12] W. Zhu, Y. Wu, S. Wang, W. Li, X. Li, J. Chen, Z. Wang, H. Tian, Organic D-A-π-A Solar Cell Sensitizers with Improved Stability and Spectral Response, Adv. Funct. Mater. 21 (2011) 756–763. https://doi.org/10.1002/adfm.201001801.

[13] M. Liang, J. Chen, Arylamine organic dyes for dye-sensitized solar cells, Chem. Soc. Rev. 42 (2013) 3453. https://doi.org/10.1039/c3cs35372a.

[14] S. Mathew, A. Yella, P. Gao, R. Humphry-Baker, B.F.E. Curchod, N. Ashari-Astani, I. Tavernelli, U. Rothlisberger, M.K. Nazeeruddin, M. Grätzel, Dye-sensitized solar cells with 13% efficiency achieved through the molecular engineering of porphyrin sensitizers, Nat. Chem. 6 (2014) 242–247. https://doi.org/10.1038/nchem.1861.

[15] W. Ghann, H. Kang, T. Sheikh, S. Yadav, T. Chavez-Gil, F. Nesbitt, J. Uddin, Fabrication, Optimization and Characterization of Natural Dye Sensitized Solar Cell, Sci. Rep. 7 (2017) 41470. https://doi.org/10.1038/srep41470.

[16] J. Gong, S. Krishnan, Mathematical Modeling of Dye-Sensitized Solar Cells, in: Dye. Sol. Cells, Elsevier, 2019: pp. 51–81. https://doi.org/10.1016/B978-0-12-814541-8.00002-1.

[17] A. Carella, F. Borbone, R. Centore, Research Progress on Photosensitizers for DSSC, Front. Chem. 6 (2018). https://doi.org/10.3389/fchem.2018.00481.

[18] R. El-Shishtawy, S. Elroby, A. Asiri, K. Müllen, Optical Absorption Spectra and Electronic Properties of Symmetric and Asymmetric Squaraine Dyes for Use in DSSC Solar Cells: DFT and TD-DFT Studies, Int. J. Mol. Sci. 17 (2016) 487. https://doi.org/10.3390/ijms17040487.

[19] N. Nath Ghosh, A. Chakraborty, S. Pal, A. Pramanik, P. Sarkar, Modulating triphenylamine-based organic dyes for their potential application in dye-sensitized solar cells: a first principle theoretical study, Phys. Chem. Chem. Phys. 16 (2014) 25280–25287. https://doi.org/10.1039/C4CP03621B.

[20] H.G. Yang, C.H. Sun, S.Z. Qiao, J. Zou, G. Liu, S.C. Smith, H.M. Cheng, G.Q. Lu, Anatase TiO2 single crystals with a large percentage of reactive facets, Nature. 453 (2008) 638–641. https://doi.org/10.1038/nature06964.

[21] Z. Xu, S. Gao, X. Lu, Y. Li, Y. Li, S. Wei, Theoretical analysis of the absorption spectrum, electronic structure, excitation, and intramolecular electron transfer of D–A′–π–A porphyrin dyes for dye-sensitized solar cells, Phys. Chem. Chem. Phys. 22 (2020) 14846–14856. https://doi.org/10.1039/D0CP01664K.

[22] S. Shalini, R. Balasundaraprabhu, T.S. Kumar, N. Prabavathy, S. Senthilarasu, S.

Prasanna, Status and outlook of sensitizers/dyes used in dye sensitized solar cells (DSSC): a review, Int. J. Energy Res. 40 (2016) 1303–1320. https://doi.org/10.1002/er.3538.

[23] S. Ganesan, B. Muthuraaman, V. Mathew, J. Madhavan, P. Maruthamuthu, S. Austin Suthanthiraraj, Performance of a new polymer electrolyte incorporated with diphenylamine in nanocrystalline dye-sensitized solar cell, Sol. Energy Mater. Sol. Cells. 92 (2008) 1718–1722. https://doi.org/10.1016/j.solmat.2008.08.004.

[24] Y. Li, X. Li, Y. Xu, Theoretical screening of high-efficiency sensitizers with D-π-A framework for DSSCs by altering promising donor group, Sol. Energy. 196 (2020) 146–156. https://doi.org/10.1016/j.solener.2019.11.092.

[25] S. Agrawal, N.J. English, K.R. Thampi, J.M.D. MacElroy, Perspectives on ab initio molecular simulation of excited-state properties of organic dye molecules in dye-sensitised solar cells, Phys. Chem. Chem. Phys. 14 (2012) 12044. https://doi.org/10.1039/c2cp42031g.

[26] M.P. Balanay, D.H. Kim, DFT/TD-DFT molecular design of porphyrin analogues for use in dye-sensitized solar cells, Phys. Chem. Chem. Phys. 10 (2008) 5121. https://doi.org/10.1039/b806097e.

[27] L. Yu, S. Zhang, M. Zhang, J. Chen, Superhydrophobicity construction with dye-sensitised TiO 2 on fabric surface for both oil/water separation and water bulk contaminants purification, Appl. Surf. Sci. 425 (2017) 46–55. https://doi.org/10.1016/j.apsusc.2017.06.329.

[28] M. Megala, B.J.M. Rajkumar, Theoretical study of anthoxanthin dyes for dye sensitized solar cells (DSSCs), J. Comput. Electron. 15 (2016) 557–568. https://doi.org/10.1007/s10825-016-0791-8.

[29] J.R. Durrant, S.A. Haque, E. Palomares, Towards optimisation of electron transfer processes in dye sensitised solar cells, Coord. Chem. Rev. 248 (2004) 1247–1257. https://doi.org/10.1016/j.ccr.2004.03.014.

[30] A. Remorino, R.M. Hochstrasser, Three-Dimensional Structures by Two-Dimensional Vibrational Spectroscopy, Acc. Chem. Res. 45 (2012) 1896–1905. https://doi.org/10.1021/ar3000025.

[31] S. Sreeja, B. Pesala, Co-sensitization aided efficiency enhancement in betanin–chlorophyll solar cell, Mater. Renew. Sustain. Energy. 7 (2018) 25. https://doi.org/10.1007/s40243-018-0132-x.

[32] V. Madurai Ramakrishnan, S. Pitchaiya, N. Muthukumarasamy, K. Kvamme, G. Rajesh, S. Agilan, A. Pugazhendhi, D. Velauthapillai, Performance of TiO2 nanoparticles synthesized by microwave and solvothermal methods as photoanode in dye-sensitized solar cells (DSSC), Int. J. Hydrogen Energy. 45 (2020) 27036–27046. https://doi.org/10.1016/j.ijhydene.2020.07.018.

[33] R.K. Chava, W.-M. Lee, S.-Y. Oh, K.-U. Jeong, Y.-T. Yu, Improvement in light harvesting and device performance of dye sensitized solar cells using electrophoretic deposited hollow TiO2 NPs scattering layer, Sol. Energy Mater. Sol. Cells. 161 (2017) 255–262. https://doi.org/10.1016/j.solmat.2016.11.037.

[34] M. Azzouzi, T. Kirchartz, J. Nelson, Factors Controlling Open-Circuit Voltage Losses

in Organic Solar Cells, Trends Chem. 1 (2019) 49–62. https://doi.org/10.1016/j.trechm.2019.01.010.

[35] S.A. Haque, S. Handa, K. Peter, E. Palomares, M. Thelakkat, J.R. Durrant, Supermolecular Control of Charge Transfer in Dye-Sensitized Nanocrystalline TiO2 Films: Towards a Quantitative Structure-Function Relationship, Angew. Chemie Int. Ed. 44 (2005) 5740–5744. https://doi.org/10.1002/anie.200500363.

[36] S. Mathew, H. Imahori, Tunable, strongly-donating perylene photosensitizers for dye-sensitized solar cells, J. Mater. Chem. 21 (2011) 7166. https://doi.org/10.1039/c1jm10993f.

[37] H. Feng, R. Li, Y. Song, X. Li, B. Liu, Novel D-π-A-π-A coumarin dyes for highly efficient dye-sensitized solar cells: Effect of π-bridge on optical, electrochemical, and photovoltaic performance, J. Power Sources. 345 (2017) 59–66. https://doi.org/10.1016/j.jpowsour.2017.01.115.

[38] H. Jia, X. Ju, M. Zhang, Z. Ju, H. Zheng, Effects of heterocycles containing different atoms as π-bridges on the performance of dye-sensitized solar cells, Phys. Chem. Chem. Phys. 17 (2015) 16334–16340. https://doi.org/10.1039/C5CP02194D.

[39] F.M. Jradi, X. Kang, D. O'Neil, G. Pajares, Y.A. Getmanenko, P. Szymanski, T.C. Parker, M.A. El-Sayed, S.R. Marder, Near-Infrared Asymmetrical Squaraine Sensitizers for Highly Efficient Dye Sensitized Solar Cells: The Effect of π-Bridges and Anchoring Groups on Solar Cell Performance, Chem. Mater. 27 (2015) 2480–2487. https://doi.org/10.1021/cm5045946.

[40] X. Li, Y. Hu, I. Sanchez-Molina, Y. Zhou, F. Yu, S.A. Haque, W. Wu, J. Hua, H. Tian, N. Robertson, Insight into quinoxaline containing D–π–A dyes for dye-sensitized solar cells with cobalt and iodine based electrolytes: the effect of π-bridge on the HOMO energy level and photovoltaic performance, J. Mater. Chem. A. 3 (2015) 21733–21743. https://doi.org/10.1039/C5TA07254A.

[41] X. Lu, Y. Shao, S. Wei, Z. Zhao, K. Li, C. Guo, W. Wang, M. Zhang, W. Guo, Effect of the functionalized π-bridge on porphyrin sensitizers for dye-sensitized solar cells: an in-depth analysis of electronic structure, spectrum, excitation, and intramolecular electron transfer, J. Mater. Chem. C. 3 (2015) 10129–10139. https://doi.org/10.1039/C5TC02286J.

[42] D.S. Patil, K.C. Avhad, N. Sekar, Linear correlation between DSSC efficiency, intramolecular charge transfer characteristics, and NLO properties – DFT approach, Comput. Theor. Chem. 1138 (2018) 75–83. https://doi.org/10.1016/j.comptc.2018.06.006.

[43] M.J. Frisch, G.W. Trucks, H.B. Schlegel, G.E. Scuseria, M.A. Robb, J.R. Cheeseman, G. Scalmani, V. Barone, B. Mennucci, G.A. Petersson, H. Nakatsuji, M. Caricato, X. Li, H.P. Hratchian, A.F. Izmaylov, J. Bloino, G. Zheng, J.L. Sonnenberg, M. Hada, M. Ehara, K. Toyota, R. Fukuda, J. Hasegawa, M. Ishida, T. Nakajima, Y. Honda, O. Kitao, H. Nakai, T. Vreven, J.A. Montgomery Jr., J.E. Peralta, F. Ogliaro, M. Bearpark, J.J. Heyd, E. Brothers, K.N. Kudin, V.N. Staroverov, R. Kobayashi, J. Normand, K. Raghavachari, A. Rendell, J.C. Burant, S.S. Iyengar, J. Tomasi, M. Cossi, N. Rega, J.M. Millam, M. Klene, J.E. Knox, J.B. Cross, V. Bakken, C. Adamo, J. Jaramillo, R. Gomperts, R.E. Stratmann, O. Yazyev, A.J. Austin, R. Cammi, C. Pomelli, J.W. Ochterski, R.L. Martin, K. Morokuma, V.G. Zakrzewski, G.A. Voth, P. Salvador, J.J.

Dannenberg, S. Dapprich, A.D. Daniels, Ö. Farkas, J.B. Foresman, J. V Ortiz, J. Cioslowski, D.J. Fox, Gaussian09 Revision D.01, Gaussian Inc. Wallingford CT, Gaussian 09 Revis. C.01. (2010).

[44] J.A.P. M.J. Frisch, G.W. Trucks, H.B. Schlegel, G.E. Scuseria, M.A. Robb, J.R. Cheeseman, J.A.Montgomery, T. Vreven, K.N. Kudin, J.C. Burant, J.M. Millam, S.S. Iyengar, J. Tomasi, V. Barone, B. Mennucci, M. Cossi, G. Scalmani, N. Rega, G.A. Petersson, H.Nakatsuj, GaussView 5, Semichem Inc. , Shawnee Mission. KS. (2009).

[45] A. Fitri, A.T. Benjelloun, M. Benzakour, M. Mcharfi, M. Hamidi, M. Bouachrine, Theoretical investigation of new thiazolothiazole-based D-π-A organic dyes for efficient dye-sensitized solar cell, Spectrochim. Acta Part A Mol. Biomol. Spectrosc. 124 (2014) 646–654. https://doi.org/10.1016/j.saa.2014.01.052.

[46] S. El Mzioui, S.M. Bouzzine, İ. Sidir, M. Bouachrine, M.N. Bennani, M. Bourass, M. Hamidi, Theoretical investigation on π-spacer effect of the D–π–A organic dyes for dye-sensitized solar cell applications: a DFT and TD-BHandH study, J. Mol. Model. 25 (2019) 92. https://doi.org/10.1007/s00894-019-3963-1.

[47] M. Lazrak, H. Toufik, S. Ennehary, S.M. Bouzzine, F. Lamchouri, Effect of Exchange–correlation Functionals on Ground State Geometries, Optoelectronic and Charge Transfer of Triphenylamine-based Dyes, Orbital Electron. J. Chem. 14 (2022). https://doi.org/10.17807/orbital.v14i1.1682.

[48] R. Soto-Rojo, J. Baldenebro-López, D. Glossman-Mitnik, Study of chemical reactivity in relation to experimental parameters of efficiency in coumarin derivatives for dye sensitized solar cells using DFT, Phys. Chem. Chem. Phys. 17 (2015) 14122–14129. https://doi.org/10.1039/C5CP01387A.

[49] Q. Alkhatib, W. Helal, A.T. Afaneh, Assessment of time-dependent density functionals for the electronic excitation energies of organic dyes used in DSSCs, New J. Chem. 46 (2022) 7682–7694. https://doi.org/10.1039/D2NJ00210H.

[50] H. Bouaamlat, T. Abram, M. Bouachrine, M. Abarkan, Organic dyes based on selenophene for efficient dye-sensitized solar cell, J. Mol. Model. 27 (2021) 333. https://doi.org/10.1007/s00894-021-04953-4.

[51] T. Delgado-Montiel, J. Baldenebro-López, R. Soto-Rojo, D. Glossman-Mitnik, Quantum chemical study of the effect of π-bridge on the optical and electronic properties of sensitizers for DSSCs incorporating dioxythiophene and thiophene units, Theor. Chem. Acc. 135 (2016) 235. https://doi.org/10.1007/s00214-016-1989-3.

[52] Z.M.E. Fahim, S.M. Bouzzine, A.A. Youssef, M. Bouachrine, M. Hamidi, Ground state geometries, UV/vis absorption spectra and charge transfer properties of triphenylamine-thiophenes based dyes for DSSCs: A TD-DFT benchmark study, Comput. Theor. Chem. 1125 (2018) 39–48. https://doi.org/10.1016/j.comptc.2018.01.002.

[53] T. Delgado-Montiel, J. Baldenebro-López, R. Soto-Rojo, D. Glossman-Mitnik, Theoretical Study of the Effect of π-Bridge on Optical and Electronic Properties of Carbazole-Based Sensitizers for DSSCs, Molecules. 25 (2020) 3670. https://doi.org/10.3390/molecules25163670.

[54] T. Lu, F. Chen, Multiwfn: A multifunctional wavefunction analyzer, J. Comput. Chem. 33 (2012) 580–592. https://doi.org/10.1002/jcc.22885.

[55] F. Amerikheirabadi, C. Diaz, N. Mohan, R.R. Zope, T. Baruah, A DFT analysis of the ground and charge-transfer excited states of Sc 3 N@I h –C 80 fullerene coupled with metal-free and zinc-phthalocyanine, Phys. Chem. Chem. Phys. 20 (2018) 25841–25848. https://doi.org/10.1039/C8CP03849J.

[56] L.-C.C. Coetzee, A.S. Adeyinka, N. Magwa, A Theoretical Evaluation of the Efficiencies of Metal-Free 1,3,4-Oxadiazole Dye-Sensitized Solar Cells: Insights from Electron–Hole Separation Distance Analysis, Energies. 15 (2022) 4913. https://doi.org/10.3390/en15134913.

[57] N.M. O'boyle, A.L. Tenderholt, K.M. Langner, cclib: A library for package-independent computational chemistry algorithms, J. Comput. Chem. 29 (2008) 839–845. https://doi.org/10.1002/jcc.20823.

[58] F. Xu, T.T. Testoff, L. Wang, X. Zhou, Cause, Regulation and Utilization of Dye Aggregation in Dye-Sensitized Solar Cells, Molecules. 25 (2020) 4478. https://doi.org/10.3390/molecules25194478.

[59] P. Li, Z. Wang, C. Song, H. Zhang, Rigid fused π-spacers in D–π–A type molecules for dye-sensitized solar cells: a computational investigation, J. Mater. Chem. C. 5 (2017) 11454–11465. https://doi.org/10.1039/C7TC03112B.

[60] R.M. El-Shishtawy, A.M. Asiri, S.G. Aziz, S.A.K. Elroby, Molecular design of donor-acceptor dyes for efficient dye-sensitized solar cells I: a DFT study, J. Mol. Model. 20 (2014) 2241. https://doi.org/10.1007/s00894-014-2241-5.

[61] T.-H. Wang, C.-H. Hsiao, S.-H. Chen, C.-M. Hsiao, L.-Y. Chen, G.-M. Li, B.-C. Hsueh, A DFT study on structures, frontier molecular orbitals and UV–vis spectra of [M(L)(N3)(C7H5N)(PPh3)] (M= Ru and Fe; L= Tp and Cp), J. Organomet. Chem. 791 (2015) 72–81. https://doi.org/10.1016/j.jorganchem.2015.05.014.

[62] A. Iwaszuk, P.A. Mulheran, M. Nolan, TiO2 nanocluster modified-rutile TiO2 photocatalyst: a first principles investigation, J. Mater. Chem. A. 1 (2013) 2515. https://doi.org/10.1039/c2ta01582j.

SUPPORTING INFORMATION

Computational Insights into bis-N,N-dimethylaniline based D-π-A Photosensitizers Bearing Divergent-Type of π-Linkers for DSSCs

Harun NALÇAKAN[1], Gülbin KURTAY[2,*], Kübra SARIKAVAK[2], Nilgün ŞEN[3,4], Fatma SEVİN[2]

[1]Department of Chemistry, Faculty of Science, Ankara University, 06100, Ankara, Turkey

[2]Department of Chemistry, Faculty of Science, Hacettepe University, 06800, Ankara, Turkey

[3]Turkish National Police Academy, Institute of Forensic Sciences, 06580, Ankara, Turkey

[4]Centre for Defence Chemistry, Cranfield University, Shrivenham, SN6 8LA, United Kingdom

corresponding author: gulbinkurtay@hacettepe.edu.tr

Table of Contents

Table S1. Optimized geometries and localized-orbital locator (LOL) plots of investigated photosensitizers [M06-2X/6-31G(d,p) solvent model: CPCM, $\varepsilon_{ethanol}$ =24.55]. 6

Table S1 (*cont.*). Optimized geometries and localized-orbital locator (LOL) plots of investigated photosensitizers [M06-2X/6-31G(d,p) solvent model: CPCM, $\varepsilon_{ethanol}$ =24.55]. 7

Table S1 (*cont.*). Optimized geometries and localized-orbital locator (LOL) plots of investigated photosensitizers [M06-2X/6-31G(d,p) solvent model: CPCM, $\varepsilon_{ethanol}$ =24.55]. 8

Table S1 (*cont.*). Optimized geometries and localized-orbital locator (LOL) plots of investigated photosensitizers [M06-2X/6-31G(d,p) solvent model: CPCM, $\varepsilon_{ethanol}$ =24.55]. 9

Table S1 (*cont.*). Optimized geometries and localized-orbital locator (LOL) plots of investigated photosensitizers [M06-2X/6-31G(d,p) solvent model: CPCM, $\varepsilon_{ethanol}$ =24.55]. 10

Table S1 (*cont.*). Optimized geometries and localized-orbital locator (LOL) plots of investigated photosensitizers [M06-2X/6-31G(d,p) solvent model: CPCM, $\varepsilon_{ethanol}$ =24.55]. 11

Table S1 (*cont.*). Optimized geometries and localized-orbital locator (LOL) plots of investigated photosensitizers [M06-2X/6-31G(d,p) solvent model: CPCM, $\varepsilon_{ethanol}$ =24.55]. 12

Table S2. Selected bond lengths (d_n, Å), bond angle (θ_n, °), and dihedral angle (ω_n, °) values [M06-2X/6-31G(d,p) solvent model: CPCM, $\varepsilon_{ethanol}$ =24.55]. 13

Table S3. Computed dipole moment values of investigated sensitizers (in Debye, D) [M06-2X/6-31G(d,p) solvent model: CPCM, $\varepsilon_{ethanol}$ =24.55]..... 14

S1. Chemical hardness (η), hyper-hardness (Γ), chemical potential (μ), electronegativity (χ), electrophilicity index (ω), electron-accepting power (ω^+), and electron-donating power (ω^-)..... 15

Table S4. Calculated values of global descriptors (all values are in eV) [M06-2X/6-31G(d,p) solvent model: CPCM, $\varepsilon_{ethanol}$ =24.55]. 18

Figure S1. Diagram of the frontier orbital energy levels (from the LUMO+4 to HOMO-4) 19

Table S5. Frontier orbitals' contour plots of the investigated dye molecules. The threshold of contours is ±0.02 au [M06-2X/6-31G(d,p) solvent model: CPCM, $\varepsilon_{ethanol}$ =24.55]. 20

Table S5 (*cont.*). Frontier orbitals' contour plots of the investigated dye molecules. The threshold of contours is ±0.02 au [M06-2X/6-31G(d,p) solvent model: CPCM, $\varepsilon_{ethanol}$ =24.55]. 21

Table S5 (*cont.*). Frontier orbitals' contour plots of the investigated dye molecules. The threshold of contours is ±0.02 au [M06-2X/6-31G(d,p) solvent model: CPCM, $\varepsilon_{ethanol}$ =24.55]. 22

Table S5 (*cont.*). Frontier orbitals' contour plots of the investigated dye molecules. The threshold of contours is ±0.02 au [M06-2X/6-31G(d,p) solvent model: CPCM, $\varepsilon_{ethanol}$ =24.55]. 23

Table S5 (*cont.*). Frontier orbitals' contour plots of the investigated dye molecules. The threshold of contours is ±0.02 au [M06-2X/6-31G(d,p) solvent model: CPCM, $\varepsilon_{ethanol}$ =24.55]. 24

Table S5 (*cont.*). Frontier orbitals' contour plots of the investigated dye molecules. The threshold of contours is ±0.02 au [M06-2X/6-31G(d,p) solvent model: CPCM, $\varepsilon_{ethanol}$ =24.55]. 25

Table S5 (*cont.*). Frontier orbitals' contour plots of the investigated dye molecules. The threshold of contours is ±0.02 au [M06-2X/6-31G(d,p) solvent model: CPCM, $\varepsilon_{ethanol}$ =24.55]. 26

Table S6. DFT-calculated IP and EA values *via* Koopman's theorem *or* delta-SCF method [M06-2X//6-31G(d,p) solvent model: CPCM, $\varepsilon_{ethanol}$ = 24.55]. 27

S2. Electrostatic potential (ESP) map 28

S3. Dipole Moment (μ) 28

Table S7 (*cont.*). Electrostatic potential (ESP) map representing the corresponding charge density distributions isodensity (0.001e/Bohr^3) and calculated dipole moment vector [M06-2X/6-31G(d,p) solvent model: CPCM, $\varepsilon_{ethanol}$ =24.55]. 30

Table S7 (*cont.*). Electrostatic potential (ESP) map representing the corresponding charge density distributions isodensity (0.001e/Bohr^3) and calculated dipole moment vector [M06-2X/6-31G(d,p) solvent model: CPCM, $\varepsilon_{ethanol}$ =24.55]. 31

S4. Natural bond orbital (NBO) analysis 32

Table S8. Absorption wavelengths (λ, nm) oscillator strengths (*f*), and the orbitals of the investigated molecules involved in the transitions [M06-2x/6-31G(d,p) solvent model: CPCM, $\varepsilon_{ethanol}$ = 24.55]. 33

Table S8 (*cont.*). Absorption wavelengths (λ, nm) oscillator strengths (*f*), and the orbitals of the investigated molecules involved in the transitions [M06-2x/6-31G(d,p) solvent model: CPCM, $\varepsilon_{ethanol}$ = 24.55]..... 34

Table S9. (a) PDOS plots for the studied photosensitizers (b) Density of state (DOS) plots and bandgap values. [M06-2x/6-31G(d,p) solvent model: CPCM, $\varepsilon_{ethanol}$ = 24.55]. 35

Table S9 (*cont.*). (a) PDOS plots for the studied photosensitizers (b) Density of state (DOS) plots and bandgap values. [M06-2x/6-31G(d,p) solvent model: CPCM, $\varepsilon_{ethanol}$ = 24.55]. 36

Table S9 (*cont.*). (a) PDOS plots for the studied photosensitizers (b) Density of state (DOS) plots and bandgap values. [M06-2x/6-31G(d,p) solvent model: CPCM, $\varepsilon_{ethanol}$ = 24.55]. 37

Table S9 (*cont.*). (a) PDOS plots for the studied photosensitizers (b) Density of state (DOS) plots and bandgap values. [M06-2x/6-31G(d,p) solvent model: CPCM, $\varepsilon_{ethanol}$ = 24.55]. 38

Table S9 (*cont.*). (a) PDOS plots for the studied photosensitizers (b) Density of state (DOS) plots and bandgap values. [M06-2x/6-31G(d,p) solvent model: CPCM, $\varepsilon_{ethanol}$ = 24.55]. 39

Table S9 (*cont.*). (a) PDOS plots for the studied photosensitizers (b) Density of state (DOS) plots and bandgap values. [M06-2x/6-31G(d,p) solvent model: CPCM, $\varepsilon_{ethanol}$ = 24.55]. 40

Table S9 (*cont.*). (a) PDOS plots for the studied photosensitizers (b) Density of state (DOS) plots and bandgap values. [M06-2x/6-31G(d,p) solvent model: CPCM, $\varepsilon_{ethanol}$ = 24.55]. 41

Table S10. Electron density differentiation maps (EDDMs) and the corresponding percent contributions of the different fragments on the investigated systems [M06-2x/6-31G(d,p) solvent model: CPCM, $\varepsilon_{ethanol}$ = 24.55]..... 42

Table S10 (*cont.*). Electron density differentiation maps (EDDMs) and the corresponding percent contributions of the different fragments on the investigated systems [M06-2x/6-31G(d,p) solvent model: CPCM, $\varepsilon_{ethanol}$ = 24.55]..... 43

Table S10 (*cont.*). Electron density differentiation maps (EDDMs) and the corresponding percent contributions of the different fragments on the investigated systems [M06-2x/6-31G(d,p) solvent model: CPCM, $\varepsilon_{ethanol}$ = 24.55]..... 44

Table S11. Atom- and fragment-based electron-hole analysis of the investigated systems [M06-2x/6-31G(d,p) solvent model: CPCM, $\varepsilon_{ethanol}$ = 24.55]..... 45

Table S12. Atom- and fragment-based electron-hole analysis of the investigated systems [M06-2x/6-31G(d,p) solvent model: CPCM, $\varepsilon_{ethanol}$ = 24.55]..... 46

Table S12 (*cont.*). Atom- and fragment-based electron-hole analysis of the investigated systems [M06-2x/6-31G(d,p) solvent model: CPCM, $\varepsilon_{ethanol}$ = 24.55]. 47

Table S12 (*cont.*). Atom- and fragment-based electron-hole analysis of the investigated systems [M06-2x/6-31G(d,p) solvent model: CPCM, $\varepsilon_{ethanol}$ = 24.55]. 48

Table S12 (*cont.*). Atom- and fragment-based electron-hole analysis of the investigated systems [M06-2x/6-31G(d,p) solvent model: CPCM, $\varepsilon_{ethanol}$ = 24.55]. 49

Table S12 (*cont.*). Atom- and fragment-based electron-hole analysis of the investigated systems [M06-2x/6-31G(d,p) solvent model: CPCM, $\varepsilon_{ethanol}$ = 24.55]. 50

Table S12 (*cont.*). Atom- and fragment-based electron-hole analysis of the investigated systems [M06-2x/6-31G(d,p) solvent model: CPCM, $\varepsilon_{ethanol}$ = 24.55]. 51

Table S12 (*cont.*). Atom- and fragment-based electron-hole analysis of the investigated systems [M06-2x/6-31G(d,p) solvent model: CPCM, $\varepsilon_{ethanol}$ = 24.55]. 52

Table S12 (*cont.*). Atom- and fragment-based electron-hole analysis of the investigated systems [M06-2x/6-31G(d,p) solvent model: CPCM, $\varepsilon_{ethanol}$ = 24.55]. 53

Table S12 (*cont.*). Atom- and fragment-based electron-hole analysis of the investigated systems [M06-2x/6-31G(d,p) solvent model: CPCM, $\varepsilon_{ethanol}$ = 24.55]. 54

Table S12 (*cont.*). Atom- and fragment-based electron-hole analysis of the investigated systems [M06-2x/6-31G(d,p) solvent model: CPCM, $\varepsilon_{ethanol}$ = 24.55]. 55

Table S12 (*cont.*). Atom- and fragment-based electron-hole analysis of the investigated systems [M06-2x/6-31G(d,p) solvent model: CPCM, $\varepsilon_{ethanol}$ = 24.55]. 56

Table S12 (*cont.*). Atom- and fragment-based electron-hole analysis of the investigated systems [M06-2x/6-31G(d,p) solvent model: CPCM, $\varepsilon_{ethanol}$ = 24.55]. 57

Table S12 (*cont.*). Atom- and fragment-based electron-hole analysis of the investigated systems [M06-2x/6-31G(d,p) solvent model: CPCM, $\varepsilon_{ethanol}$ = 24.55]. 58

Table S12 (*cont.*). Atom- and fragment-based electron-hole analysis of the investigated systems [M06-2x/6-31G(d,p) solvent model: CPCM, $\varepsilon_{ethanol}$ = 24.55]. 59

Table S12 (*cont.*). Atom- and fragment-based electron-hole analysis of the investigated systems [M06-2x/6-31G(d,p) solvent model: CPCM, $\varepsilon_{ethanol}$ = 24.55]. 60

Table S12 (*cont.*). Atom- and fragment-based electron-hole analysis of the investigated systems [M06-2x/6-31G(d,p) solvent model: CPCM, $\varepsilon_{ethanol}$ = 24.55]. 61

Table S12 (*cont.*). Atom- and fragment-based electron-hole analysis of the investigated systems [M06-2x/6-31G(d,p) solvent model: CPCM, $\varepsilon_{ethanol}$ = 24.55]. 62

Table S12 (*cont.*). Atom- and fragment-based electron-hole analysis of the investigated systems [M06-2x/6-31G(d,p) solvent model: CPCM, $\varepsilon_{ethanol}$ = 24.55]. 63

Table S12 (*cont.*). Atom- and fragment-based electron-hole analysis of the investigated systems [M06-2x/6-31G(d,p) solvent model: CPCM, $\varepsilon_{ethanol}$ = 24.55]. 64

Table S12 (*cont.*). Atom- and fragment-based electron-hole analysis of the investigated systems [M06-2x/6-31G(d,p) solvent model: CPCM, $\varepsilon_{ethanol}$ = 24.55]. 65

Table S12 (*cont.*). Atom- and fragment-based electron-hole analysis of the investigated systems [M06-2x/6-31G(d,p) solvent model: CPCM, $\varepsilon_{ethanol}$ = 24.55]. 66

Table S13. Atom- and fragment-based transition density and color correlation matrix (where the y-axis is the originating, and the x-axis is the receiving fragment for the excited electron) of the investigated systems [M06-2x/6-31G(d,p) solvent model: CPCM, $\varepsilon_{ethanol}$ = 24.55]. 67

Table S13 (*cont.*). Atom- and fragment-based transition density and color correlation matrix (where the y-axis is the originating, and the x-axis is the receiving fragment for the excited electron) of the investigated systems [M06-2x/6-31G(d,p) solvent model: CPCM, $\varepsilon_{ethanol}$ = 24.55]. 68

Table S13 (*cont.*). Atom- and fragment-based transition density and color correlation matrix (where the y-axis is the originating, and the x-axis is the receiving fragment for the excited electron) of the investigated systems [M06-2x/6-31G(d,p) solvent model: CPCM, $\varepsilon_{ethanol}$ = 24.55]. 69

Table S13 (*cont.*). Atom- and fragment-based transition density and color correlation matrix (where the y-axis is the originating, and the x-axis is the receiving fragment for the excited electron) of the investigated systems [M06-2x/6-31G(d,p) solvent model: CPCM, $\varepsilon_{ethanol}$ = 24.55]. 70

Table S13 (*cont.*). Atom- and fragment-based transition density and color correlation matrix (where the y-axis is the originating, and the x-axis is the receiving fragment for the excited electron) of the investigated systems [M06-2x/6-31G(d,p) solvent model: CPCM, $\varepsilon_{ethanol}$ = 24.55]. 71

Table S13 (*cont.*). Atom- and fragment-based transition density and color correlation matrix (where the y-axis is the originating, and the x-axis is the receiving fragment for the excited electron) of the investigated systems [M06-2x/6-31G(d,p) solvent model: CPCM, $\varepsilon_{ethanol}$ = 24.55]. 72

Table S13 (*cont.*). Atom- and fragment-based transition density and color correlation matrix (where the y-axis is the originating, and the x-axis is the receiving fragment for the excited electron) of the investigated systems [M06-2x/6-31G(d,p) solvent model: CPCM, $\varepsilon_{ethanol}$ = 24.55]. 73

Table SC-1. Optimized Cartesian Coordinates of the D-δ_1-A | [M06-2X/6-31G(d,p) solvent model: CPCM, $\varepsilon_{ethanol}$ =24.55]. 74

Table SC-2. Optimized Cartesian Coordinates of the D-ε_1-δ_1-A | [M06-2X/6-31G(d,p) solvent model: CPCM, $\varepsilon_{ethanol}$ =24.55]. 75

Table SC-3. Optimized Cartesian Coordinates of the D-ε_2-δ_1-A | [M06-2X/6-31G(d,p) solvent model: CPCM, $\varepsilon_{ethanol}$ =24.55]. 76

Table SC-4. Optimized Cartesian Coordinates of the D-ε_3-δ_1-A | [M06-2X/6-31G(d,p) solvent model: CPCM, $\varepsilon_{ethanol}$ =24.55]. 77

Table SC-5. Optimized Cartesian Coordinates of the D-ε_4-δ_1-A | [M06-2X/6-31G(d,p) solvent model: CPCM, $\varepsilon_{ethanol}$ =24.55]. 78

Table SC-6. Optimized Cartesian Coordinates of the D-ε_5-δ_1-A | [M06-2X/6-31G(d,p) solvent model: CPCM, $\varepsilon_{ethanol}$ =24.55]. 79

Table SC-7. Optimized Cartesian Coordinates of the D-ε_6-δ_1-A | [M06-2X/6-31G(d,p) solvent model: CPCM, $\varepsilon_{ethanol}$ =24.55]. 80

Table SC-8. Optimized Cartesian Coordinates of the D-δ_2-A | [M06-2X/6-31G(d,p) solvent model: CPCM, $\varepsilon_{ethanol}$ =24.55]. 81

Table SC-9. Optimized Cartesian Coordinates of the D-ε_1-δ_2-A | [M06-2X/6-31G(d,p) solvent model: CPCM, $\varepsilon_{ethanol}$ =24.55]. 82

Table SC-10. Optimized Cartesian Coordinates of the D-ε_2-δ_2-A | [M06-2X/6-31G(d,p) solvent model: CPCM, $\varepsilon_{ethanol}$ =24.55]. 83

Table SC-11. Optimized Cartesian Coordinates of the D-ε_3-δ_2-A | [M06-2X/6-31G(d,p) solvent model: CPCM, $\varepsilon_{ethanol}$ =24.55]. 84

Table SC-12. Optimized Cartesian Coordinates of the D-ε_4-δ_2-A | [M06-2X/6-31G(d,p) solvent model: CPCM, $\varepsilon_{ethanol}$ =24.55]. 85

Table SC-13. Optimized Cartesian Coordinates of the D-ε_5-δ_2-A | [M06-2X/6-31G(d,p) solvent model: CPCM, $\varepsilon_{ethanol}$ =24.55]. 86

Table SC-14. Optimized Cartesian Coordinates of the D-ε_6-δ_2-A | [M06-2X/6-31G(d,p) solvent model: CPCM, $\varepsilon_{ethanol}$ =24.55]. 87

Table SC-15. Optimized Cartesian Coordinates of the D-δ_3-A | [M06-2X/6-31G(d,p) solvent model: CPCM, $\varepsilon_{ethanol}$ =24.55]. 88

Table SC-16. Optimized Cartesian Coordinates of the D-ε_1-δ_3-A | [M06-2X/6-31G(d,p) solvent model: CPCM, $\varepsilon_{ethanol}$ =24.55]. 89

Table SC-17. Optimized Cartesian Coordinates of the D-ε_2-δ_3-A | [M06-2X/6-31G(d,p) solvent model: CPCM, $\varepsilon_{ethanol}$ =24.55]. 90

Table SC-18. Optimized Cartesian Coordinates of the D-ε_3-δ_3-A | [M06-2X/6-31G(d,p) solvent model: CPCM, $\varepsilon_{ethanol}$ =24.55]. 91

Table SC-19. Optimized Cartesian Coordinates of the D-ε_4-δ_3-A | [M06-2X/6-31G(d,p) solvent model: CPCM, $\varepsilon_{ethanol}$ =24.55]. 92

Table SC-20. Optimized Cartesian Coordinates of the D-ε_5-δ_3-A | [M06-2X/6-31G(d,p) solvent model: CPCM, $\varepsilon_{ethanol}$ =24.55]. 93

Table SC-21. Optimized Cartesian Coordinates of the D-ε_6-δ_3-A | [M06-2X/6-31G(d,p) solvent model: CPCM, $\varepsilon_{ethanol}$ =24.55]. 94

Table SC-22. Optimized Cartesian Coordinates of the D-δ_1-A@Ti_5O_{10}| [M06-2X/6-31G(d,p) solvent model: CPCM, $\varepsilon_{ethanol}$ =24.55]. 95

Table SC-23. Optimized Cartesian Coordinates of the D-ε_3-δ_1-A@Ti_5O_{10}| [M06-2X/6-31G(d,p) solvent model: CPCM, $\varepsilon_{ethanol}$ =24.55]. 96

Table SC-24. Optimized Cartesian Coordinates of the D-ε_3-δ_2-A@Ti_5O_{10}| [M06-2X/6-31G(d,p) solvent model: CPCM, $\varepsilon_{ethanol}$ =24.55]. 97

Table SC-25. Optimized Cartesian Coordinates of the D-ε_3-δ_3-A@Ti_5O_{10}| [M06-2X/6-31G(d,p) solvent model: CPCM, $\varepsilon_{ethanol}$ =24.55]. 98

Table SC-26. Optimized Cartesian Coordinates of the D-ε_6-δ_1-A@Ti_5O_{10}| [M06-2X/6-31G(d,p) solvent model: CPCM, $\varepsilon_{ethanol}$ =24.55]. 99

Table SC-26 (*cont*). Optimized Cartesian Coordinates of the D-ε_6-δ_1-A@Ti_5O_{10}| [M06-2X/6-31G(d,p) solvent model: CPCM, $\varepsilon_{ethanol}$ =24.55]. 100

Table SC-27. Optimized Cartesian Coordinates of the D-ε_6-δ_2-A@Ti_5O_{10}| [M06-2X/6-31G(d,p) solvent model: CPCM, $\varepsilon_{ethanol}$ =24.55]. 101

Table SC-27 (*cont*). Optimized Cartesian Coordinates of the D-ε_6-δ_2-A@Ti_5O_{10}| [M06-2X/6-31G(d,p) solvent model: CPCM, $\varepsilon_{ethanol}$ =24.55]. 102

Table SC-28. Optimized Cartesian Coordinates of the D-ε_6-δ_3-A@Ti_5O_{10}| [M06-2X/6-31G(d,p) solvent model: CPCM, $\varepsilon_{ethanol}$ =24.55]. 103

Table SC-28 (*cont*). Optimized Cartesian Coordinates of the D-ε_6-δ_3-A@Ti_5O_{10}| [M06-2X/6-31G(d,p) solvent model: CPCM, $\varepsilon_{ethanol}$ =24.55]. 104

Table S1. Optimized geometries and localized-orbital locator (LOL) plots of investigated photosensitizers [M06-2X/6-31G(d,p) solvent model: CPCM, $\varepsilon_{ethanol}$ =24.55].

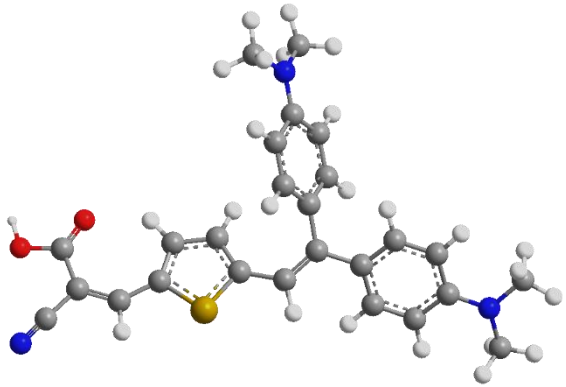
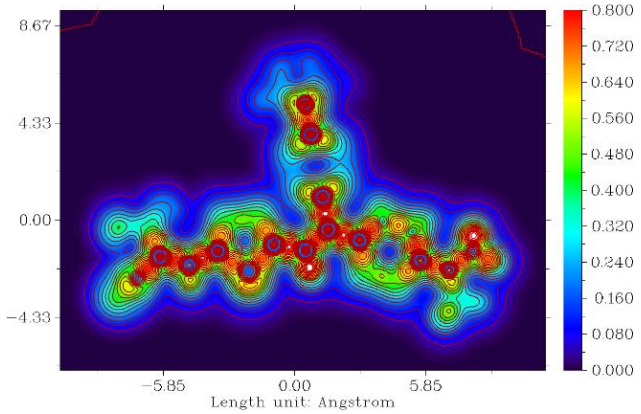
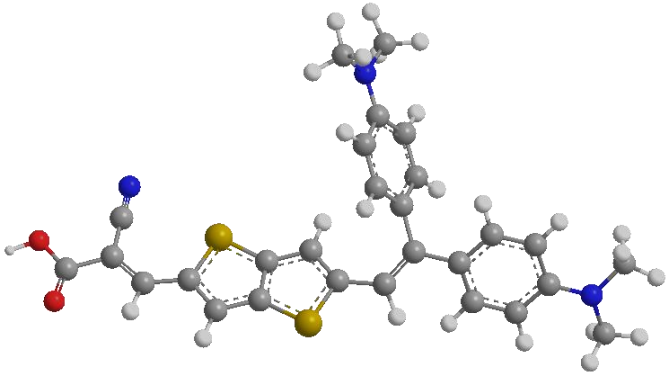
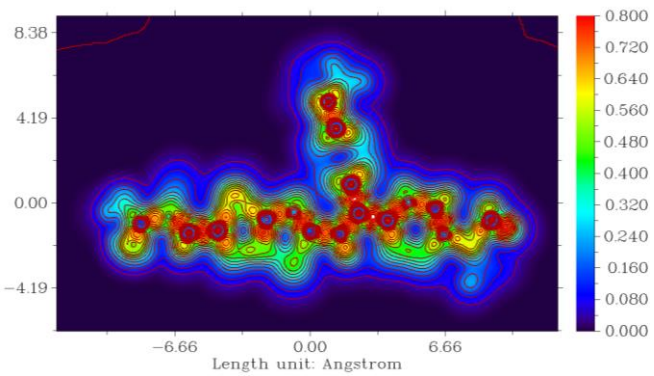
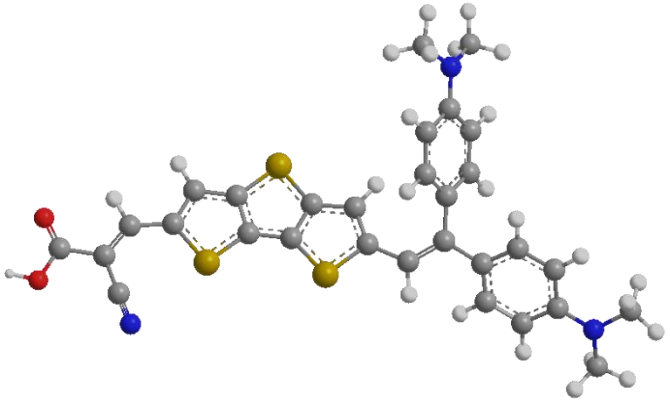
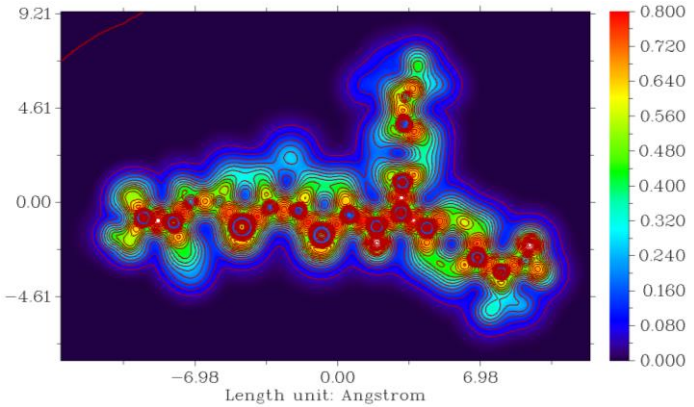
ENTRY	OPTIMIZED GEOMETRY	LOL
D-δ_1-A		
D-δ_2-A		
D-δ_3-A		

Table S1 (*cont.*). Optimized geometries and localized-orbital locator (LOL) plots of investigated photosensitizers [M06-2X/6-31G(d,p) solvent model: CPCM, $\varepsilon_{ethanol}$ =24.55].

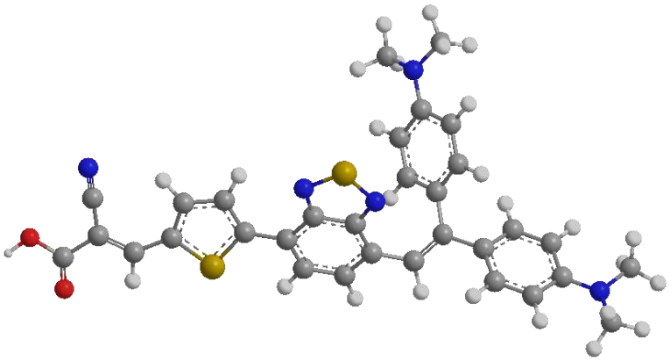
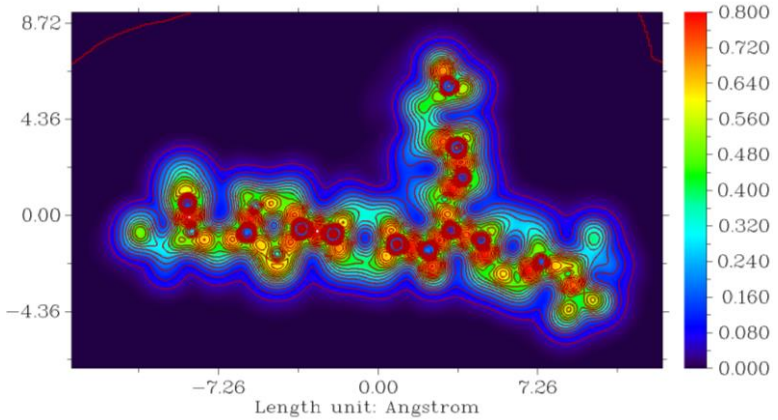
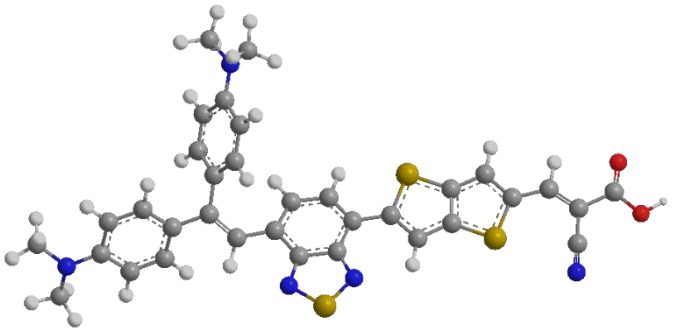
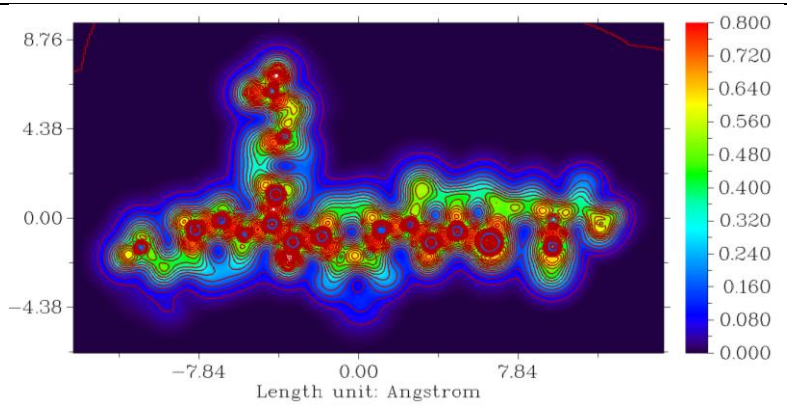
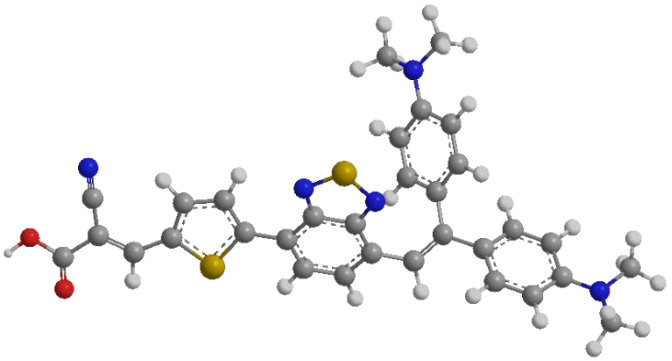
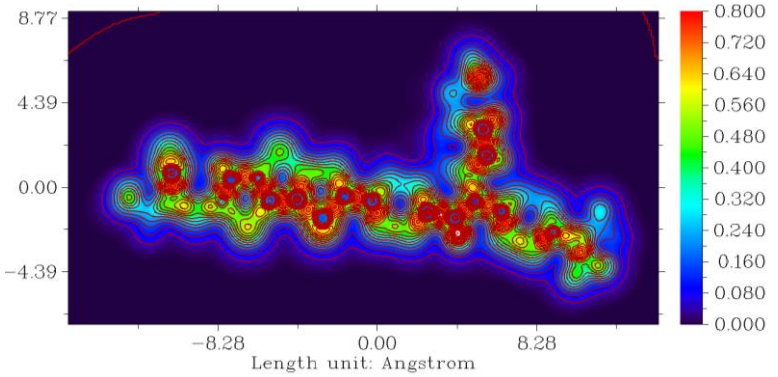
ENTRY	OPTIMIZED GEOMETRY	LOL
D-ε_1-δ_1-A		
D-ε_1-δ_2-A		
D-ε_1-δ_3-A		

Table S1 (*cont.*). Optimized geometries and localized-orbital locator (LOL) plots of investigated photosensitizers [M06-2X/6-31G(d,p) solvent model: CPCM, $\varepsilon_{ethanol}$ =24.55].

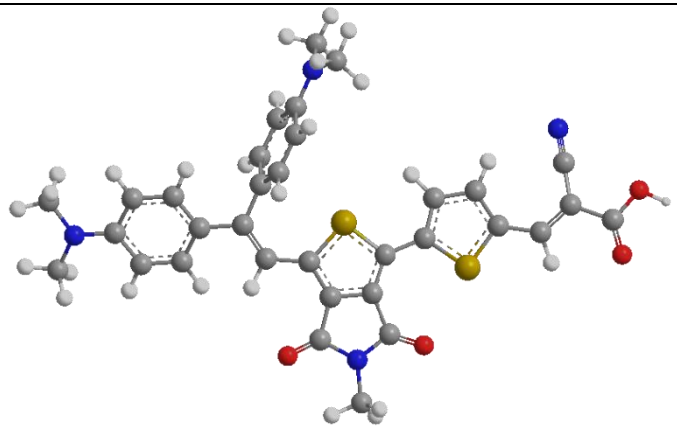
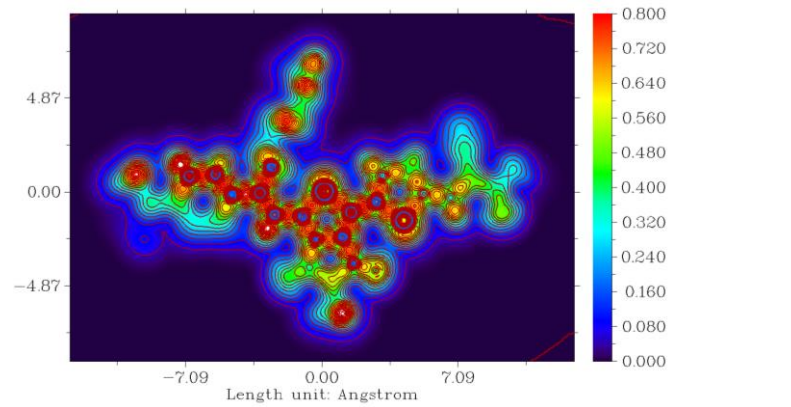
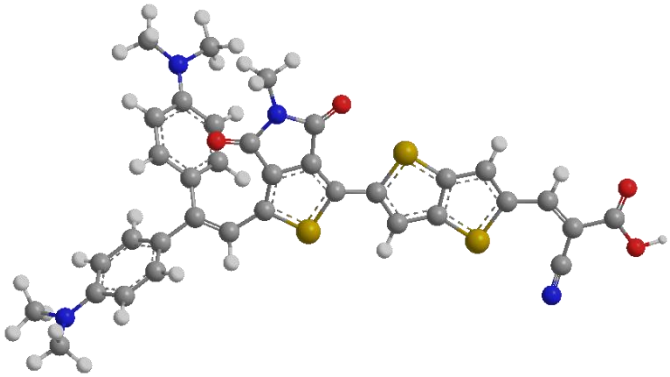
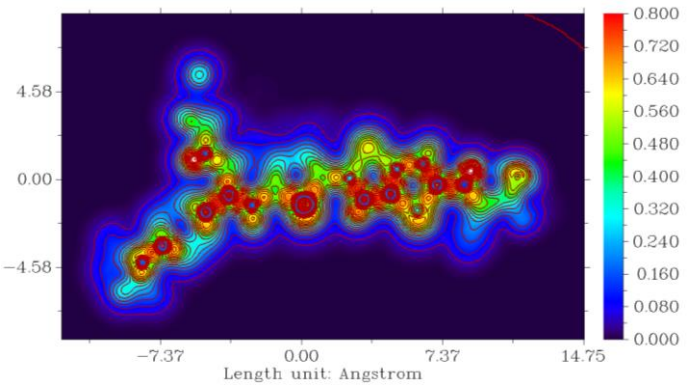
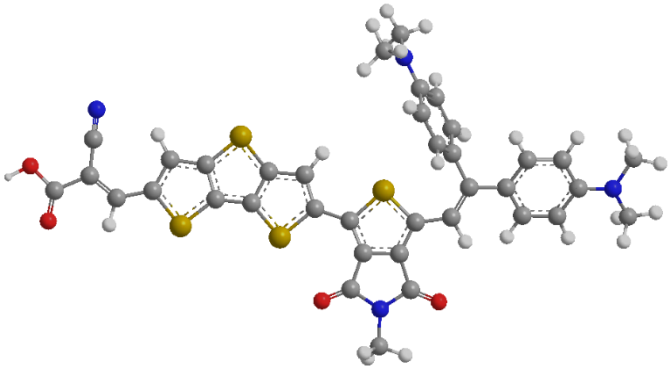
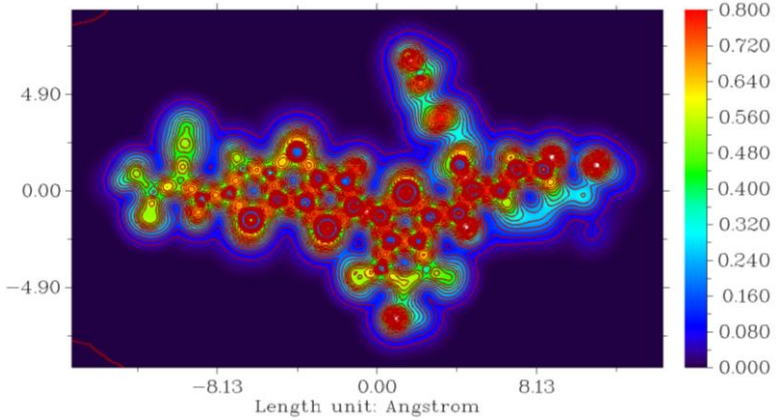
ENTRY	OPTIMIZED GEOMETRY	LOL
D-ε_2-δ_1-A		
D-ε_2-δ_2-A		
D-ε_2-δ_3-A		

Table S1 (*cont.*). Optimized geometries and localized-orbital locator (LOL) plots of investigated photosensitizers [M06-2X/6-31G(d,p) solvent model: CPCM, $\varepsilon_{ethanol}$ =24.55].

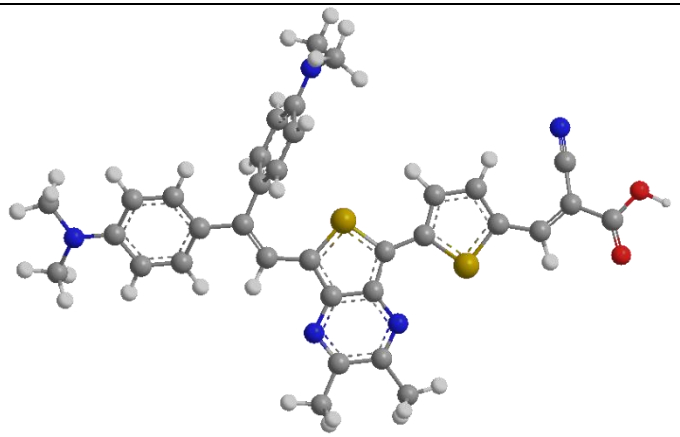
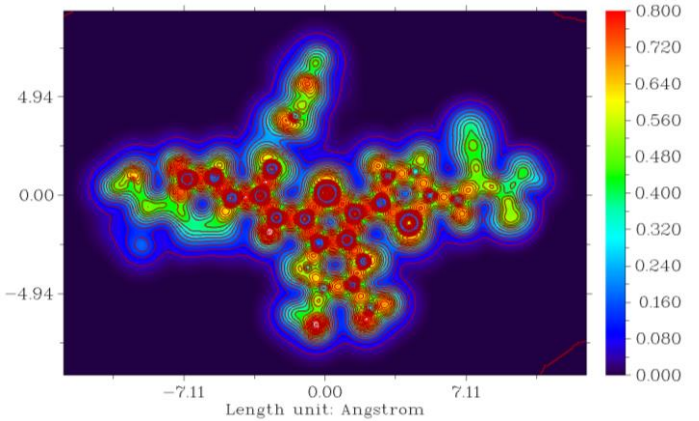
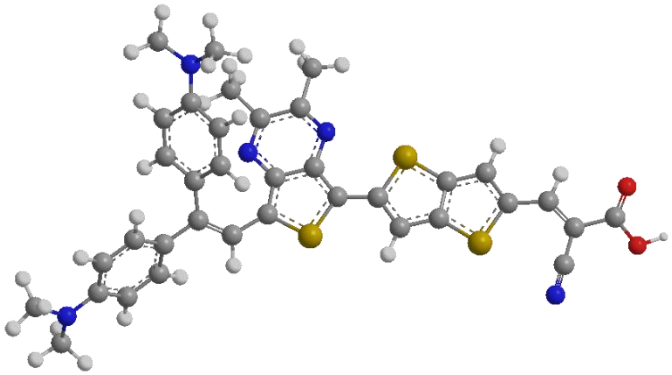
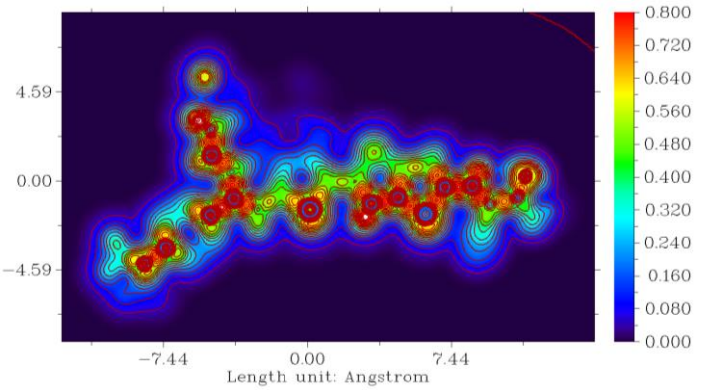
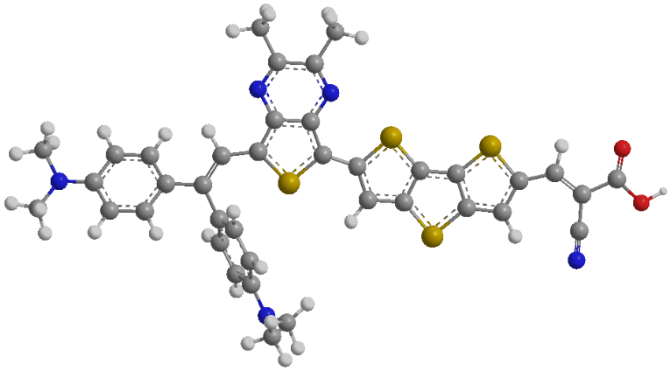
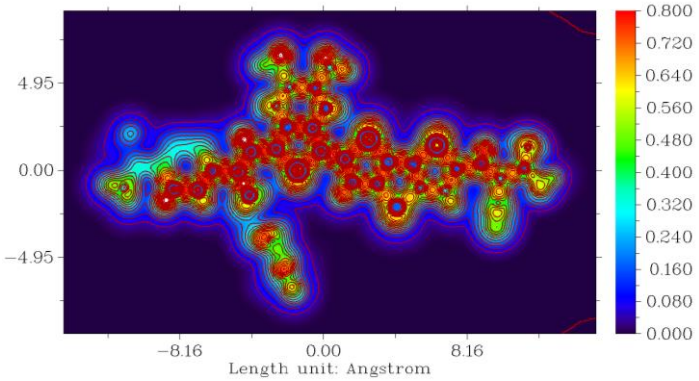
ENTRY	OPTIMIZED GEOMETRY	LOL
D-ε_3-δ_1-A		
D-ε_3-δ_2-A		
D-ε_3-δ_3-A		

Table S1 (*cont.*). Optimized geometries and localized-orbital locator (LOL) plots of investigated photosensitizers [M06-2X/6-31G(d,p) solvent model: CPCM, $\varepsilon_{ethanol}$ =24.55].

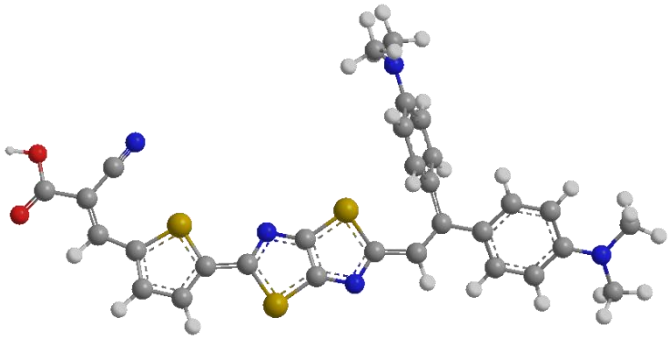
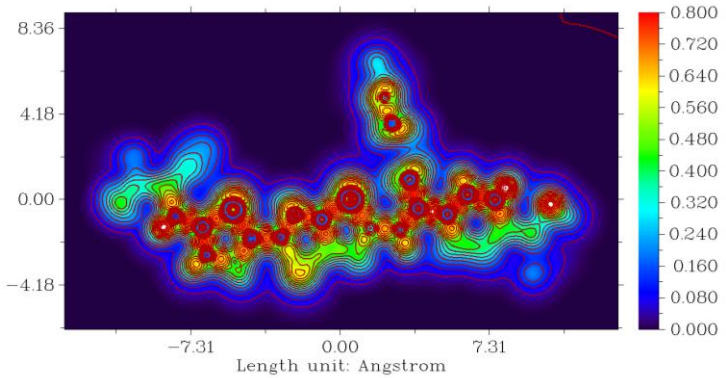
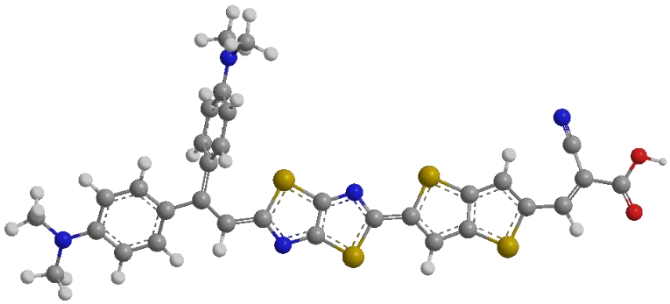
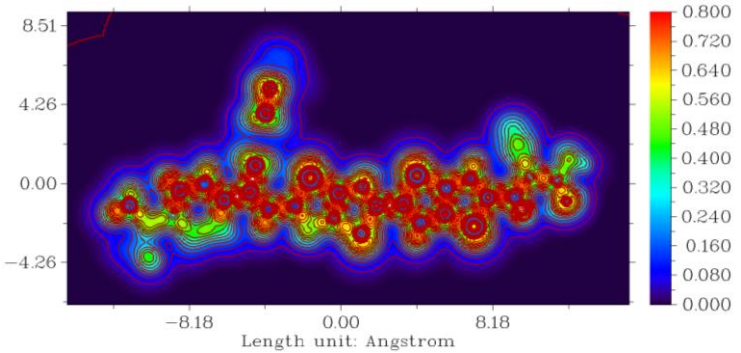
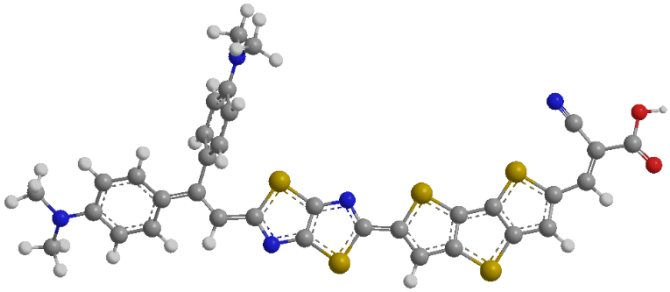
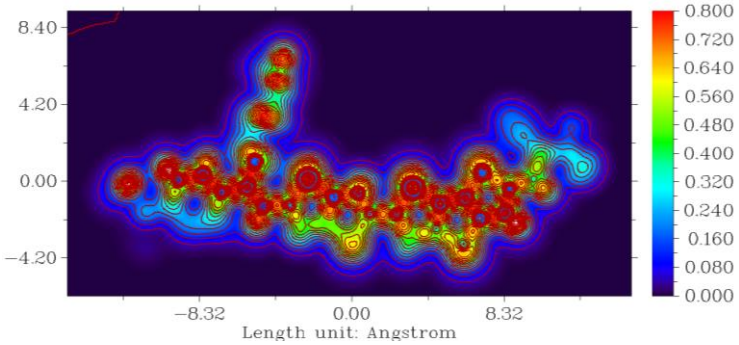
ENTRY	OPTIMIZED GEOMETRY	LOL
D-Ɛ$_4$-δ$_1$-A		
D-Ɛ$_4$-δ$_2$-A		
D-Ɛ$_4$-δ$_3$-A		

Table S1 (*cont.*). Optimized geometries and localized-orbital locator (LOL) plots of investigated photosensitizers [M06-2X/6-31G(d,p) solvent model: CPCM, $\varepsilon_{ethanol}$ =24.55].

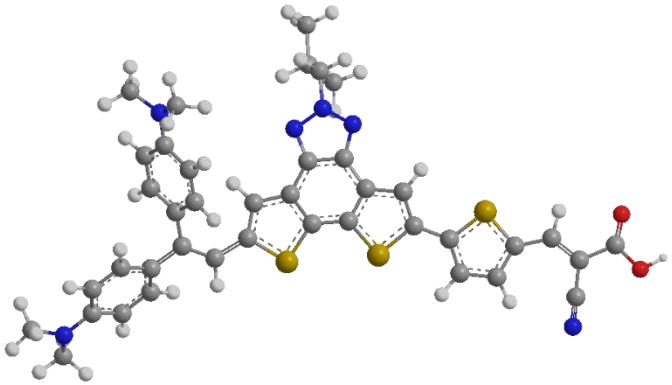
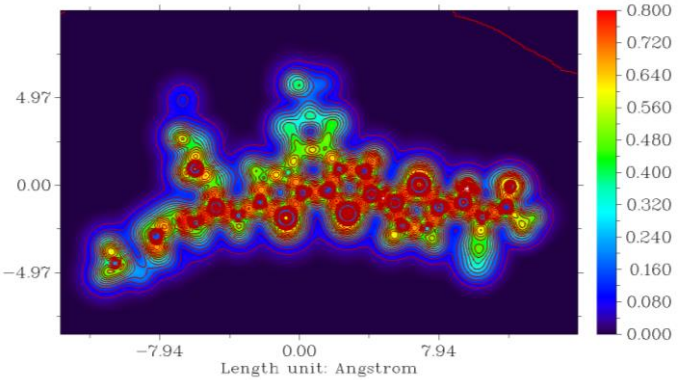
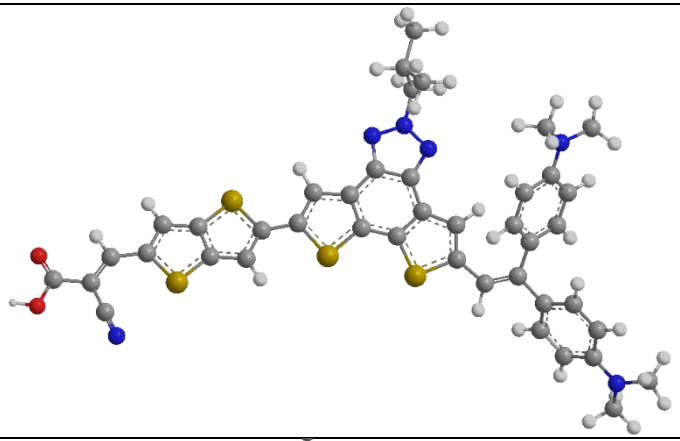
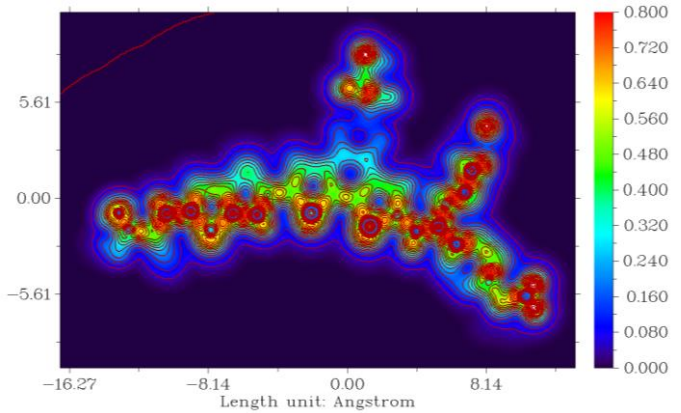
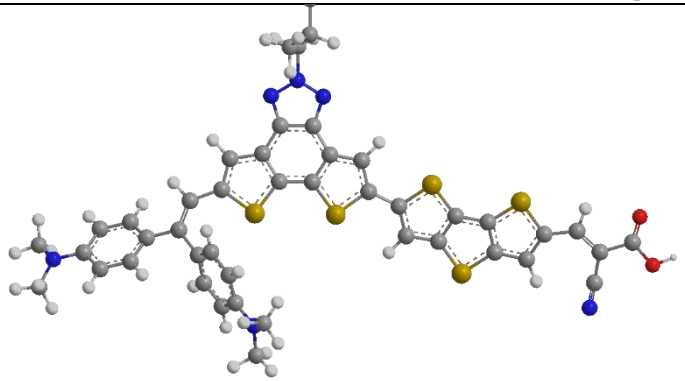
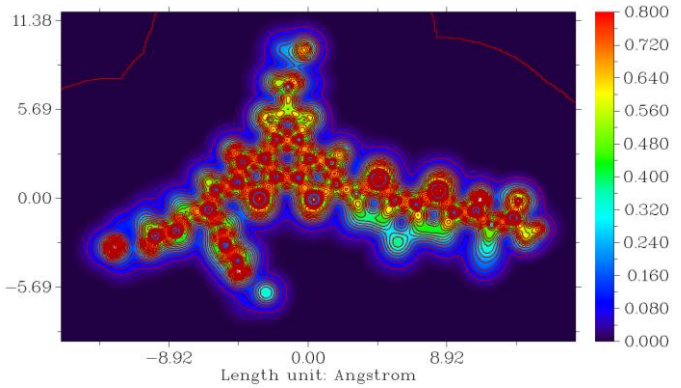
ENTRY	OPTIMIZED GEOMETRY	LOL
D-ε_5-δ_1-A		
D-ε_5-δ_2-A		
D-ε_5-δ_3-A		

Table S1 (*cont.*). Optimized geometries and localized-orbital locator (LOL) plots of investigated photosensitizers [M06-2X/6-31G(d,p) solvent model: CPCM, $\varepsilon_{ethanol}$ =24.55].

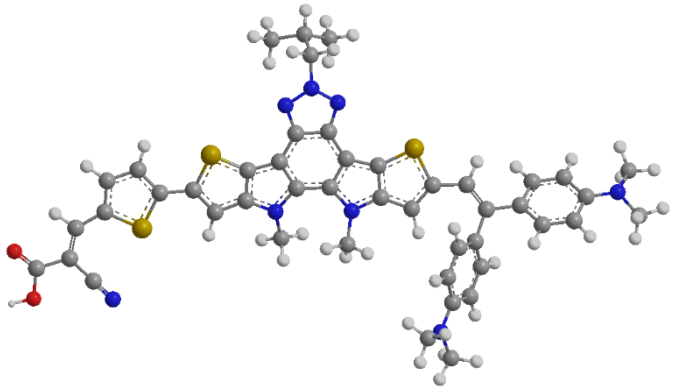
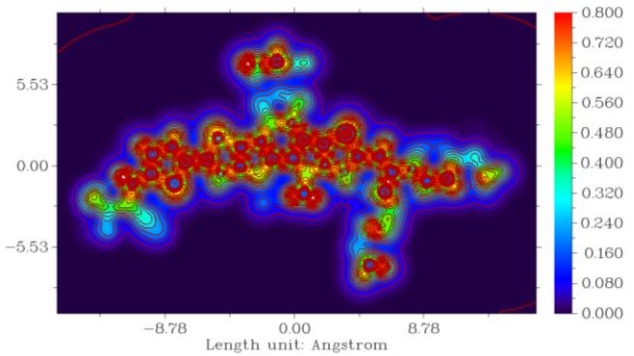
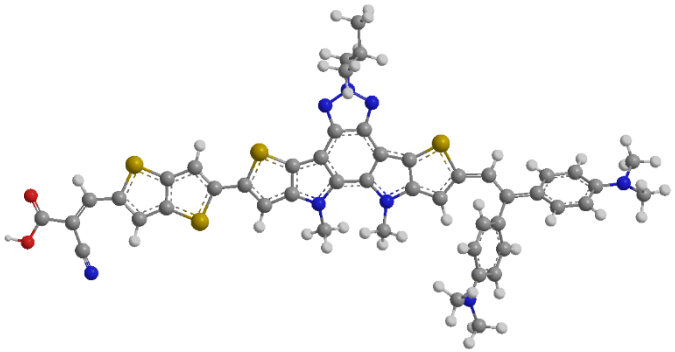
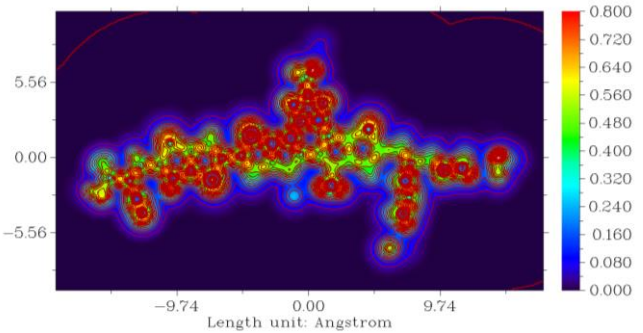
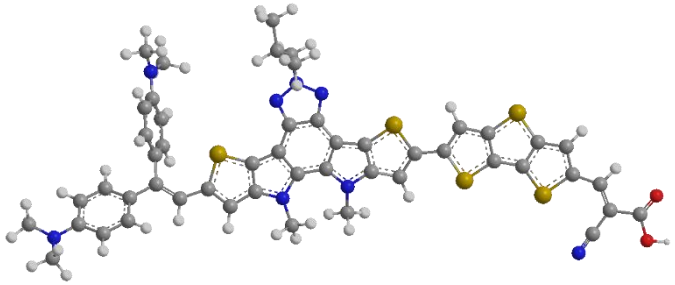
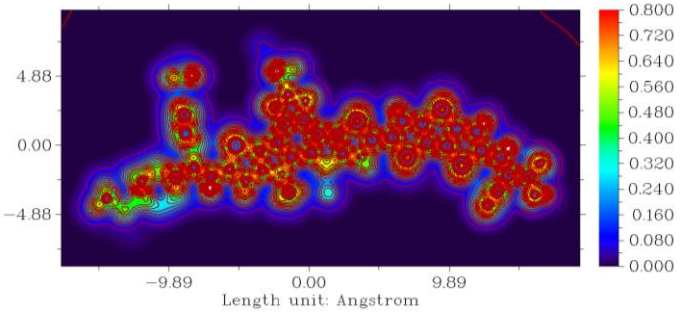
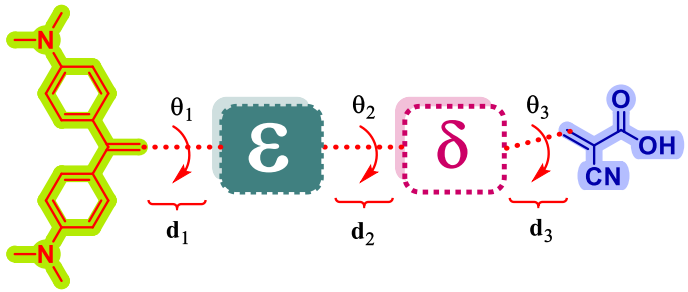
ENTRY	OPTIMIZED GEOMETRY	LOL
D-Ɛ$_6$-δ$_1$-A		
D-Ɛ$_6$-δ$_2$-A		
D-Ɛ$_6$-δ$_3$-A		

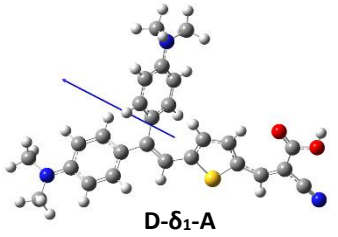
Table S2. Selected bond lengths (d_n, Å), bond angle (θ_n, °), and dihedral angle (ω_n, °) values [M06-2X/6-31G(d,p) solvent model: CPCM, $\varepsilon_{ethanol}$ =24.55].

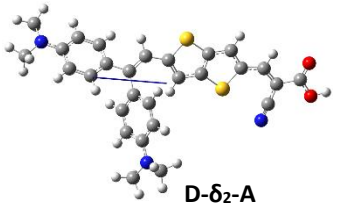


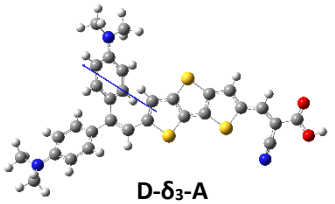
Entry	d_1	d_2	d_3	θ_1	θ_2	θ_3	ω_1	ω_2	ω_3
D-δ_1-A	1.450	-	1.426	127.330	-	134.447	20.779	-	178.424
D-ε_1-δ_1-A	1.465	1.460	1.432	127.885	122.451	129.185	-43.181	-165.139	179.515
D-ε_2-δ_1-A	1.443	1.446	1.434	128.374	119.291	117.736	-6.101	179.484	-179.780
D-ε_3-δ_1-A	1.439	1.434	1.425	128.863	121.362	118.054	-4.595	179.163	-179.778
D-ε_4-δ_1-A	1.449	1.448	1.431	128.995	121.146	125.934	7.693	-179.881	-179.949
D-ε_5-δ_1-A	1.457	1.448	1.432	127.307	119.834	118.014	-26.590	174.993	-179.310
D-ε_6-δ_1-A	1.456	1.444	1.424	127.882	119.332	126.112	-17.634	-172.159	-179.735
D-δ_2-A	1.453	-	1.423	127.666	-	125.456	23.172	-	-179.413
D-ε_1-δ_2-A	1.460	1.460	1.428	128.310	119.288	125.399	-29.024	-171.764	179.996
D-ε_2-δ_2-A	1.451	1.449	1.430	126.404	119.500	125.237	39.396	178.756	-179.688
D-ε_3-δ_2-A	1.451	1.438	1.424	126.694	121.772	125.343	-36.026	178.996	179.968
D-ε_4-δ_2-A	1.449	1.449	1.434	129.176	121.528	117.202	-5.486	-175.865	-179.766
D-ε_5-δ_2-A	1.456	1.449	1.428	127.648	120.020	125.310	22.768	-163.533	-179.239
D-ε_6-δ_2-A	1.456	1.447	1.431	127.641	119.400	117.285	-20.478	-159.793	-179.668
D-δ_3-A	1.455	-	1.424	127.373	-	125.300	21.730	-	179.817
D-ε_1-δ_3-A	1.467	1.461	1.431	127.924	122.584	117.353	-44.117	-168.447	179.962
D-ε_2-δ_3-A	1.443	1.447	1.432	128.609	119.218	117.188	6.426	179.376	178.977
D-ε_3-δ_3-A	1.440	1.439	1.429	129.193	121.447	117.343	5.101	179.043	179.007
D-ε_4-δ_3-A	1.450	1.449	1.429	128.968	121.353	125.198	-9.800	179.174	-179.890
D-ε_5-δ_3-A	1.453	1.450	1.432	129.213	119.930	117.279	14.405	-159.837	-179.893
D-ε_6-δ_3-A	1.452	1.448	1.427	130.041	119.851	125.267	8.060	166.710	-179.900

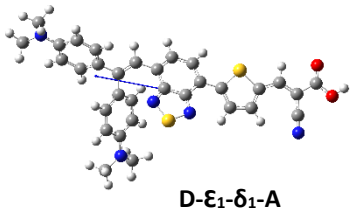
Table S3. Computed dipole moment values of investigated sensitizers (in Debye, D) [Mo6-2X/6-31G(d,p) solvent model: CPCM, $\varepsilon_{ethanol}$ =24.55].

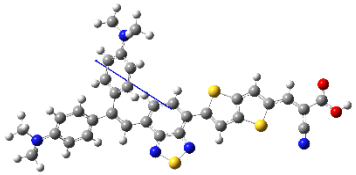
Entry	μ_x	μ_y	μ_z	μ_{normal}
D-δ_1-A	12.1092	6.2502	-1.5949	13.7201
D-ε_1-δ_1-A	9.5308	-0.1578	-2.2545	9.7950
D-ε_2-δ_1-A	-8.8576	4.3393	-0.5369	9.8780
D-ε_3-δ_1-A	-10.6170	-1.9116	0.1510	10.7888
D-ε_4-δ_1-A	6.7511	-0.5963	0.2316	6.7813
D-ε_5-δ_1-A	-10.5029	5.7543	-0.3264	11.9803
D-ε_6-δ_1-A	6.8529	-3.8418	-0.6728	7.8851
D-δ_2-A	9.8246	0.3348	1.6149	9.9621
D-ε_1-δ_2-A	-10.9463	6.9762	-2.1333	13.1545
D-ε_2-δ_2-A	-9.0358	2.6390	-0.9151	9.4577
D-ε_3-δ_2-A	-12.5928	7.0094	-1.1688	14.4595
D-ε_4-δ_2-A	-8.8604	-0.2884	-0.0099	8.8651
D-ε_5-δ_2-A	9.9867	6.4414	-1.1139	11.9359
D-ε_6-δ_2-A	9.2890	-4.9729	0.4580	10.5463
D-δ_3-A	9.6782	6.2195	-2.2942	11.7308
D-ε_1-δ_3-A	9.9112	-0.3212	-2.3364	10.1879
D-ε_2-δ_3-A	8.8597	5.0042	-0.7682	10.2043
D-ε_3-δ_3-A	-10.4524	1.4421	0.3678	10.5578
D-ε_4-δ_3-A	-6.7371	-1.0126	0.1381	6.8142
D-ε_5-δ_3-A	-7.6122	0.2006	1.4646	7.7544
D-ε_6-δ_3-A	-6.9648	0.9917	-0.1885	7.0376

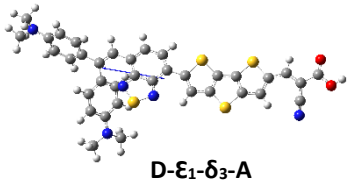

D-δ_1-A

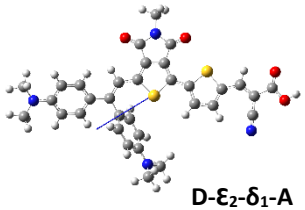

D-δ_2-A

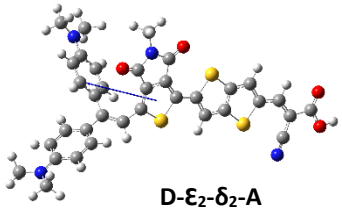

D-δ_3-A

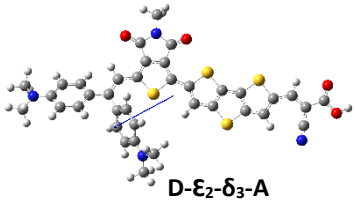

D-ε_1-δ_1-A

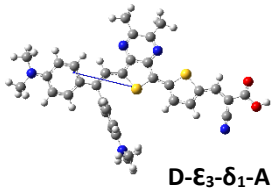

D-ε_1-δ_2-A

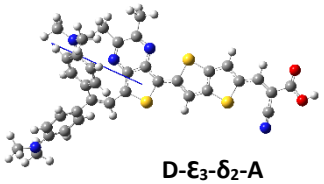

D-ε_1-δ_3-A

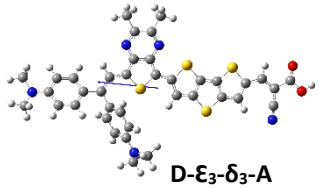

D-ε_2-δ_1-A

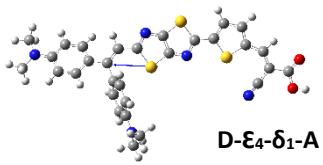

D-ε_2-δ_2-A

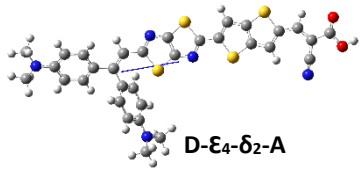

D-ε_2-δ_3-A

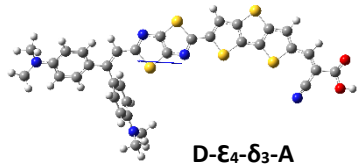

D-ε_3-δ_1-A

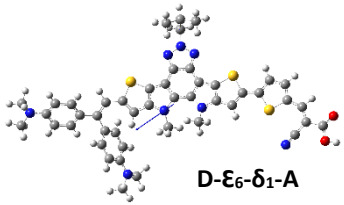

D-ε_3-δ_2-A

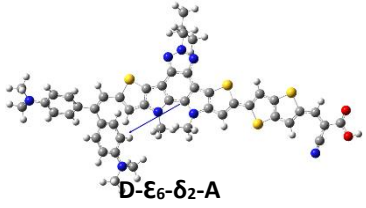

D-ε_3-δ_3-A

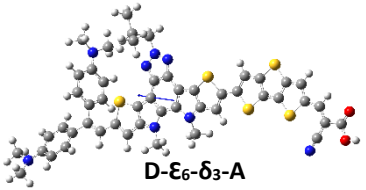

D-ε_4-δ_1-A

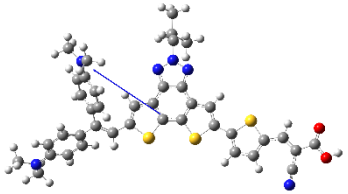

D-ε_4-δ_2-A

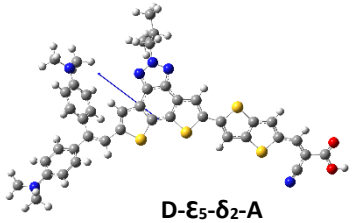

D-ε_4-δ_3-A

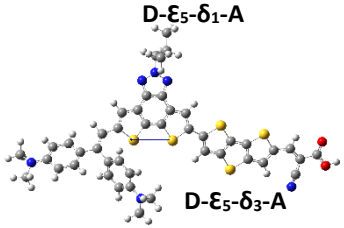

D-ε_6-δ_1-A


D-ε_6-δ_2-A


D-ε_6-δ_3-A


D-ε_5-δ_1-A


D-ε_5-δ_2-A


D-ε_5-δ_3-A

S1. Chemical hardness (η), hyper-hardness (Γ), chemical potential (μ), electronegativity (χ), electrophilicity index (ω), electron-accepting power (ω^+), and electron-donating power (ω^-)

The below discussed global reactivity descriptors were all calculated from Koopman's theory of closed-shell compounds where I and A values are expressed as the negative values of HOMO and LUMO energies, respectively.

Chemical hardness (η) is defined as the second derivative of energy with respect to the number of electrons, according to the Parr-Pearson model, whose general expression is shown below (**Equation S1**).

$$\eta = (\partial^2 E/\partial N^2)_{\upsilon(r)} \quad \textbf{Equation S1}$$

Basically, chemical hardness is an important concept describing the chemical reactivity and chemical stability of the target molecule. It can be calculated by using **Equation S2,** where I is the ionization potential and A is the electron affinity.

$$\eta = \frac{1}{2}(I - A) \quad \textbf{Equation S2}$$

The higher the value of the chemical hardness stands for the higher the resistance to the transfer of intermolecular charge. Thus, excellent energy of conversion is obtained by the lower chemical hardness values, which are desirable in DSSCs. In this scope, the value of chemical hardness of the model dye was calculated as 2.082 eV, and the investigated values of the chemical hardness of the candidate sensitizers varied from 1.772 eV (D-ε_1-δ_1-A) to 2.025 eV (D-ε_6-δ_3-A). It is noteworthy that all of the systems under examination display a congruity between their bandgap energies and chemical hardness values, with the minimum chemical hardness value being correlated with the smallest bandgap energy.

Hyper-hardness (Γ), a novel global descriptor, is defined as the third derivative of energy with respect to the total number of electrons in the system under study. The hyper-hardness values obtained from these calculations, using **Equation S3**, can be utilized to assess the stability or reactivity of target molecules. Furthermore, these findings can be associated with the maximum hardness and minimum polarizability.

$$\Gamma = \varepsilon_{LUMO} - 2\,\varepsilon_{HOMO} + \varepsilon_{HOMO-1} \quad \textbf{Equation S3}$$

where ε represents the energy of the optimized geometry, a positive value of hyper-hardness (Γ) indicates an increase in stability, while a negative value, or a value closer to zero (0), is suggestive of the instability or reactivity of the dye molecules. Regarding the model dye, the hyper-hardness value was determined to be 3.684 eV, implying a high degree of stability. In contrast, the investigated

molecules exhibit a range of hyper-hardness values, ranging from 2.721 eV to 3.684 eV. Notably, the D-ε_3-δ_n-A and D-ε_6-δ_n-A series were observed to be more reactive than the other studied molecules.

Chemical potential (μ) and **electronegativity (χ = -μ)** are comparable, as both descriptors provide valuable insights into the electronic properties of molecules. Chemical potential (**Equation S4**) measures the escape tendency of an electron from a molecule, with higher values indicating a higher degree of reactivity or instability. In contrast, electronegativity describes a molecule's ability to retain its electrons and prevent their release, thereby indicating the molecule's tendency towards stability. Due to these similarities, chemical potential and electronegativity can be considered analogous, and understanding both is crucial for analyzing chemical reactivity and comprehending the electronic properties of molecules.

$$\mu = -(\varepsilon_{HOMO} + \varepsilon_{LUMO})/2 \qquad \textbf{Equation S4}$$

Therefore, chemical potential is a descriptor that is closely linked to the availability of electrons in a given reagent. A reagent with a higher electronic chemical potential has a greater capacity to donate its electrons to other molecules, making it a proficient electron donor. Conversely, a reagent with a lower electronic chemical potential has a higher affinity for electrons and can effectively accept electrons from other molecules, making it a competent electron acceptor. Based on the results obtained in this study, it was observed that the D-ε_6-δ_n-A series was particularly effective in facilitating electron transfer from the photosensitizer to the TiO_2 semiconductor.

Electrophilicity index (ω), which has been given in the following expression (**Equation S5)** gauges the energy stabilization when a system receives an additional electronic charge from the environment. A lower value of the electrophilicity value indicates enhanced chemical reactivity.

$$\omega = \frac{\mu^2}{2\eta} \qquad \textbf{Equation S5}$$

where μ is the chemical potential and η is the chemical hardness. In this scope, the value of the electrophilicity of the model dye was calculated as 3.842 eV. The electrophilicity values of the investigated sensitizers varied from 3.972 eV to 4.576 eV.

Electron-accepting power (ω^+) and electron-donating power (ω^-) The concept of stabilization energy is a crucial parameter in the study of molecular structures, as it provides valuable information on the stability and reactivity of molecules. In this context, the value of ω is a commonly used descriptor for quantifying stabilization energies in molecular structures. The ω^+ value, in particular, represents the electron-accepting ability of a molecule, and a higher value indicates a greater capacity for electron acceptance. As a result, higher values of both ω and ω^+ are desirable, as they indicate increased

stability and reactivity in molecular structures. Given the importance of this parameter, it is crucial to accurately measure and analyze the values of ω and ω^+ in order to gain insights into the electronic properties of molecules and their potential applications in a variety of chemical reactions (**Equation S6**).

$$\omega^+ = \frac{(I+3A)^2}{16(I-A)} \qquad \omega^- = \frac{(3I+A)^2}{16(\mathrm{I}-\mathrm{A})} \qquad \textbf{Equation S6}$$

According to the calculations, Ɛ containing molecules (D-$Ɛ_n$-δ_n-A) displayed higher ω^+ values compared to the D-δ_n-A type molecules. Furthermore, the calculated values of electron-donating powers (ω^-) for both the reference and designed dyes indicate a consistent trend of electrophilicity and electron-accepting power.

Table S4. Calculated values of global descriptors (all values are in eV) [M06-2X/6-31G(d,p) solvent model: CPCM, $\varepsilon_{ethanol}$ =24.55].

Entry	ε_{HOMO}	ε_{LUMO}	ε_g	I	A	η	Γ	μ	χ	ω	ω^+	ω^-
D-δ_1-A	-6.083	-1.918	4.165	6.083	1.918	2.082	3.684	-4.000	4.000	3.842	2.102	6.103
D-ε_1-δ_1-A	-6.100	-2.221	3.879	6.100	2.221	1.940	3.446	-4.160	4.160	4.462	2.624	6.784
D-ε_2-δ_1-A	-6.150	-2.238	3.911	6.150	2.238	1.956	3.451	-4.194	4.194	4.497	2.644	6.838
D-ε_3-δ_1-A	-5.848	-2.258	3.589	5.848	2.258	1.795	2.832	-4.053	4.053	4.576	2.774	6.827
D-ε_4-δ_1-A	-6.138	-2.253	3.885	6.138	2.253	1.942	3.443	-4.196	4.196	4.532	2.677	6.872
D-ε_5-δ_1-A	-5.967	-2.138	3.829	5.967	2.138	1.914	3.232	-4.053	4.053	4.290	2.503	6.555
D-ε_6-δ_1-A	-5.709	-2.070	3.639	5.709	2.070	1.819	2.885	-3.889	3.889	4.157	2.440	6.329
D-δ_2-A	-6.035	-1.986	4.049	6.035	1.986	2.025	3.512	-4.011	4.011	3.972	2.220	6.231
D-ε_1-δ_2-A	-6.030	-2.257	3.773	6.030	2.257	1.886	3.235	-4.143	4.143	4.550	2.714	6.858
D-ε_2-δ_2-A	-6.136	-2.226	3.910	6.136	2.226	1.955	3.509	-4.181	4.181	4.471	2.625	6.806
D-ε_3-δ_2-A	-5.851	-2.201	3.650	5.851	2.201	1.825	2.992	-4.026	4.026	4.442	2.657	6.683
D-ε_4-δ_2-A	-6.125	-2.252	3.872	6.125	2.252	1.936	3.398	-4.188	4.188	4.530	2.678	6.866
D-ε_5-δ_2-A	-5.949	-2.133	3.816	5.949	2.133	1.908	3.211	-4.041	4.041	4.279	2.497	6.538
D-ε_6-δ_2-A	-5.694	-2.097	3.597	5.694	2.097	1.798	2.857	-3.896	3.896	4.220	2.497	6.393
D-δ_3-A	-5.987	-2.035	3.952	5.987	2.035	1.976	3.370	-4.011	4.011	4.070	2.312	6.322
D-ε_1-δ_3-A	-6.076	-2.213	3.864	6.076	2.213	1.932	3.401	-4.144	4.144	4.446	2.615	6.759
D-ε_2-δ_3-A	-6.107	-2.234	3.873	6.107	2.234	1.936	3.380	-4.171	4.171	4.492	2.648	6.819
D-ε_3-δ_3-A	-5.772	-2.227	3.545	5.772	2.227	1.772	2.721	-4.000	4.000	4.513	2.735	6.734
D-ε_4-δ_3-A	-6.117	-2.222	3.895	6.117	2.222	1.947	3.423	-4.169	4.169	4.464	2.622	6.792
D-ε_5-δ_3-A	-5.957	-2.151	3.806	5.957	2.151	1.903	3.191	-4.054	4.054	4.317	2.528	6.582
D-ε_6-δ_3-A	-5.687	-2.105	3.581	5.687	2.105	1.791	2.871	-3.896	3.896	4.238	2.514	6.410

Abbreviations: ε_{HOMO} (HOMO' energy), ε_{LUMO} (LUMO' energy), ε_g (bandgap energy), I (ionization potential), A (electron affinity), η (chemical hardness), Γ (hyper-hardness), μ (chemical potential), χ (electronegativity), ω (electrophilicity index), electron-accepting power (ω^+), electron-donating power (ω^-)

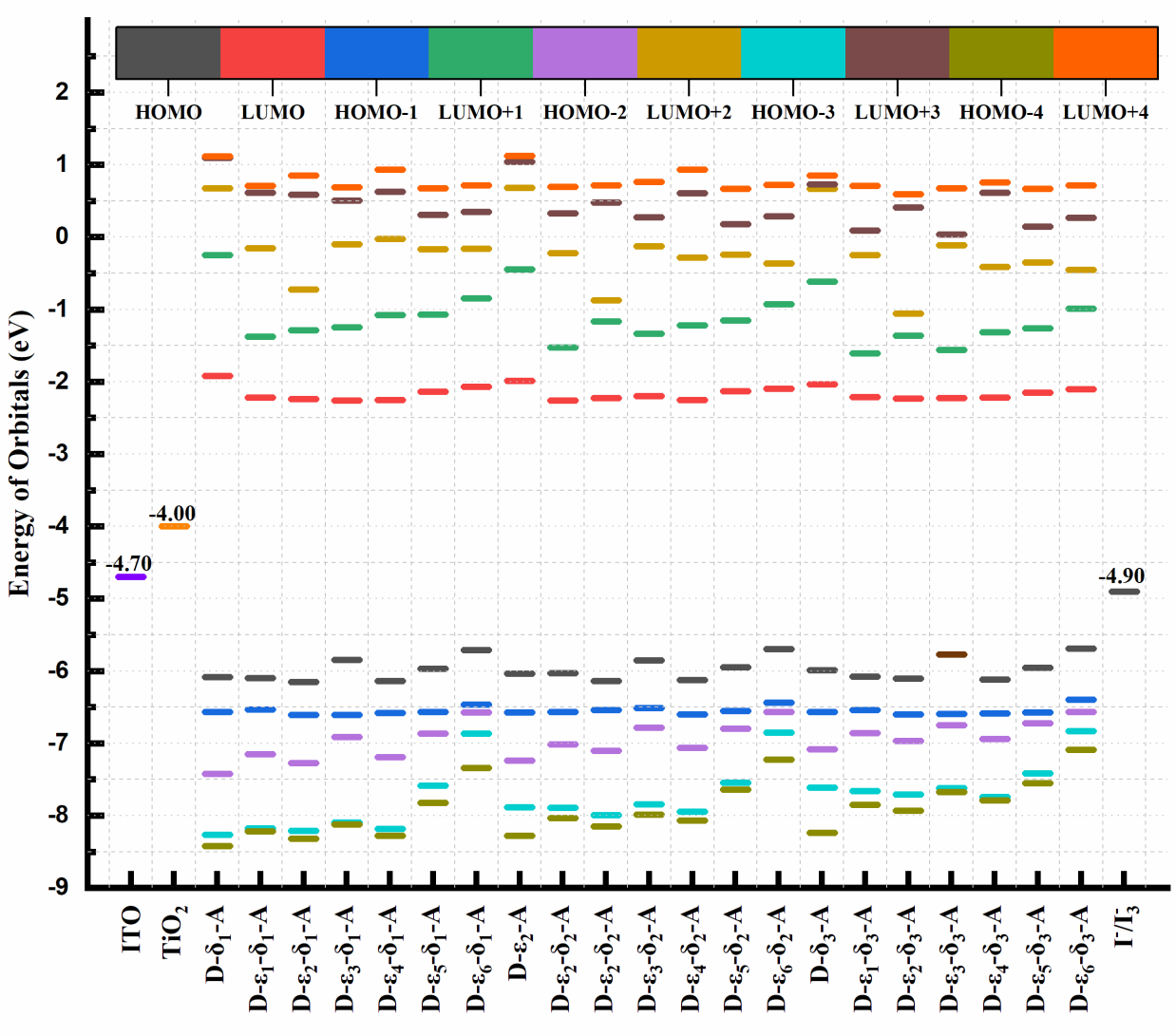


Figure S1. Diagram of the frontier orbital energy levels (from the LUMO+4 to HOMO-4)

Table S5. Frontier orbitals' contour plots of the investigated dye molecules. The threshold of contours is ±0.02 au [M06-2X/6-31G(d,p) solvent model: CPCM, $\varepsilon_{ethanol}$ =24.55].

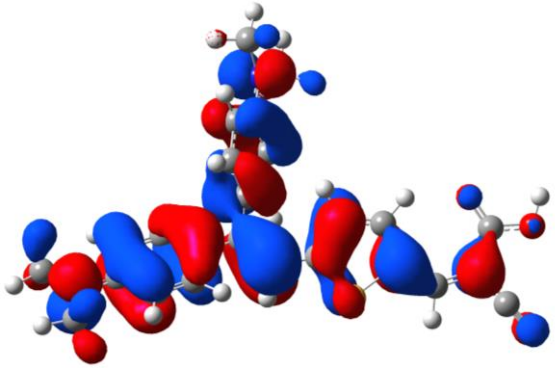
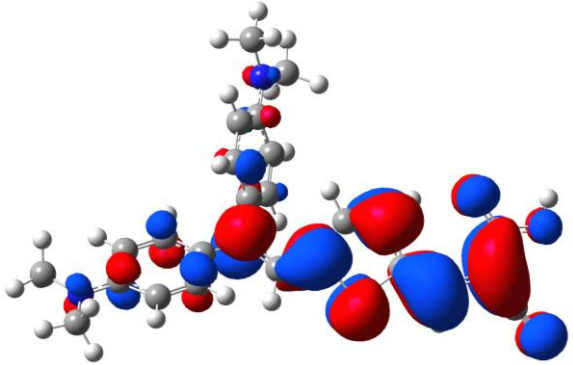
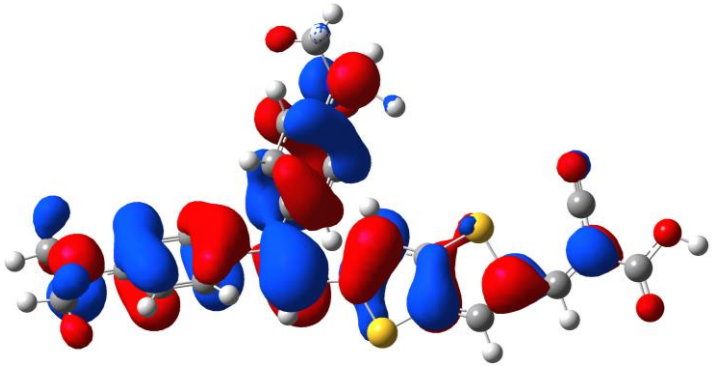
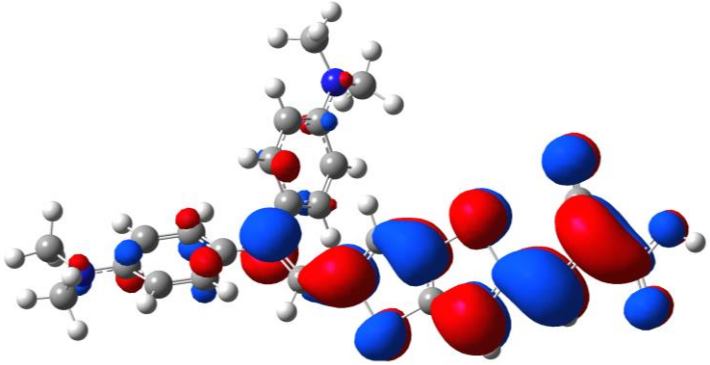
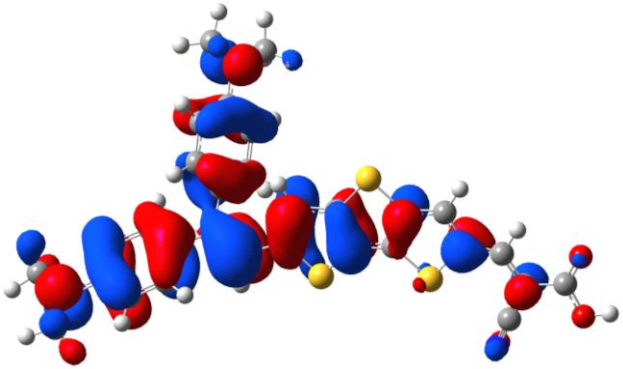
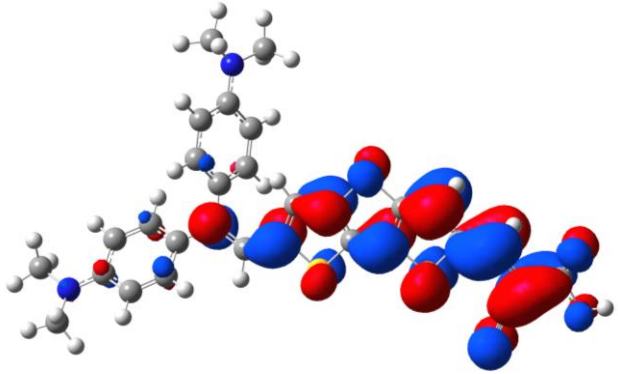
ENTRY	HOMO	LUMO
D-δ_1-A		
D-δ_2-A		
D-δ_3-A		

Table S5 (*cont.*). Frontier orbitals' contour plots of the investigated dye molecules. The threshold of contours is ±0.02 au [M06-2X/6-31G(d,p) solvent model: CPCM, $\varepsilon_{ethanol}$ =24.55].

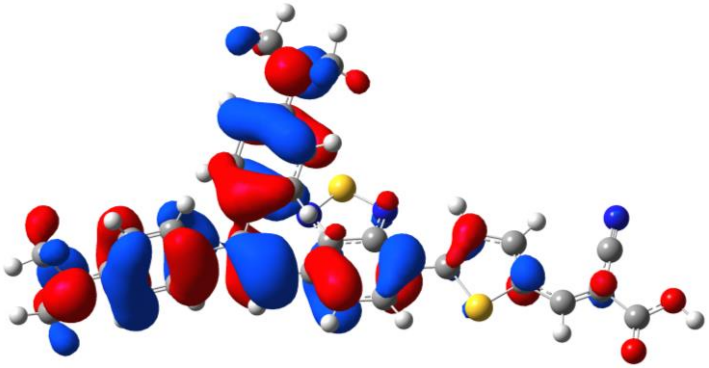
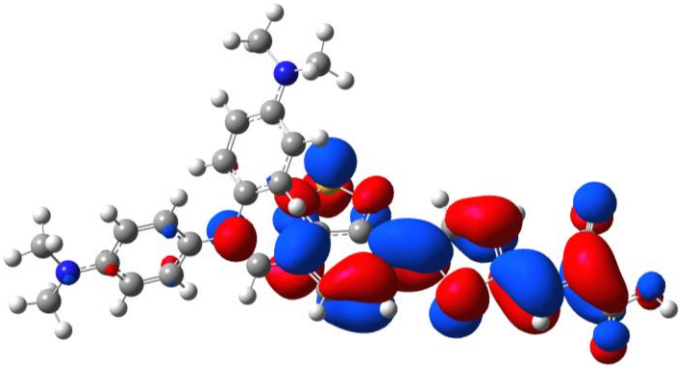
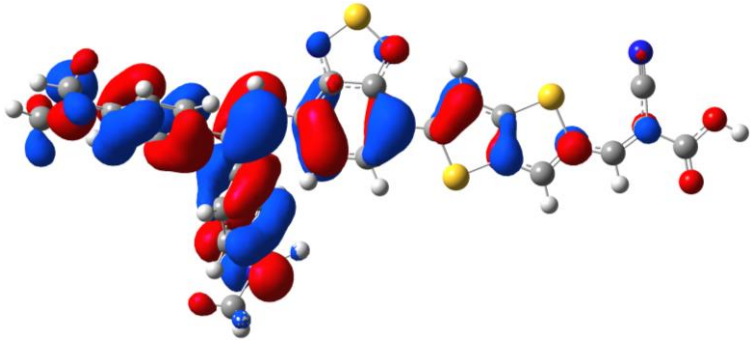
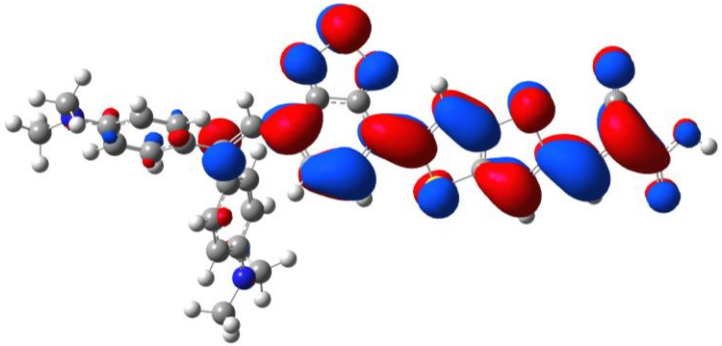
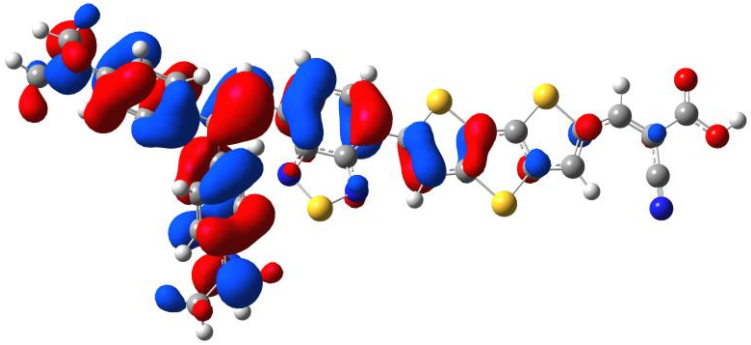
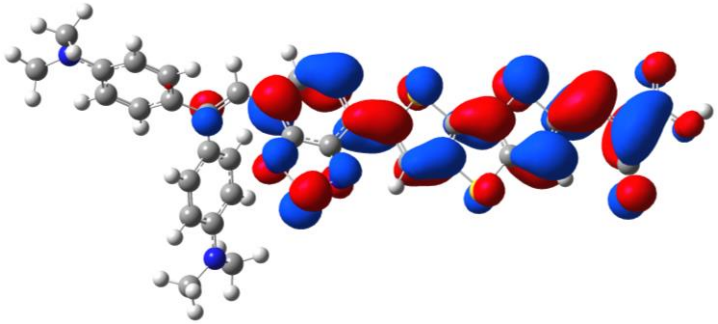
ENTRY	HOMO	LUMO
D-ε_1-δ_1-A		
D- ε_1-δ_2-A		
D- ε_1-δ_3-A		

Table S5 (*cont.*). Frontier orbitals' contour plots of the investigated dye molecules. The threshold of contours is ±0.02 au [M06-2X/6-31G(d,p) solvent model: CPCM, $\varepsilon_{ethanol}$ =24.55].

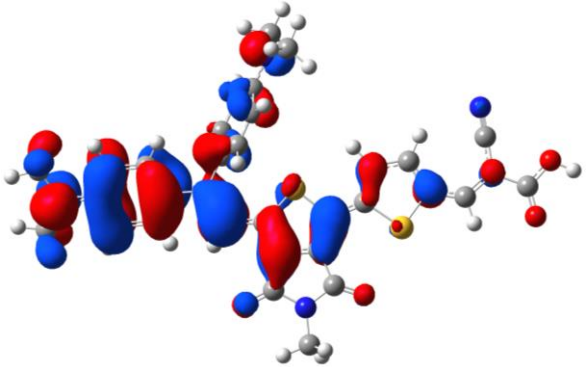
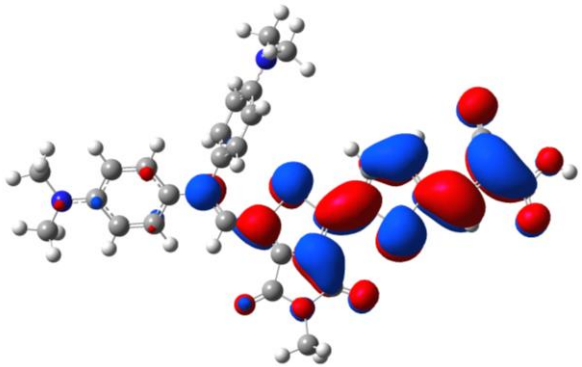
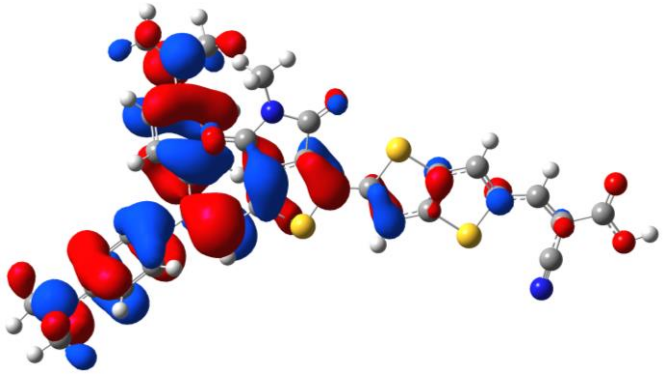
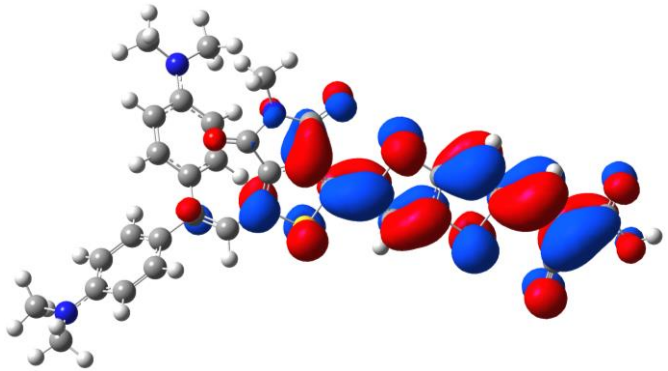
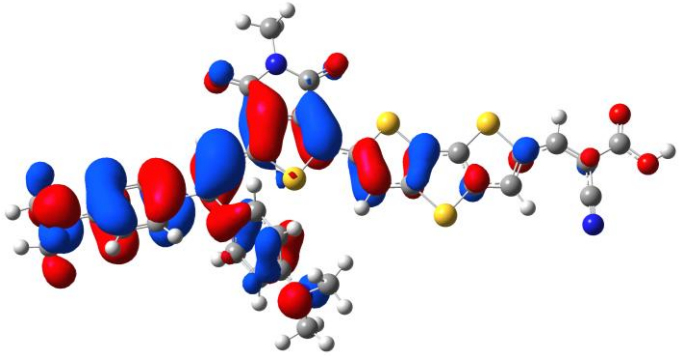
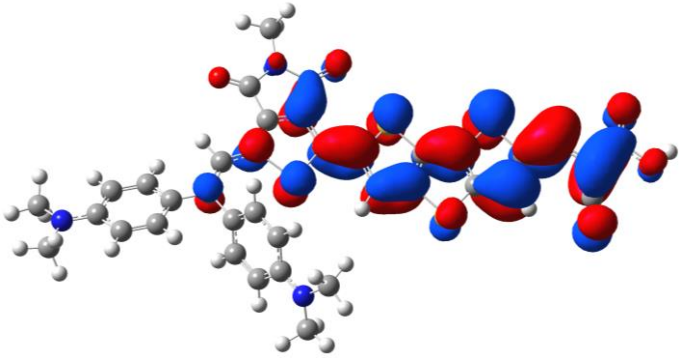
ENTRY	HOMO	LUMO
D-ε_2-δ_1-A		
D-ε_2-δ_2-A		
D-ε_2-δ_3-A		

Table S5 (*cont.*). Frontier orbitals' contour plots of the investigated dye molecules. The threshold of contours is ±0.02 au [M06-2X/6-31G(d,p) solvent model: CPCM, $\varepsilon_{ethanol}$ =24.55].

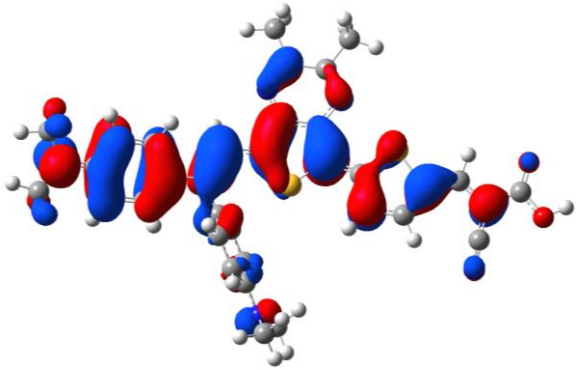
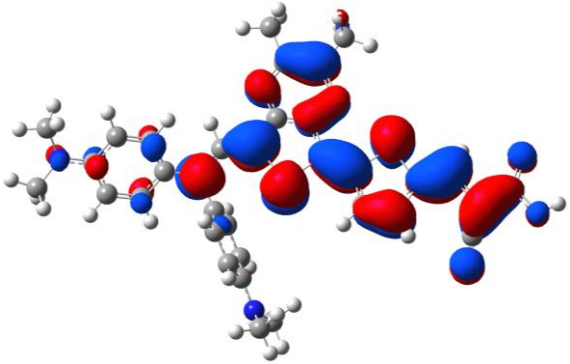
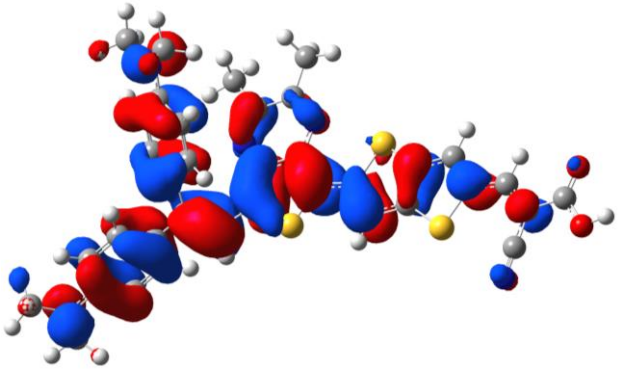
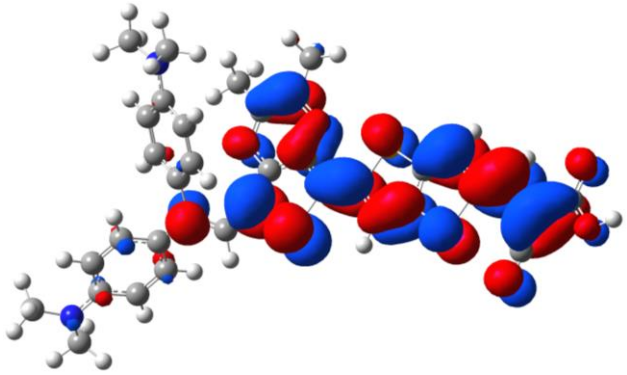
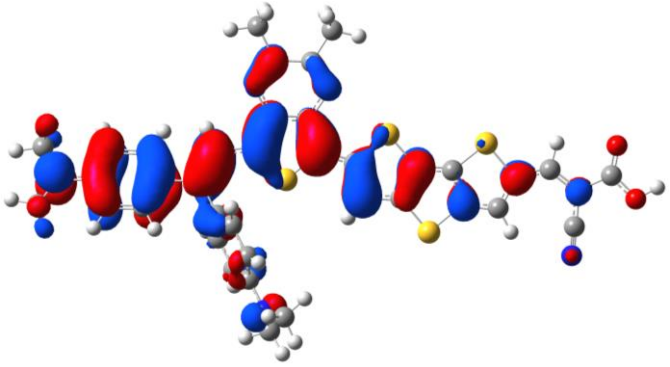
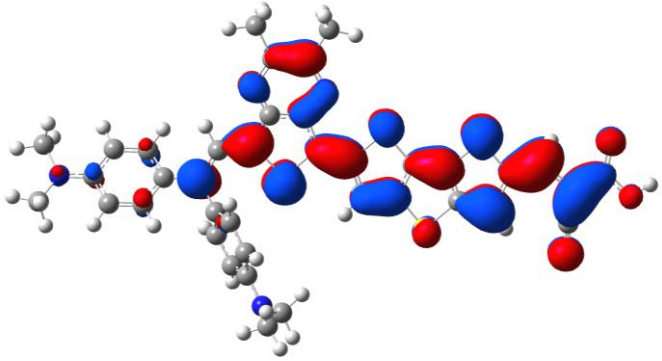
ENTRY	HOMO	LUMO
D-Ɛ$_3$-δ$_1$-A		
D-Ɛ$_3$-δ$_2$-A		
D-Ɛ$_3$-δ$_3$-A		

Table S5 (*cont.*). Frontier orbitals' contour plots of the investigated dye molecules. The threshold of contours is ±0.02 au [M06-2X/6-31G(d,p) solvent model: CPCM, $\varepsilon_{ethanol}$ =24.55].

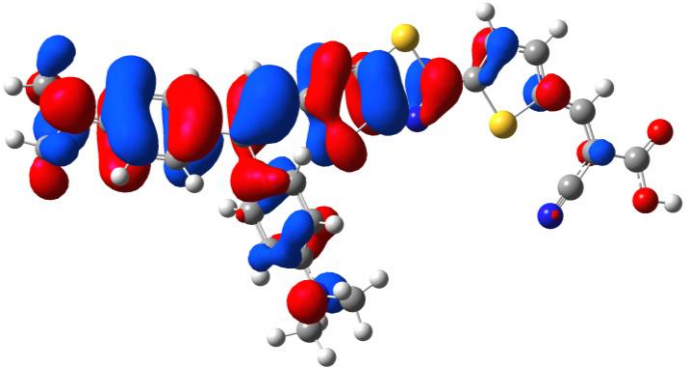
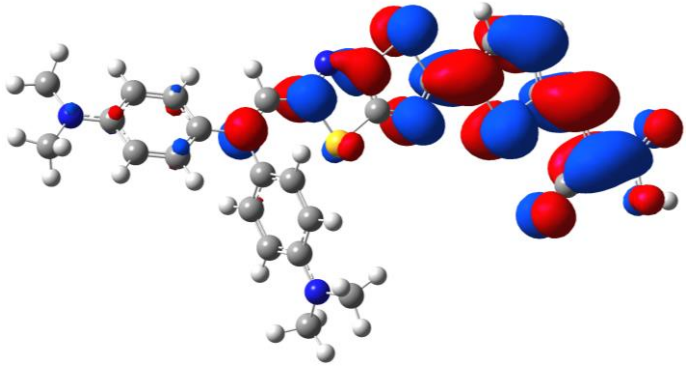
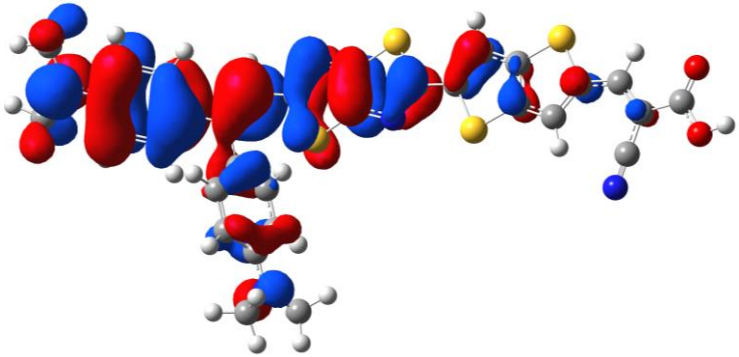
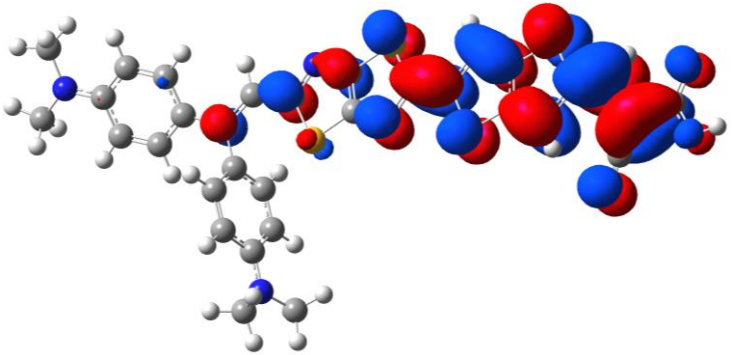
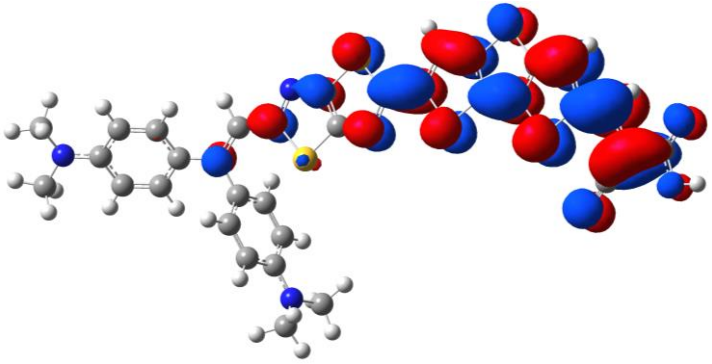
ENTRY	HOMO	LUMO
D-Ɛ$_4$-δ$_1$-A		
D-Ɛ$_4$-δ$_2$-A		
D-Ɛ$_4$-δ$_3$-A		

Table S5 (*cont.*). Frontier orbitals' contour plots of the investigated dye molecules. The threshold of contours is ±0.02 au [M06-2X/6-31G(d,p) solvent model: CPCM, $\varepsilon_{ethanol}$ =24.55].

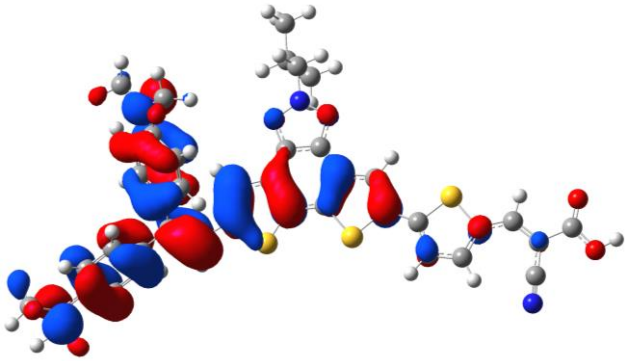
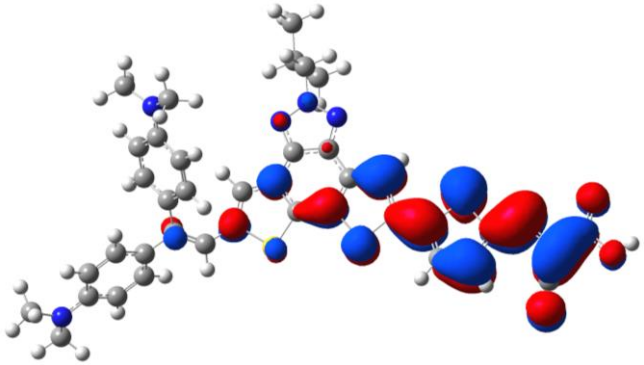
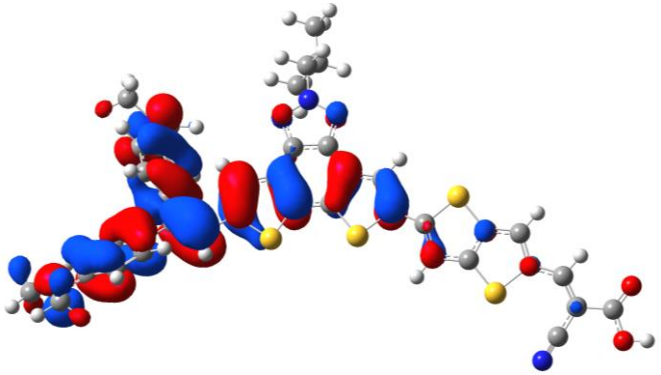
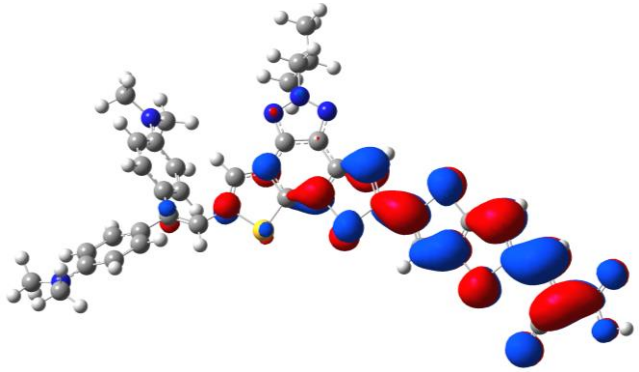
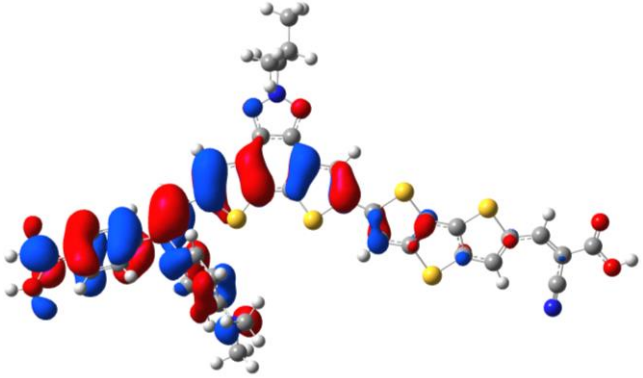
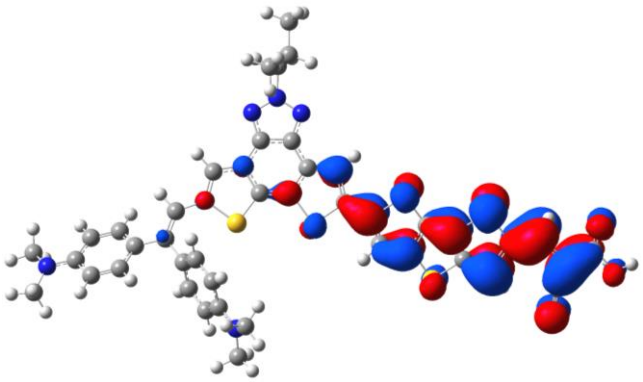
ENTRY	HOMO	LUMO
D-ε_5-δ_1-A		
D-ε_5-δ_2-A		
D-ε_5-δ_3-A		

Table S5 (*cont.*). Frontier orbitals' contour plots of the investigated dye molecules. The threshold of contours is ±0.02 au [M06-2X/6-31G(d,p) solvent model: CPCM, $\varepsilon_{ethanol}$ =24.55].

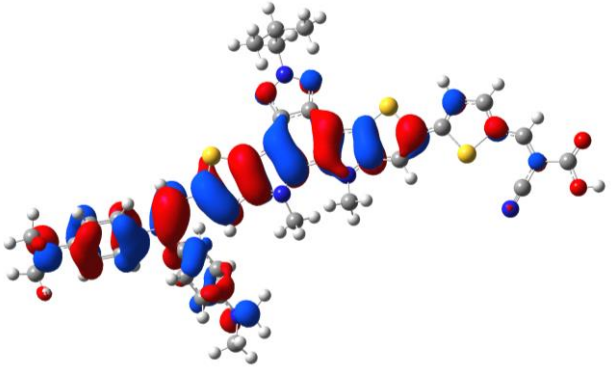
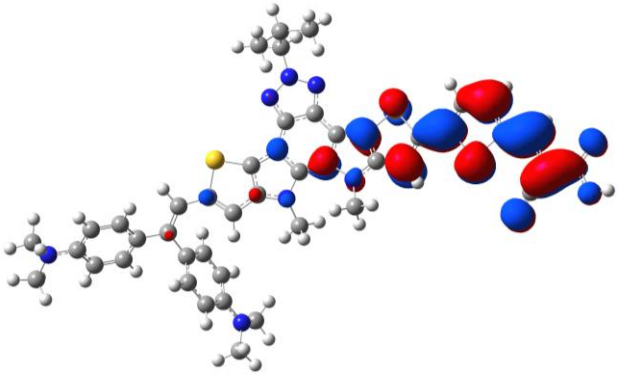
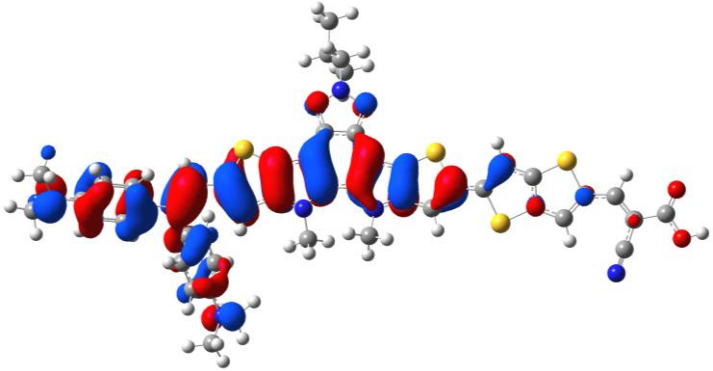
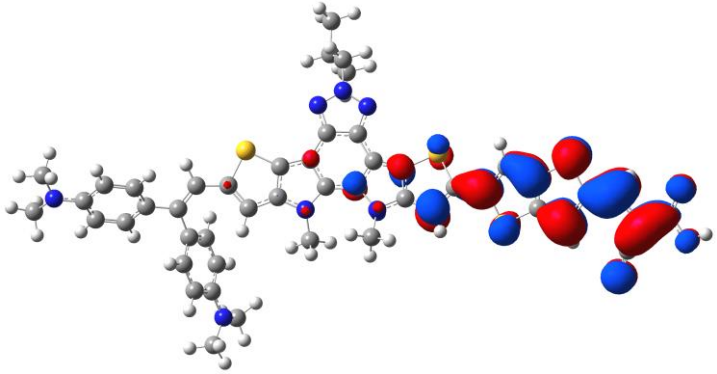
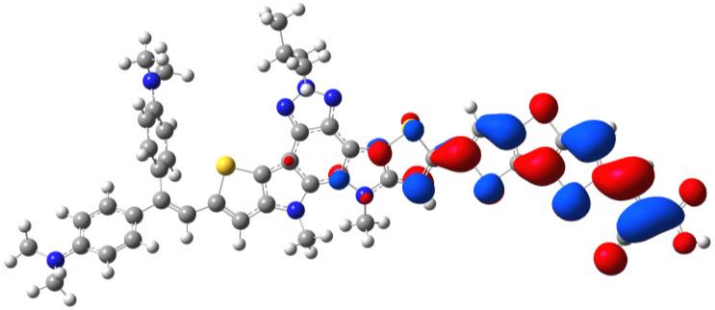
ENTRY	HOMO	LUMO
D-ε_6-δ_1-A		
D-ε_6-δ_2-A		
D-ε_6-δ_3-A		

Table S6. DFT-calculated IP and EA values *via* Koopman's theorem *or* delta-SCF method [M06-2X//6-31G(d,p) solvent model: CPCM, $\varepsilon_{ethanol} = 24.55$].

Entry	SCF Energies (eV)					Koopman's theorem	
	Neutral	Cation	Anion	I	A	I	A
D-δ_1-A (*model dye*)	-1718.134	-1717.940	-1718.236	**5.267**	**2.794**	**6.083**	**1.918**
D-ε_1-δ_1-A	-2455.511	-2455.316	-2455.622	5.327	3.017	6.100	2.221
D-ε_2-δ_1-A	-2589.915	-2589.720	-2590.028	5.292	3.089	6.150	2.238
D-ε_3-δ_1-A	-2534.122	-2533.936	-2534.235	**5.064**	**3.054**	**5.848**	**2.258**
D-ε_4-δ_1-A	-2776.297	-2776.102	-2776.411	5.288	3.100	6.138	2.253
D-ε_5-δ_1-A	-3218.572	-3218.381	-3218.682	5.206	2.990	5.967	2.138
D-ε_6-δ_1-A	-3560.190	-3560.007	-3560.298	**4.991**	**2.926**	**5.709**	**2.070**
D-δ_2-A	-2192.485	-2192.292	-2192.590	5.245	2.841	6.035	1.986
D-ε_1-δ_2-A	-2929.859	-2929.666	-2929.969	5.248	3.003	6.030	2.257
D-ε_2-δ_2-A	-3064.256	-3064.058	-3064.368	5.371	3.046	6.136	2.226
D-ε_3-δ_2-A	-3008.463	-3008.275	-3008.572	**5.098**	**2.973**	**5.851**	**2.201**
D-ε_4-δ_2-A	-3250.638	-3250.444	-3250.751	5.279	3.074	6.125	2.252
D-ε_5-δ_2-A	-3692.918	-3692.727	-3693.026	5.190	2.961	5.949	2.133
D-ε_6-δ_2-A	-4034.532	-4034.349	-4034.640	**4.978**	**2.952**	**5.694**	**2.097**
D-δ_3-A	-2666.828	-2666.637	-2666.934	5.205	2.886	5.987	2.035
D-ε_1-δ_3-A	-3404.199	-3404.003	-3404.309	5.316	2.995	6.076	2.213
D-ε_2-δ_3-A	-3538.602	-3538.408	-3538.713	5.279	3.043	6.107	2.234
D-ε_3-δ_3-A	-3482.808	-3482.624	-3482.918	**5.006**	**2.987**	**5.772**	**2.227**
D-ε_4-δ_3-A	-3724.984	-3724.789	-3725.095	5.300	3.024	6.117	2.222
D-ε_5-δ_3-A	-4167.261	-4167.070	-4167.371	5.184	2.990	5.957	2.151
D-ε_6-δ_3-A	-4508.878	-4508.695	-4508.986	**4.978**	**2.943**	**5.687**	**2.105**

S2. Electrostatic potential (ESP) map

An electrostatic potential map (ESP) is defined as a color scheme representing the electrostatic potential at the molecular surface. The charge distribution in a molecule can be visualized using ESP charts. The collected data contains critical information that may be utilized to analyze the possible electroactive sub-fragments of the target molecules, and the results can be used to build chemical reactivity patterns. In this scope, the ESP maps of the investigated photosensitizers are illustrated in **Table S7**. Based on the provided ESP maps, electron-deficient (positive) regions are represented by blue, whereas electron-rich regions are symbolized by red color. Green-colored regions may be considered to have zero electrostatic potentials, and the regions of intermediate electron density are signified by yellow color. In other words, the brief descriptions of the potential values provided by various colors may be listed in descending order of red > orange > yellow > green > blue. Our analysis revealed that all the molecules investigated displayed similar ESP maps with comparable values as electronegative and electropositive poles. Due to the strongly polarized nitrile and carboxylic acid functional groups, the anchoring (cyanoacrylic acid) group was the most electroactive domain across the whole system. It is apparent that the electron density moves from the donor to the conjugation spacer, and finally, to the anchoring group. Based on the ESP maps, it can be inferred that the electron distribution is favorable for the transfer of electrons from the donor to the anchoring unit.

S3. Dipole Moment (μ)

Molecules with a large dipole moment are typically characterized by an asymmetric distribution of electronic charge. This feature makes these molecules more reactive and susceptible to changes in their electronic structure and properties under the influence of an external electric field. In the studied conjugated systems, the local dipole moment (μ_{normal}) of the ground state induces polarization upon electron excitation, resulting in differentiated dipole moments. The μ value denotes the degree of charge distribution within the studied molecules, with positive charge tending to localize on the donor fragment and negative charge tending to localize over the acceptor fragment. The differentiation between the negative and positive charge following excitation results in a decrease in the binding energy of the D-ε_n-δ_n-A system, thereby facilitating charge transfer. Therefore, it is crucial to explore the reactivity, stability, and charge transfer properties that reflect the corresponding nonlinear optical (NLO) property of the donor-π-bridge-acceptor scaffold. In our research, we calculated the μnormal values of the sensitizers using **Equation S7.**

$$\mu_{normal} = \frac{\mu_x^2+\mu_y^2+\mu_z^2}{2} \qquad \textbf{Equation S7}$$

Table S7. Electrostatic potential (ESP) map representing the corresponding charge density distributions isodensity (0.001e/Bohr^3) and calculated dipole moment vector [M06-2X/6-31G(d,p) solvent model: CPCM, $\varepsilon_{ethanol}$ =24.55].

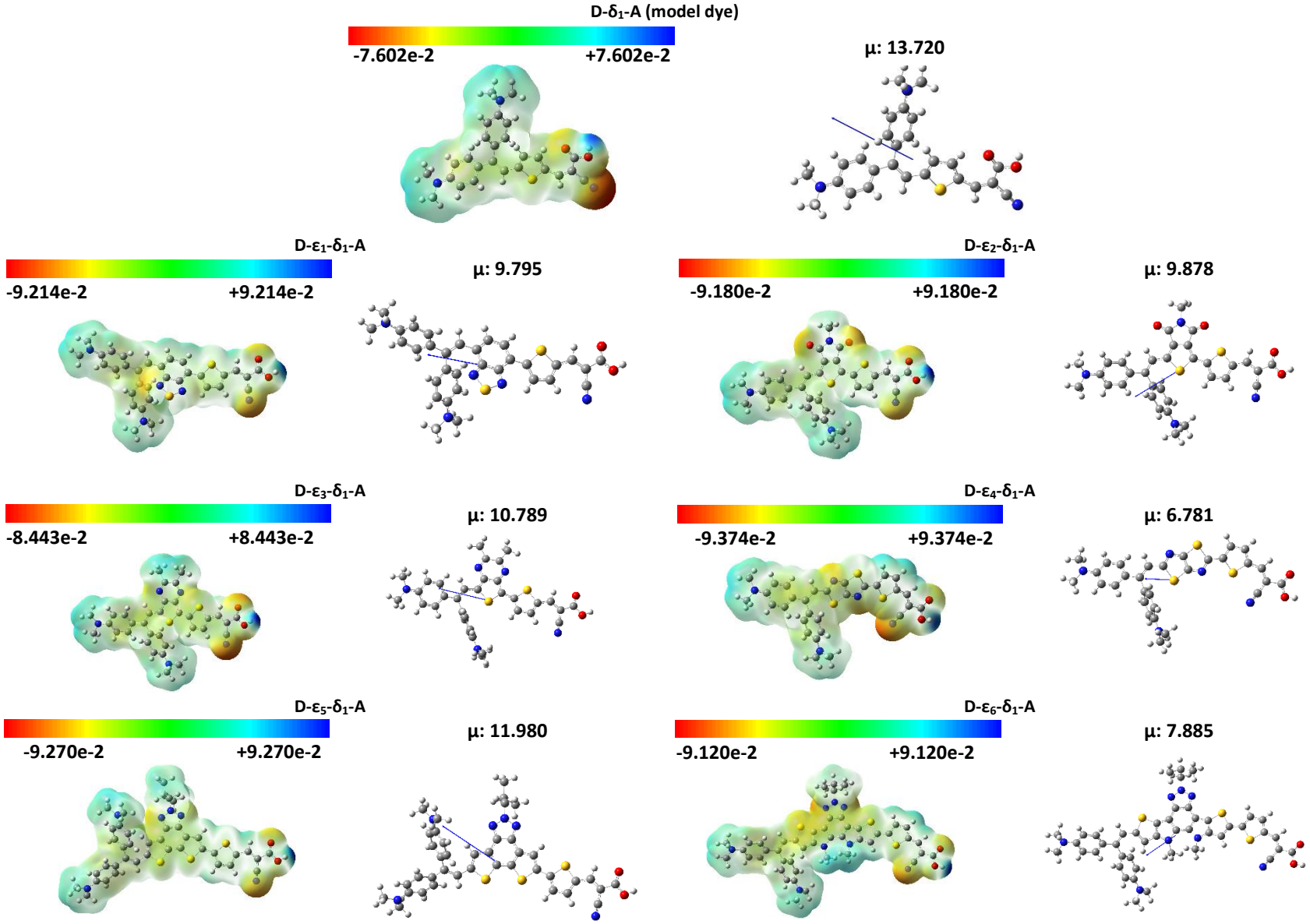


Table S7 (*cont.*). Electrostatic potential (ESP) map representing the corresponding charge density distributions isodensity (0.001e/Bohr^3) and calculated dipole moment vector [M06-2X/6-31G(d,p) solvent model: CPCM, $\varepsilon_{ethanol}$ =24.55].

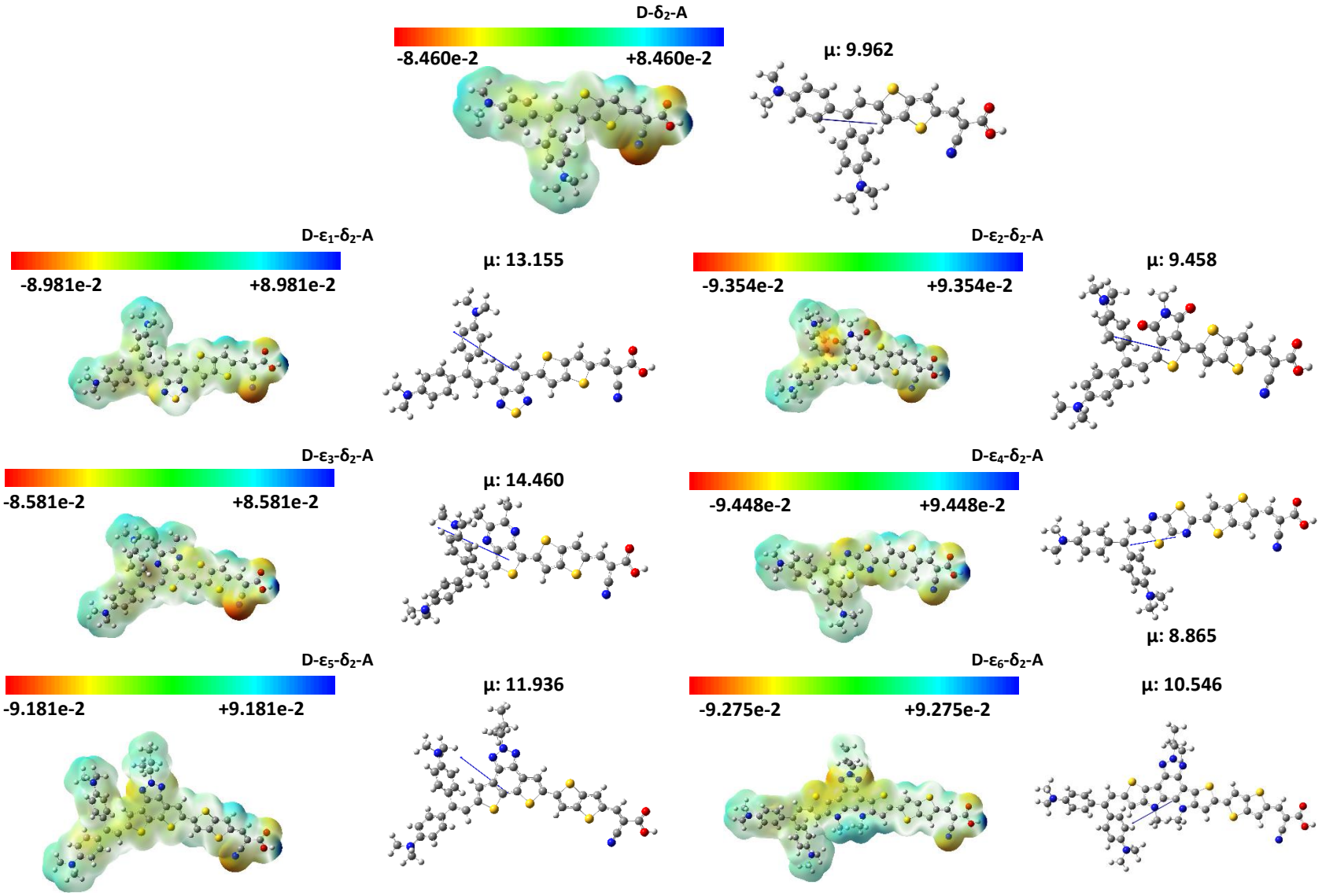
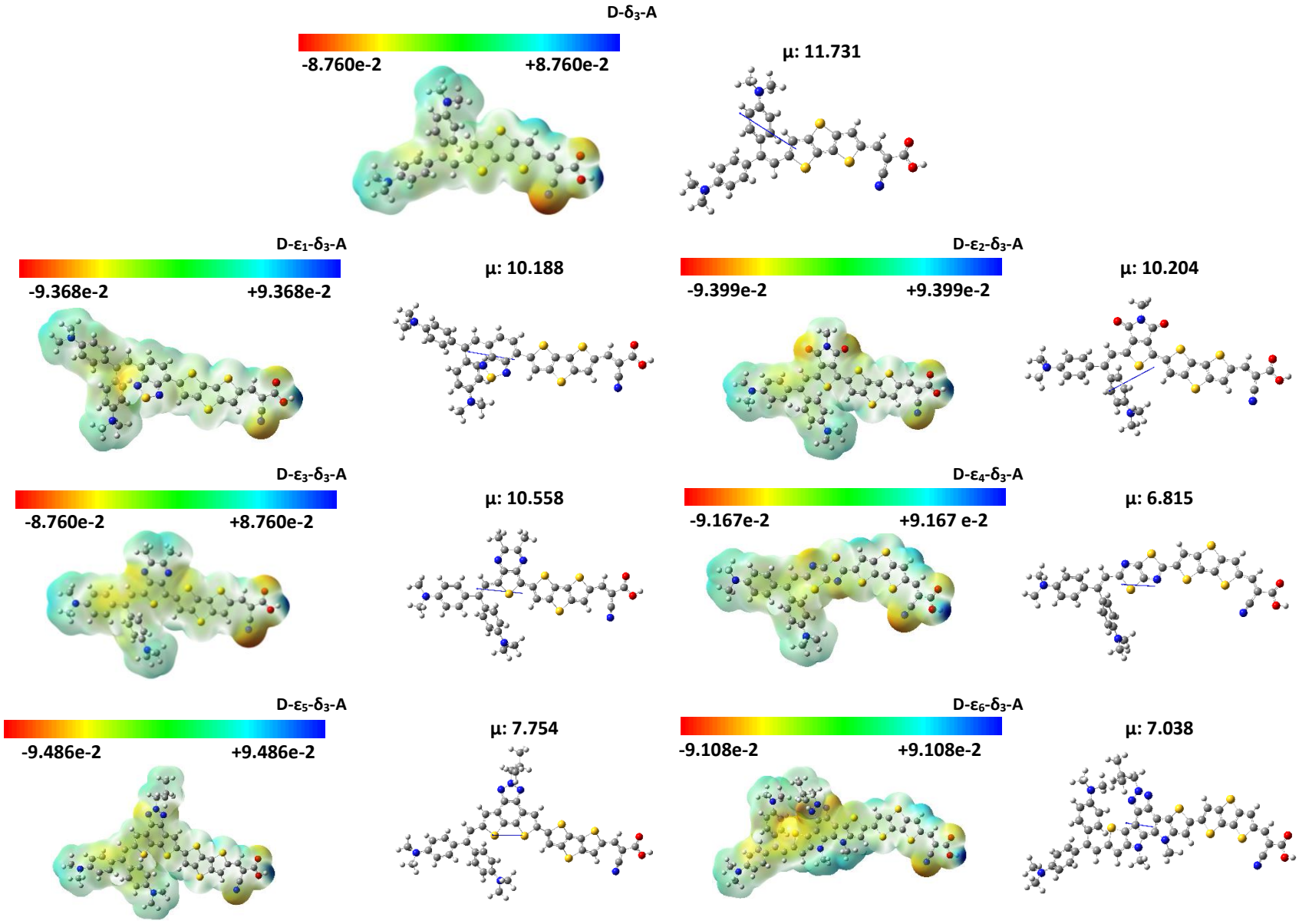


Table S7 (*cont.*). Electrostatic potential (ESP) map representing the corresponding charge density distributions isodensity (0.001e/Bohr^3) and calculated dipole moment vector [M06-2X/6-31G(d,p) solvent model: CPCM, $\varepsilon_{ethanol}$ =24.55].



S4. Natural bond orbital (NBO) analysis

To investigate the charge distribution and electron transfer patterns of the target dye molecules, a Natural Bond Orbital (NBO) analysis was performed using the optimized geometries of the ground state (S0). This analysis provides a deeper understanding of the electronic structure and properties of the molecules under study, thereby shedding light on their potential applications in various chemical reactions. The natural charges calculated on the atoms of the dye molecules' fragments provide valuable insights into the intramolecular charge delocalization within the molecules. These natural charge values were determined for different fragments of the molecules, including the donor (q^{Donor}), π-bridge (q^{ε}, q^{δ}), acceptor ($q^{Acceptor}$), and the difference in natural charges between the donor and acceptor fragments (Δq^{D-A}). The obtained results for these natural charges are presented in the below given table providing detailed information on the charge distribution and delocalization within the dye molecules. As anticipated, the acceptor units of all the investigated systems exhibited the highest negative charges. The positive charge difference values (Δq^{D-A}) between the donor and acceptor units provide compelling evidence for successful charge separation, with higher values indicating more effective charge separation. The obtained values indicate that the series of dyes with the thiophene (δ_1), thieno[3,2-b]thiophene (δ_2) fragments exhibit robust charge separation, suggesting the impact of the electron-withdrawing properties of the δ_1 and δ_2 units, which promote charge separation in the photosensitizer systems. It is worth noting that all candidates demonstrated better charge separation than the model dye molecule.

Entry	q^{donor}	q^{π}		$q^{acceptor}$	Δq^{d-a}
		q^{ε}	q^{δ}		
D-δ_1-A	0.12561	-	0.08067	-0.20626	0.33187
D-ε_1-δ_1-A	0.09875	-0.06794	0.10537	-0.13616	0.23491
D-ε_2-δ_1-A	0.16072	-0.14707	0.11274	-0.12637	0.28709
D-ε_3-δ_1-A	0.12255	-0.01259	0.07107	-0.18103	0.30358
D-ε_4-δ_1-A	0.12760	-0.10361	0.09401	-0.11800	0.24560
D-ε_5-δ_1-A	0.07509	-0.033	0.09218	-0.13396	0.20905
D-ε_6-δ_1-A	0.04474	0.03516	0.07417	-0.15409	0.19883
D-δ_2-A	0.10169	-	0.06672	-0.16842	0.27011
D-ε_1-δ_2-A	0.10478	-0.07987	0.11668	-0.14159	0.24637
D-ε_2-δ_2-A	0.13585	-0.13762	0.13123	-0.12947	0.26532
D-ε_3-δ_2-A	0.09818	-0.01378	0.08064	-0.16502	0.26320
D-ε_4-δ_2-A	0.12115	-0.11358	0.11551	-0.12309	0.24424
D-ε_5-δ_2-A	0.07442	-0.04644	0.10827	-0.13625	0.21067
D-ε_6-δ_2-A	0.04387	0.00855	0.09064	-0.14307	0.18694
D-δ_3-A	0.08576	-	0.07175	-0.15748	0.24324
D-ε_1-δ_3-A	0.09036	-0.08194	0.12906	-0.13748	0.22784
D-ε_2-δ_3-A	0.15182	-0.16541	0.14496	-0.13133	0.28315
D-ε_3-δ_3-A	0.10225	-0.03768	0.0883	-0.15288	0.25513
D-ε_4-δ_3-A	0.11932	-0.12202	0.13239	-0.12967	0.24899
D-ε_5-δ_3-A	0.07717	-0.06192	0.11939	-0.13463	0.21180
D-ε_6-δ_3-A	0.04311	-0.00118	0.10137	-0.14333	0.18644

Table S8. Absorption wavelengths (λ, nm) oscillator strengths (*f*), and the orbitals of the investigated molecules involved in the transitions [M06-2x/6-31G(d,p) solvent model: CPCM, $\varepsilon_{ethanol}$ = 24.55].

Entry	λ	*f*	Transitions (%) *(only major contributions are indicated)*
D-δ$_1$-A **(*model dye*)**	***481***	***1.24***	HOMO→LUMO (91%)
	373	0.37	HOMO-1→LUMO (91%)
	316	0.11	HOMO-2→LUMO (83%)
D-ε$_1$-δ$_1$-A	***514***	***0.86***	HOMO→LUMO (79%), HOMO→LUMO+1 (10%)
	402	0.59	HOMO-2→LUMO (26%), HOMO-1→LUMO (54%)
	372	0.13	HOMO-2→LUMO (28%), HOMO-1→LUMO (28%), HOMO→LUMO+1 (31%)
D-ε$_2$-δ$_1$-A	***490***	***1.18***	HOMO-2→LUMO (10%), HOMO→LUMO (76%)
	388	0.32	HOMO-1→LUMO (76%), HOMO-1→LUMO+1 (15%)
	385	0.33	HOMO→LUMO+1 (81%)
D-ε$_3$-δ$_1$-A	***593***	***1.30***	HOMO→LUMO (91%)
	410	0.24	HOMO-1→LUMO (82%)
	398	0.16	HOMO→LUMO+1 (75%)
D-ε$_4$-δ$_1$-A	***483***	***1.50***	HOMO-2→LUMO (13%), HOMO→LUMO (73%), HOMO→LUMO+1 (10%)
	377	0.27	HOMO-1→LUMO (75%), HOMO-1→LUMO+1 (17%)
	360	0.13	HOMO-2→LUMO (40%), HOMO→LUMO+1 (42%)
D-ε$_5$-δ$_1$-A	***477***	***1.80***	HOMO-2→LUMO (18%), HOMO→LUMO (65%), HOMO→LUMO+1 (12%)
	379	0.09	HOMO-2→LUMO (38%), HOMO→LUMO+1 (44%)
	351	0.43	HOMO-2→LUMO (26%), HOMO→LUMO (31%), HOMO→LUMO+1 (28%)
D-ε$_6$-δ$_1$-A	***506***	***1.97***	HOMO-1→LUMO (19%), HOMO→LUMO (68%)
	391	0.60	HOMO-1→LUMO (18%), HOMO→LUMO+1 (64%)
	362	0.38	HOMO-4→LUMO (10%), HOMO-1→LUMO (36%), HOMO→LUMO (29%), HOMO→LUMO+1 (17%)
D-ε$_2$-A	***486***	***1.30***	HOMO→LUMO (88%)
	365	0.39	HOMO-1→LUMO (87%)
	330	0.13	HOMO-2→LUMO (74%), HOMO→LUMO+1 (15%)
D-ε$_2$-δ$_2$-A	***533***	***1.32***	HOMO→LUMO (80%), HOMO→LUMO+1 (10%)
	393	0.66	HOMO-2→LUMO (40%), HOMO-1→LUMO (16%), HOMO→LUMO+1 (31%)
	383	0.52	HOMO-1→LUMO (63%), HOMO→LUMO+1 (18%)
D-ε$_2$-δ$_2$-A	***474***	***1.43***	HOMO-2→LUMO (15%), HOMO→LUMO (67%), HOMO→LUMO+1 (14%)
	393	0.12	HOMO-2→LUMO (11%), HOMO-→LUMO+1 (69%)
	370	0.52	HOMO-2-→LUMO (46%), HOMO-1→LUMO (27%), HOMO→LUMO (12%)
D-ε$_3$-δ$_2$-A	***574***	***1.34***	HOMO→LUMO (84%)
	420	051	HOMO-2→LUMO (31%), HOMO-1→LUMO (19%), HOMO→LUMO+1 (35%)
	392	0.12	HOMO-1→LUMO (38%), HOMO→LUMO+1 (37%)
D-ε$_4$-δ$_2$-A	***475***	***2.05***	HOMO-2→LUMO (17%), HOMO→LUMO (65%), HOMO→LUMO+1 (14%)
	374	0.16	HOMO-2→LUMO (42%), HOMO-1→LUMO (10%), HOMO→LUMO+1 (29%)
	364	0.13	HOMO-1→LUMO (60%), HOMO-1→LUMO+1 (20%)
D-ε$_5$-δ$_2$-A	***471***	***2.03***	HOMO-2→LUMO (19%), HOMO→LUMO (59%), HOMO→LUMO+1 (17%)
	384	0.27	HOMO-2→LUMO (36%), HOMO→LUMO+1 (43%)
	355	0.40	HOMO-2→LUMO (24%), HOMO→LUMO (38%), HOMO→LUMO+1 (23%)
D-ε$_6$-δ$_2$-A	***492***	***2.37***	HOMO-1→LUMO (19%), HOMO→LUMO (62%), HOMO→LUMO+1 (10%)
	395	0.42	HOMO-1→LUMO (13%), HOMO→LUMO+1 (62%), HOMO→LUMO+2 (11%)
	368	0.53	HOMO-4→LUMO (17%), HOMO-1→LUMO (31%), HOMO→LUMO (35%)

Table S8 (*cont.*). Absorption wavelengths (λ, nm) oscillator strengths (*f*), and the orbitals of the investigated molecules involved in the transitions [M06-2x/6-31G(d,p) solvent model: CPCM, $\varepsilon_{ethanol}$ = 24.55].

Entry	λ	*f*	**Transitions (%)** *(only major contributions are indicated)*
D-δ$_3$-A	***485***	***1.55***	HOMO→LUMO (83%)
	356	0.23	HOMO-2→LUMO (14%), HOMO-1→LUMO (69%), HOMO-1→LUMO+1 (11%)
	345	0.07	HOMO-2→LUMO (43%), HOMO-1→LUMO (14%), HOMO→LUMO+1 (24%)
D-ε$_1$-δ$_3$-A	***505***	***1.24***	HOMO→LUMO (63%), HOMO→LUMO+1 (23%)
	413	0.79	HOMO-2→LUMO (51%), HOMO-1→LUMO (10%), HOMO→LUMO+1 (25%)
	378	0.06	HOMO-1→LUMO (44%), HOMO-1→LUMO+1 (21%), HOMO→LUMO+1 (16%)
D-ε$_2$-δ$_3$-A	***486***	***1.75***	HOMO-2→LUMO (16%), HOMO→LUMO (62%), HOMO→LUMO+1 (18%)
	397	0.29	HOMO-2→LUMO (31%), HOMO→LUMO+1 (51%)
	376	0.45	HOMO-1→LUMO (50%), HOMO-1→LUMO+1 (24%)
D-ε$_3$-δ$_3$-A	***585***	***1.60***	HOMO→LUMO (80%), HOMO→LUMO+1 (13%)
	430	0.31	HOMO-2→LUMO (13%), HOMO→LUMO+1 (69%)
	393	0.18	HOMO-2→LUMO (14%), HOMO-1→LUMO (60%), HOMO-1→LUMO+1 (15%)
D-ε$_4$-δ$_3$-A	***475***	***2.04***	HOMO-2→LUMO (19%), HOMO→LUMO (59%), HOMO→LUMO+1 (17%)
	383	0.33	HOMO-2→LUMO (44%), HOMO→LUMO+1 (36%)
	360	0.26	HOMO-1→LUMO (58%), HOMO-1→LUMO+1 (29%)
D-ε$_5$-δ$_3$-A	***466***	***2.08***	HOMO-2→LUMO (24%), HOMO→LUMO (49%), HOMO→LUMO+1 (19%)
	393	0.32	HOMO-3→LUMO (10%), HOMO-2→LUMO (35%), HOMO→LUMO+1 (43%)
	360	0.40	HOMO-2→LUMO (16%), HOMO→LUMO (46%), HOMO→LUMO+1 (22%)
D-ε$_6$-δ$_3$-A			HOMO-1→LUMO (20%), HOMO→LUMO (58%), HOMO→LUMO+1 (11%)
	491	***2.53***	HOMO-4→LUMO (11%), HOMO-1→LUMO (14%), HOMO→LUMO+1 (54%),
	394	0.52	HOMO→LUMO+2 (14%)
	371	0.60	HOMO-4→LUMO (18%), HOMO-1→LUMO (22%), HOMO→LUMO (39%),
			HOMO→LUMO+1 (12%)

Table S9. (a) PDOS plots for the studied photosensitizers (b) Density of state (DOS) plots and bandgap values. [M06-2x/6-31G(d,p) solvent model: CPCM, $\varepsilon_{ethanol}$ = 24.55].

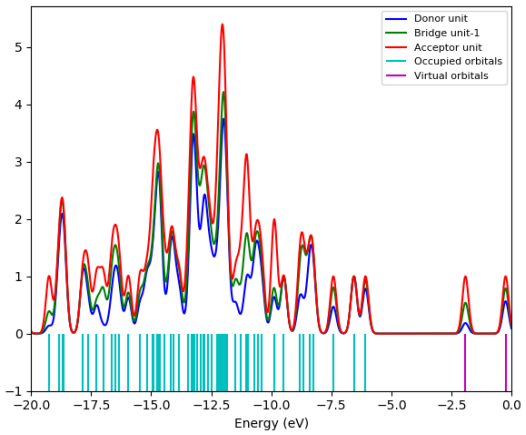
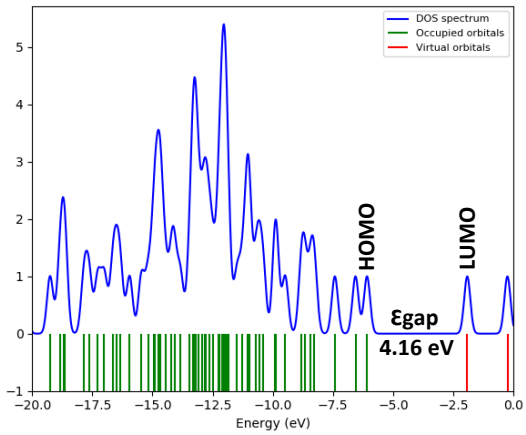
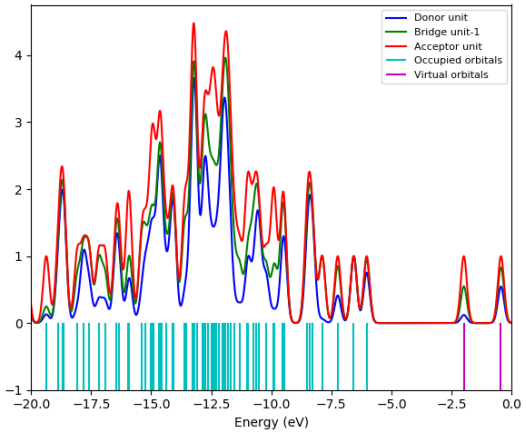
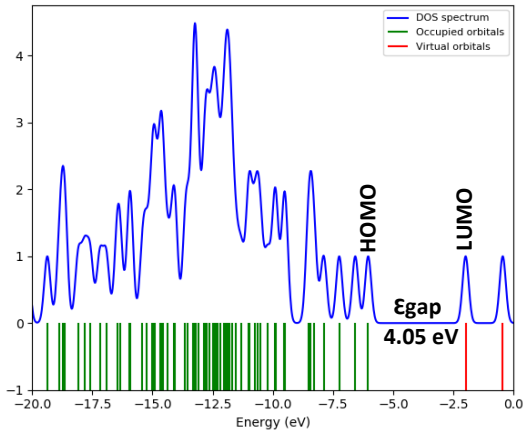
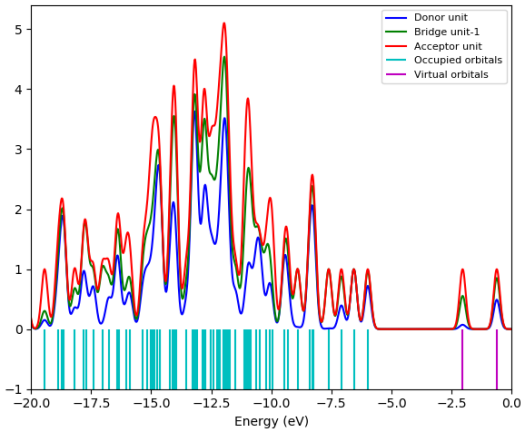
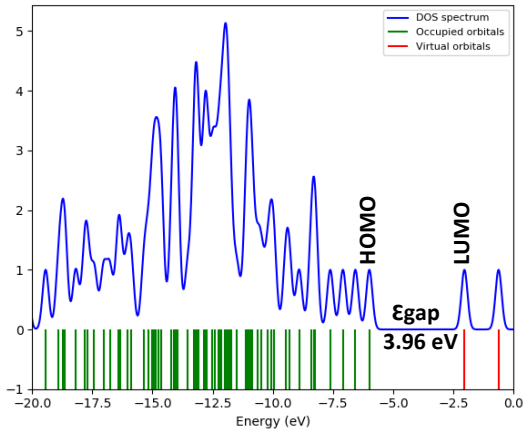
Entry	PDOS	DOS
D-δ1-A (model dye)		
D-δ2-A		
D-δ3-A		

Table S9 (*cont.*). (a) PDOS plots for the studied photosensitizers (b) Density of state (DOS) plots and bandgap values. [M06-2x/6-31G(d,p) solvent model: CPCM, $\varepsilon_{ethanol}$ = 24.55].

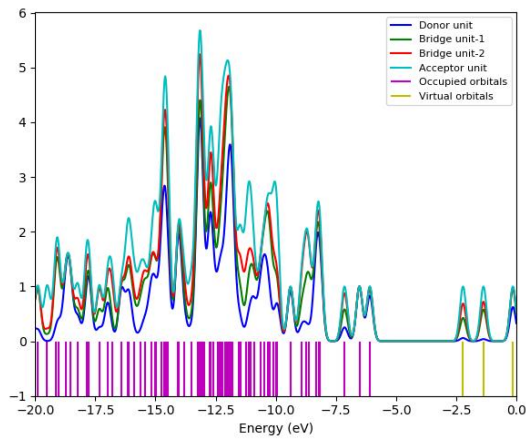
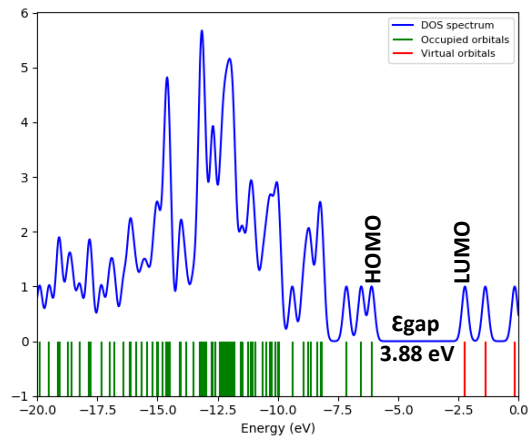
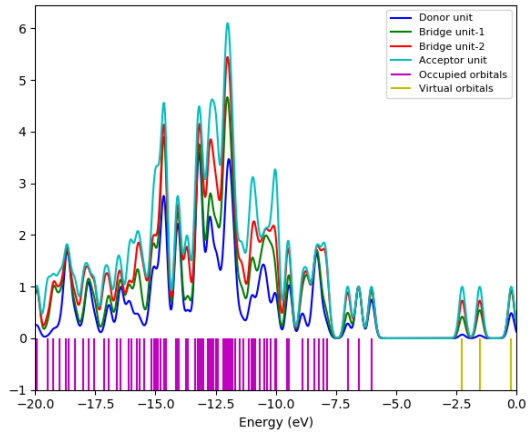
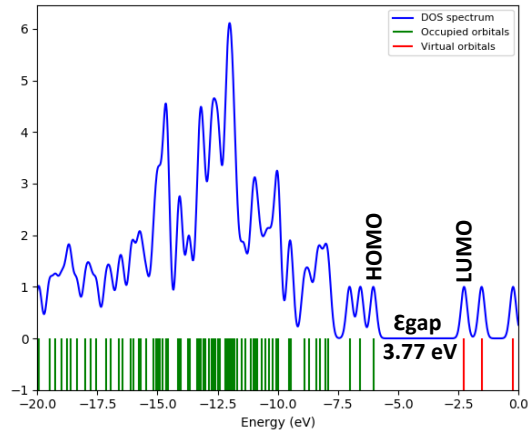
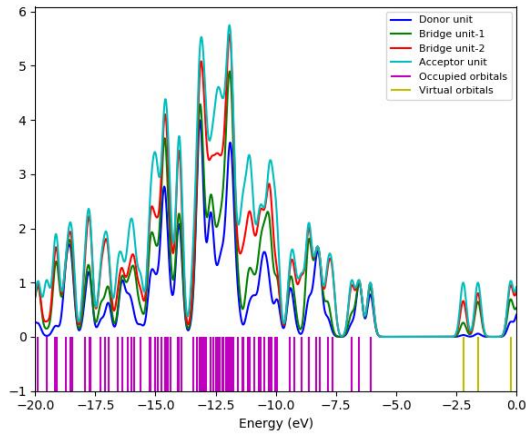
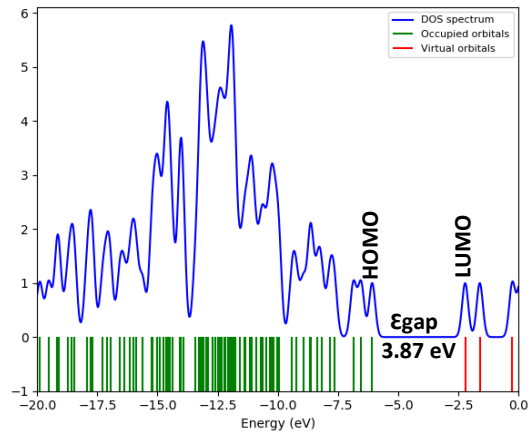
Entry	PDOS	DOS
D-ε₁-δ₁-A		
D-ε₁-δ₂-A		
D-ε₁-δ₃-A		

Table S9 (*cont.*). (a) PDOS plots for the studied photosensitizers (b) Density of state (DOS) plots and bandgap values. [M06-2x/6-31G(d,p) solvent model: CPCM, $\varepsilon_{ethanol}$ = 24.55].

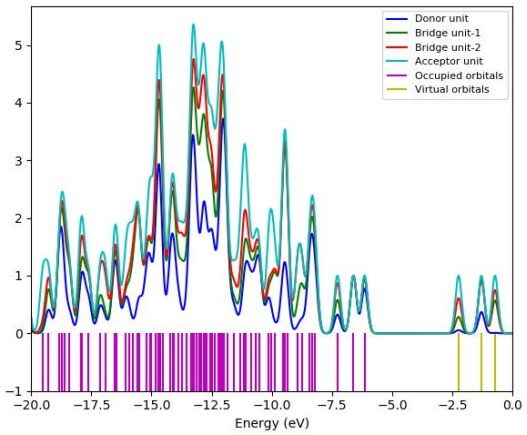
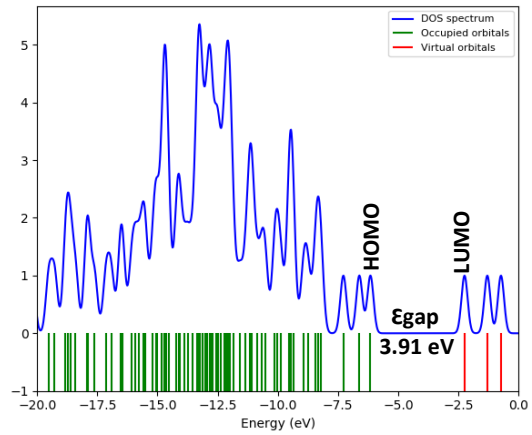
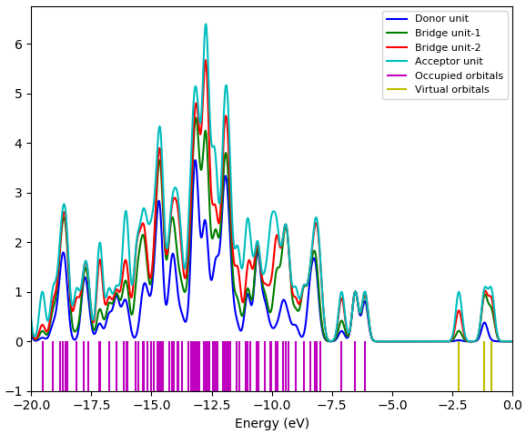
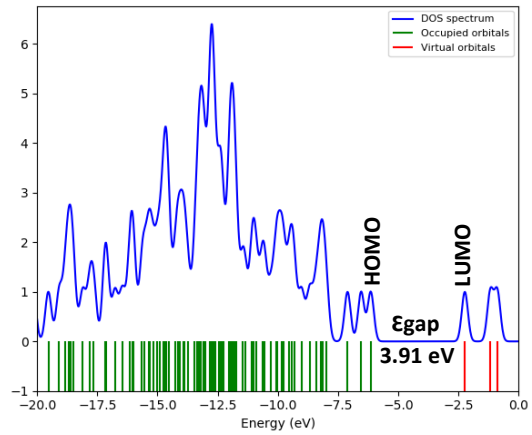
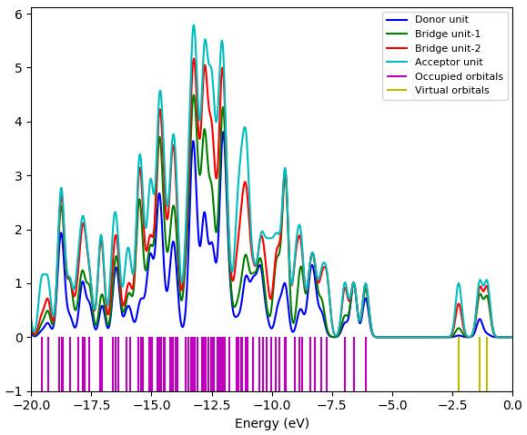
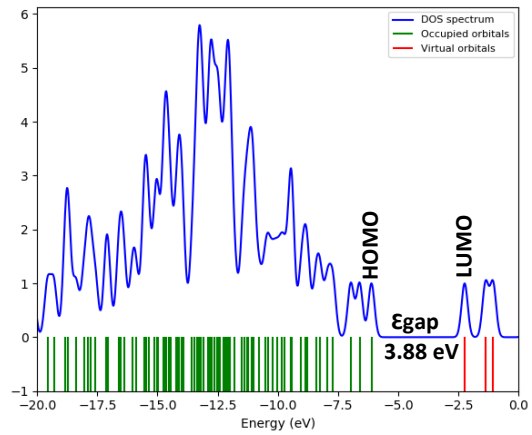
Entry	PDOS	DOS
D-ε₂-δ₁-A		
D-ε₂-δ₂-A		
D-ε₂-δ₃-A		

Table S9 (*cont.*). (a) PDOS plots for the studied photosensitizers (b) Density of state (DOS) plots and bandgap values. [M06-2x/6-31G(d,p) solvent model: CPCM, $\varepsilon_{ethanol}$ = 24.55].

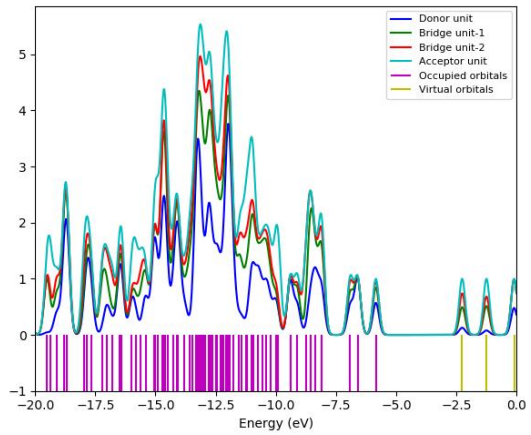
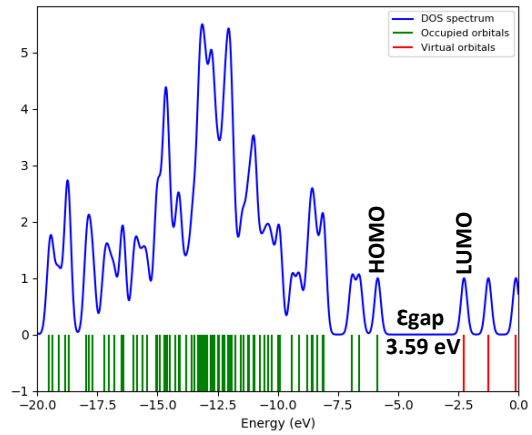
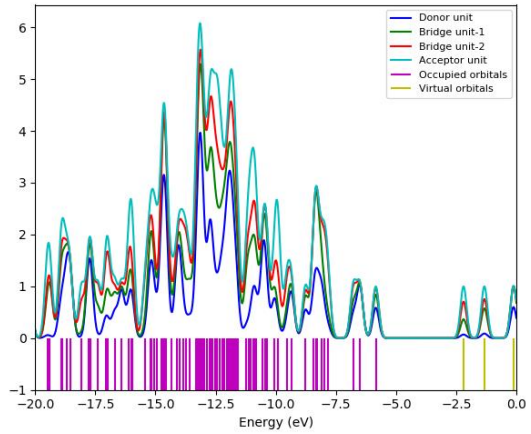
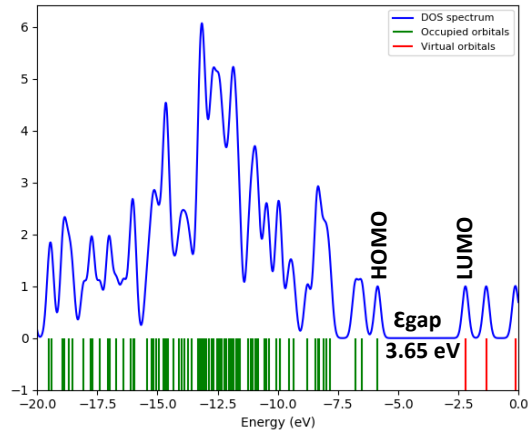
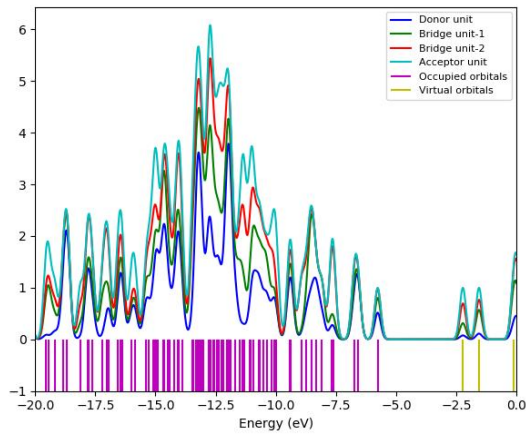
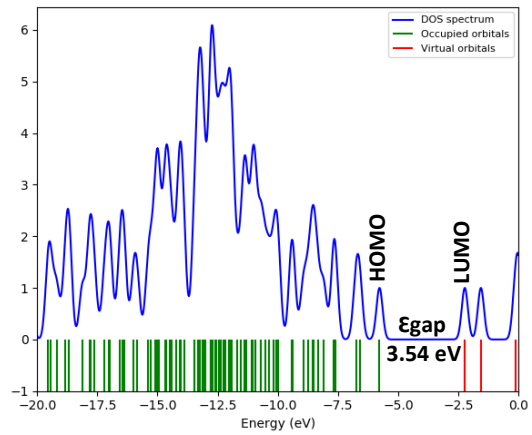
Entry	PDOS	DOS
D-ε3-δ1-A		
D-ε3-δ2-A		
D-ε3-δ3-A		

Table S9 (*cont.*). (a) PDOS plots for the studied photosensitizers (b) Density of state (DOS) plots and bandgap values. [M06-2x/6-31G(d,p) solvent model: CPCM, $\varepsilon_{ethanol}$ = 24.55].

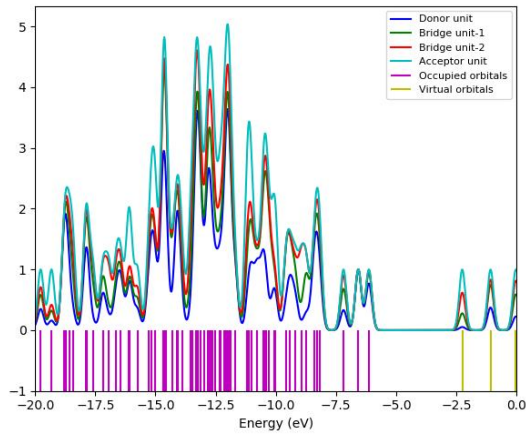
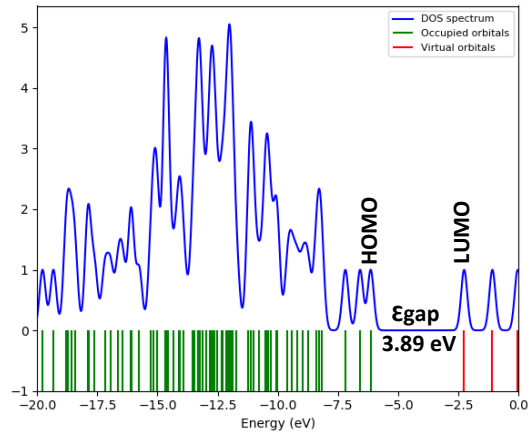
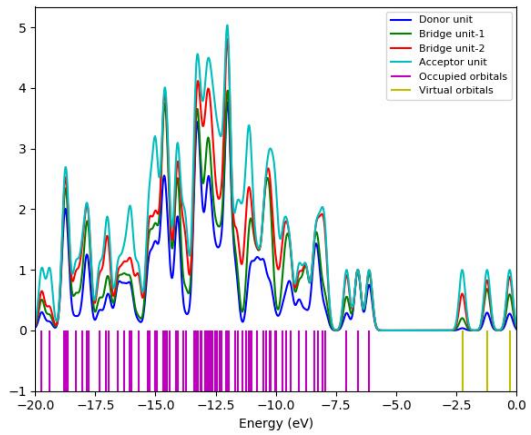
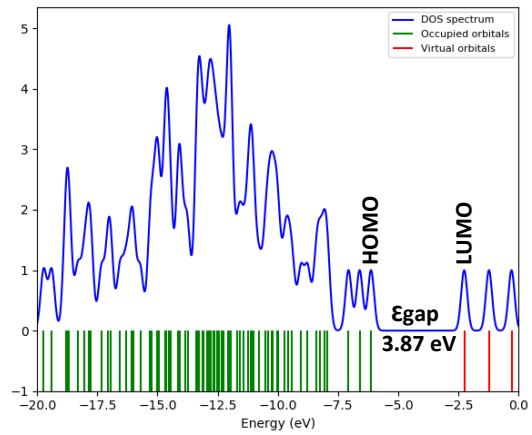
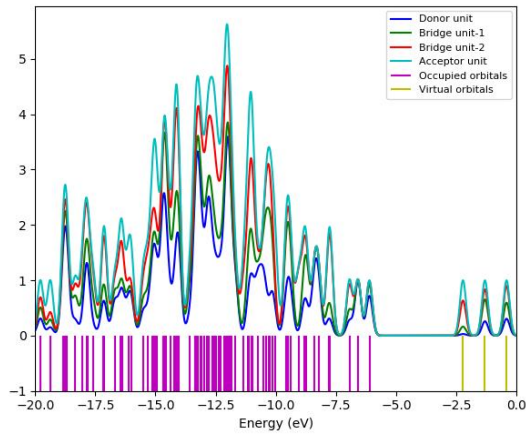
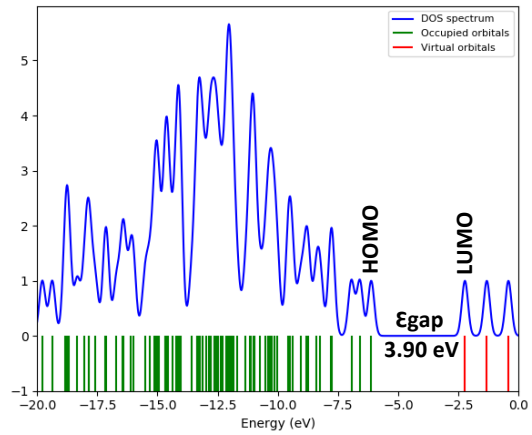
Entry	PDOS	DOS
D-ε4-δ1-A		
D-ε4-δ2-A		
D-ε4-δ3-A		

Table S9 (*cont.*). (a) PDOS plots for the studied photosensitizers (b) Density of state (DOS) plots and bandgap values. [M06-2x/6-31G(d,p) solvent model: CPCM, $\varepsilon_{ethanol}$ = 24.55].

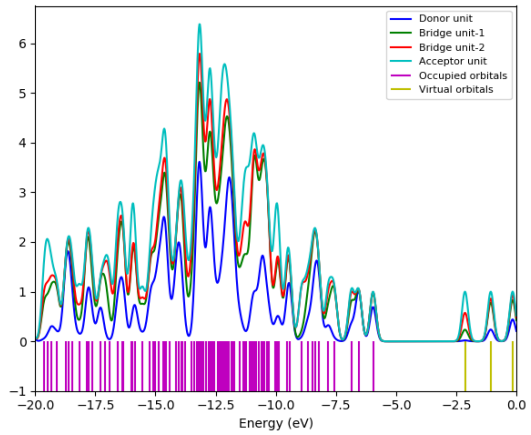
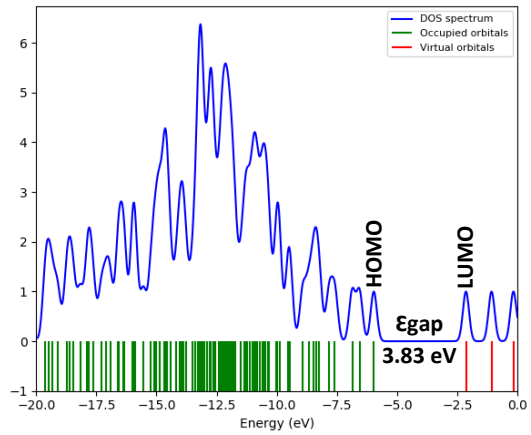
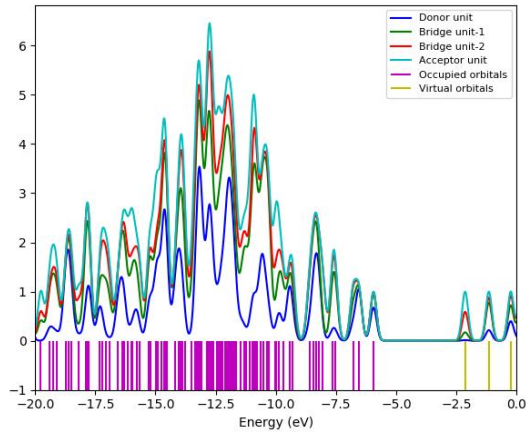
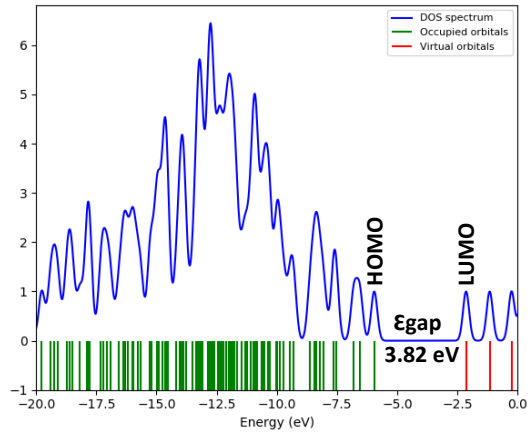
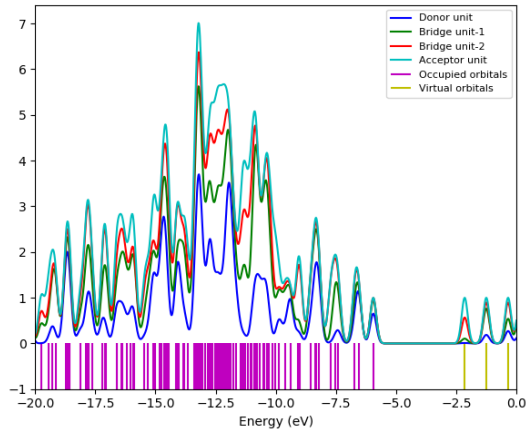
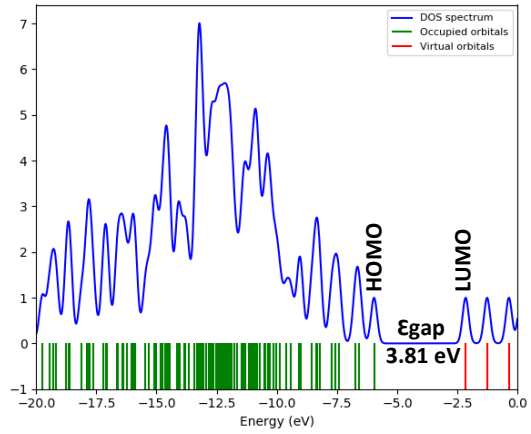
Entry	PDOS	DOS
D-ε5-δ1-A		
D-ε5-δ2-A		
D-ε5-δ3-A		

Table S9 (*cont.*). (a) PDOS plots for the studied photosensitizers (b) Density of state (DOS) plots and bandgap values. [M06-2x/6-31G(d,p) solvent model: CPCM, $\varepsilon_{ethanol}$ = 24.55].

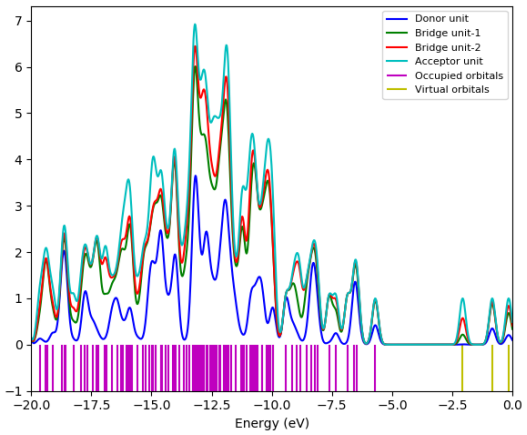
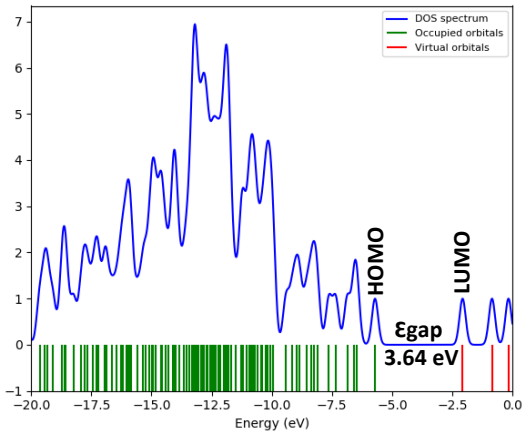
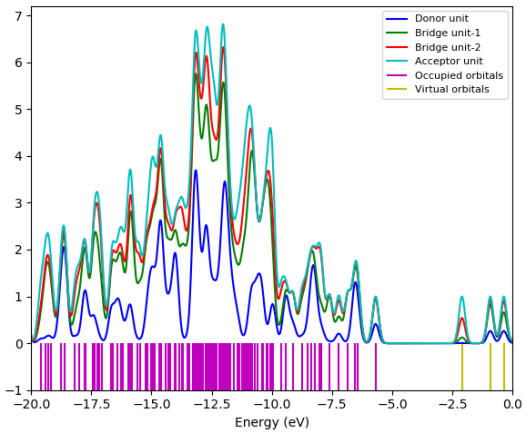
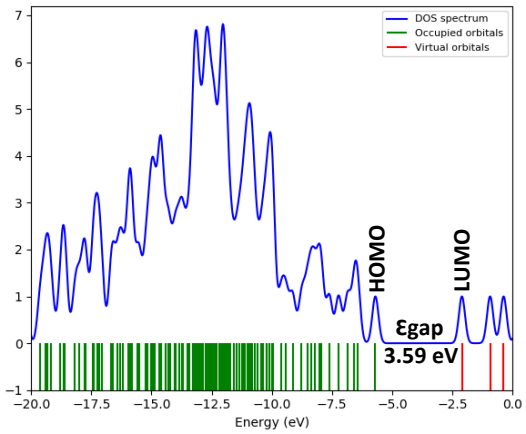
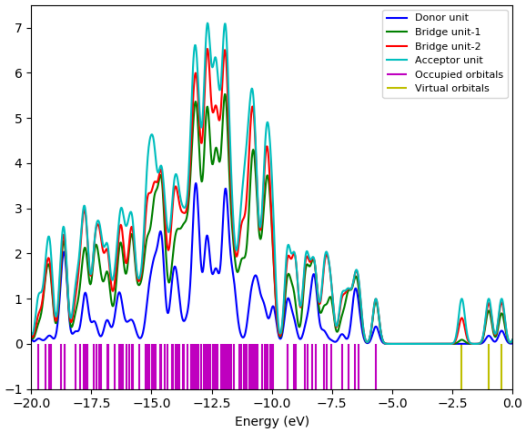
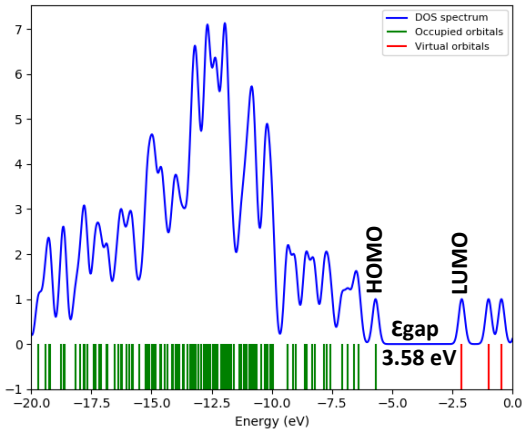
Entry	PDOS	DOS
D-ε$_6$-δ$_1$-A		
D-ε$_6$-δ$_2$-A		
D-ε$_6$-δ$_3$-A		

Table S10. Electron density differentiation maps (EDDMs) and the corresponding percent contributions of the different fragments on the investigated systems [M06-2x/6-31G(d,p) solvent model: CPCM, $\varepsilon_{ethanol} = 24.55$].

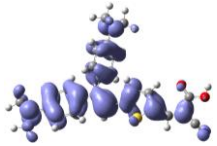
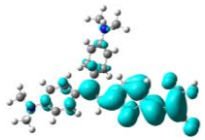
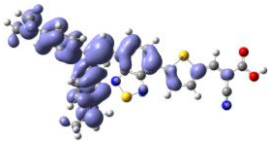
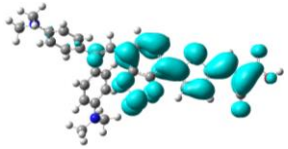
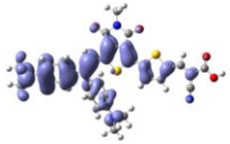
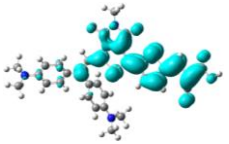
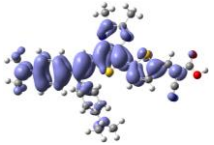
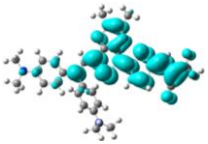
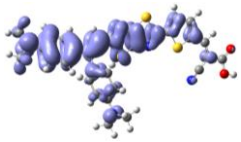
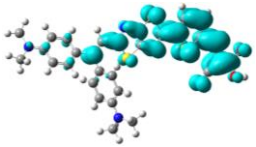
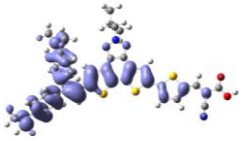
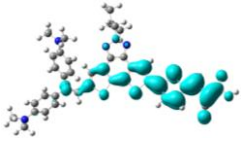
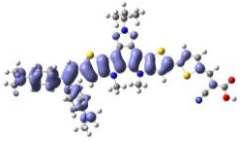
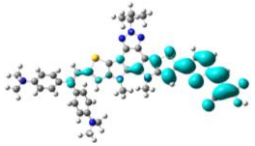
Entry	absorption λ_{max}	*f*	change	contribution %				EDDM BEFORE *(where the excited electron density is coming from)*	EDDM AFTER *(where the excited electron density is going to)*
				D	ε	δ	A		
D-δ$_1$-A (*model dye*)	481	1.24	**Before**	79	-	15	7		
			After	18	-	36	46		
			Net	**-61**	**-**	**21**	**39**		
D-ε$_1$-δ$_1$-A	514	0.86	**Before**	83	12	4	1		
			After	6	37	26	31		
			Net	**-77**	**25**	**22**	**30**		
D-ε$_2$-δ$_1$-A	490	1.18	**Before**	78	16	5	2		
			After	5	23	33	39		
			Net	**-73**	**7**	**28**	**37**		
D-ε$_3$-δ$_1$-A	593	1.30	**Before**	57	27	11	5		
			After	13	37	24	26		
			Net	**-44**	**10**	**13**	**21**		
D-ε$_4$-δ$_1$-A	483	1.50	**Before**	77	18	4	1		
			After	5	23	24	38		
			Net	**-72**	**5**	**20**	**37**		
D-ε$_5$-δ$_1$-A	477	1.80	**Before**	69	27	3	1		
			After	2	21	34	43		
			Net	**-67**	**-6**	**31**	**42**		
D-ε$_6$-δ$_1$-A	506	1.97	**Before**	42	53	3	1		
			After	1	21	36	43		
			Net	**-41**	**-32**	**33**	**42**		

Table S10 (*cont.*). Electron density differentiation maps (EDDMs) and the corresponding percent contributions of the different fragments on the investigated systems [M06-2x/6-31G(d,p) solvent model: CPCM, $\varepsilon_{ethanol} = 24.55$].

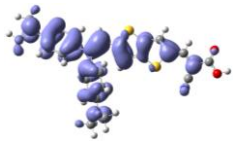
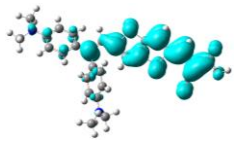
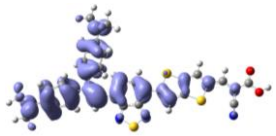
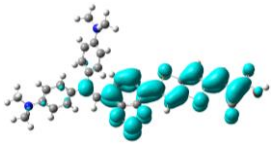
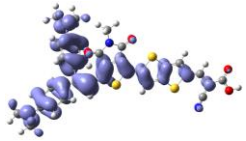
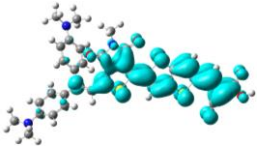
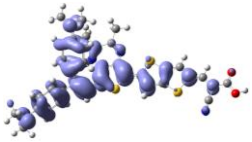
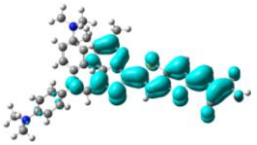
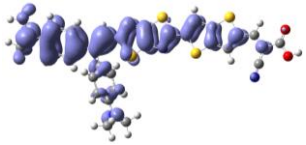
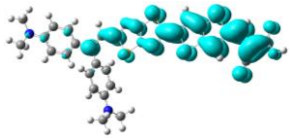
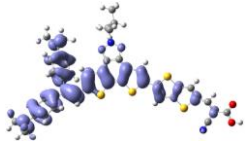
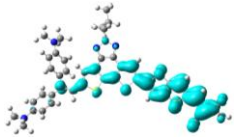
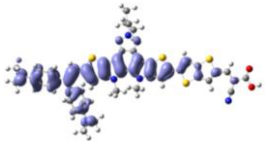
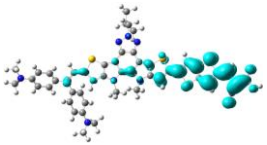
Entry	absorption λ_{max}	*f*	change	contribution %				EDDM BEFORE *(where the excited electron density is coming from)*	EDDM AFTER *(where the excited electron density is going to)*
				D	ε	δ	A		
D-δ$_2$-A	486	1.30	**Before**	75	-	20	5		
			After	12	-	43	45		
			Net	**-63**	**-**	**23**	**40**		
D-ε$_1$-δ$_2$-A	533	1.32	**Before**	75	16	7	2		
			After	7	35	31	27		
			Net	**-68**	**19**	**24**	**25**		
D-ε$_2$-δ$_2$-A	474	1.43	**Before**	80	13	5	1		
			After	3	19	41	38		
			Net	**-77**	**6**	**36**	**37**		
D-ε$_3$-δ$_2$-A	574	1.34	**Before**	59	25	13	3		
			After	7	29	34	29		
			Net	**-52**	**24**	**21**	**26**		
D-ε$_4$-δ$_2$-A	475	2.05	**Before**	75	19	5	1		
			After	4	17	40	39		
			Net	**-71**	**-2**	**35**	**38**		
D-ε$_5$-δ$_2$-A	471	2.03	**Before**	68	28	4	1		
			After	1	16	42	41		
			Net	**-67**	**-12**	**38**	**40**		
D-ε$_6$-δ$_2$-A	492	2.37	**Before**	41	54	4	1		
			After	0	12	42	46		
			Net	**-41**	**-42**	**38**	**45**		

Table S10 (*cont.*). Electron density differentiation maps (EDDMs) and the corresponding percent contributions of the different fragments on the investigated systems [M06-2x/6-31G(d,p) solvent model: CPCM, $\varepsilon_{ethanol} = 24.55$].

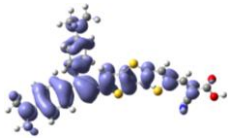
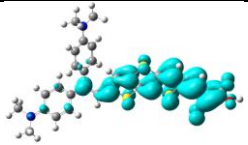
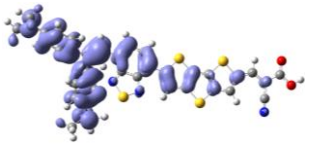
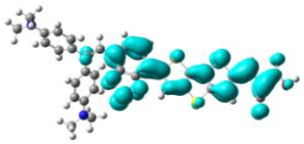
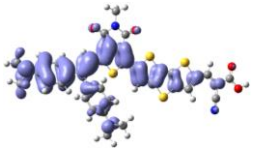
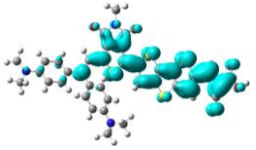
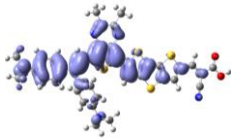
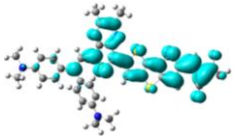
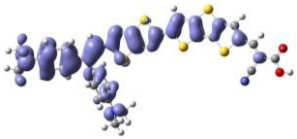
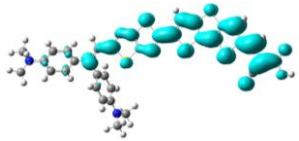
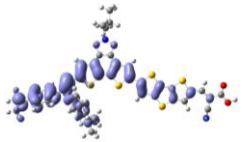
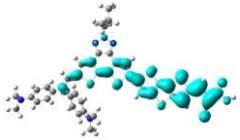
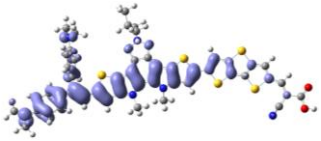
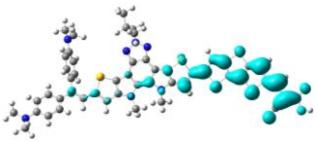
Entry	absorption λ_{max}	*f*	change	contribution %				EDDM BEFORE *(where the excited electron density is coming from)*	EDDM AFTER *(where the excited electron density is going to)*
				D	ε	δ	A		
D-δ$_3$-A	485	1.55	**Before**	72	-	25	3		
			After	7	-	48	45		
			Net	**-65**	**-**	**23**	**42**		
D-ε$_1$-δ$_3$-A	505	1.24	**Before**	78	13	8	1		
			After	3	23	40	34		
			Net	**-75**	**10**	**32**	**33**		
D-ε$_2$-δ$_3$-A	486	1.75	**Before**	72	17	9	1		
			After	3	14	45	38		
			Net	**-69**	**-3**	**36**	**37**		
D-ε$_3$-δ$_3$-A	585	1.6	**Before**	52	29	18	2		
			After	8	24	38	30		
			Net	**-44**	**-5**	**20**	**28**		
D-ε$_4$-δ$_3$-A	475	2.04	**Before**	72	20	7	1		
			After	3	13	47	37		
			Net	**-69**	**-7**	**40**	**36**		
D-ε$_5$-δ$_3$-A	466	2.08	**Before**	65	30	5	1		
			After	1	9	46	43		
			Net	**-64**	**-21**	**41**	**42**		
D-ε$_6$-δ$_3$-A	491	2.53	**Before**	39	55	5	1		
			After	0	9	48	43		
			Net	**-39**	**-46**	**43**	**42**		

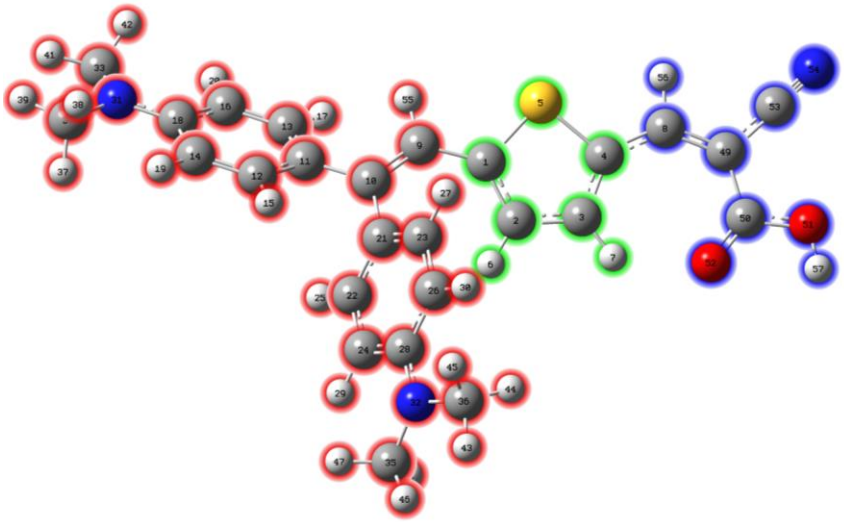
Table S11. Atom- and fragment-based electron-hole analysis of the investigated systems [M06-2x/6-31G(d,p) solvent model: CPCM, $\varepsilon_{ethanol}$ = 24.55].

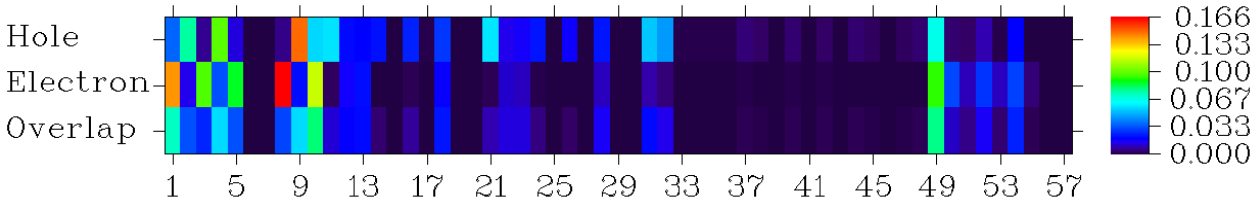
Entry	Hole (%)				Electron (%)				Overlap (%)				Difference (%)			
	D	Ɛ	δ	A	D	Ɛ	δ	A	D	Ɛ	δ	A	D	Ɛ	δ	A
D-δ_1-A	66.01	-	23.10	10.89	25.58	-	37.43	36.99	41.10	-	29.40	20.07	-40.43	-	14.33	26.10
D-δ_2-A	58.89	-	32.50	8.61	20.93	-	45.66	33.41	35.11	-	38.52	16.96	-37.95	-	13.16	24.80
D-δ_3-A	49.77	-	42.63	7.60	16.97	-	52.24	30.79	29.06	-	47.19	15.30	-32.80	-	9.61	23.19
D-ε_1-δ_1-A	67.19	20.94	8.79	3.08	11.03	59.09	16.64	13.24	27.22	35.17	12.09	6.39	-56.17	38.16	7.85	10.16
D-ε_1-δ_2-A	56.75	25.54	14.65	3.06	14.32	54.97	20.97	10.65	28.50	37.47	17.15	5.71	-42.44	29.44	5.42	7.58
D-ε_1-δ_3-A	56.81	21.54	19.05	2.60	10.13	58.04	22.59	9.24	23.99	35.36	20.75	4.90	-46.68	36.50	3.54	6.64
D-ε_2-δ_1-A	54.80	26.69	13.47	5.04	16.54	33.15	27.25	23.06	30.10	29.75	19.16	10.78	-38.26	6.46	13.78	18.02
D-ε_2-δ_2-A	51.92	23.19	20.04	4.85	13.31	32.98	33.74	19.98	26.28	27.66	26.00	9.84	-38.62	9.79	13.70	15.13
D-ε_2-δ_3-A	42.07	24.13	29.21	4.60	14.71	30.34	37.63	17.31	24.88	27.05	33.16	8.92	-27.35	6.21	8.42	12.72
D-ε_3-δ_1-A	43.62	34.42	15.42	6.54	16.21	45.11	21.30	17.38	26.59	39.41	18.12	10.66	-27.41	10.69	5.88	10.84
D-ε_3-δ_2-A	45.19	31.69	18.67	4.45	12.89	48.05	25.12	13.94	24.14	39.02	21.66	7.88	-32.30	16.37	6.45	9.49
D-ε_3-δ_3-A	38.08	33.71	24.97	3.25	14.83	44.92	28.58	11.67	23.76	38.91	26.71	6.16	-23.24	11.22	3.61	8.42
D-ε_4-δ_1-A	48.49	33.66	12.74	5.11	16.27	35.53	26.38	21.81	28.09	34.58	18.33	10.55	-32.22	1.87	13.64	16.71
D-ε_4-δ_2-A	42.75	31.41	20.94	4.91	15.48	33.39	31.49	19.63	25.73	32.38	25.68	9.81	-27.26	1.98	10.55	14.73
D-ε_4-δ_3-A	36.93	29.89	28.63	4.55	14.72	32.23	36.86	16.19	23.32	31.04	32.49	8.58	-22.21	2.35	8.23	11.63
D-ε_5-δ_1-A	34.00	47.11	13.59	5.30	9.98	39.04	26.61	24.36	18.43	42.89	19.01	11.37	-24.02	-8.06	13.03	19.06
D-ε_5-δ_2-A	32.20	44.22	18.97	4.61	10.66	37.54	31.49	20.32	18.53	40.74	24.44	9.68	-21.55	-6.68	12.52	15.70
D-ε_5-δ_3-A	26.07	39.96	29.05	4.93	8.98	32.86	37.39	20.76	15.30	36.24	32.95	10.12	-17.09	-7.09	8.34	15.84
D-ε_6-δ_1-A	12.69	66.74	14.32	6.25	4.46	33.86	32.18	29.50	7.53	47.53	21.47	13.57	-8.23	-32.88	17.86	23.25
D-ε_6-δ_2-A	12.10	61.58	21.13	5.20	4.41	28.32	38.66	28.61	7.30	41.76	28.58	12.19	-7.69	-33.25	17.53	23.41
D-ε_6-δ_3-A	9.52	56.68	28.91	4.88	3.35	25.73	46.01	24.92	5.65	38.19	36.47	11.03	-6.18	-30.95	17.09	20.03

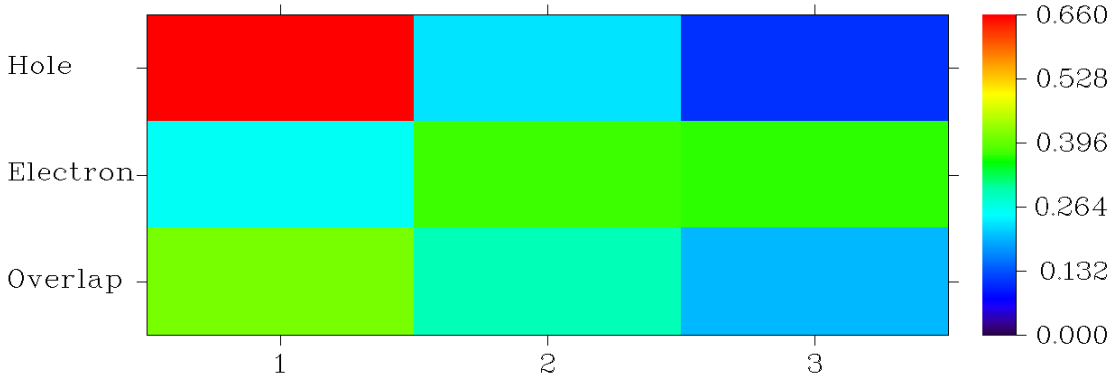
Table S12. Atom- and fragment-based electron-hole analysis of the investigated systems [M06-2x/6-31G(d,p) solvent model: CPCM, $\varepsilon_{ethanol}$ = 24.55].

D-δ_1-A

Fragment 1: Donor unit (D)-Atom indices: 9-48,55
Fragment 2: Bridge unit-1 (δ)-Atom indices: 1-7
Fragment 3: Acceptor unit (A)-Atom indices: 8,49-54,56-57





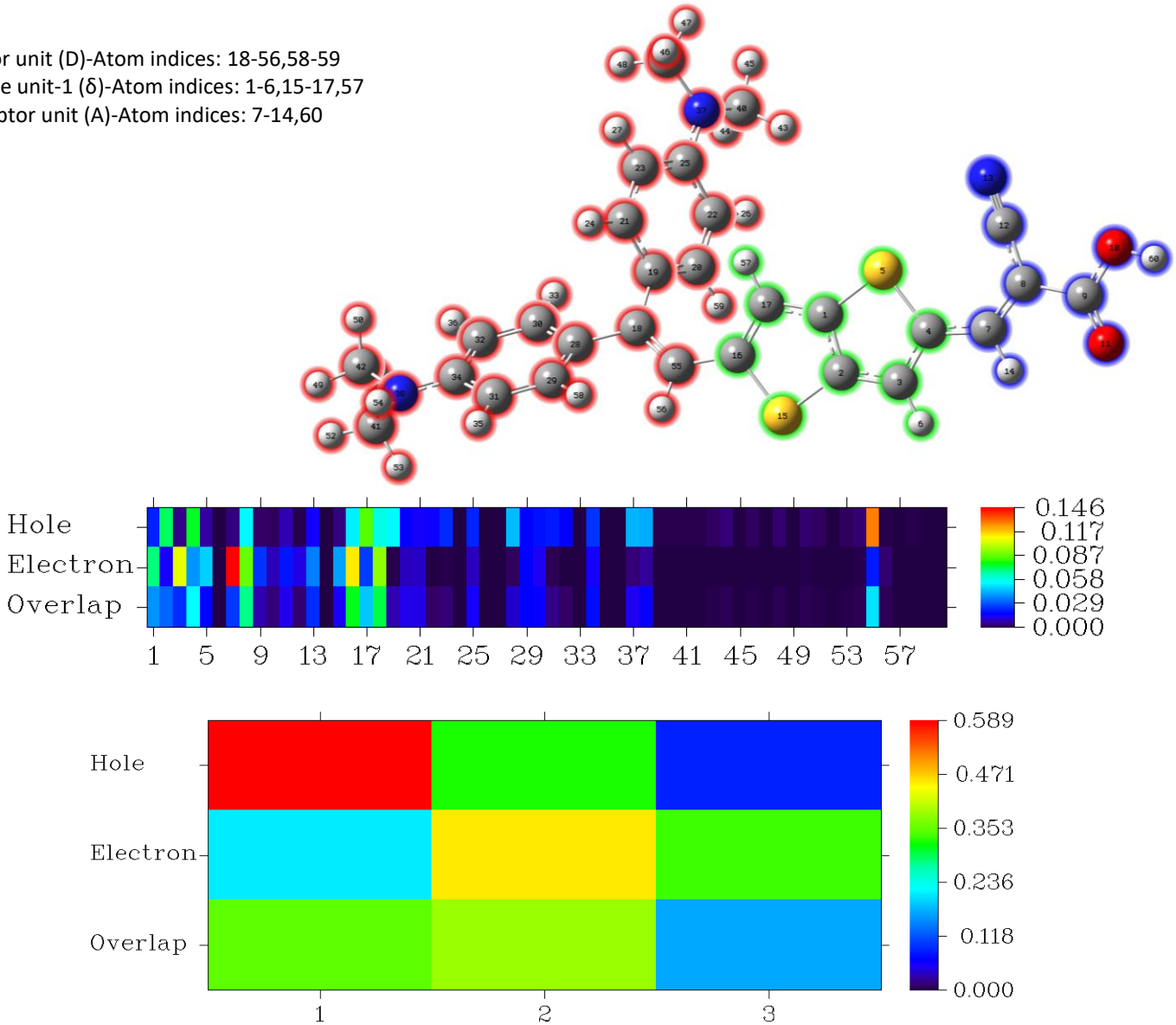


(***x-axis*** 1: Fragment 1, 2: Fragment 2, 3: Fragment 3)

Table S12 (*cont.*). Atom- and fragment-based electron-hole analysis of the investigated systems [M06-2x/6-31G(d,p) solvent model: CPCM, $\varepsilon_{ethanol}$ = 24.55].

D-δ_2-A

Fragment 1: Donor unit (D)-Atom indices: 18-56,58-59
Fragment 2: Bridge unit-1 (δ)-Atom indices: 1-6,15-17,57
Fragment 3: Acceptor unit (A)-Atom indices: 7-14,60

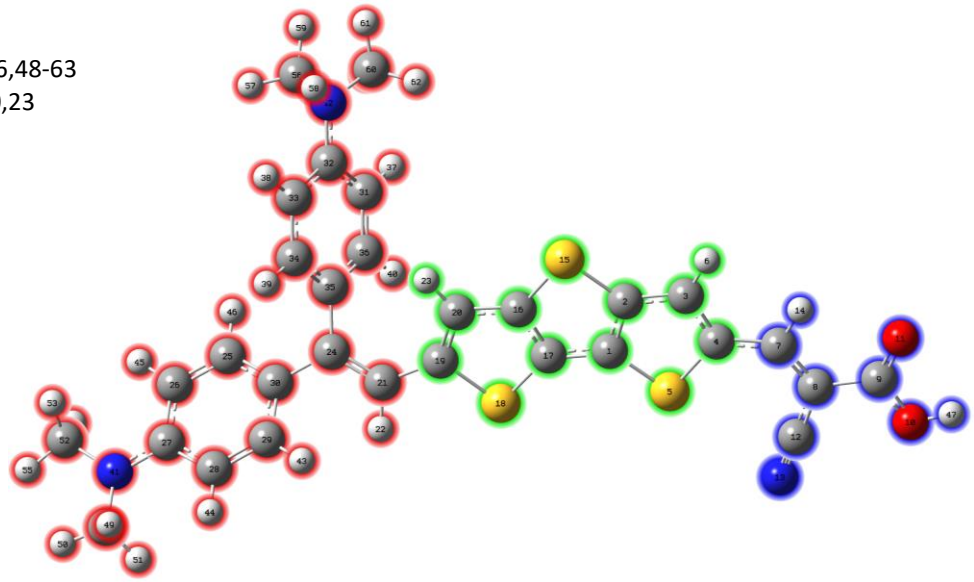


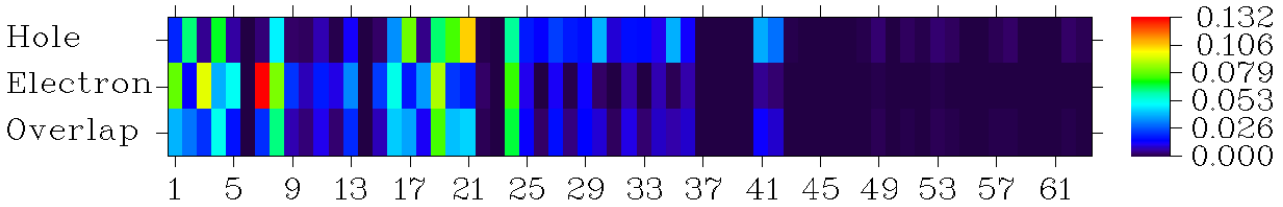
(***x-axis*** 1: Fragment 1, 2: Fragment 2, 3: Fragment 3)

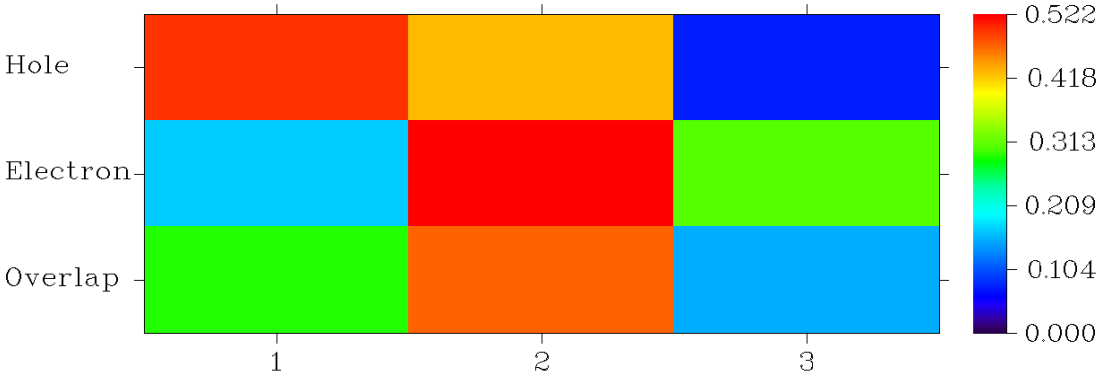
Table S12 (*cont.*). Atom- and fragment-based electron-hole analysis of the investigated systems [M06-2x/6-31G(d,p) solvent model: CPCM, $\varepsilon_{ethanol}$ = 24.55].

D-δ_3-A

Fragment 1: Donor unit (D)-Atom indices: 21-22,24-46,48-63
Fragment 2: Bridge unit-1 (δ)-Atom indices: 1-6,15-20,23
Fragment 3: Acceptor unit (A)-Atom indices: 7-14,47





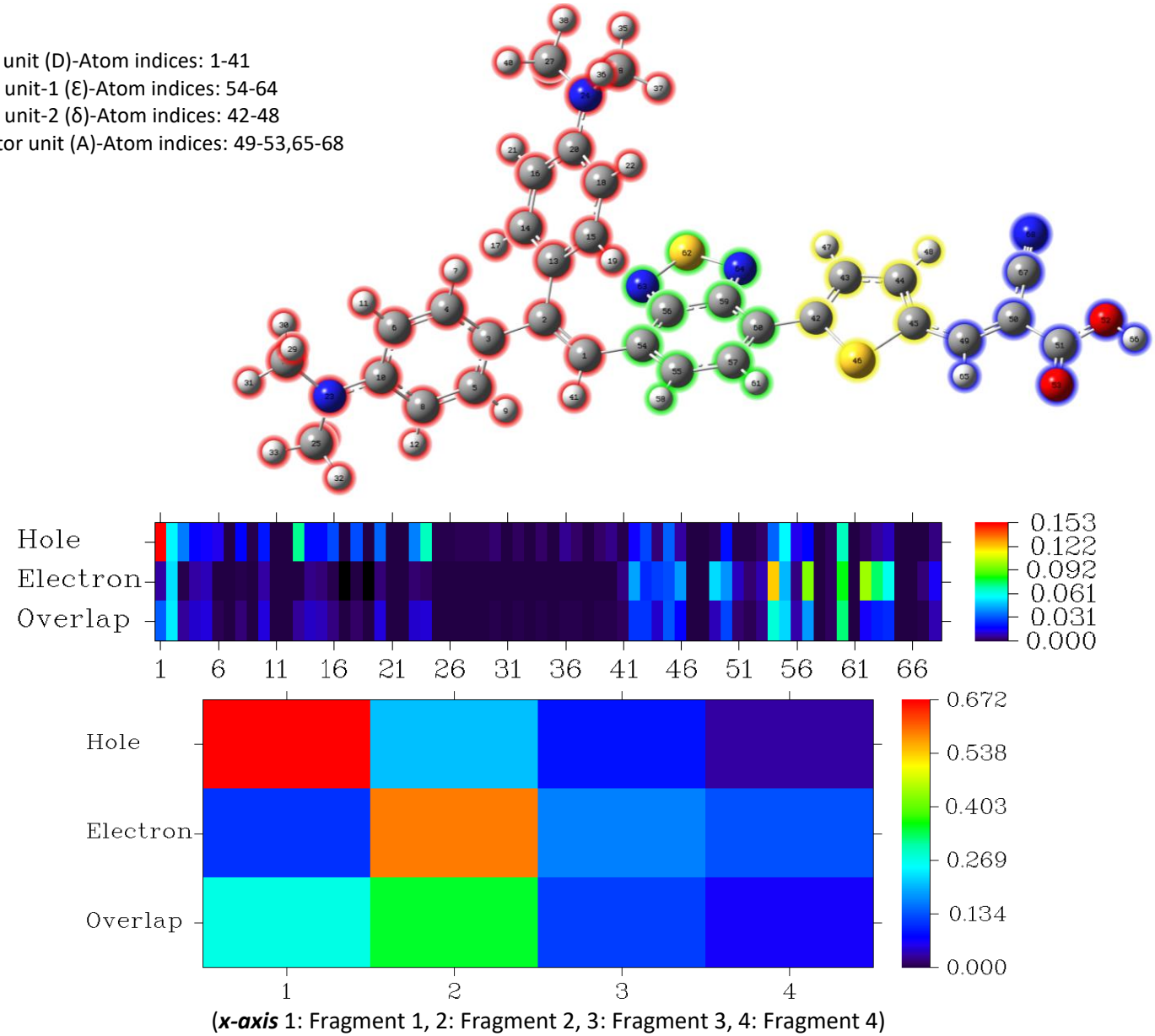


(***x-axis*** 1: Fragment 1, 2: Fragment 2, 3: Fragment 3)

Table S12 (*cont.*). Atom- and fragment-based electron-hole analysis of the investigated systems [M06-2x/6-31G(d,p) solvent model: CPCM, $\varepsilon_{ethanol}$ = 24.55].

D-ε_1-δ_1-A

Fragment 1: Donor unit (D)-Atom indices: 1-41
Fragment 2: Bridge unit-1 (Ɛ)-Atom indices: 54-64
Fragment 3: Bridge unit-2 (δ)-Atom indices: 42-48
Fragment 4: Acceptor unit (A)-Atom indices: 49-53,65-68

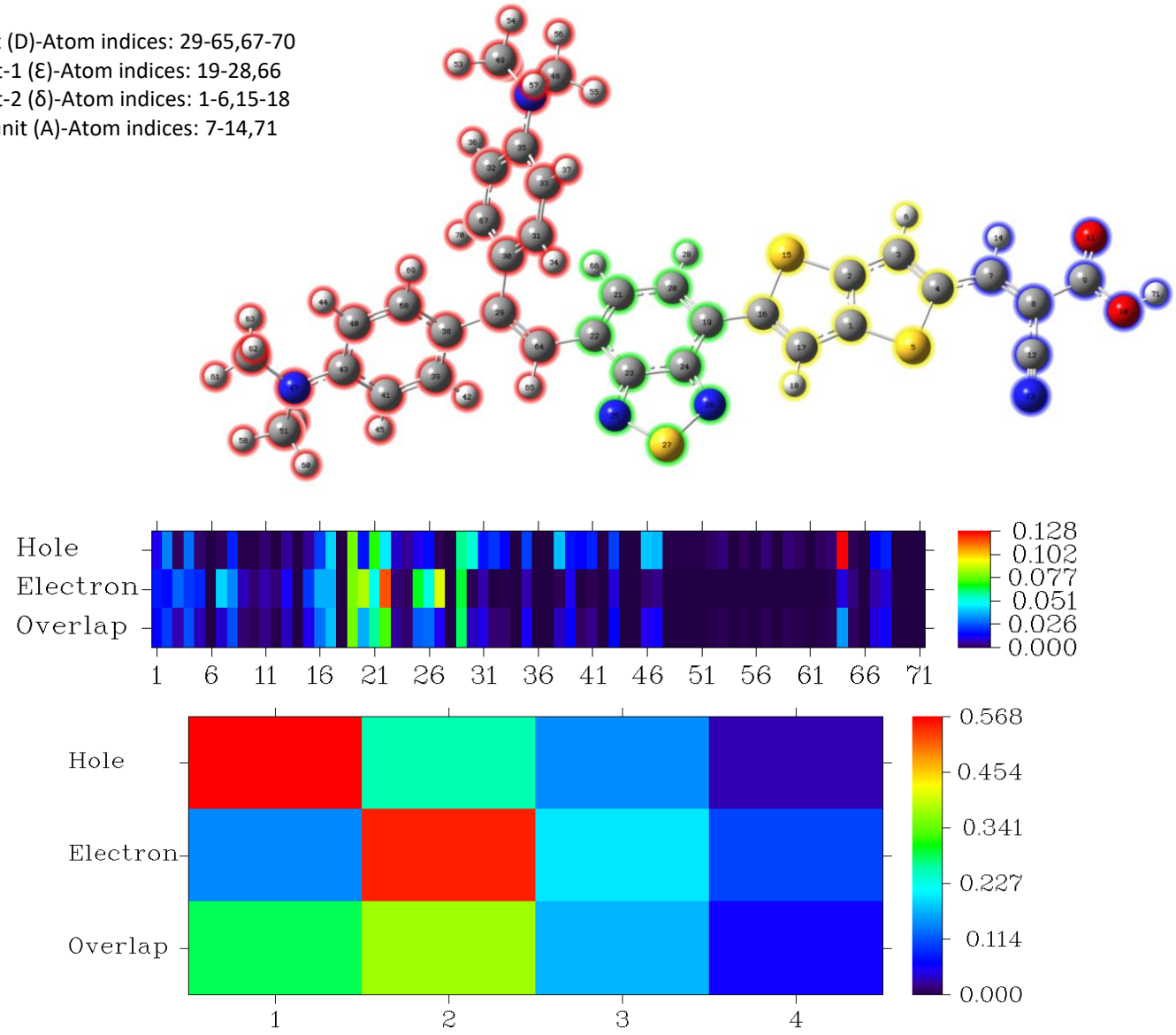


(***x-axis*** 1: Fragment 1, 2: Fragment 2, 3: Fragment 3, 4: Fragment 4)

Table S12 (*cont.*). Atom- and fragment-based electron-hole analysis of the investigated systems [M06-2x/6-31G(d,p) solvent model: CPCM, $\varepsilon_{ethanol}$ = 24.55].

D-ε_1-δ_2-A

Fragment 1: Donor unit (D)-Atom indices: 29-65,67-70
Fragment 2: Bridge unit-1 (ε)-Atom indices: 19-28,66
Fragment 3: Bridge unit-2 (δ)-Atom indices: 1-6,15-18
Fragment 4: Acceptor unit (A)-Atom indices: 7-14,71

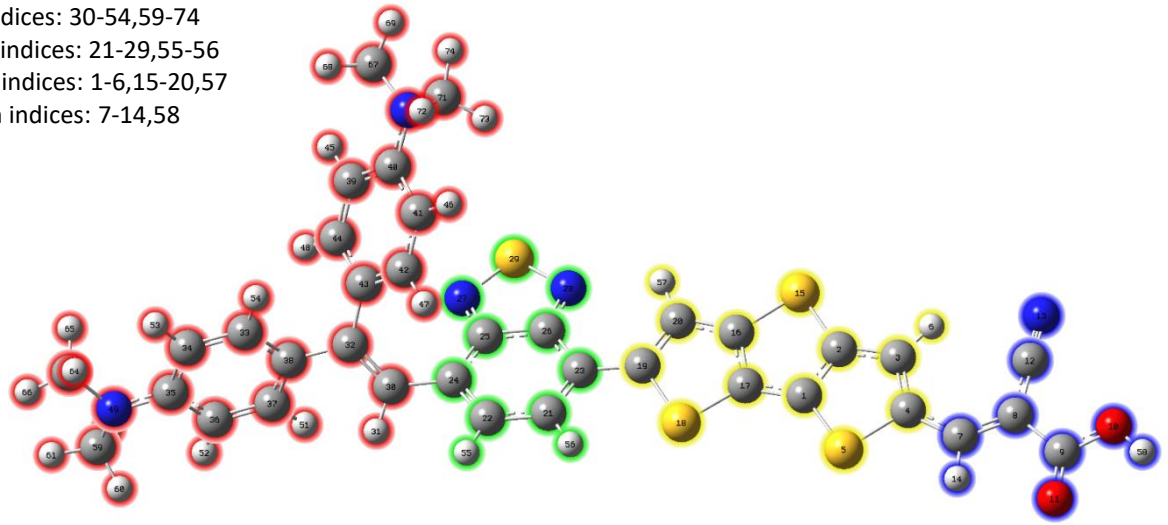


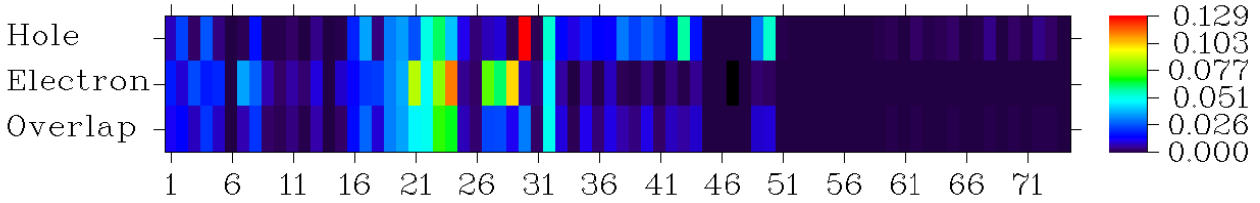
(***x-axis*** 1: Fragment 1, 2: Fragment 2, 3: Fragment 3, 4: Fragment 4)

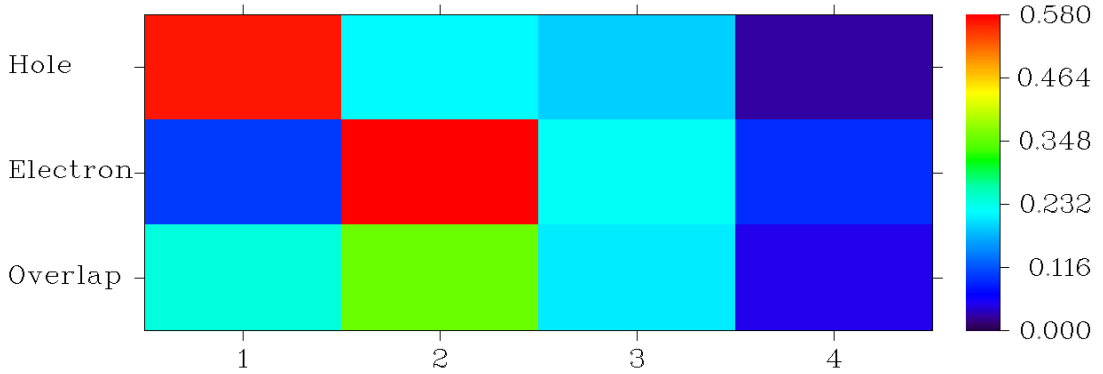
Table S12 (*cont.*). Atom- and fragment-based electron-hole analysis of the investigated systems [M06-2x/6-31G(d,p) solvent model: CPCM, $\varepsilon_{ethanol}$ = 24.55].

D-ε_1-δ_3-A

Fragment 1: Donor unit (D)-Atom indices: 30-54,59-74
Fragment 2: Bridge unit-1 (ε)-Atom indices: 21-29,55-56
Fragment 3: Bridge unit-2 (δ)-Atom indices: 1-6,15-20,57
Fragment 4: Acceptor unit (A)-Atom indices: 7-14,58





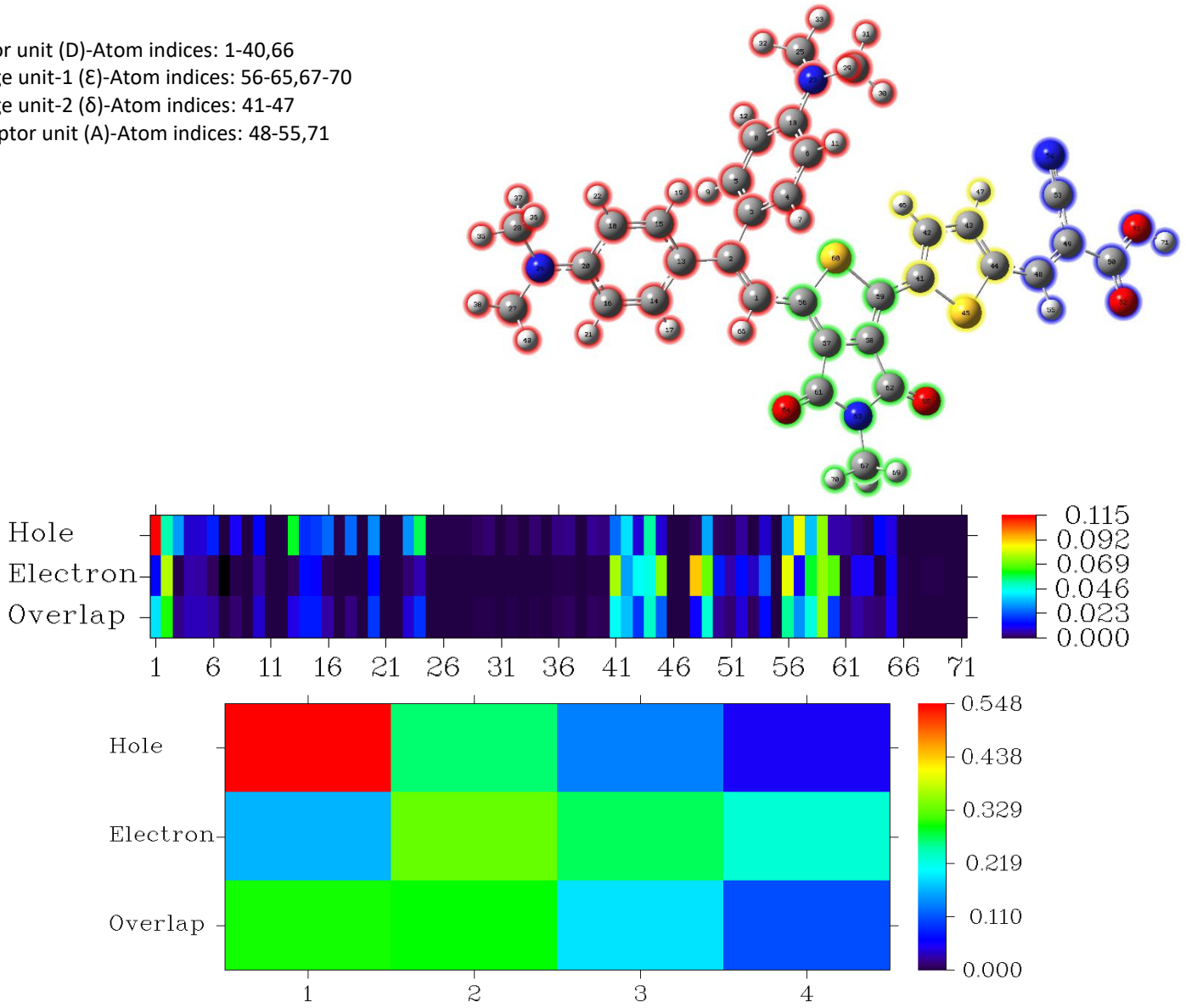


(***x-axis*** 1: Fragment 1, 2: Fragment 2, 3: Fragment 3, 4: Fragment 4)

Table S12 (*cont.*). Atom- and fragment-based electron-hole analysis of the investigated systems [M06-2x/6-31G(d,p) solvent model: CPCM, $\varepsilon_{ethanol}$ = 24.55].

D-Ɛ$_2$-δ$_1$-A

Fragment 1: Donor unit (D)-Atom indices: 1-40,66
Fragment 2: Bridge unit-1 (Ɛ)-Atom indices: 56-65,67-70
Fragment 3: Bridge unit-2 (δ)-Atom indices: 41-47
Fragment 4: Acceptor unit (A)-Atom indices: 48-55,71

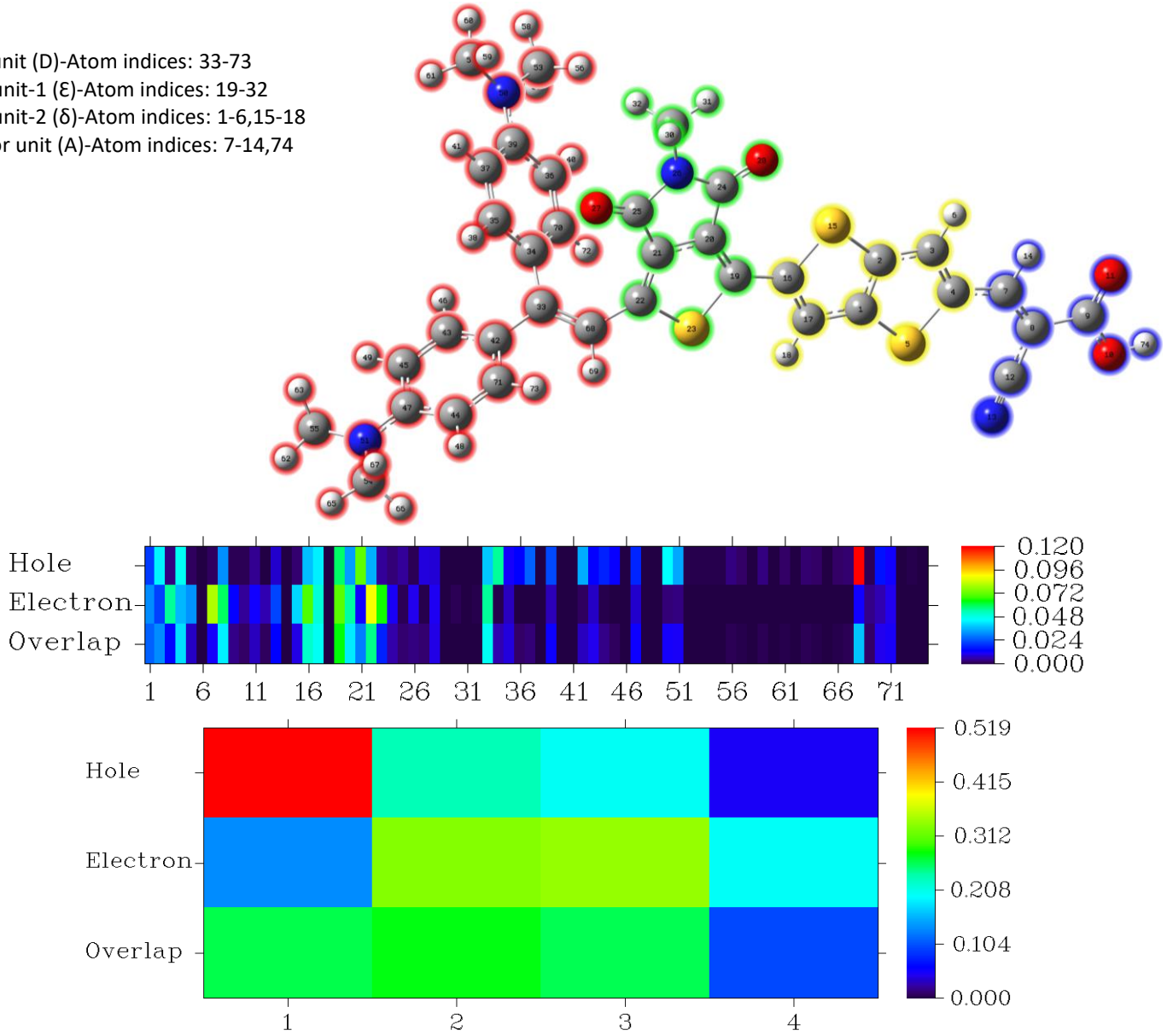


(***x-axis*** 1: Fragment 1, 2: Fragment 2, 3: Fragment 3, 4: Fragment 4)

Table S12 (*cont.*). Atom- and fragment-based electron-hole analysis of the investigated systems [M06-2x/6-31G(d,p) solvent model: CPCM, $\varepsilon_{ethanol}$ = 24.55].

D-ε_2-δ_2-A

Fragment 1: Donor unit (D)-Atom indices: 33-73
Fragment 2: Bridge unit-1 (ε)-Atom indices: 19-32
Fragment 3: Bridge unit-2 (δ)-Atom indices: 1-6,15-18
Fragment 4: Acceptor unit (A)-Atom indices: 7-14,74

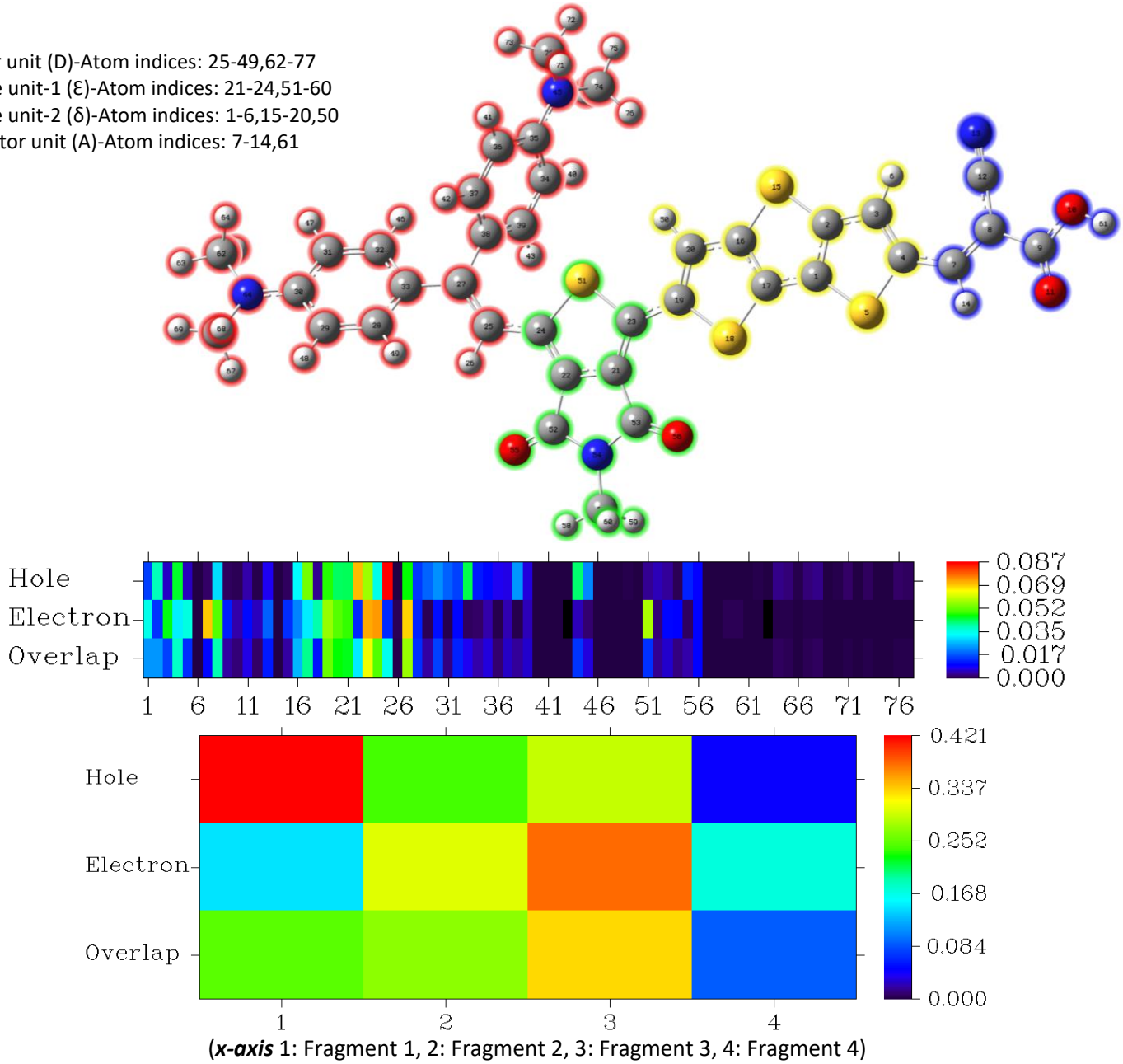


(***x-axis*** 1: Fragment 1, 2: Fragment 2, 3: Fragment 3, 4: Fragment 4)

Table S12 (*cont.*). Atom- and fragment-based electron-hole analysis of the investigated systems [M06-2x/6-31G(d,p) solvent model: CPCM, $\varepsilon_{ethanol}$ = 24.55].

D-ε_2-δ_3-A

Fragment 1: Donor unit (D)-Atom indices: 25-49,62-77
Fragment 2: Bridge unit-1 (Ɛ)-Atom indices: 21-24,51-60
Fragment 3: Bridge unit-2 (δ)-Atom indices: 1-6,15-20,50
Fragment 4: Acceptor unit (A)-Atom indices: 7-14,61

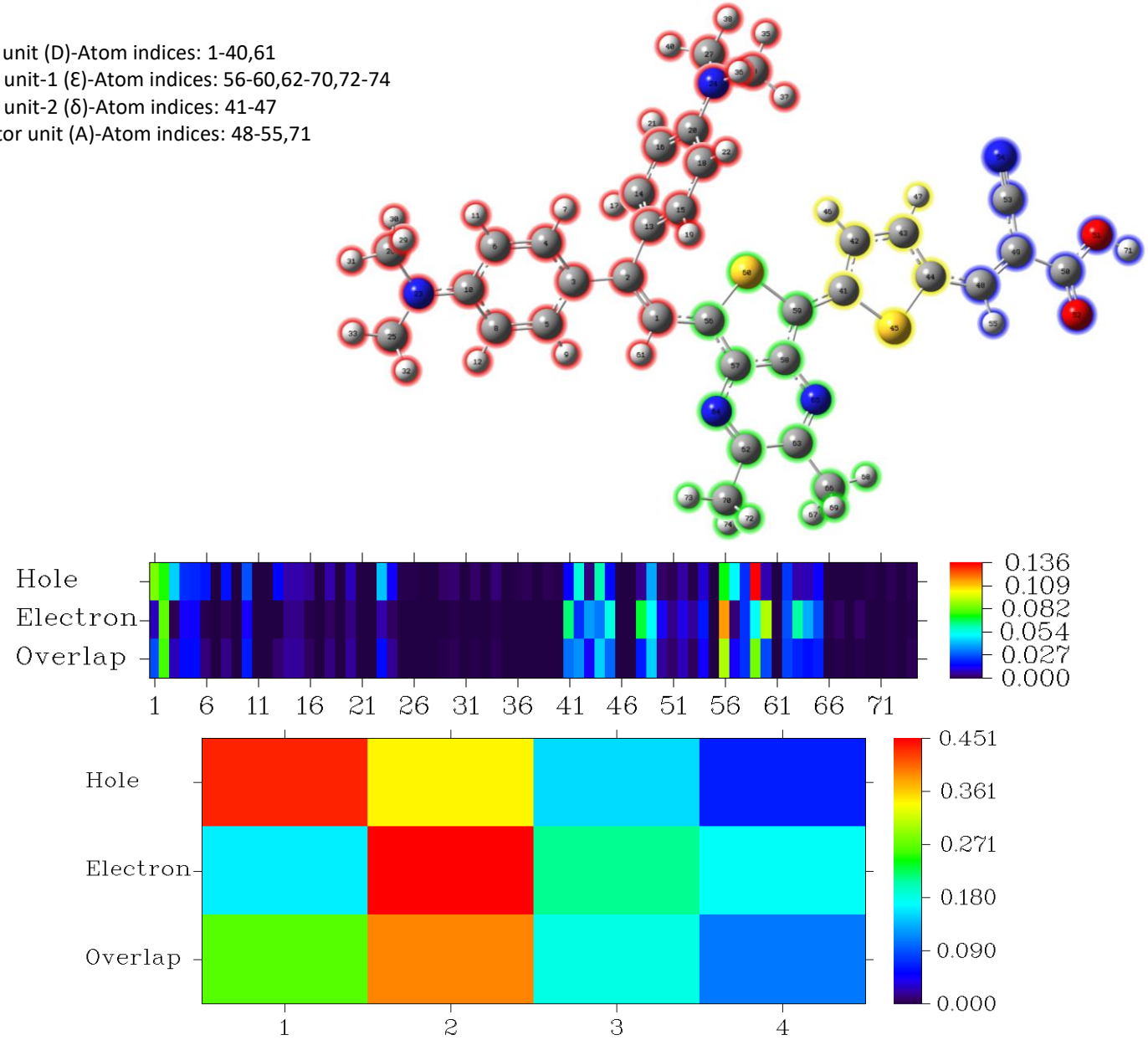


(***x-axis*** 1: Fragment 1, 2: Fragment 2, 3: Fragment 3, 4: Fragment 4)

Table S12 (*cont.*). Atom- and fragment-based electron-hole analysis of the investigated systems [M06-2x/6-31G(d,p) solvent model: CPCM, $\varepsilon_{ethanol}$ = 24.55].

D-Ɛ$_3$-δ$_1$-A

Fragment 1: Donor unit (D)-Atom indices: 1-40,61
Fragment 2: Bridge unit-1 (Ɛ)-Atom indices: 56-60,62-70,72-74
Fragment 3: Bridge unit-2 (δ)-Atom indices: 41-47
Fragment 4: Acceptor unit (A)-Atom indices: 48-55,71

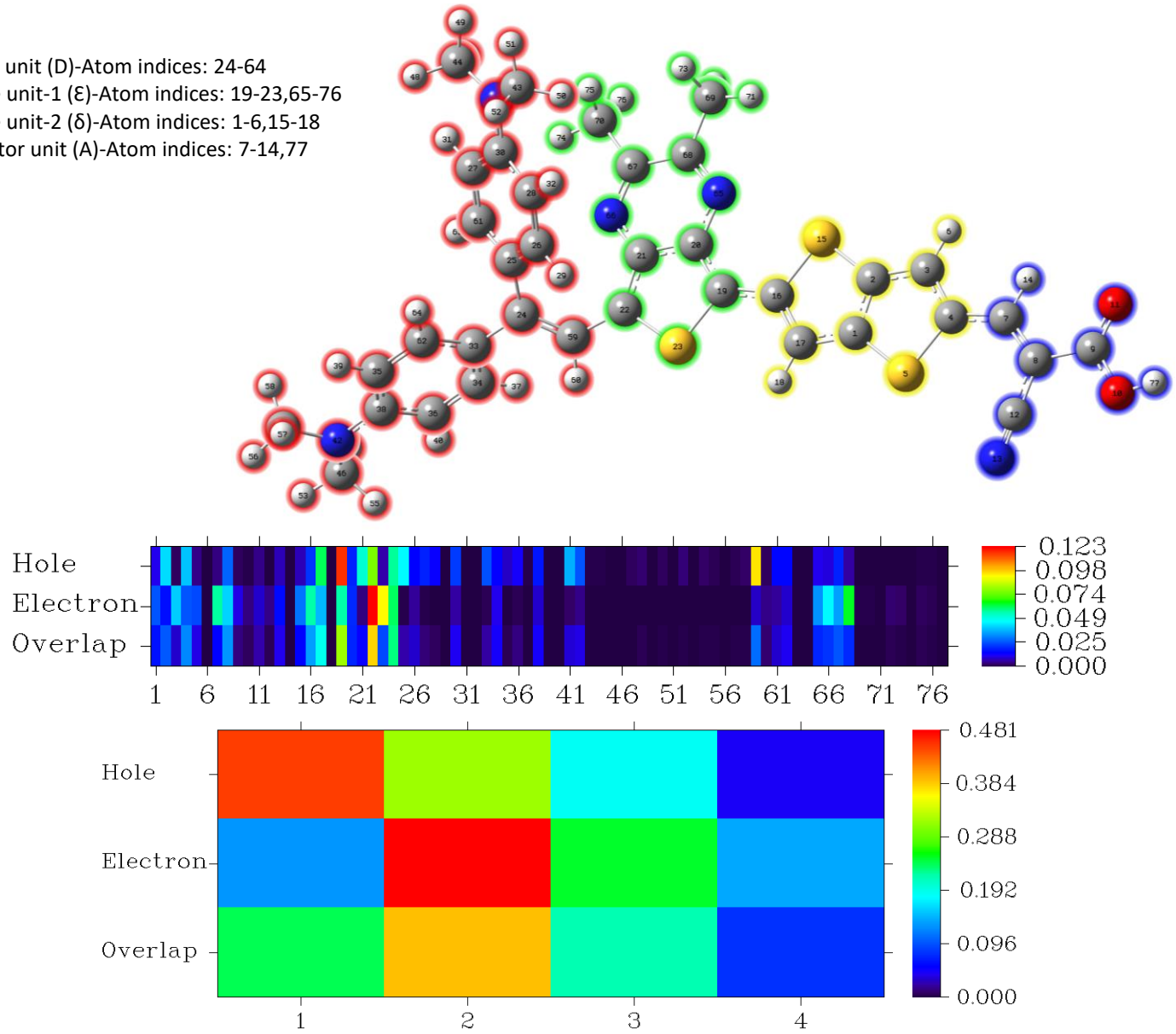


(***x-axis*** 1: Fragment 1, 2: Fragment 2, 3: Fragment 3, 4: Fragment 4)

Table S12 (*cont.*). Atom- and fragment-based electron-hole analysis of the investigated systems [M06-2x/6-31G(d,p) solvent model: CPCM, $\varepsilon_{ethanol}$ = 24.55].

D-ε_3-δ_2-A

Fragment 1: Donor unit (D)-Atom indices: 24-64
Fragment 2: Bridge unit-1 (ε)-Atom indices: 19-23,65-76
Fragment 3: Bridge unit-2 (δ)-Atom indices: 1-6,15-18
Fragment 4: Acceptor unit (A)-Atom indices: 7-14,77

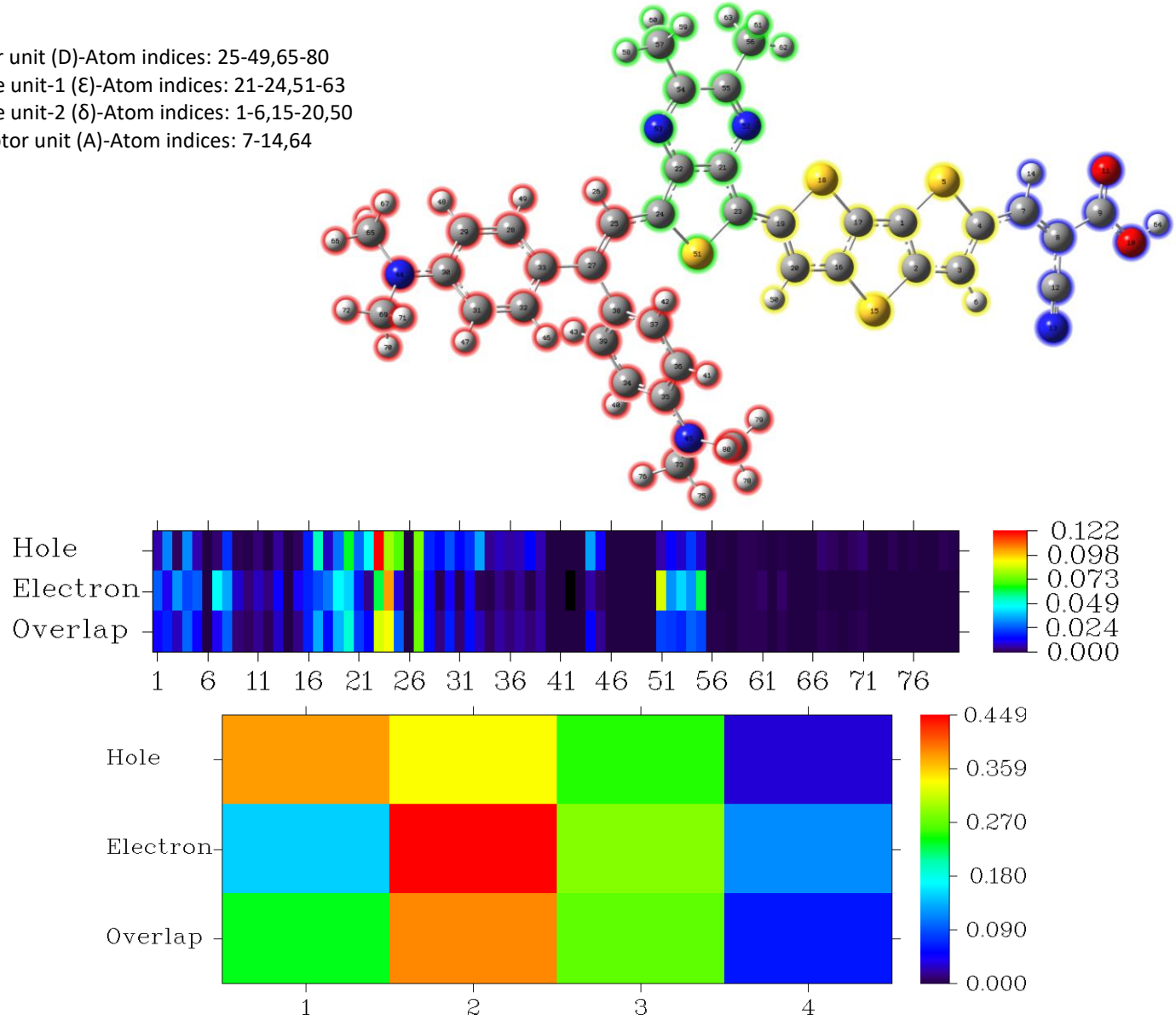


(***x-axis*** 1: Fragment 1, 2: Fragment 2, 3: Fragment 3, 4: Fragment 4)

Table S12 (*cont.*). Atom- and fragment-based electron-hole analysis of the investigated systems [M06-2x/6-31G(d,p) solvent model: CPCM, $\varepsilon_{ethanol}$ = 24.55].

D-ε_3-δ_3-A

Fragment 1: Donor unit (D)-Atom indices: 25-49,65-80
Fragment 2: Bridge unit-1 (ε)-Atom indices: 21-24,51-63
Fragment 3: Bridge unit-2 (δ)-Atom indices: 1-6,15-20,50
Fragment 4: Acceptor unit (A)-Atom indices: 7-14,64

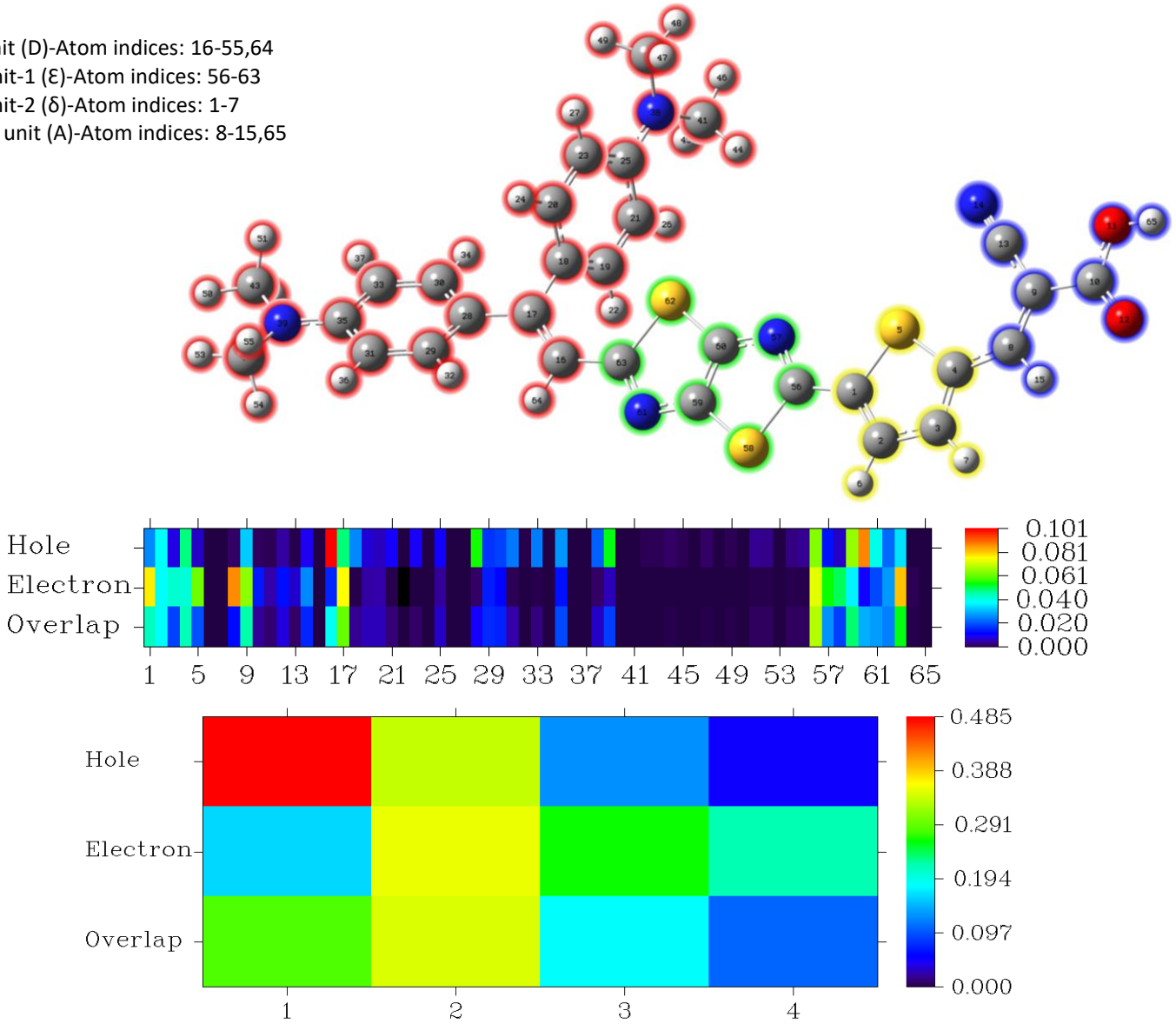


(***x-axis*** 1: Fragment 1, 2: Fragment 2, 3: Fragment 3, 4: Fragment 4)

Table S12 (*cont.*). Atom- and fragment-based electron-hole analysis of the investigated systems [M06-2x/6-31G(d,p) solvent model: CPCM, $\varepsilon_{ethanol}$ = 24.55].

D-Ɛ$_4$-δ$_1$-A

Fragment 1: Donor unit (D)-Atom indices: 16-55,64
Fragment 2: Bridge unit-1 (Ɛ)-Atom indices: 56-63
Fragment 3: Bridge unit-2 (δ)-Atom indices: 1-7
Fragment 4: Acceptor unit (A)-Atom indices: 8-15,65

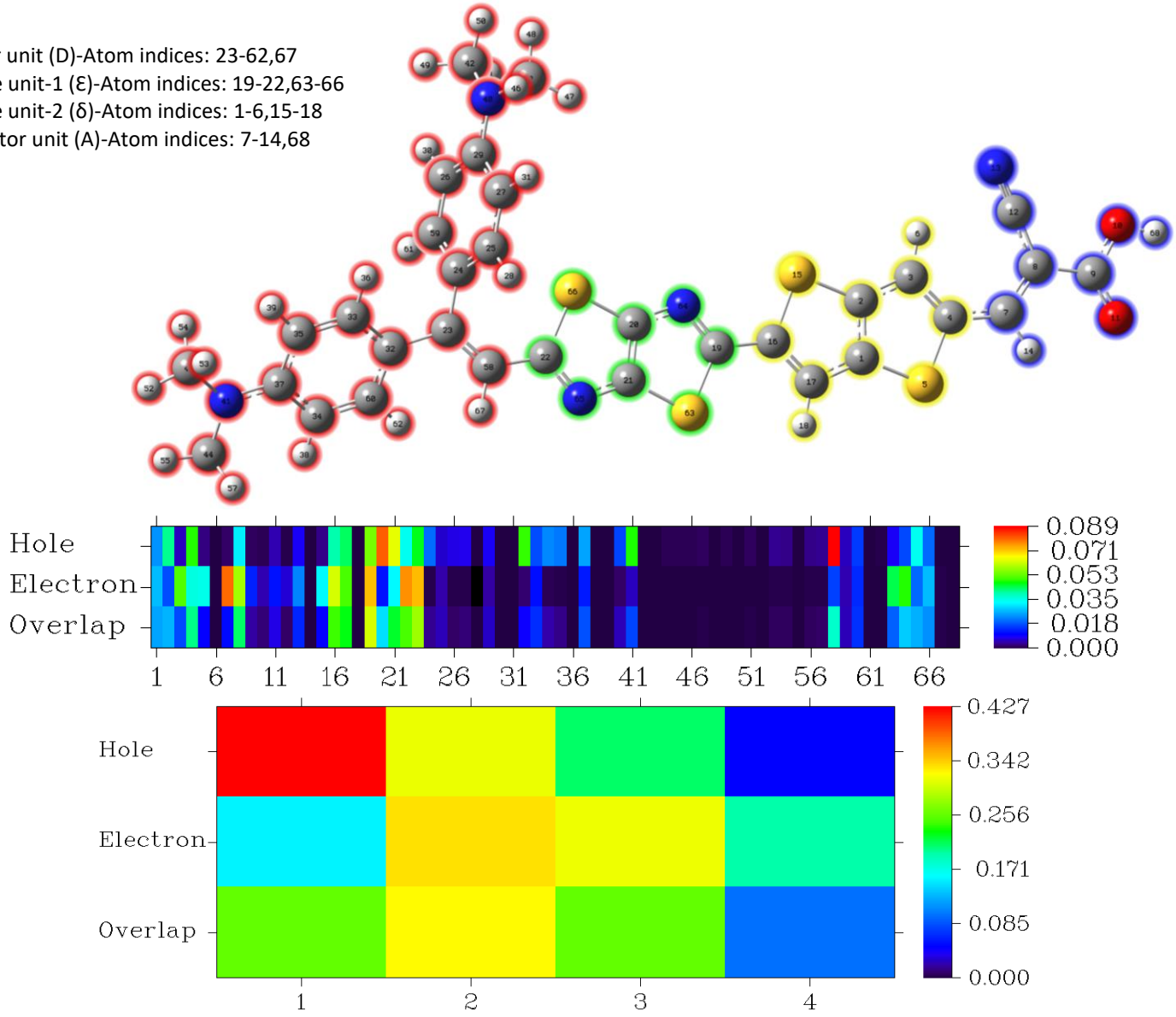


(***x-axis*** 1: Fragment 1, 2: Fragment 2, 3: Fragment 3, 4: Fragment 4)

Table S12 (*cont.*). Atom- and fragment-based electron-hole analysis of the investigated systems [M06-2x/6-31G(d,p) solvent model: CPCM, $\varepsilon_{ethanol}$ = 24.55].

D-ε_4-δ_2-A

Fragment 1: Donor unit (D)-Atom indices: 23-62,67
Fragment 2: Bridge unit-1 (ε)-Atom indices: 19-22,63-66
Fragment 3: Bridge unit-2 (δ)-Atom indices: 1-6,15-18
Fragment 4: Acceptor unit (A)-Atom indices: 7-14,68

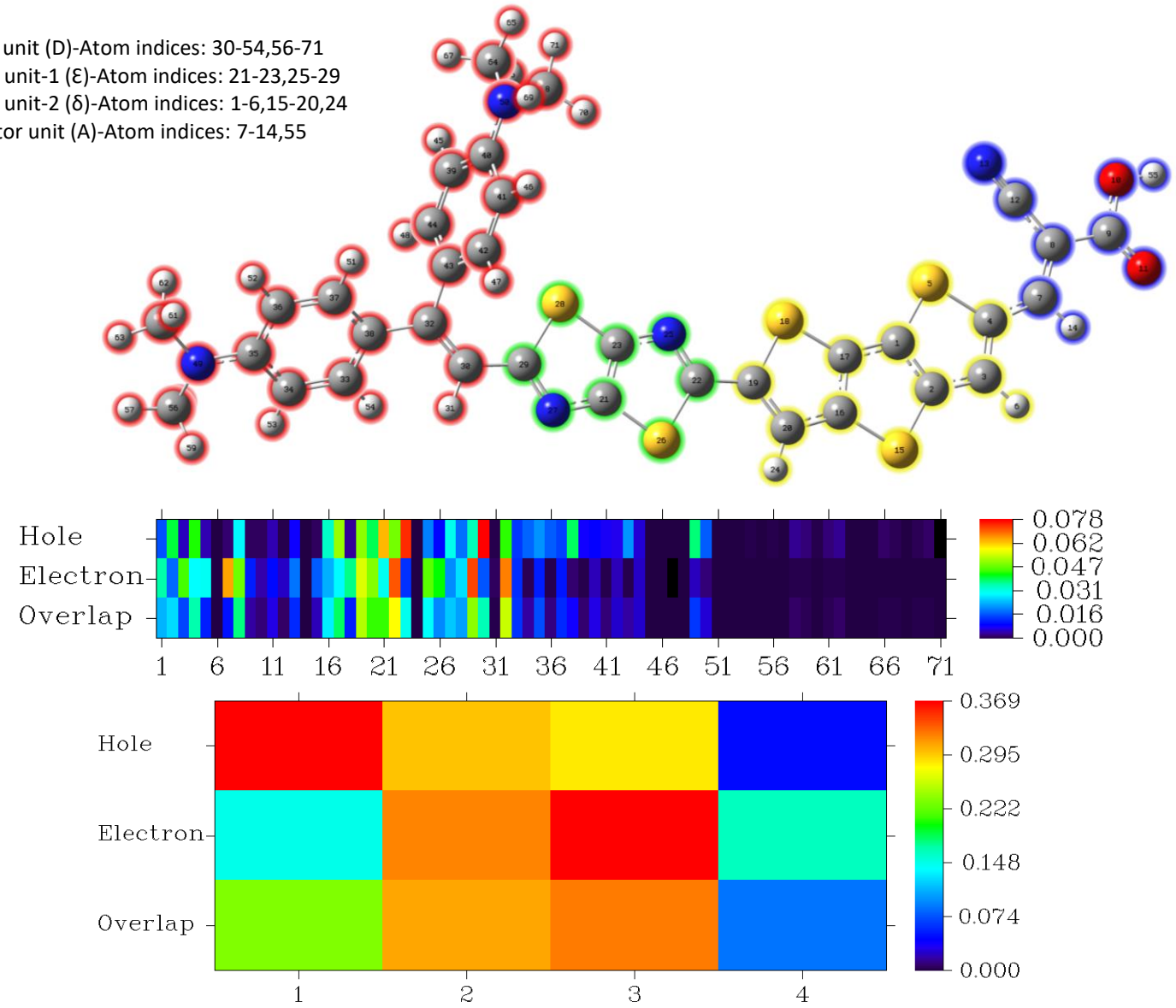


(***x-axis*** 1: Fragment 1, 2: Fragment 2, 3: Fragment 3, 4: Fragment 4)

Table S12 (*cont.*). Atom- and fragment-based electron-hole analysis of the investigated systems [M06-2x/6-31G(d,p) solvent model: CPCM, $\varepsilon_{ethanol}$ = 24.55].

D-ε_4-δ_3-A

Fragment 1: Donor unit (D)-Atom indices: 30-54,56-71
Fragment 2: Bridge unit-1 (ε)-Atom indices: 21-23,25-29
Fragment 3: Bridge unit-2 (δ)-Atom indices: 1-6,15-20,24
Fragment 4: Acceptor unit (A)-Atom indices: 7-14,55

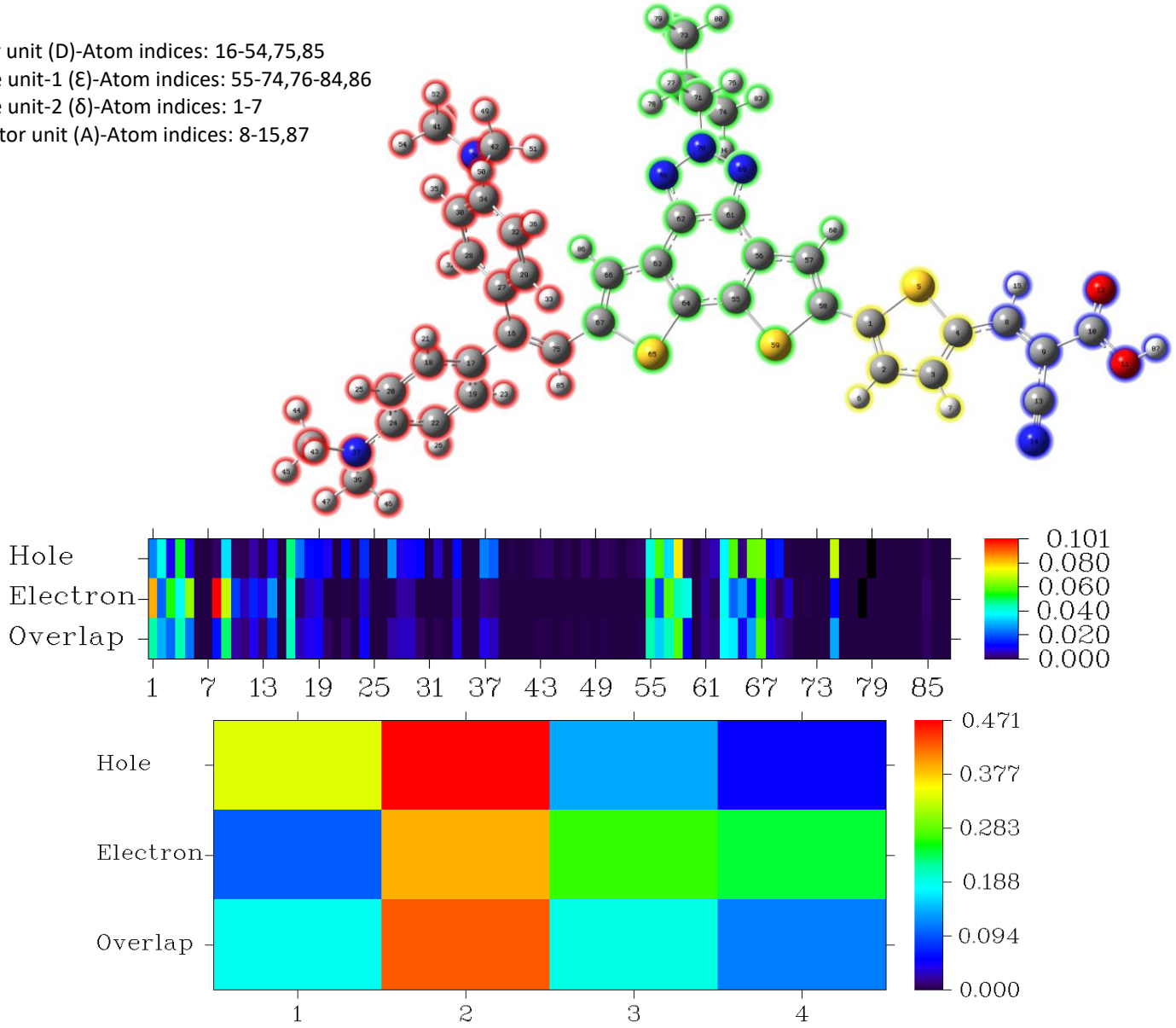


(***x-axis*** 1: Fragment 1, 2: Fragment 2, 3: Fragment 3, 4: Fragment 4)

Table S12 (*cont.*). Atom- and fragment-based electron-hole analysis of the investigated systems [M06-2x/6-31G(d,p) solvent model: CPCM, $\varepsilon_{ethanol}$ = 24.55].

D-ε_5-δ_1-A

Fragment 1: Donor unit (D)-Atom indices: 16-54,75,85
Fragment 2: Bridge unit-1 (ε)-Atom indices: 55-74,76-84,86
Fragment 3: Bridge unit-2 (δ)-Atom indices: 1-7
Fragment 4: Acceptor unit (A)-Atom indices: 8-15,87

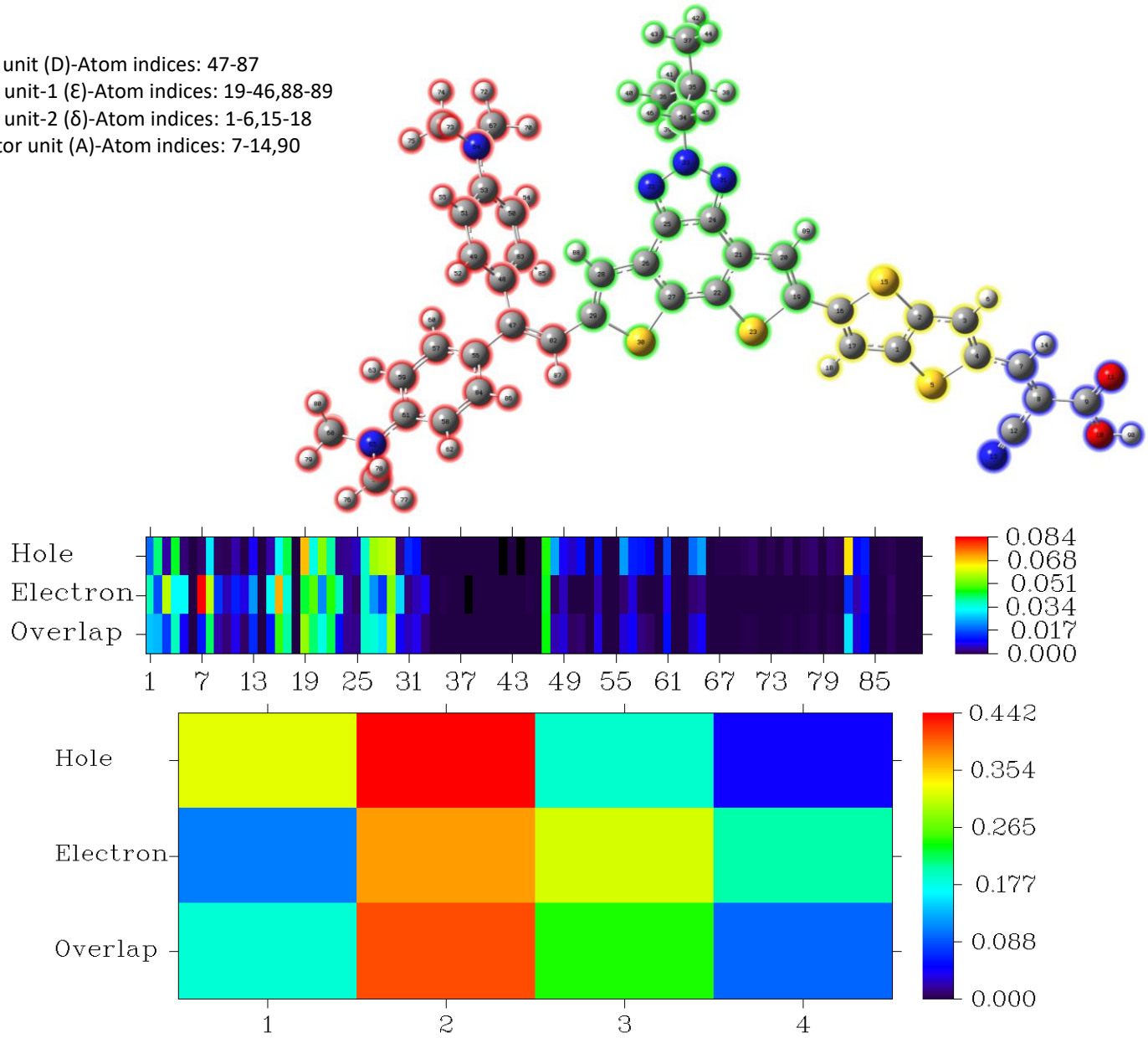


(***x-axis*** 1: Fragment 1, 2: Fragment 2, 3: Fragment 3, 4: Fragment 4)

Table S12 (*cont.*). Atom- and fragment-based electron-hole analysis of the investigated systems [M06-2x/6-31G(d,p) solvent model: CPCM, $\varepsilon_{ethanol}$ = 24.55].

D-ε_5-δ_2-A

Fragment 1: Donor unit (D)-Atom indices: 47-87
Fragment 2: Bridge unit-1 (Ɛ)-Atom indices: 19-46,88-89
Fragment 3: Bridge unit-2 (δ)-Atom indices: 1-6,15-18
Fragment 4: Acceptor unit (A)-Atom indices: 7-14,90

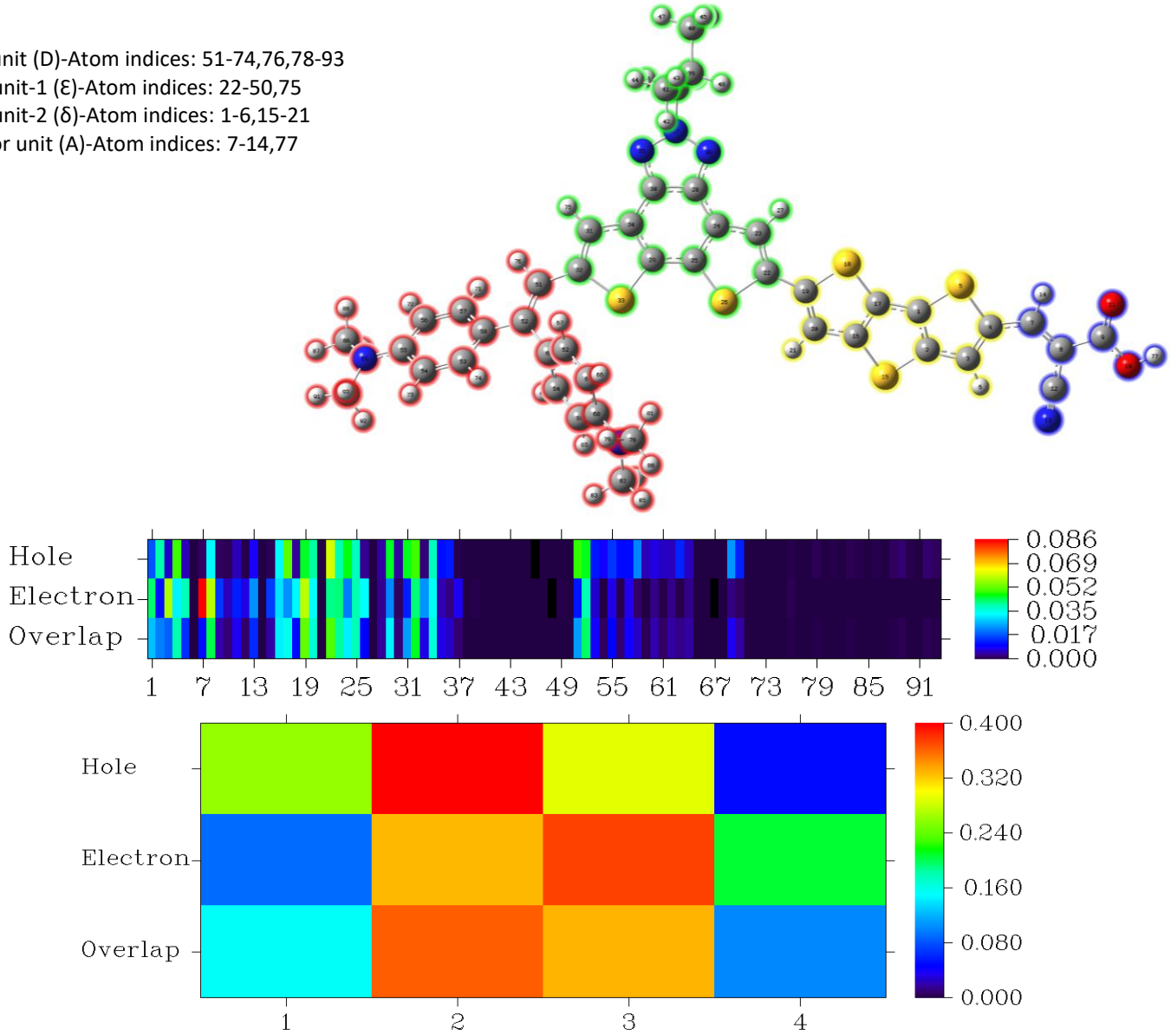


(***x-axis*** 1: Fragment 1, 2: Fragment 2, 3: Fragment 3, 4: Fragment 4)

Table S12 (*cont.*). Atom- and fragment-based electron-hole analysis of the investigated systems [M06-2x/6-31G(d,p) solvent model: CPCM, $\varepsilon_{ethanol}$ = 24.55].

D-ε_5-δ_3-A

Fragment 1: Donor unit (D)-Atom indices: 51-74,76,78-93
Fragment 2: Bridge unit-1 (ε)-Atom indices: 22-50,75
Fragment 3: Bridge unit-2 (δ)-Atom indices: 1-6,15-21
Fragment 4: Acceptor unit (A)-Atom indices: 7-14,77

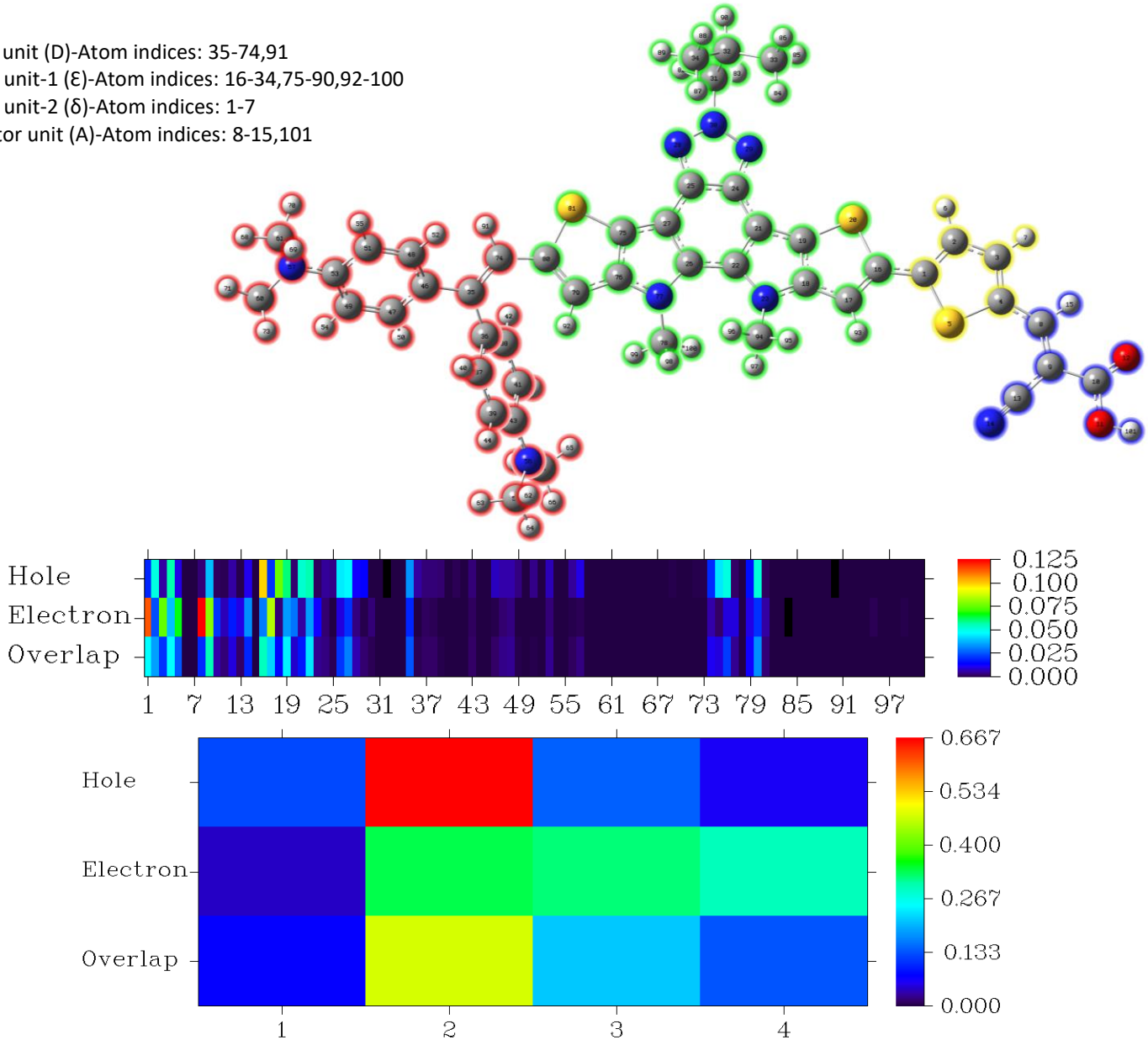


(***x-axis*** 1: Fragment 1, 2: Fragment 2, 3: Fragment 3, 4: Fragment 4)

Table S12 (*cont.*). Atom- and fragment-based electron-hole analysis of the investigated systems [M06-2x/6-31G(d,p) solvent model: CPCM, $\varepsilon_{ethanol}$ = 24.55].

D-ε_6-δ_1-A

Fragment 1: Donor unit (D)-Atom indices: 35-74,91
Fragment 2: Bridge unit-1 (ε)-Atom indices: 16-34,75-90,92-100
Fragment 3: Bridge unit-2 (δ)-Atom indices: 1-7
Fragment 4: Acceptor unit (A)-Atom indices: 8-15,101

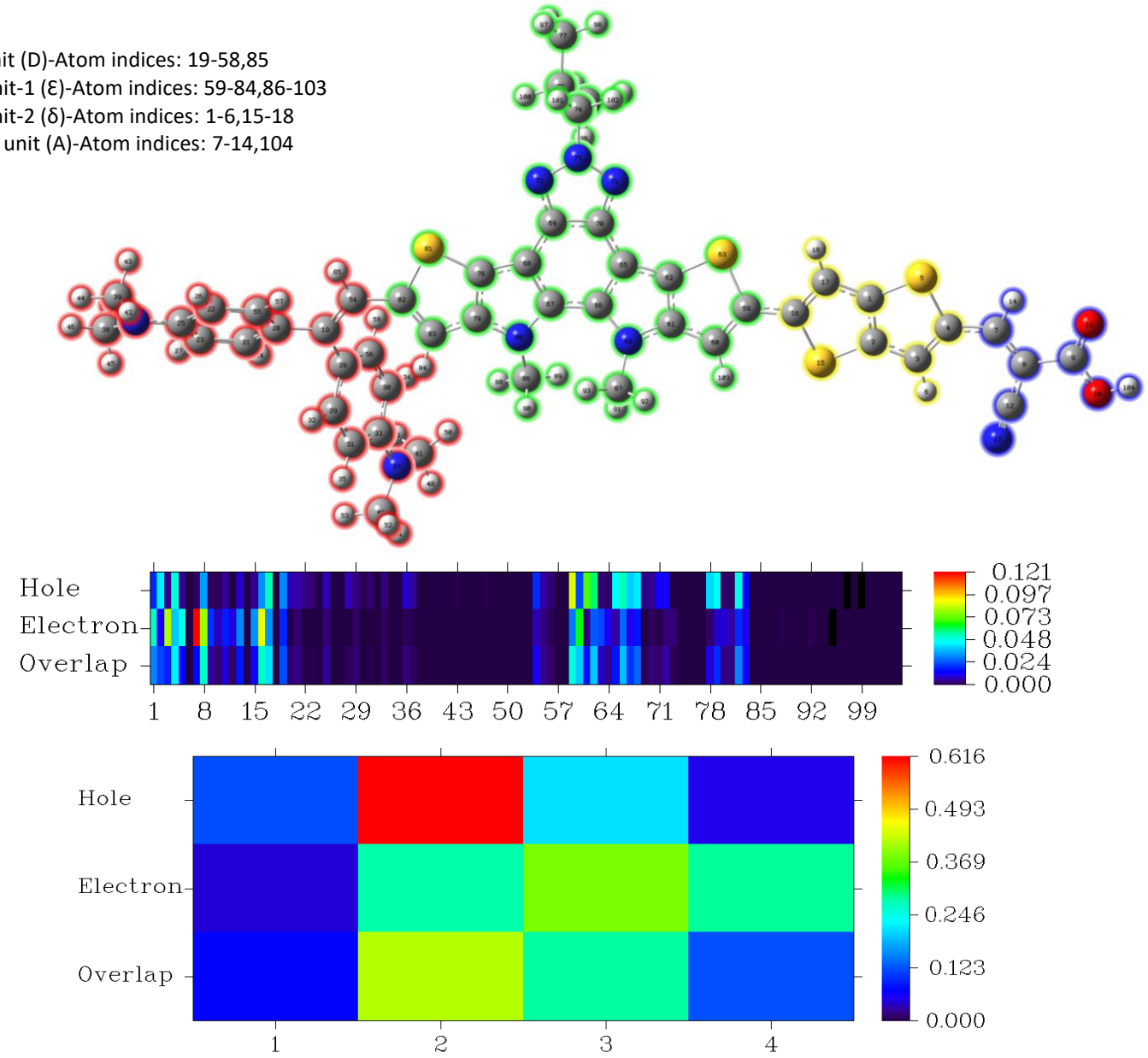


(***x-axis*** 1: Fragment 1, 2: Fragment 2, 3: Fragment 3, 4: Fragment 4)

Table S12 (*cont.*). Atom- and fragment-based electron-hole analysis of the investigated systems [M06-2x/6-31G(d,p) solvent model: CPCM, $\varepsilon_{ethanol}$ = 24.55].

D-ε_6-δ_2-A

Fragment 1: Donor unit (D)-Atom indices: 19-58,85
Fragment 2: Bridge unit-1 (ε)-Atom indices: 59-84,86-103
Fragment 3: Bridge unit-2 (δ)-Atom indices: 1-6,15-18
Fragment 4: Acceptor unit (A)-Atom indices: 7-14,104

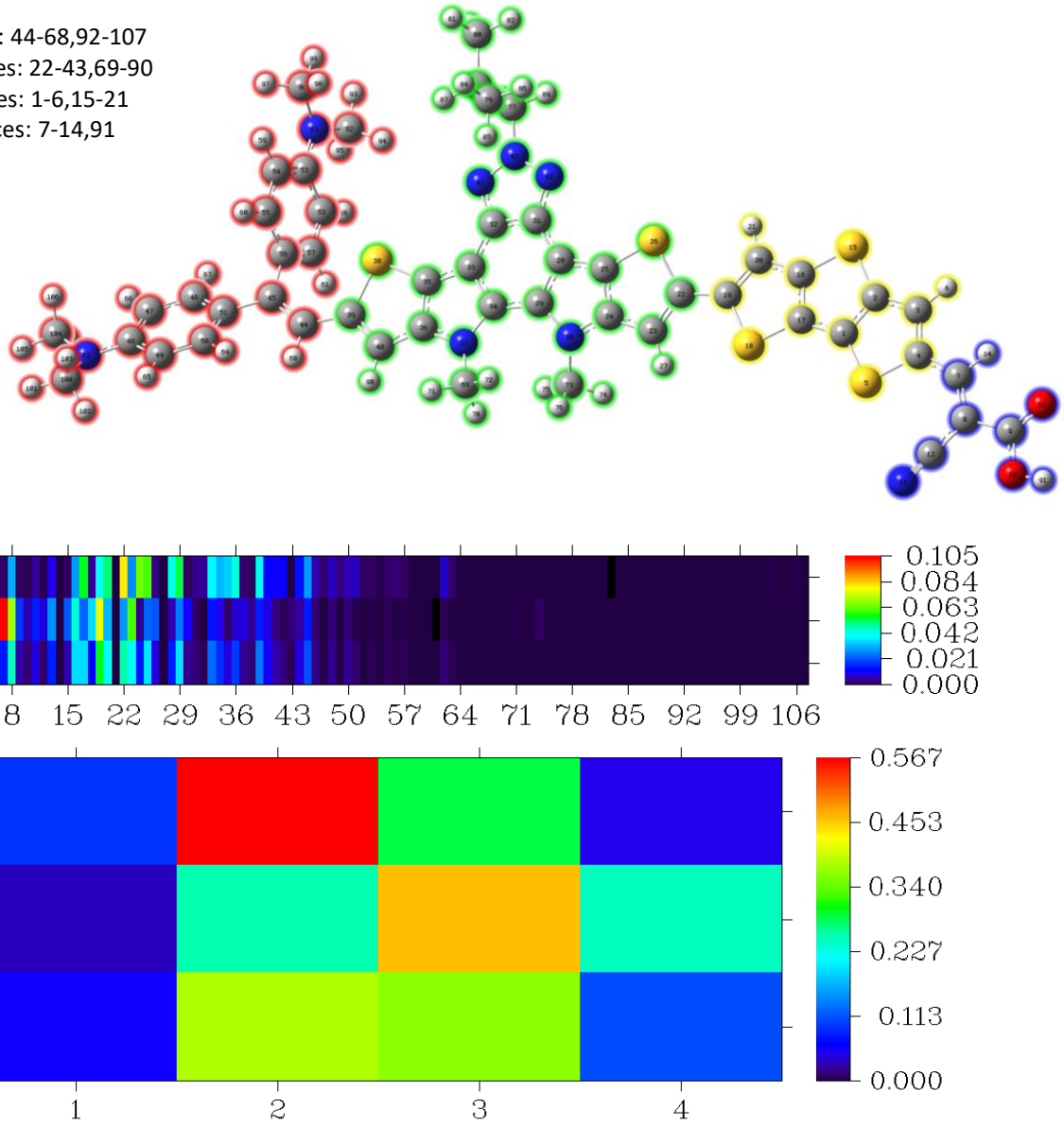


(***x-axis*** 1: Fragment 1, 2: Fragment 2, 3: Fragment 3, 4: Fragment 4)

Table S12 (*cont.*). Atom- and fragment-based electron-hole analysis of the investigated systems [M06-2x/6-31G(d,p) solvent model: CPCM, $\varepsilon_{ethanol}$ = 24.55].

D-ε_6-δ_3-A

Fragment 1: Donor unit (D)-Atom indices: 44-68,92-107
Fragment 2: Bridge unit-1 (Ɛ)-Atom indices: 22-43,69-90
Fragment 3: Bridge unit-2 (δ)-Atom indices: 1-6,15-21
Fragment 4: Acceptor unit (A)-Atom indices: 7-14,91



(***x-axis*** 1: Fragment 1, 2: Fragment 2, 3: Fragment 3, 4: Fragment 4)

Table S13. Atom- and fragment-based transition density and color correlation matrix (where the y-axis is the originating, and the x-axis is the receiving fragment for the excited electron) of the investigated systems [M06-2x/6-31G(d,p) solvent model: CPCM, $\varepsilon_{ethanol}$ = 24.55].

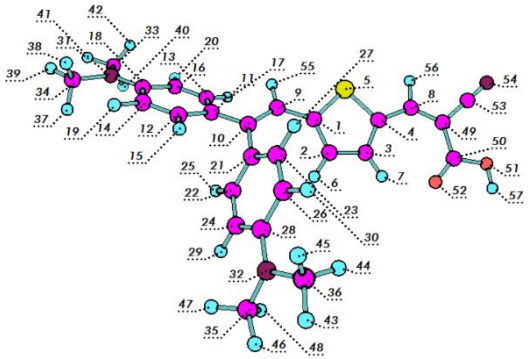
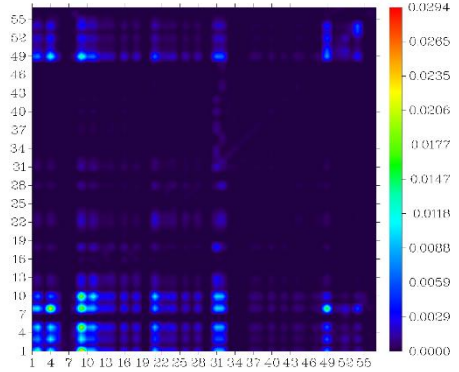
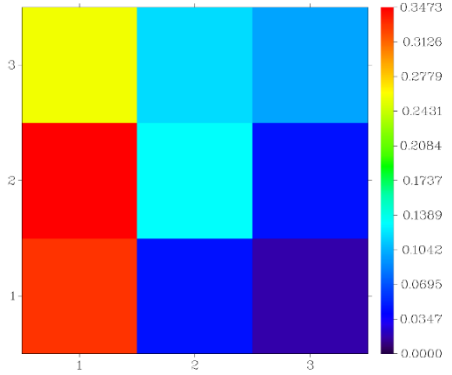
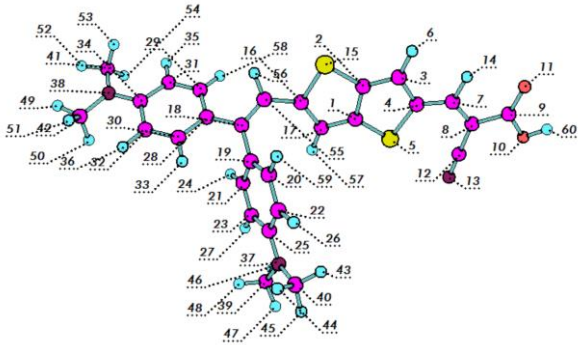
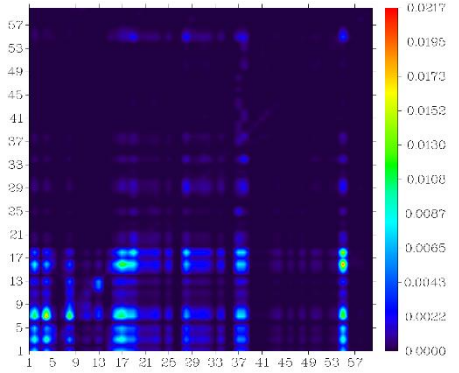
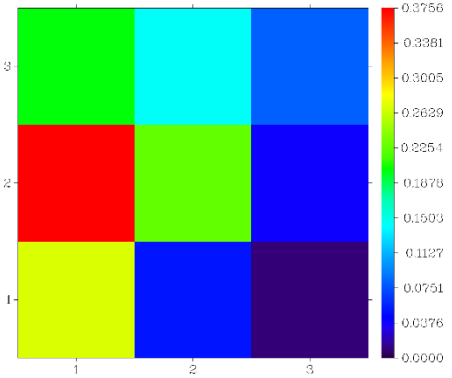
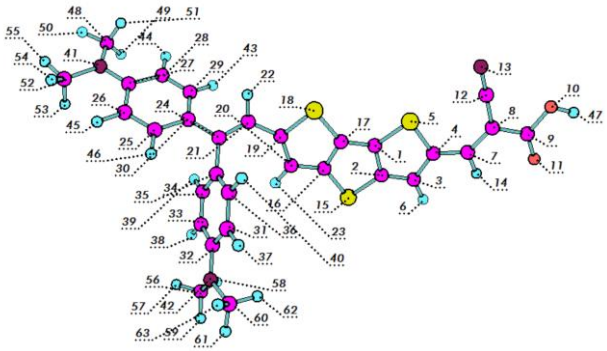
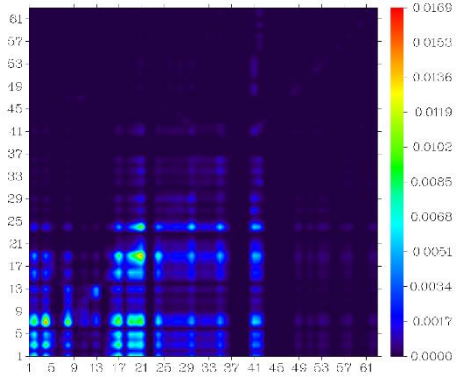
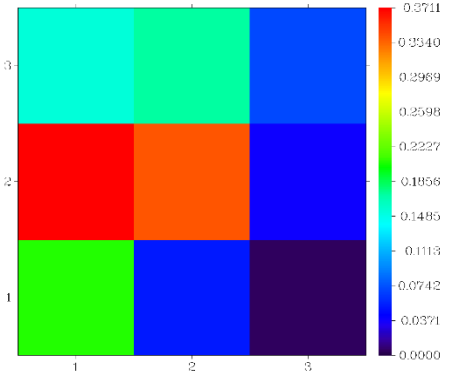
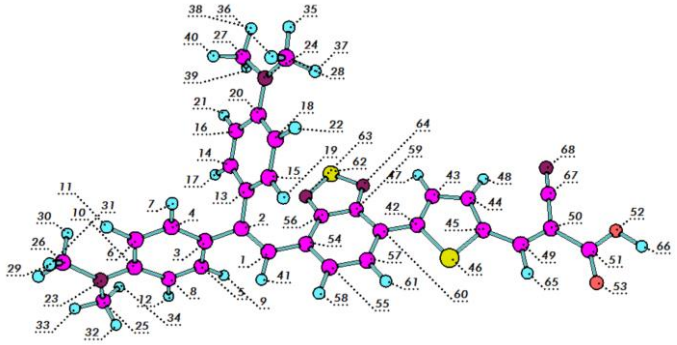
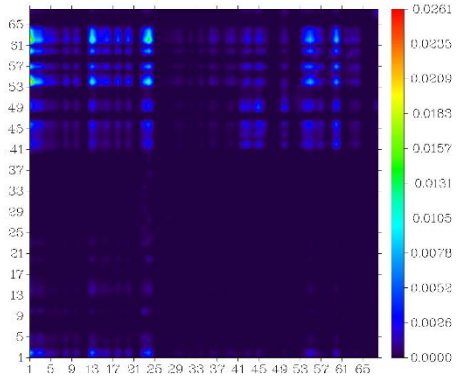
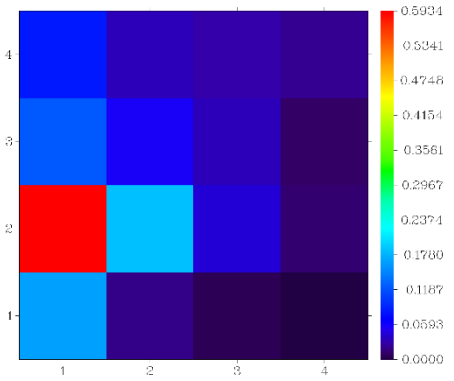
 **D-δ$_1$-A** (***model dye***)		
 **D-δ$_2$-A**		
 **D-δ$_3$-A**		

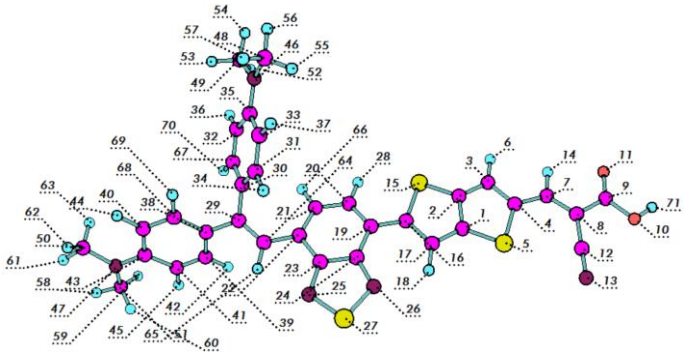
Table S13 (*cont.*). Atom- and fragment-based transition density and color correlation matrix (where the y-axis is the originating, and the x-axis is the receiving fragment for the excited electron) of the investigated systems [M06-2x/6-31G(d,p) solvent model: CPCM, $\varepsilon_{ethanol}$ = 24.55].



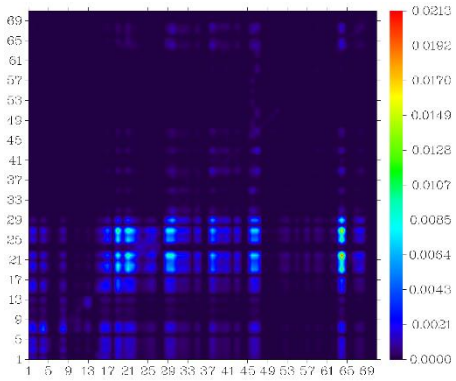
D-ε₁-δ₁-A

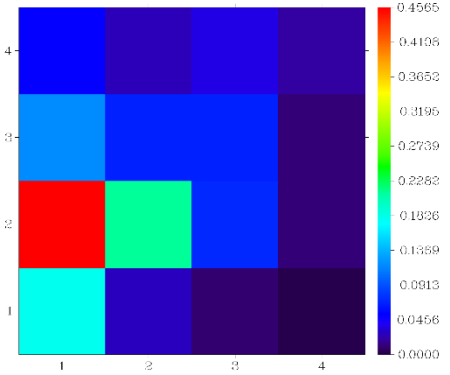


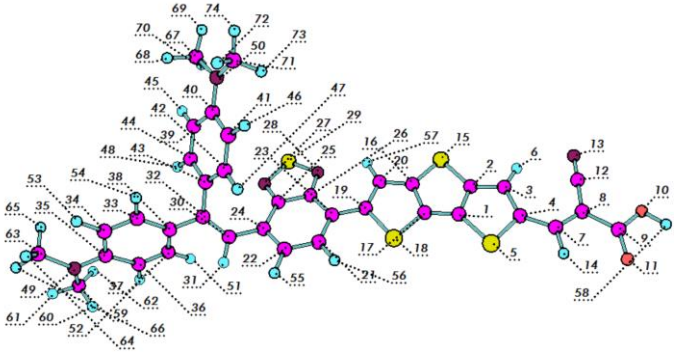




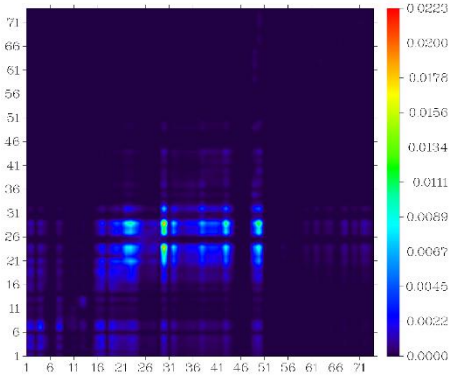
D-ε₁-δ₂-A







D-ε₁-δ₃-A



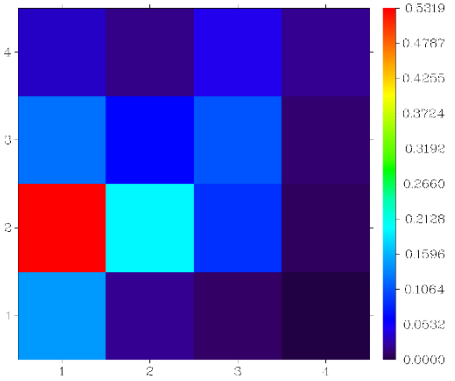
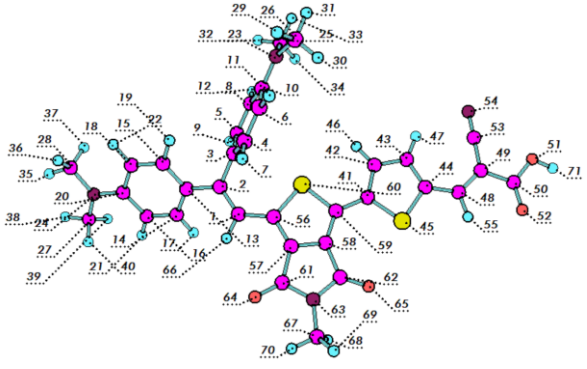
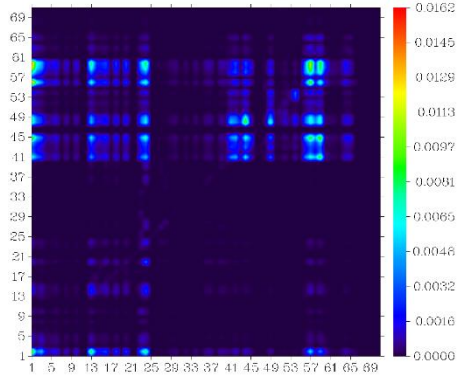
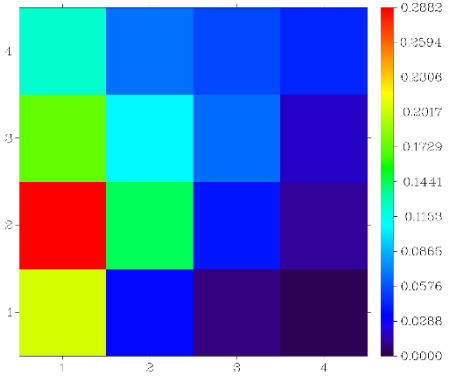


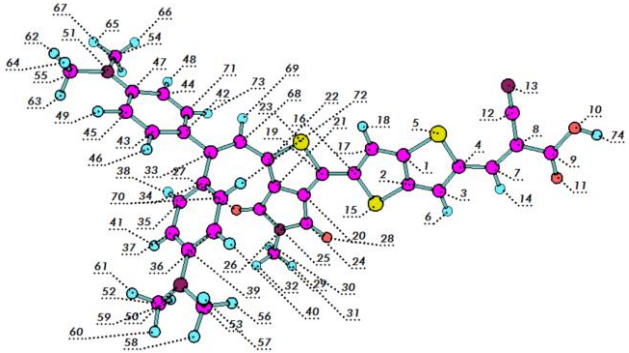
Table S13 (*cont.*). Atom- and fragment-based transition density and color correlation matrix (where the y-axis is the originating, and the x-axis is the receiving fragment for the excited electron) of the investigated systems [M06-2x/6-31G(d,p) solvent model: CPCM, $\varepsilon_{ethanol} = 24.55$].



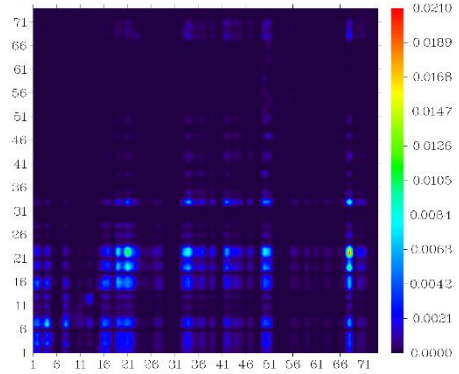
D-ε₂-δ₁-A

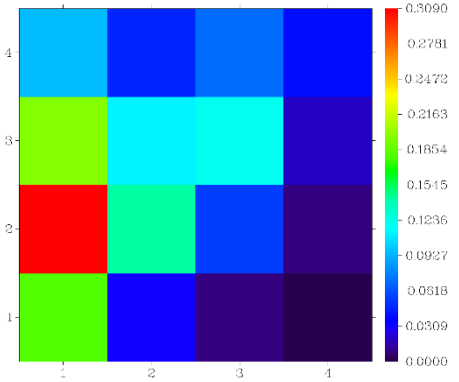


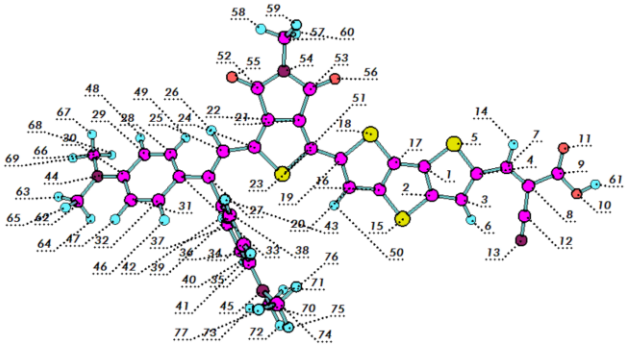




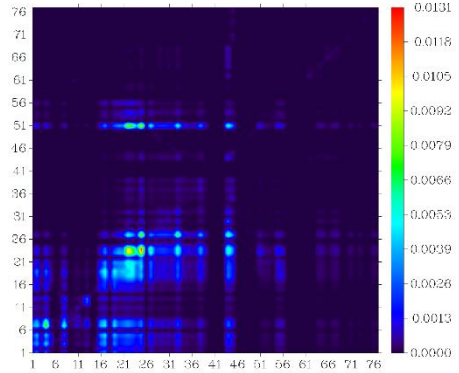
D-ε₂-δ₂-A







D-ε₂-δ₃-A



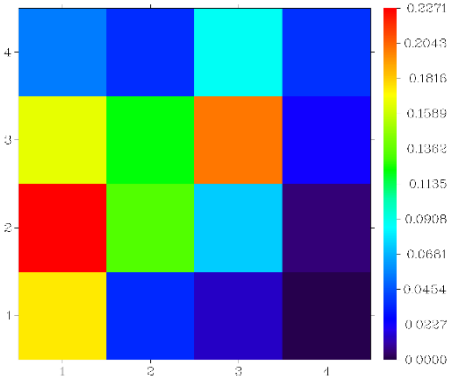
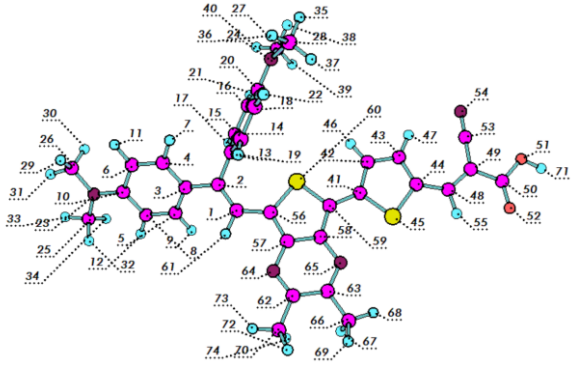
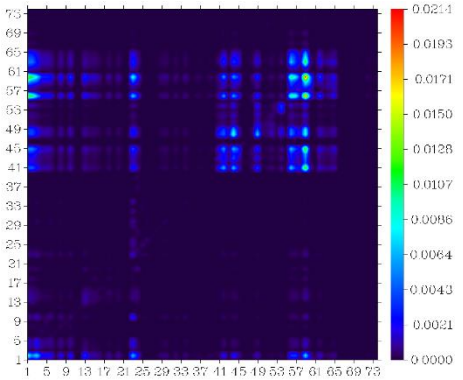
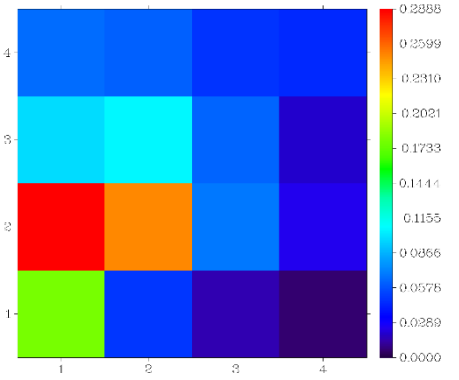


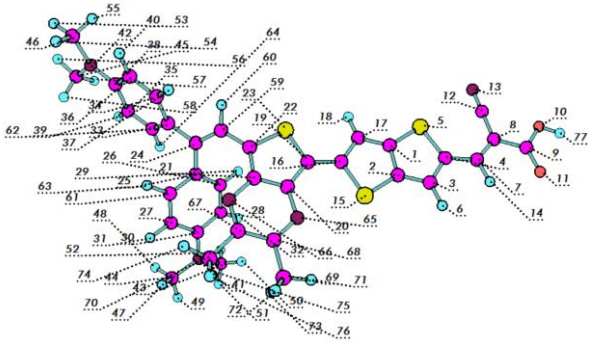
Table S13 (*cont.*). Atom- and fragment-based transition density and color correlation matrix (where the y-axis is the originating, and the x-axis is the receiving fragment for the excited electron) of the investigated systems [M06-2x/6-31G(d,p) solvent model: CPCM, $\varepsilon_{ethanol}$ = 24.55].



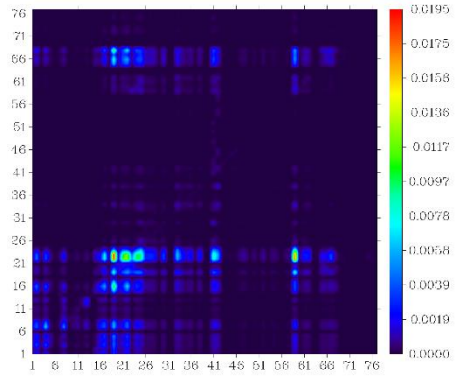
D-ε$_3$-δ$_1$-A

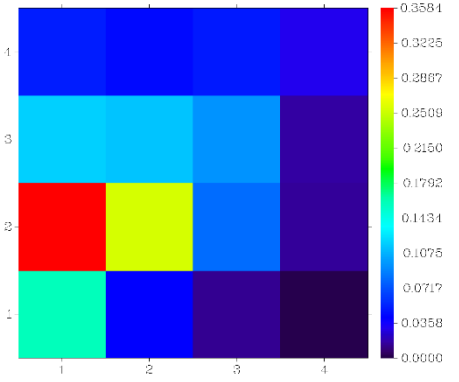


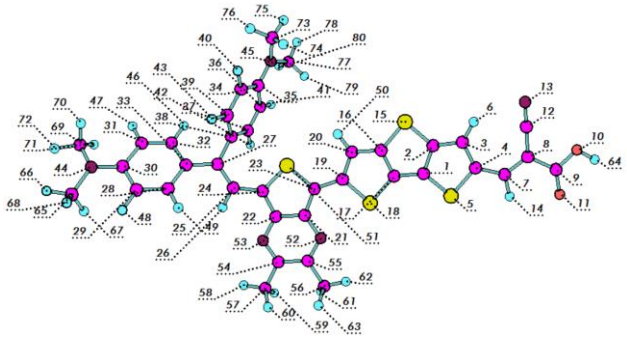




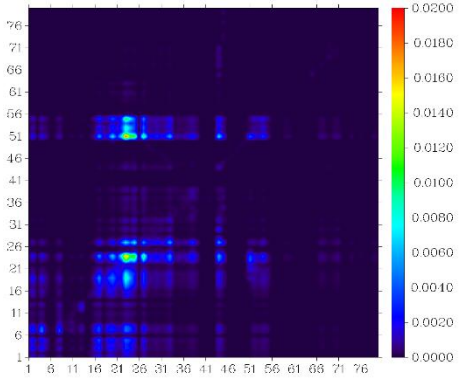
D-ε$_3$-δ$_2$-A







D-ε$_3$-δ$_3$-A



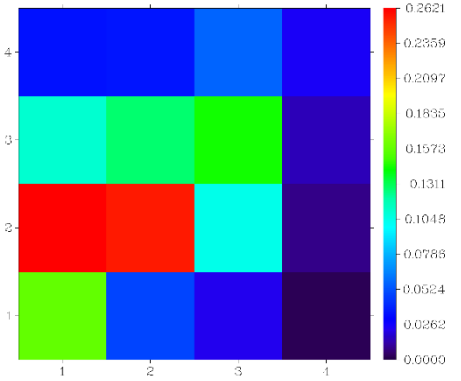
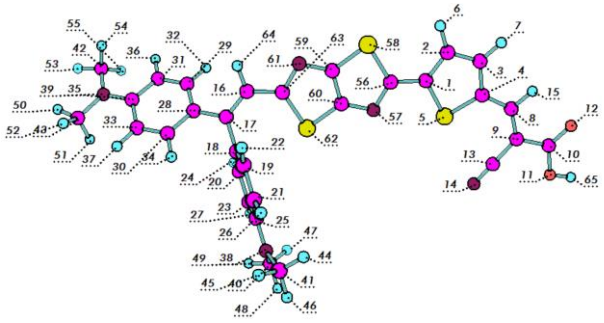
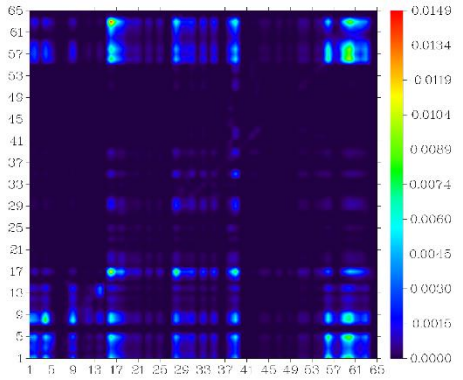
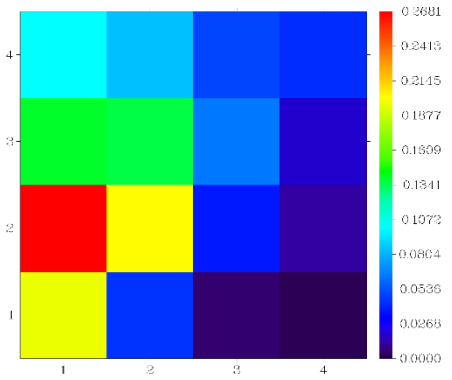


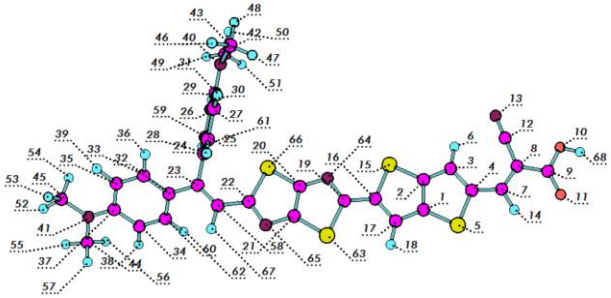
Table S13 (*cont.*). Atom- and fragment-based transition density and color correlation matrix (where the y-axis is the originating, and the x-axis is the receiving fragment for the excited electron) of the investigated systems [M06-2x/6-31G(d,p) solvent model: CPCM, $\varepsilon_{ethanol} = 24.55$].



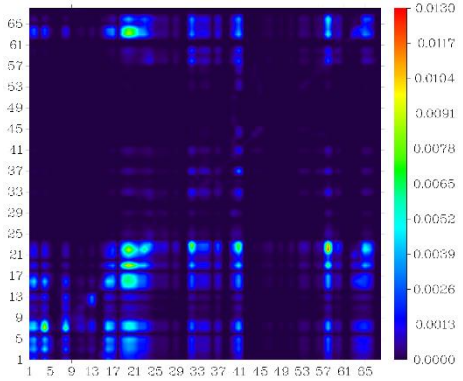
D-ε$_4$-δ$_1$-A

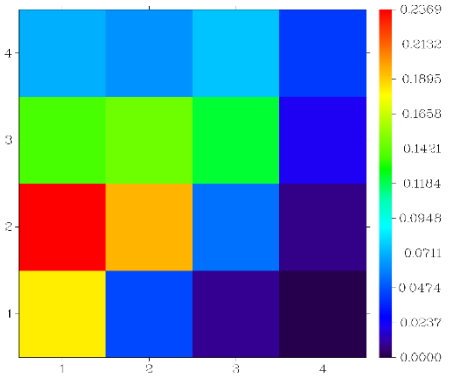


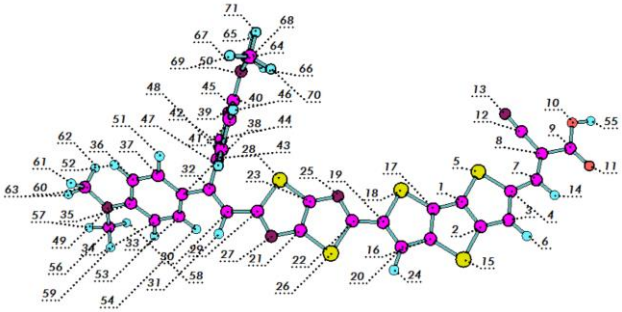




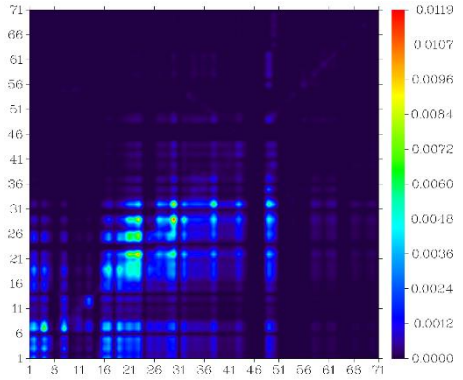
D-ε$_4$-δ$_2$-A







D-ε$_4$-δ$_3$-A



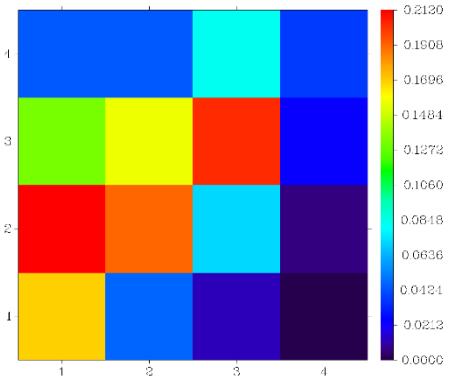
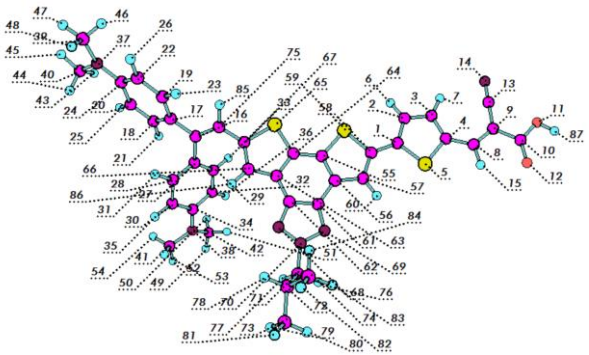
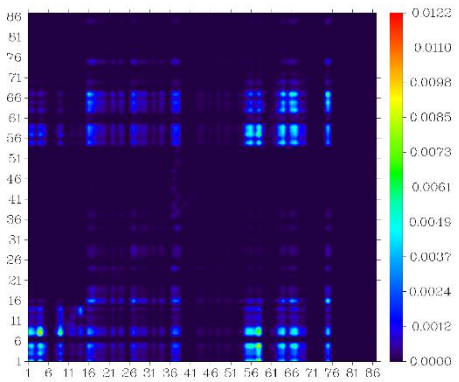
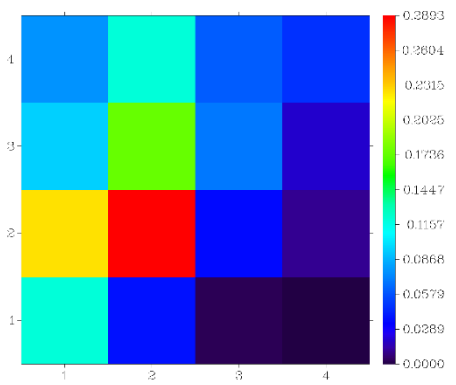


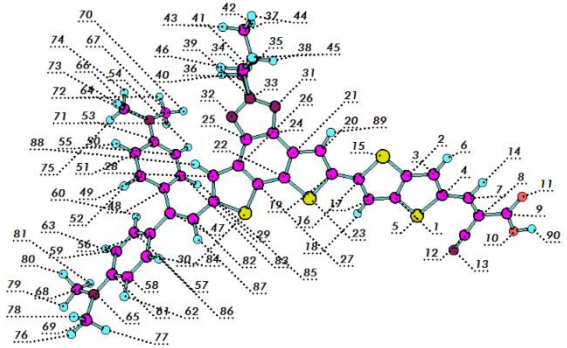
Table S13 (*cont.*). Atom- and fragment-based transition density and color correlation matrix (where the y-axis is the originating, and the x-axis is the receiving fragment for the excited electron) of the investigated systems [M06-2x/6-31G(d,p) solvent model: CPCM, $\varepsilon_{ethanol}$ = 24.55].



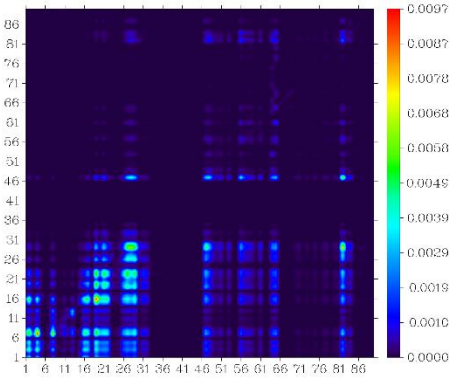
D-ε$_5$-δ$_1$-A

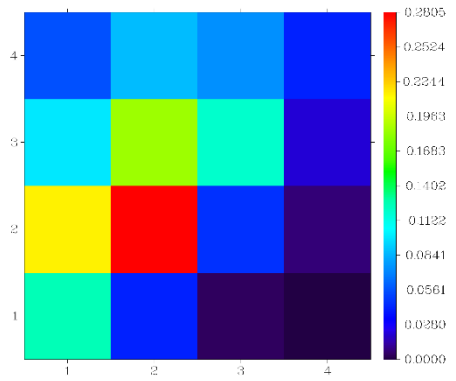


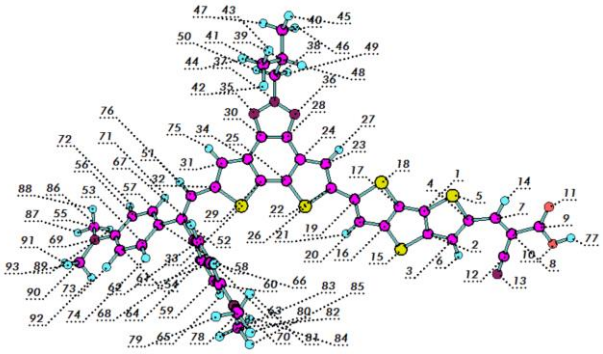




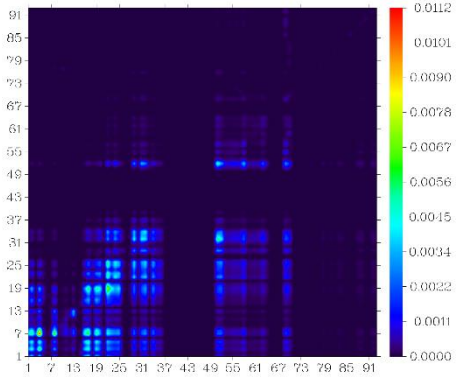
D-ε$_5$-δ$_2$-A







D-ε$_5$-δ$_3$-A



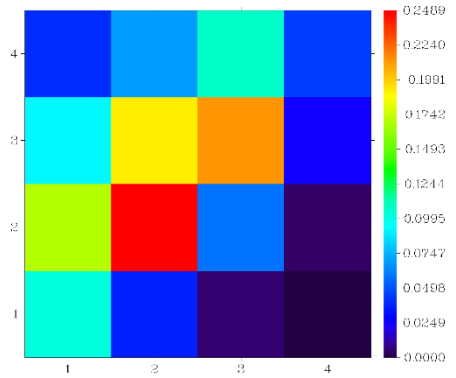
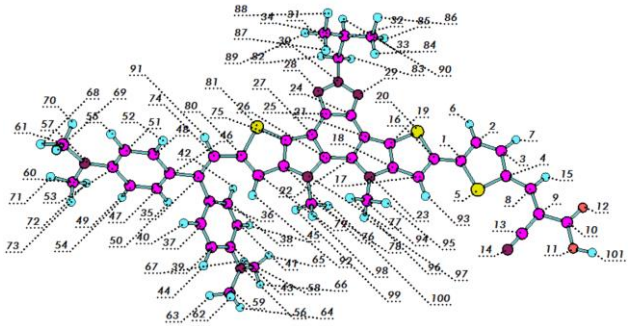
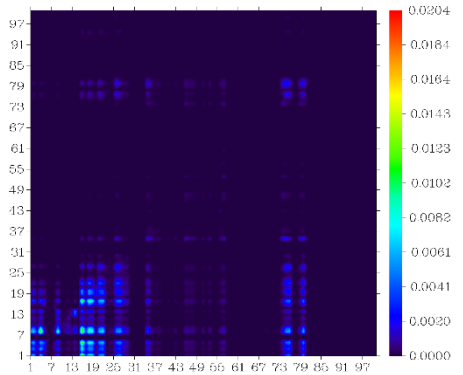
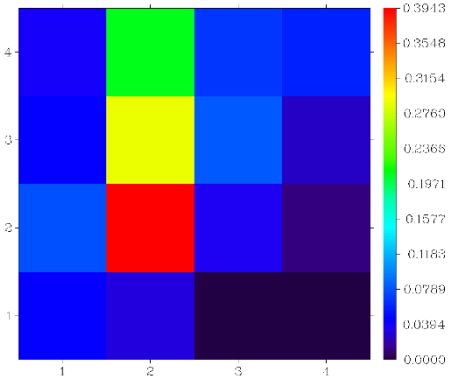


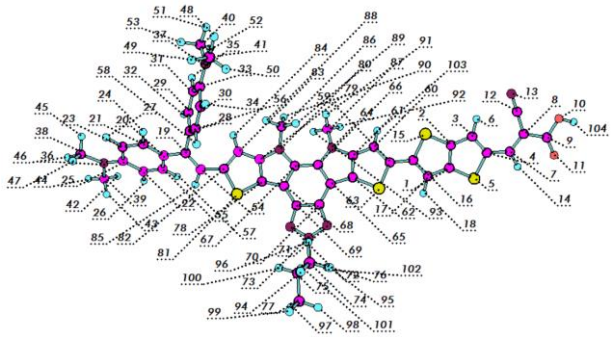
Table S13 (*cont.*). Atom- and fragment-based transition density and color correlation matrix (where the y-axis is the originating, and the x-axis is the receiving fragment for the excited electron) of the investigated systems [M06-2x/6-31G(d,p) solvent model: CPCM, $\varepsilon_{ethanol}$ = 24.55].



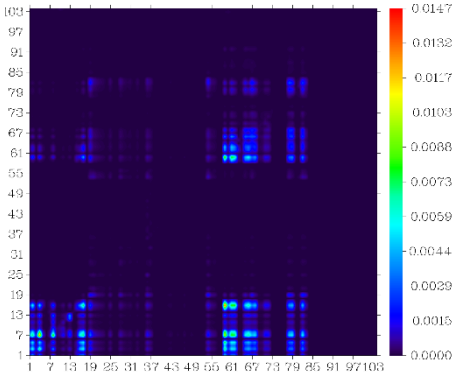
D-ε$_6$-δ$_1$-A

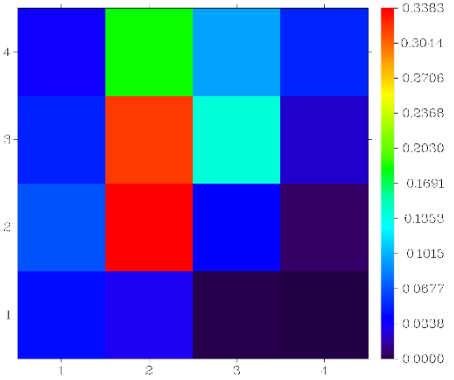


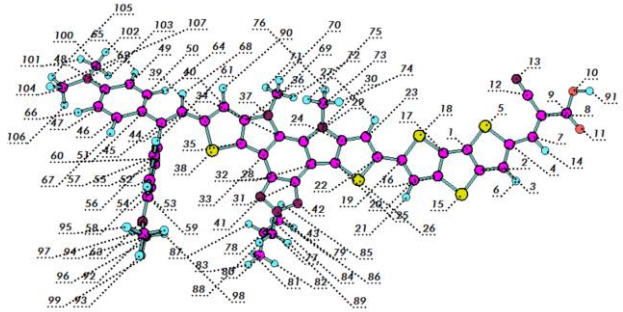




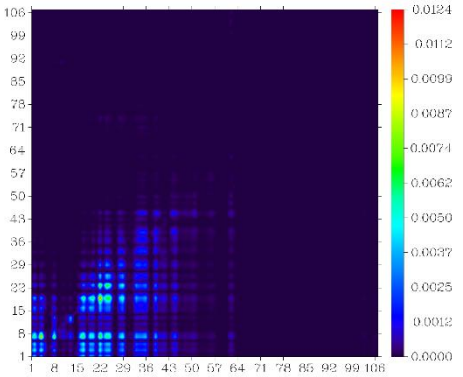
D-ε$_6$-δ$_2$-A







D-ε$_6$-δ$_3$-A



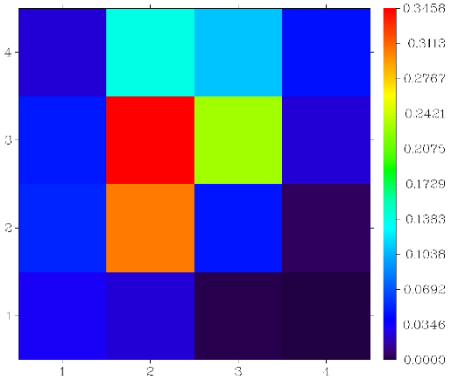


Table SC-1. Optimized Cartesian Coordinates of the D-δ_1-A | [M06-2X/6-31G(d,p) solvent model: CPCM, $\varepsilon_{ethanol}$ =24.55].

C	-0.946064	-1.085369	0.013891
C	-1.640048	-0.030692	-0.573403
C	-3.029965	-0.193566	-0.563747
C	-3.449615	-1.380982	0.030575
S	-2.050706	-2.287800	0.569975
H	-1.141467	0.825888	-1.007752
H	-3.726538	0.516633	-0.981055
C	-4.715376	-1.992205	0.269212
C	0.475827	-1.336261	0.150872
C	1.485012	-0.426001	0.080183
C	2.887017	-0.881371	0.020231
C	3.929227	-0.100172	0.543644
C	3.243017	-2.114390	-0.549638
C	5.244905	-0.530645	0.534674
H	3.698676	0.865053	0.984707
C	4.552356	-2.561220	-0.574465
H	2.477440	-2.727761	-1.016194
C	5.594980	-1.784634	-0.016592
H	6.005644	0.111057	0.961194
H	4.770337	-3.511089	-1.046544
C	1.236698	1.034512	0.105429
C	1.790574	1.886016	-0.857530
C	0.440389	1.615068	1.099924
C	1.530927	3.248061	-0.861097
H	2.425380	1.467233	-1.634016
C	0.182654	2.975197	1.126013
H	0.008845	0.978933	1.868166
C	0.719394	3.832809	0.137563
H	1.963145	3.860285	-1.642749
H	-0.436558	3.374324	1.919700
N	6.892135	-2.226451	-0.016581
N	0.471956	5.183266	0.155581
C	7.230647	-3.463025	-0.694475
C	7.950514	-1.344640	0.437216
C	0.911315	6.003326	-0.957001
C	-0.493653	5.718437	1.096405
H	8.004729	-0.425363	-0.160565
H	7.805879	-1.061308	1.485597
H	8.904340	-1.863995	0.357710
H	7.001070	-3.421829	-1.767438
H	8.296837	-3.651236	-0.577523
H	6.688594	-4.310992	-0.261747
H	-0.579990	6.793403	0.944543
H	-1.487318	5.268278	0.969678
H	-0.172792	5.549401	2.130017
H	0.615376	7.035700	-0.776103
H	2.001660	5.979061	-1.057672
H	0.473269	5.677071	-1.910016
C	-6.017552	-1.626041	0.039943
C	-6.499486	-0.372712	-0.570519
O	-7.838816	-0.334882	-0.634888
O	-5.804307	0.534168	-0.974175
C	-7.024335	-2.563253	0.447888
N	-7.821776	-3.333600	0.786114
H	0.745946	-2.378056	0.304805
H	-4.630845	-2.969711	0.742225
H	-8.087727	0.509517	-1.043038

Table SC-2. Optimized Cartesian Coordinates of the D-ε_1-δ_1-A | [M06-2X/6-31G(d,p) solvent model: CPCM, $\varepsilon_{ethanol}$ =24.55].

C	2.274652	-1.567158	-0.099072
C	3.285418	-0.665074	-0.175930
C	4.687450	-1.142520	-0.163496
C	5.688484	-0.500500	-0.906801
C	5.071963	-2.267770	0.579559
C	6.993402	-0.965547	-0.935079
H	5.434248	0.381931	-1.486683
C	6.372073	-2.746794	0.568946
H	4.337107	-2.764447	1.206985
C	7.370905	-2.114635	-0.204837
H	7.724027	-0.431667	-1.529768
H	6.615770	-3.607646	1.179039
C	3.051720	0.788357	-0.338964
C	3.810705	1.731665	0.364219
C	2.058293	1.277559	-1.194605
C	3.565651	3.091780	0.261242
H	4.605084	1.389538	1.022126
C	1.800591	2.634267	-1.318359
H	1.476519	0.577571	-1.788345
C	2.536455	3.581966	-0.573321
H	4.179071	3.775907	0.834127
H	1.032015	2.957537	-2.009322
N	8.659244	-2.596058	-0.243835
N	2.264579	4.930683	-0.658755
C	9.049135	-3.650057	0.673347
C	9.694181	-1.796799	-0.872106
C	3.204950	5.874584	-0.083485
C	1.363945	5.401276	-1.694433
H	9.480181	-1.644144	-1.934885
H	9.803670	-0.810342	-0.400686
H	10.644508	-2.323708	-0.796412
H	8.458969	-4.555868	0.500861
H	10.096192	-3.897869	0.503801
H	8.925771	-3.356360	1.725116
H	1.264447	6.483103	-1.612779
H	1.721694	5.158088	-2.705064
H	0.368080	4.965010	-1.570928
H	2.842792	6.886844	-0.259694
H	3.286555	5.733843	0.998784
H	4.210265	5.781764	-0.517725
H	2.530588	-2.621224	-0.184824
C	-3.496092	-0.599356	0.177601
C	-4.186298	0.495858	0.667031
C	-5.580562	0.397047	0.503407
C	-5.975800	-0.779861	-0.108549
S	-4.590313	-1.768801	-0.476744
H	-3.688730	1.338463	1.125015
H	-6.271576	1.166845	0.821004
C	-7.271585	-1.275812	-0.463110
C	-8.490027	-0.704606	-0.276172
C	-9.688815	-1.443968	-0.750937
O	-10.820083	-0.774200	-0.510058
O	-9.648476	-2.524345	-1.293424
C	0.838757	-1.301469	0.022499
C	-0.081010	-2.056568	-0.669477
C	0.280905	-0.303268	0.900083
C	-1.480345	-1.822025	-0.615204
H	0.277391	-2.845596	-1.323437
C	-1.143554	-0.054875	0.951433
C	-2.054864	-0.833852	0.152504
H	-2.112858	-2.445980	-1.240538
S	-0.094430	1.405312	2.517665
N	0.967869	0.449893	1.754762
N	-1.472754	0.896496	1.822597
H	-7.310143	-2.246805	-0.954488
H	-11.560759	-1.304746	-0.845066
C	-8.682510	0.567216	0.345923
N	-8.829729	1.600384	0.850053

Table SC-3. Optimized Cartesian Coordinates of the D-ε_2-δ_1-A | [M06-2X/6-31G(d,p) solvent model: CPCM, $\varepsilon_{ethanol}$ =24.55].

C	-2.475822	-1.164810	0.270305	S	4.260244	-1.459129	-0.037334
C	-3.242399	-0.047444	0.155384	H	2.392224	1.627621	-0.340043
C	-2.654470	1.306250	0.305559	H	4.943674	2.070118	-0.560484
C	-2.062403	1.703670	1.509597	C	6.692442	-0.279748	-0.352742
C	-2.679050	2.232428	-0.744555	C	7.686828	0.626555	-0.535564
C	-1.490487	2.957210	1.659909	C	9.089195	0.131476	-0.558418
H	-2.043287	1.007919	2.344640	O	9.967055	1.120676	-0.748402
C	-2.094085	3.482245	-0.621929	O	9.400136	-1.029014	-0.421539
H	-3.147667	1.956541	-1.685637	C	7.462381	2.027466	-0.706641
C	-1.483490	3.880938	0.590371	N	7.272400	3.162331	-0.844509
H	-1.046501	3.218677	2.612181	H	7.043304	-1.304212	-0.238714
H	-2.113492	4.153066	-1.471499	C	-1.036978	-1.264738	0.298215
C	-4.687882	-0.140545	-0.103970	C	-0.330435	-2.438286	0.416663
C	-5.268218	-1.262491	-0.720466	C	1.072683	-2.320750	0.301151
C	-5.554076	0.905202	0.254689	C	1.505258	-1.039655	0.084211
C	-6.629189	-1.352809	-0.945421	S	0.114767	0.035617	0.040790
H	-4.634480	-2.073932	-1.065618	C	-0.671276	-3.860742	0.613704
C	-6.919728	0.833347	0.042721	C	1.652974	-3.680780	0.439513
H	-5.144349	1.794207	0.724775	N	0.562801	-4.530297	0.618807
C	-7.501520	-0.306956	-0.557997	O	-1.749543	-4.399920	0.746730
H	-7.018256	-2.232636	-1.442390	O	2.808431	-4.050289	0.410282
H	-7.539261	1.667764	0.346452	H	-2.956723	-2.139734	0.293302
N	-0.916806	5.123740	0.727634	C	0.706880	-5.961722	0.788816
N	-8.851423	-0.393846	-0.765354	H	1.181875	-6.400770	-0.090678
C	-0.801521	5.987439	-0.432085	H	1.312587	-6.178231	1.670791
C	-0.138018	5.422319	1.914845	H	-0.291513	-6.378423	0.915458
C	-9.400948	-1.536901	-1.469355	H	10.857861	0.734964	-0.753059
C	-9.700088	0.744173	-0.467333				
H	-0.760914	5.390634	2.815145				
H	0.693230	4.717070	2.049163				
H	0.272639	6.427098	1.826825				
H	-1.788173	6.228993	-0.841174				
H	-0.326291	6.920680	-0.133265				
H	-0.201836	5.531481	-1.231616				
H	-10.731473	0.491385	-0.708053				
H	-9.654341	1.005288	0.595835				
H	-9.415885	1.630203	-1.049355				
H	-10.483445	-1.433394	-1.524094				
H	-9.008296	-1.617295	-2.491312				
H	-9.175786	-2.470575	-0.942477				
C	2.832142	-0.487422	-0.078041				
C	3.142833	0.847824	-0.280685				
C	4.520592	1.087292	-0.400926				
C	5.275701	-0.068938	-0.291694				

Table SC-4. Optimized Cartesian Coordinates of the D-ε_3-δ_1-A | [M06-2X/6-31G(d,p) solvent model: CPCM, $\varepsilon_{ethanol}$ =24.55].

C	-2.464209	-1.110291	0.233462	S	4.221738	-1.376058	-0.059412
C	-3.260549	-0.012265	0.141276	H	2.422420	1.762277	-0.274287
C	-4.712967	-0.132478	-0.067301	H	4.981320	2.159879	-0.437505
C	-5.581094	0.910463	0.293971	C	6.680773	-0.224103	-0.290337
C	-5.300290	-1.274427	-0.638693	C	7.702341	0.669449	-0.422027
C	-6.952562	0.817742	0.128192	C	9.089163	0.147437	-0.441133
H	-5.167891	1.816511	0.727138	O	9.994953	1.123393	-0.578219
C	-6.667240	-1.386210	-0.815925	O	9.379322	-1.024233	-0.344738
H	-4.669271	-2.086670	-0.986816	C	7.508298	2.078266	-0.542774
C	-7.539812	-0.342970	-0.424342	N	7.340598	3.221506	-0.640918
H	-7.571534	1.652964	0.431120	H	7.012106	-1.258591	-0.211143
H	-7.060621	-2.282348	-1.279338	C	-1.026932	-1.185144	0.244331
C	-2.692239	1.355532	0.258730	C	-0.315550	-2.390683	0.322451
C	-2.686985	2.237143	-0.828009	C	1.094813	-2.234696	0.207490
C	-2.135473	1.803173	1.461237	C	1.486257	-0.910611	0.038174
C	-2.112281	3.495683	-0.738475	S	0.089258	0.118881	0.030914
H	-3.122585	1.919596	-1.771912	H	-2.922659	-2.095851	0.261482
C	-1.572807	3.065393	1.576841	C	-0.070092	-4.638513	0.525098
H	-2.131440	1.139434	2.322116	C	1.381798	-4.476012	0.419841
C	-1.542969	3.947659	0.473812	N	-0.886357	-3.621304	0.477974
H	-2.109065	4.130293	-1.615657	N	1.941045	-3.306814	0.264597
H	-1.153631	3.365330	2.529097	C	2.266749	-5.684741	0.489820
N	-8.896874	-0.451718	-0.582830	H	2.020971	-6.395526	-0.305155
N	-0.991625	5.204693	0.580275	H	3.307602	-5.379037	0.388192
C	-9.451205	-1.607424	-1.261355	H	2.136951	-6.207550	1.442534
C	-9.744983	0.691365	-0.304387	C	-0.650219	-6.012760	0.690509
C	-0.792860	5.990481	-0.623400	H	10.874609	0.713531	-0.583646
C	-0.211613	5.531761	1.759747	H	-0.265534	-6.496209	1.593853
H	-9.672703	0.990961	0.747065	H	-1.735192	-5.939090	0.759630
H	-9.483265	1.558440	-0.924856	H	-0.388343	-6.654053	-0.156926
H	-10.780811	0.423644	-0.507449				
H	-9.195099	-2.533331	-0.735119				
H	-10.536521	-1.521138	-1.280330				
H	-9.091460	-1.690943	-2.295483				
H	0.182999	6.541568	1.655041				
H	-0.833133	5.507350	2.660436				
H	0.630417	4.840792	1.905808				
H	-0.338068	6.942751	-0.353476				
H	-0.141166	5.485200	-1.349940				
H	-1.748699	6.203666	-1.112006				
C	2.810222	-0.373123	-0.085050				
C	3.156940	0.966118	-0.233159				
C	4.537345	1.179838	-0.321003				
C	5.275510	0.006142	-0.243700				

Table SC-5. Optimized Cartesian Coordinates of the D-ε_4-δ_1-A | [M06-2X/6-31G(d,p) solvent model: CPCM, $\varepsilon_{ethanol}$ =24.55].

C	-4.347503	-1.902705	0.329741
C	-5.162336	-2.986882	0.576613
C	-6.524509	-2.675600	0.412534
C	-6.746112	-1.360905	0.042056
S	-5.243900	-0.489894	-0.105473
H	-4.792096	-3.963855	0.863744
H	-7.333029	-3.382520	0.556730
C	-8.053848	-0.823659	-0.180455
C	-8.439570	0.425477	-0.543653
C	-9.893876	0.693739	-0.701835
O	-10.134669	1.958960	-1.056214
O	-10.756836	-0.135752	-0.529893
C	-7.521094	1.494378	-0.782457
N	-6.767932	2.354144	-0.974554
H	-8.869839	-1.529702	-0.035962
C	2.928917	-1.445217	0.439233
C	3.806662	-0.433302	0.218994
C	3.381410	0.987812	0.263448
C	2.877011	1.545810	1.443612
C	3.489483	1.821698	-0.856108
C	2.470911	2.868841	1.507568
H	2.798139	0.922654	2.330877
C	3.067459	3.141089	-0.820158
H	3.894182	1.419801	-1.781240
C	2.548085	3.704079	0.369362
H	2.091262	3.254066	2.445556
H	3.145108	3.738999	-1.719561
C	5.229316	-0.712420	-0.043285
C	5.664379	-1.939541	-0.571926
C	6.217261	0.247876	0.227165
C	7.002272	-2.209713	-0.792570
H	4.933859	-2.693686	-0.849678
C	7.562333	-0.002861	0.016752
H	5.921370	1.213457	0.626535
C	7.997124	-1.248476	-0.492415
H	7.278113	-3.166290	-1.218659
H	8.281070	0.773053	0.249354
N	2.147403	5.015143	0.420193
N	9.324649	-1.511243	-0.696771
C	2.113274	5.801592	-0.797957
C	1.493164	5.516276	1.613595
C	9.727882	-2.768368	-1.297144
C	10.307401	-0.468088	-0.474978
H	0.580660	4.953203	1.850609
H	2.159822	5.465156	2.481417
H	1.223910	6.560017	1.459029
H	1.447370	5.363551	-1.553398
H	1.755962	6.803363	-0.563986
H	3.112548	5.894742	-1.236799
H	11.298697	-0.860300	-0.696808
H	10.128473	0.404482	-1.116276
H	10.300990	-0.131721	0.567986
H	10.813868	-2.794642	-1.371679
H	9.408851	-3.620056	-0.685959
H	9.309178	-2.894630	-2.303830
C	-2.902363	-1.826867	0.388547
N	-2.237208	-0.729827	0.122229
S	-1.932891	-3.232716	0.822622
C	-0.524556	-2.246373	0.618997
C	-0.911436	-0.972093	0.248423
N	0.796328	-2.498172	0.749345
S	0.499357	0.017918	0.067325
C	1.481864	-1.402158	0.488372
H	3.300983	-2.460887	0.539500
H	-11.095171	2.070219	-1.143748

Table SC-6. Optimized Cartesian Coordinates of the D-ε_5-δ_1-A | [M06-2X/6-31G(d,p) solvent model: CPCM, $\varepsilon_{ethanol}$ =24.55].

C	5.439993	-0.991464	0.159404	H	-11.197148	-5.173737	-0.546533
C	5.839969	-2.285198	0.440704	H	-8.407800	-6.104340	-2.228970
C	7.236633	-2.433459	0.503393	H	-10.170478	-6.039726	-2.178162
C	7.918626	-1.250854	0.270503	H	-9.268716	-4.806569	-3.083245
S	6.799344	0.051788	-0.033134	H	-5.229880	5.086809	4.153997
H	5.141891	-3.098297	0.602603	H	-5.302907	3.376814	4.628883
H	7.726223	-3.374527	0.716008	H	-3.885192	4.012025	3.767402
C	9.319208	-0.953956	0.244599	H	-6.716504	5.546385	2.723789
C	10.375780	-1.786788	0.434659	H	-6.640769	4.885695	1.089140
C	11.744012	-1.211475	0.355722	H	-7.687781	4.120380	2.302653
O	12.688294	-2.134465	0.561345	C	1.605281	-0.303009	-0.119572
O	11.978295	-0.045976	0.132402	C	2.261624	0.924956	-0.243079
C	10.244840	-3.183292	0.705833	C	3.675769	0.803108	-0.157851
N	10.128527	-4.315401	0.924970	C	4.088156	-0.489796	0.026041
H	9.599883	0.079155	0.045816	S	2.735243	-1.600637	0.097390
C	-4.748050	-1.260278	0.065850	H	4.353010	1.647257	-0.225128
C	-5.925871	-2.106934	-0.225557	C	1.435283	2.078789	-0.431480
C	-7.071490	-2.071937	0.583386	C	0.027182	1.970666	-0.481597
C	-5.946162	-2.989354	-1.315699	C	-0.632093	0.706818	-0.343206
C	-8.161898	-2.893161	0.346593	C	0.188003	-0.411525	-0.172285
H	-7.102682	-1.390306	1.428481	S	-0.761594	-1.855967	-0.045606
C	-7.028140	-3.814616	-1.573509	C	-2.017140	0.384623	-0.366342
H	-5.103556	-3.007688	-2.001040	C	-2.260263	-0.956827	-0.213970
C	-8.165098	-3.803184	-0.734388	N	-0.479431	3.199093	-0.665073
H	-9.016024	-2.828636	1.009147	N	1.762673	3.370288	-0.585058
H	-6.996821	-4.457698	-2.444222	N	0.591740	3.965488	-0.709416
C	-4.985963	0.048452	0.723054	C	0.481658	5.390243	-1.002970
C	-5.946233	0.945308	0.241833	C	0.060785	5.632734	-2.454877
C	-4.273511	0.423067	1.868658	C	-0.024402	7.137878	-2.700788
C	-6.160027	2.178170	0.841898	C	1.026386	4.958228	-3.426697
H	-6.537275	0.673518	-0.628857	C	-3.505471	-1.712236	-0.239492
C	-4.478987	1.643361	2.490246	H	1.467761	5.815569	-0.803787
H	-3.541146	-0.264917	2.282372	H	-0.243232	5.815855	-0.305443
C	-5.417383	2.568646	1.977756	H	-0.936361	5.193939	-2.582669
H	-6.910925	2.837720	0.425217	H	-0.715985	7.619545	-2.003444
H	-3.912343	1.875313	3.383323	H	0.959977	7.603597	-2.582147
N	-9.232566	-4.639160	-0.962682	H	-0.371167	7.338820	-3.717532
N	-5.600794	3.800518	2.564782	H	0.728425	5.157134	-4.459514
C	-9.268241	-5.429560	-2.178192	H	2.043173	5.342086	-3.286140
C	-10.460658	-4.442440	-0.216024	H	1.050355	3.873788	-3.284131
C	-6.721986	4.621443	2.148446	H	-3.411587	-2.744514	-0.569346
C	-4.975335	4.073771	3.844851	H	-2.802134	1.118146	-0.499435
H	-10.296791	-4.592119	0.856259	H	13.553167	-1.698148	0.499137
H	-10.879029	-3.437040	-0.360644				

Table SC-7. Optimized Cartesian Coordinates of the D-ε_6-δ_1-A | [M06-2X/6-31G(d,p) solvent model: CPCM, $\varepsilon_{ethanol}$ =24.55].

C	-7.396686	0.308946	0.089335	H	7.865850	1.419824	-1.701162
C	-8.328588	1.294261	0.363011	C	10.858327	0.153139	-0.677000
C	-9.650281	0.828845	0.278854	H	11.029516	-1.552958	0.654358
C	-9.748336	-0.510697	-0.057880	H	10.244688	1.748876	-2.015780
S	-8.159211	-1.206992	-0.266425	N	4.650743	-5.630326	1.108477
H	-8.060337	2.315541	0.605690	N	12.212967	0.348907	-0.832587
H	-10.526116	1.443357	0.453601	C	4.101515	-5.901696	2.423628
C	-10.989832	-1.193969	-0.202273	C	5.089788	-6.750269	0.297412
C	-11.252953	-2.490337	-0.519347	C	13.131637	-0.654995	-0.329482
C	-12.670925	-2.919725	-0.596592	C	12.680222	1.264979	-1.855929
O	-12.789452	-4.213911	-0.912510	H	4.802784	-6.609045	-0.749381
O	-13.614099	-2.188159	-0.397049	H	6.178580	-6.895696	0.336995
C	-10.233816	-3.457872	-0.774971	H	4.605959	-7.658519	0.654925
N	-9.399534	-4.237027	-0.978146	H	3.235906	-5.262447	2.624410
H	-11.872477	-0.580161	-0.029068	H	3.764736	-6.937098	2.459892
C	-5.957841	0.430212	0.083298	H	4.836004	-5.745204	3.226205
C	-5.032569	-0.512857	-0.303580	H	13.768982	1.293768	-1.835200
C	-3.715804	-0.023082	-0.137397	H	12.357647	0.968367	-2.863895
C	-3.644237	1.273609	0.358647	H	12.315802	2.279449	-1.666133
S	-5.214042	1.926421	0.650911	H	14.152309	-0.342813	-0.547512
C	-2.281379	1.640609	0.407934	H	13.039377	-0.759101	0.756218
C	-1.553722	0.511089	-0.039089	H	12.963681	-1.641759	-0.783263
N	-2.444884	-0.491845	-0.389797	C	5.754169	0.662400	-0.159763
C	-1.578742	2.849493	0.686727	C	1.943211	1.474375	0.001160
C	-0.181253	2.924508	0.502285	C	2.061044	0.113690	-0.244107
C	-0.120079	0.547752	-0.078981	N	0.810558	-0.461262	-0.291641
C	0.566158	1.766699	0.133307	C	0.627591	-1.896053	-0.109630
N	0.214028	4.171759	0.791239	C	3.393407	-0.368492	-0.322845
N	-2.016945	4.051781	1.083683	C	4.298780	0.648899	-0.124958
N	-0.912828	4.779583	1.123818	S	3.500812	2.207223	0.142646
C	-0.943367	6.201509	1.448420	H	0.029695	6.431045	1.886235
C	-1.214609	7.090033	0.227121	H	-1.719743	6.331504	2.204794
C	-2.613969	6.865082	-0.343719	H	-2.707810	5.854600	-0.753029
C	-0.143096	6.913676	-0.848060	H	-3.383754	6.990698	0.423462
C	6.598692	-0.395257	-0.079930	H	-2.812570	7.577420	-1.149149
C	6.125265	-1.764555	0.251275	H	-0.192427	5.909899	-1.282381
C	6.372463	-2.841695	-0.605462	H	-0.292783	7.637464	-1.653625
C	5.419281	-2.027232	1.429487	H	0.862168	7.054954	-0.440197
C	5.898075	-4.116868	-0.331162	H	-1.156965	8.116027	0.612559
H	6.942958	-2.675186	-1.515715	H	6.197492	1.648767	-0.281960
C	4.945690	-3.295438	1.728908	H	3.678247	-1.392231	-0.525816
H	5.230712	-1.213676	2.124945	H	-5.297952	-1.494087	-0.680344
C	5.154111	-4.375040	0.840575	C	-2.203347	-1.626150	-1.272773
H	6.111430	-4.914237	-1.031975	H	-3.038289	-1.703410	-1.971228
H	4.418803	-3.448741	2.662422	H	-1.295824	-1.445807	-1.848691
C	8.049363	-0.215217	-0.308006	H	-2.113390	-2.564064	-0.721484
C	8.988547	-1.049589	0.315619	H	0.552363	-2.425746	-1.061395
C	8.555089	0.786865	-1.149349	H	1.486259	-2.283738	0.442646
C	10.353081	-0.878177	0.144567	H	-0.268400	-2.076377	0.484753
H	8.638879	-1.851043	0.960034	H	-13.735521	-4.428074	-0.946868
C	9.915303	0.972722	-1.336264				

Table SC-8. Optimized Cartesian Coordinates of the D-δ_2-A | [M06-2X/6-31G(d,p) solvent model: CPCM, $\varepsilon_{ethanol}$ =24.55].

C	-2.162545	-0.797732	-0.073544
C	-2.384396	-1.982063	0.632055
C	-3.741578	-2.302730	0.785110
C	-4.567140	-1.360143	0.191431
S	-3.646627	-0.059235	-0.563321
H	-4.129477	-3.175736	1.296530
C	-5.986333	-1.465758	0.207297
C	-6.942836	-0.655079	-0.323896
C	-8.363734	-1.035624	-0.137080
O	-9.201018	-0.156864	-0.699922
O	-8.730778	-2.025022	0.456261
C	-6.650146	0.539048	-1.050354
N	-6.406699	1.506815	-1.640895
H	-6.374626	-2.339072	0.729316
S	-0.880538	-2.702207	1.101902
C	0.027003	-1.398658	0.344911
C	-0.799739	-0.463806	-0.242534
C	2.383111	-0.504729	0.196290
C	2.007734	0.928870	0.201430
C	1.212724	1.468394	1.219890
C	2.454406	1.802183	-0.797137
C	0.849501	2.804421	1.231768
C	2.091759	3.140691	-0.812089
H	3.097055	1.421472	-1.586592
C	1.263492	3.677155	0.198605
H	0.248124	3.174182	2.052759
H	2.459156	3.772114	-1.611296
C	3.813127	-0.838046	0.028670
C	4.226259	-2.036160	-0.574119
C	4.822766	0.029834	0.472196
C	5.563440	-2.369409	-0.705832
C	6.165842	-0.287215	0.356607
H	4.545637	0.973816	0.932413
C	6.576666	-1.507849	-0.226078
H	5.822556	-3.296198	-1.202136
H	6.900718	0.418027	0.724229
N	0.876403	4.996415	0.181563
N	7.904774	-1.840583	-0.326645
C	1.483110	5.901244	-0.776351
C	0.196196	5.552149	1.336216
C	8.290397	-3.021851	-1.074864
C	8.914479	-0.855078	0.010045
H	-0.748928	5.031605	1.521258
H	0.804808	5.491932	2.249030
H	-0.032758	6.599207	1.142126
H	1.277229	5.579342	-1.802247
H	1.054436	6.894149	-0.646988
H	2.572486	5.972533	-0.651963
H	9.900524	-1.293211	-0.137644
H	8.837737	0.047358	-0.611402
H	8.834307	-0.553736	1.059831
H	9.373456	-3.129415	-1.034807
H	7.847264	-3.923372	-0.639200
H	7.985049	-2.965152	-2.128554
C	1.476184	-1.502097	0.369766
H	1.860145	-2.508642	0.518793
H	-0.433715	0.405387	-0.772091
H	3.480613	-2.712447	-0.982285
H	0.874754	0.820845	2.024511
H	-10.107384	-0.465116	-0.540215

Table SC-9. Optimized Cartesian Coordinates of the D-ε_1-δ_2-A | [M06-2X/6-31G(d,p) solvent model: CPCM, $\varepsilon_{ethanol}$ =24.55].

C	4.834148	-0.631700	-0.041134	H	-4.073353	6.091548	-1.321325
C	4.802904	0.656379	-0.567537	H	-5.342819	6.139435	-0.080018
C	6.076738	1.206755	-0.793169	H	-3.975492	7.271029	-0.012377
C	7.085271	0.328461	-0.434915	H	-1.820431	5.425431	1.845042
S	6.451586	-1.192282	0.186377	H	-2.741215	6.920096	1.671039
H	6.275644	2.191736	-1.197923	H	-3.388719	5.594911	2.661241
C	8.468550	0.653500	-0.571937	H	-10.922792	-3.610481	-1.467169
C	9.579480	-0.071260	-0.276942	H	-9.604242	-3.124551	-2.552947
C	10.905891	0.544282	-0.537192	H	-9.296663	-4.244834	-1.209295
O	11.912496	-0.266951	-0.197598	H	-11.648057	-1.951975	-0.376413
O	11.060464	1.650413	-1.002593	H	-10.662122	-1.226054	0.894956
C	9.538653	-1.391119	0.268843	H	-10.746853	-0.457843	-0.704328
N	9.498140	-2.461767	0.711520	C	-3.243321	-1.174681	0.016208
H	8.668170	1.642727	-0.980930	H	-3.488112	-2.232090	0.079078
S	3.173000	1.198806	-0.785902	H	-1.813992	0.919630	-1.124624
C	2.549766	-0.331929	-0.174549	C	-4.685092	2.087382	-0.745220
C	3.555275	-1.199029	0.186142	C	-6.750754	-0.109409	0.350264
H	3.369857	-2.184241	0.587985	H	-6.578158	0.803694	0.912578
C	1.106596	-0.541306	-0.111797	H	-5.309897	1.718120	-1.554258
C	0.206218	0.339776	-0.674131	H	12.745999	0.190315	-0.393275
C	-1.201441	0.173087	-0.631870				
C	-1.810188	-0.898041	-0.013421				
C	-0.909873	-1.856161	0.573694				
C	0.525547	-1.689517	0.533377				
N	-1.287505	-2.965220	1.206230				
N	1.176563	-2.681698	1.138188				
S	0.059935	-3.722767	1.696986				
H	0.578231	1.213798	-1.201720				
C	-4.272541	-0.290513	-0.035766				
C	-4.086170	1.172396	0.128329				
C	-3.319019	1.693993	1.176765				
C	-4.495509	3.455257	-0.613508				
C	-3.126178	3.056409	1.333987				
H	-2.866354	1.009757	1.889338				
C	-3.694904	3.978560	0.425430				
H	-4.976609	4.118547	-1.321436				
H	-2.538811	3.405441	2.173994				
C	-5.656328	-0.783814	-0.211347				
C	-5.936864	-1.948363	-0.941968				
C	-8.047761	-0.578354	0.220910				
C	-7.226583	-2.430910	-1.088964				
H	-5.125113	-2.473428	-1.437346				
C	-8.323115	-1.764872	-0.495394				
H	-8.851801	-0.018489	0.682173				
H	-7.384748	-3.321461	-1.684490				
N	-3.478938	5.332390	0.551085				
N	-9.604472	-2.248432	-0.614522				
C	-2.829790	5.836971	1.746498				
C	-4.263484	6.248899	-0.254843				
C	-10.716199	-1.423182	-0.180678				
C	-9.863939	-3.358861	-1.511316				

Table SC-10. Optimized Cartesian Coordinates of the D-ε_2-δ_2-A | [M06-2X/6-31G(d,p) solvent model: CPCM, $\varepsilon_{ethanol}$ =24.55].

C	4.644679	-0.748874	-0.012306
C	4.963030	0.524428	0.452514
C	6.343968	0.797803	0.441339
C	7.074802	-0.275388	-0.035216
S	6.051562	-1.639151	-0.473996
H	6.805563	1.724553	0.760477
C	8.499677	-0.244090	-0.146108
C	9.369447	-1.187241	-0.590597
C	10.819173	-0.859047	-0.589461
O	11.562911	-1.865110	-1.058818
O	11.273882	0.195222	-0.208897
C	8.965947	-2.475687	-1.059448
N	8.631384	-3.518771	-1.438298
H	8.964317	0.685902	0.177619
S	3.546964	1.408598	0.917073
C	2.535012	0.040467	0.479533
C	3.259517	-1.028526	0.000805
H	2.815157	-1.962438	-0.321331
C	1.094104	0.079345	0.626927
C	0.245529	1.037934	1.116008
C	-1.123199	0.664670	1.121589
C	-1.383891	-0.579239	0.608704
S	0.138268	-1.308922	0.140756
C	0.351827	2.399734	1.701449
C	-1.894405	1.749417	1.767119
N	-0.950944	2.752603	2.041675
O	-3.064388	1.829690	2.064947
O	1.327694	3.100914	1.873292
C	-1.309376	4.002839	2.678916
H	-1.673988	3.824451	3.692769
H	-0.415640	4.624367	2.712735
H	-2.088251	4.502993	2.100347
C	-3.804938	-0.820749	-0.010270
C	-3.958003	0.548511	-0.547869
C	-5.065659	1.338407	-0.212590
C	-3.139771	2.398648	-1.901458
C	-5.212687	2.632294	-0.684207
H	-5.819734	0.934806	0.457347
C	-4.248749	3.200848	-1.546656
H	-2.382637	2.779691	-2.575298
H	-6.078564	3.204903	-0.376218
C	-4.997112	-1.694070	-0.003062
C	-5.993010	-1.574417	-0.984841
C	-6.265743	-3.547217	0.946730
C	-7.088419	-2.419847	-1.024810
H	-5.896072	-0.807654	-1.747577
C	-7.252111	-3.441984	-0.061514
H	-6.361787	-4.287742	1.730948
H	-7.821042	-2.286322	-1.810960
N	-4.390705	4.477457	-2.037810
N	-8.325662	-4.293068	-0.100617
C	-5.436185	5.328481	-1.501569
C	-3.280559	5.090763	-2.742846
C	-8.515493	-5.262429	0.960966
C	-9.381376	-4.073673	-1.070193
H	-2.370024	5.128822	-2.129359
H	-3.048748	4.543939	-3.662678
H	-3.554031	6.107963	-3.019953
H	-5.335043	5.479607	-0.417815
H	-5.390343	6.299742	-1.992503
H	-6.425422	4.901536	-1.695108
H	-10.145644	-4.838676	-0.942467
H	-9.852814	-3.089677	-0.949095
H	-8.999161	-4.145118	-2.094572
H	-9.400309	-5.858543	0.742651
H	-7.659124	-5.941947	1.031665
H	-8.652880	-4.782880	1.939089
C	-2.612930	-1.325116	0.410551
H	-2.543391	-2.394277	0.593734
C	-3.011761	1.108238	-1.414773
C	-5.173966	-2.695847	0.963488
H	-2.155242	0.514716	-1.722921
H	-4.450406	-2.792160	1.768149
H	12.493045	-1.588556	-1.030909

Table SC-11. Optimized Cartesian Coordinates of the D-ε_3-δ_2-A | [M06-2X/6-31G(d,p) solvent model: CPCM, $\varepsilon_{ethanol}$ =24.55].

C	4.659513	-0.849073	0.021317
C	4.936338	0.437817	-0.438751
C	6.305567	0.745651	-0.455138
C	7.081186	-0.312204	-0.005140
S	6.098864	-1.705582	0.444202
H	6.735461	1.687016	-0.776689
C	8.501436	-0.246796	0.070950
C	9.409930	-1.171848	0.486193
C	10.846599	-0.806490	0.448941
O	11.631854	-1.796854	0.887343
O	11.266839	0.262786	0.067225
C	9.051953	-2.472334	0.955003
N	8.754158	-3.526782	1.334429
H	8.935283	0.696616	-0.256870
S	3.480778	1.288901	-0.857810
C	2.514365	-0.114466	-0.410153
C	3.284378	-1.167848	0.040399
H	2.872919	-2.115414	0.365776
C	1.081473	-0.094639	-0.535116
C	0.252325	0.934893	-0.968541
C	-1.131520	0.584378	-0.994443
C	-1.385072	-0.704931	-0.525215
S	0.111682	-1.469214	-0.126175
C	-3.823221	-0.911334	0.050177
C	-3.955197	0.472146	0.561316
C	-3.045165	0.999343	1.483117
C	-5.031212	2.652072	0.474963
C	-3.096590	2.325697	1.880955
H	-2.273040	0.354125	1.894365
C	-4.071835	3.201326	1.354069
H	-5.826374	3.269993	0.076342
H	-2.374807	2.682170	2.605456
C	-5.034409	-1.756756	0.016801
C	-5.204016	-2.774385	-0.934170
C	-7.184052	-2.402090	0.970825
C	-6.318218	-3.597214	-0.938704
H	-4.456735	-2.906228	-1.711533
C	-7.336769	-3.444999	0.029572
H	-7.943903	-2.228242	1.722557
H	-6.405807	-4.350715	-1.711460
N	-4.089580	4.538986	1.688473
N	-8.432727	-4.273958	0.052491
C	-3.246952	5.004858	2.773480
C	-5.232506	5.344750	1.303469
C	-9.548052	-3.952407	0.922602
C	-8.636631	-5.214854	-1.032393
H	-5.338458	5.372526	0.214122
H	-6.174077	4.969712	1.728829
H	-5.078962	6.366454	1.649120
H	-2.189348	4.842103	2.542965
H	-3.397574	6.075777	2.905189
H	-3.470486	4.501257	3.724587
H	-9.536320	-5.795539	-0.832814
H	-8.752511	-4.714899	-2.003909
H	-7.796493	-5.912776	-1.105964
H	-10.324465	-4.705748	0.796656
H	-9.240862	-3.960061	1.973495
H	-9.978959	-2.966660	0.699840
C	-2.629747	-1.429958	-0.347740
H	-2.578189	-2.500117	-0.536583
C	-4.967628	1.319554	0.099406
C	-6.064758	-1.586555	0.954168
H	-5.708019	0.931744	-0.595478
H	-5.977572	-0.801047	1.699048
N	0.682346	2.179442	-1.342184
N	-2.074467	1.458532	-1.459648
C	-1.656087	2.647268	-1.785458
C	-0.239927	3.022768	-1.714808
C	0.177216	4.410224	-2.101739
C	-2.670778	3.655500	-2.239989
H	1.250930	4.522473	-1.953661
H	-0.062664	4.611619	-3.150602
H	-0.350887	5.157330	-1.501228
H	-3.648893	3.177103	-2.286392
H	-2.724776	4.487684	-1.528733
H	-2.416825	4.075060	-3.217987
H	12.551964	-1.492387	0.835238

Table SC-12. Optimized Cartesian Coordinates of the D-ε_4-δ_2-A | [M06-2X/6-31G(d,p) solvent model: CPCM, $\varepsilon_{ethanol}$ =24.55].

C	5.590890	-1.612481	0.174529
C	5.654540	-0.240591	-0.070252
C	6.963710	0.264508	-0.189912
C	7.903925	-0.738583	-0.033917
S	7.162155	-2.306567	0.258508
H	7.208254	1.300892	-0.379818
C	9.336483	-0.688877	-0.077043
C	10.155103	0.375339	-0.278734
C	11.623542	0.136970	-0.276147
O	12.314507	1.261653	-0.481599
O	12.132915	-0.946926	-0.108450
C	9.686340	1.707827	-0.493694
N	9.293847	2.784300	-0.667570
H	9.863840	-1.629875	0.071414
S	4.071178	0.461297	-0.160550
C	3.351525	-1.107530	0.137064
C	4.270345	-2.114036	0.295035
H	4.012981	-3.148965	0.484414
C	1.906212	-1.192294	0.194880
C	-0.162531	-0.538164	0.095866
C	-0.416829	-1.852961	0.433298
C	-2.498068	-1.203957	0.363483
C	-4.914337	-0.462644	0.175906
C	-4.630007	0.994943	0.168784
C	-4.151434	1.643782	1.311934
C	-4.585115	3.130476	-0.992113
C	-3.887242	3.004715	1.318457
H	-3.974267	1.065110	2.215057
C	-4.094441	3.787141	0.160269
H	-4.756527	3.684151	-1.906643
H	-3.517610	3.459917	2.228612
C	-6.316888	-0.876019	-0.012277
C	-7.372530	-0.010196	0.314663
C	-7.983088	-2.528984	-0.672699
C	-8.698351	-0.382730	0.175079
H	-7.146057	0.977378	0.705714
C	-9.044309	-1.659288	-0.324784
H	-8.191416	-3.509944	-1.081322
H	-9.470780	0.321645	0.457621
N	-3.843302	5.137921	0.157546
N	-10.351148	-2.035148	-0.479427
C	-3.906539	5.870453	-1.093177
C	-3.162919	5.735527	1.291047
C	-10.668936	-3.373697	-0.938020
C	-11.413380	-1.137657	-0.068853
H	-3.757692	5.635613	2.205152
H	-2.179668	5.280088	1.471121
H	-3.021306	6.798286	1.099726
H	-4.911158	5.821030	-1.525636
H	-3.676942	6.917832	-0.902307
H	-3.194521	5.486861	-1.836592
H	-12.374556	-1.609654	-0.266157
H	-11.358077	-0.903893	1.001943
H	-11.376199	-0.194294	-0.625973
H	-11.750862	-3.484357	-0.990217
H	-10.259378	-3.561336	-1.937354
H	-10.276084	-4.140402	-0.258466
C	-3.936116	-1.383054	0.364644
C	-4.860869	1.772669	-0.972067
C	-6.665207	-2.138894	-0.518977
H	-5.248573	1.298179	-1.869743
H	-5.884627	-2.826356	-0.831408
S	1.086733	-2.700516	0.594835
N	1.132166	-0.160880	-0.033623
N	-1.704793	-2.234713	0.579729
S	-1.665126	0.314675	-0.036356
H	-4.205049	-2.428580	0.486525
H	13.259600	1.040005	-0.468496

Table SC-13. Optimized Cartesian Coordinates of the D-ε_5-δ_2-A | [M06-2X/6-31G(d,p) solvent model: CPCM, $\varepsilon_{ethanol}$ =24.55].

C	-6.719018	-0.864554	0.141087	H	2.249889	5.675987	-1.824439
C	-7.180561	0.290170	-0.486140	C	5.334969	-1.635695	0.051439
C	-8.582471	0.369853	-0.563920	C	5.793683	-0.296860	0.496198
C	-9.190299	-0.733071	0.010221	C	6.860845	0.354038	-0.132692
S	-8.018572	-1.878915	0.653420	C	5.584204	1.621123	1.979474
H	-9.144023	1.180436	-1.012433	C	7.273099	1.621346	0.253288
C	-10.609271	-0.889543	0.056677	H	7.375520	-0.140934	-0.952124
C	-11.370029	-1.883862	0.584272	C	6.630977	2.299425	1.313024
C	-12.847158	-1.767663	0.476763	H	5.086449	2.078884	2.825313
O	-13.475677	-2.799984	1.047257	H	8.098936	2.084127	-0.272595
O	-13.417096	-0.847358	-0.063469	C	6.353910	-2.697727	-0.096404
C	-10.825274	-3.032927	1.235940	C	7.506813	-2.723058	0.702850
N	-10.375826	-3.962642	1.762580	C	7.139509	-4.750556	-1.153962
H	-11.174366	-0.081517	-0.405086	C	8.445419	-3.737561	0.603836
S	-5.862068	1.295162	-0.995561	H	7.664970	-1.932265	1.430448
C	-4.707519	0.149415	-0.337852	C	8.279780	-4.793462	-0.320253
C	-5.306878	-0.949329	0.228985	H	6.986401	-5.507613	-1.912892
H	-4.761483	-1.758853	0.698436	H	9.312837	-3.709497	1.251475
C	-3.289169	0.430161	-0.440139	N	7.009816	3.568788	1.683361
C	-2.682015	1.624669	-0.719508	N	9.192821	-5.817592	-0.407720
C	-1.261993	1.531796	-0.735328	C	8.218048	4.140604	1.120581
C	-0.802345	0.241270	-0.460772	C	6.442651	4.158984	2.880329
S	-2.121800	-0.853289	-0.196473	C	10.449567	-5.712448	0.309096
C	-0.264632	2.530941	-0.973012	C	9.075660	-6.784985	-1.481743
C	1.112350	2.214179	-0.937594	H	5.354632	4.248758	2.793607
C	1.568783	0.885316	-0.661022	H	6.666961	3.573663	3.782780
C	0.583575	-0.077758	-0.427225	H	6.850482	5.160755	3.009179
C	2.889659	0.362700	-0.589581	H	8.133762	4.245096	0.033732
C	2.922512	-0.978347	-0.300350	H	8.369408	5.134151	1.540497
S	1.300306	-1.625223	-0.116445	H	9.106806	3.532222	1.337473
N	-0.387212	3.836432	-1.255080	H	9.863684	-7.529382	-1.375357
N	1.805005	3.333220	-1.198126	H	8.114225	-7.306178	-1.433205
N	0.862699	4.237457	-1.379823	H	9.164718	-6.322106	-2.474305
C	1.182462	5.644288	-1.595476	H	11.049285	-6.598129	0.103445
C	0.858565	6.488969	-0.360411	H	11.025215	-4.825245	0.011942
C	1.563021	5.942863	0.879553	H	10.282387	-5.663161	1.390192
C	1.250583	7.939103	-0.637402	C	4.030903	-1.917151	-0.196241
H	-0.225881	6.435903	-0.204641	C	5.182837	0.360100	1.570844
H	1.244572	4.920939	1.106305	C	6.210475	-3.730341	-1.035034
H	2.649312	5.935765	0.733935	H	4.368613	-0.132318	2.095756
H	1.340787	6.566810	1.749165	H	5.362926	-3.718561	-1.714307
H	0.981597	8.575471	0.209311	H	3.766906	-2.957813	-0.370491
H	2.332083	8.021683	-0.790993	H	3.779415	0.957124	-0.754348
H	0.749149	8.327516	-1.528658	H	-3.223229	2.547982	-0.893110
H	0.615999	5.983489	-2.465942	H	-14.431094	-2.664334	0.941855

Table SC-14. Optimized Cartesian Coordinates of the D-ε_6-δ_2-A | [M06-2X/6-31G(d,p) solvent model: CPCM, $\varepsilon_{ethanol}$ =24.55].

C	-8.685913	0.408873	-0.362125	H	7.328439	-6.731265	1.428524
C	-8.733005	-0.978797	-0.223882	C	6.716471	0.574798	-0.557183
C	-10.031804	-1.516912	-0.207590	C	9.489809	0.545814	-1.631248
C	-10.989165	-0.523603	-0.334610	C	6.444396	-1.758139	1.509578
S	-10.266880	1.075255	-0.479467	H	8.774027	1.050174	-2.274199
H	-10.261640	-2.569375	-0.109186	H	6.232860	-0.824906	2.024783
C	-12.417150	-0.603917	-0.370951	C	-4.989331	0.103984	-0.255268
C	-13.223897	-1.694083	-0.275912	C	-4.041951	-0.863600	-0.492227
C	-14.692641	-1.484444	-0.352627	C	-2.735164	-0.326047	-0.377072
O	-15.370070	-2.632232	-0.250699	C	-2.697081	1.026992	-0.066267
O	-15.217501	-0.403355	-0.492315	S	-4.286123	1.677945	0.116303
C	-12.736678	-3.026190	-0.109829	N	-1.451861	-0.796234	-0.550910
N	-12.326118	-4.101756	0.025006	C	-1.342106	1.427991	-0.054550
H	-12.956801	0.334054	-0.493086	C	-0.585251	0.265351	-0.335070
S	-7.134777	-1.646037	-0.102140	C	0.847735	0.331438	-0.376008
C	-6.428973	-0.046070	-0.267560	C	1.503383	1.584414	-0.334276
C	-7.373941	0.944245	-0.389114	C	0.728733	2.761392	-0.113184
H	-7.132661	1.992406	-0.514681	C	-0.668542	2.677930	0.071262
C	7.583677	-0.435380	-0.300538	N	-1.138135	3.912293	0.300028
C	9.025251	-0.279063	-0.596562	N	1.091909	4.045971	0.009700
C	9.996527	-0.945667	0.164607	N	-0.052047	4.664340	0.242390
C	10.841350	0.718258	-1.883638	C	-0.087063	6.087578	0.551730
C	11.352978	-0.783717	-0.068855	C	0.528425	6.383676	1.922147
H	9.679352	-1.594855	0.975628	C	-0.155536	5.570066	3.018497
C	11.816259	0.051420	-1.108919	C	0.435121	7.883769	2.194630
H	11.138854	1.363056	-2.701202	C	2.887253	1.310795	-0.437800
H	12.055896	-1.308813	0.565849	C	3.039040	-0.066968	-0.497499
C	7.146661	-1.722103	0.300338	N	1.802822	-0.674053	-0.455582
C	7.424384	-2.944782	-0.318767	S	4.424180	2.096343	-0.424438
C	6.002728	-2.949996	2.062677	C	5.262334	0.537213	-0.489832
C	6.983269	-4.149240	0.211684	C	4.383119	-0.520404	-0.529662
H	7.994685	-2.953546	-1.244129	H	4.696206	-1.554256	-0.594322
C	6.242582	-4.182545	1.413241	H	7.135047	1.528976	-0.871895
H	5.474298	-2.922064	3.007549	C	1.657064	-2.072021	-0.068899
H	7.221290	-5.067097	-0.311075	C	-1.175199	-2.041724	-1.254802
N	13.161272	0.194961	-1.370546	H	2.522827	-2.353012	0.534326
N	5.772730	-5.369409	1.932636	H	0.763258	-2.187214	0.544627
C	14.122563	-0.338199	-0.423612	H	1.599478	-2.735532	-0.934126
C	13.592412	1.236455	-2.284283	H	-1.061075	-2.883946	-0.569513
C	6.236883	-6.620498	1.363708	H	-2.004803	-2.246387	-1.933505
C	5.210146	-5.379532	3.269551	H	-0.270764	-1.925342	-1.851834
H	13.198490	1.061882	-3.290553	H	0.279872	5.801925	3.994155
H	13.271197	2.236149	-1.960045	H	-1.225659	5.803149	3.059075
H	14.679836	1.225109	-2.347096	H	-0.049447	4.494801	2.846703
H	14.018992	-1.424041	-0.332606	H	0.925585	8.465366	1.408564
H	15.129026	-0.130141	-0.784963	H	-0.612396	8.199760	2.249669
H	14.012197	0.101096	0.577736	H	0.911052	8.129525	3.147322
H	4.907477	-6.395792	3.519225	H	1.585725	6.095324	1.873739
H	5.925185	-5.032331	4.028531	H	0.448245	6.614766	-0.241648
H	4.320841	-4.743160	3.322682	H	-1.140748	6.374788	0.526107
H	5.772096	-7.447416	1.899292	H	-4.284637	-1.889790	-0.743339
H	5.948455	-6.701711	0.310790	H	-16.316976	-2.427362	-0.311528

Table SC-15. Optimized Cartesian Coordinates of the D-δ_3-A | [M06-2X/6-31G(d,p) solvent model: CPCM, $\varepsilon_{ethanol}$ =24.55].

C	-3.324398	-0.255929	-0.215397	H	9.455943	-1.865919	-0.039828
C	-3.704965	0.965572	-0.776002	H	9.096975	-2.521698	1.571454
C	-5.096184	1.139501	-0.835460	H	10.029072	-3.482130	0.419869
C	-5.780490	0.049629	-0.320670	C	3.941310	5.932625	-0.631954
S	-4.684505	-1.208975	0.245599	H	4.999896	5.666330	-0.717618
H	-5.603718	2.011080	-1.231593	H	3.465711	5.760913	-1.607527
C	-7.202534	-0.011645	-0.266242	H	3.883717	6.995652	-0.401549
C	-8.030309	-0.988052	0.195280	C	2.400748	5.873001	1.336053
C	-9.493963	-0.757466	0.119360	H	2.545660	6.947268	1.229871
O	-10.193295	-1.789876	0.602908	H	1.347440	5.641427	1.127027
O	-10.001330	0.246422	-0.327255	H	2.607612	5.608163	2.378325
C	-7.564086	-2.221589	0.744077				
N	-7.176625	-3.220982	1.186260				
H	-7.713087	0.866806	-0.657952				
S	-2.333742	1.945523	-1.248016				
C	-1.250422	0.695302	-0.684104				
C	-1.918820	-0.409339	-0.165658				
S	-0.800812	-1.610550	0.372012				
C	0.567316	-0.611279	-0.105163				
C	0.159766	0.584360	-0.656594				
C	1.896442	-1.176227	0.069120				
H	1.927272	-2.260498	0.150712				
H	0.846954	1.333750	-1.026007				
C	3.078443	-0.508423	0.099585				
C	5.512158	-0.750830	0.666713				
C	6.710359	-1.445574	0.654279				
C	6.815296	-2.700463	0.012794				
C	5.658751	-3.196769	-0.630918				
C	4.469585	-2.487837	-0.602932				
C	4.353944	-1.253895	0.054934				
C	2.500395	3.049943	1.277819				
C	3.251810	3.810815	0.352605				
C	3.958879	3.106192	-0.646726				
C	3.916655	1.720655	-0.703553				
C	3.153570	0.970165	0.197495				
C	2.461042	1.667991	1.193895				
H	1.949885	3.541334	2.070406				
H	4.544396	3.640966	-1.383900				
H	4.475896	1.207000	-1.481222				
H	1.869031	1.109637	1.914223				
N	7.993355	-3.406802	0.009249				
N	3.302672	5.183075	0.433026				
H	3.613767	-2.889111	-1.138333				
H	5.694860	-4.132920	-1.173913				
H	7.570506	-1.008812	1.146142				
H	5.468561	0.208523	1.174091				
H	-11.136333	-1.574653	0.522859				
C	8.103310	-4.604749	-0.801029				
H	7.943047	-4.401933	-1.868759				
H	9.098940	-5.027937	-0.675573				
H	7.375650	-5.359377	-0.484510				
C	9.201141	-2.780559	0.512529				

Table SC-16. Optimized Cartesian Coordinates of the D-ε_1-δ_3-A | [M06-2X/6-31G(d,p) solvent model: CPCM, $\varepsilon_{ethanol}$ =24.55].

C	-5.586515	-0.665241	-0.073731	H	9.464389	-0.740163	-1.666243
C	-6.214759	0.467343	0.450478	H	7.205503	0.153492	-1.607151
C	-7.615859	0.446813	0.333685	H	1.967124	-2.855492	-1.162084
C	-8.057798	-0.711084	-0.284446	H	-0.405385	-2.381385	-1.050932
S	-6.725166	-1.774560	-0.721778	H	-1.831382	1.487171	1.298430
H	-8.271527	1.234160	0.680742	H	-13.677257	-1.000074	-0.876036
C	-9.381635	-1.148447	-0.608052	C	10.762096	-3.828995	0.726897
C	-10.571217	-0.530224	-0.384897	H	10.139376	-4.726485	0.661742
C	-11.810680	-1.216500	-0.833888	H	11.794134	-4.127063	0.545524
O	-12.906659	-0.503741	-0.556360	H	10.686901	-3.433413	1.749603
O	-11.828482	-2.291990	-1.386932	C	11.413016	-2.116647	-0.963151
C	-10.696068	0.741595	0.253172	H	11.173292	-2.003164	-2.024894
N	-10.784413	1.774484	0.771704	H	11.569461	-1.115223	-0.538173
H	-9.472801	-2.113118	-1.105055	H	12.346648	-2.673452	-0.892109
S	-5.080082	1.620792	1.115751	C	5.230771	5.799555	-0.452561
C	-3.758572	0.563561	0.682977	H	6.224406	5.646765	-0.896828
C	-4.177103	-0.605160	0.062662	H	4.902806	6.813839	-0.677440
S	-2.837731	-1.618769	-0.337664	H	5.326504	5.713894	0.634296
C	-1.708742	-0.442575	0.328786	C	3.349475	5.306271	-2.010444
C	-2.352339	0.660036	0.838575	H	3.678152	4.983294	-3.008423
C	0.255373	-1.749740	-0.463815	H	2.337479	4.924025	-1.844781
C	1.647025	-2.028011	-0.536277	H	3.299643	6.394428	-1.997076
C	-0.274985	-0.718137	0.277188				
C	2.603083	-1.276280	0.106550				
C	2.093855	-0.224663	0.949594				
C	0.677742	0.064618	1.023312				
N	2.821092	0.546688	1.753424				
N	0.395722	1.061055	1.860117				
S	1.803465	1.561808	2.500127				
C	4.028376	-1.595408	-0.026440				
H	4.250032	-2.660371	-0.055137				
C	5.065118	-0.733850	-0.174459				
C	7.448786	-0.699598	-0.980390				
C	8.736509	-1.210288	-1.016799				
C	9.099271	-2.323012	-0.225923				
C	8.105783	-2.867562	0.617542				
C	6.822088	-2.345310	0.634493				
C	6.451222	-1.258214	-0.168938				
C	5.492733	3.028638	0.044414				
C	4.466807	3.510465	-0.798803				
C	3.678253	2.551487	-1.471725				
C	3.885397	1.194876	-1.273426				
C	4.878049	0.716589	-0.410946				
C	5.687051	1.667975	0.222096				
H	6.145020	3.720078	0.563169				
H	2.907203	2.864514	-2.164680				
H	3.264526	0.485431	-1.813843				
H	6.482638	1.332811	0.882120				
N	10.370165	-2.853596	-0.273657				
N	4.246745	4.861866	-0.960419				
H	6.091735	-2.775101	1.314370				
H	8.339928	-3.694607	1.276192				

Table SC-17. Optimized Cartesian Coordinates of the D-ε_2-δ_3-A | [M06-2X/6-31G(d,p) solvent model: CPCM, $\varepsilon_{ethanol}$ =24.55].

C	-5.079838	-0.422528	-0.143232
C	-5.459698	0.914699	-0.276884
C	-6.851415	1.107919	-0.340507
C	-7.534456	-0.093521	-0.255778
S	-6.443007	-1.464078	-0.098632
H	-7.332153	2.071309	-0.444660
C	-8.938611	-0.374458	-0.278484
C	-9.986938	0.484589	-0.370431
C	-11.359841	-0.086187	-0.372430
O	-12.296663	0.862732	-0.457991
O	-11.601803	-1.269114	-0.304026
C	-9.843826	1.902955	-0.462625
N	-9.715448	3.052415	-0.537821
H	-9.230195	-1.421606	-0.213367
S	-4.093000	2.005716	-0.327692
C	-3.010536	0.644119	-0.166667
C	-3.671435	-0.575079	-0.079266
S	-2.572371	-1.896207	0.090929
C	-1.210121	-0.786320	0.041467
C	-1.603834	0.526074	-0.098924
C	0.675146	-2.509374	0.336036
C	2.087637	-2.535188	0.412916
C	0.154258	-1.256854	0.148687
C	2.713010	-1.319148	0.290859
C	4.141897	-1.128004	0.229062
H	4.682658	-2.071387	0.227069
C	4.838089	0.033845	0.113200
C	6.905168	-1.052448	-0.831450
C	8.265707	-1.072100	-1.077103
C	9.093650	0.001868	-0.671089
C	8.467390	1.097735	-0.033667
C	7.102777	1.099359	0.198513
C	6.282076	0.022917	-0.175428
C	2.947793	2.916555	1.688901
C	2.895627	3.863752	0.641130
C	3.521505	3.521909	-0.580731
C	4.160753	2.302498	-0.733971
C	4.181104	1.351236	0.293845
C	3.576045	1.694405	1.508068
H	2.496072	3.134788	2.648401
H	3.510339	4.214160	-1.413157
H	4.640669	2.071506	-1.681383
H	3.594308	0.980930	2.328168
N	10.444700	-0.017432	-0.894207
N	2.273758	5.075584	0.807162
H	6.658282	1.955391	0.697425
H	9.051463	1.953447	0.281263
H	8.688093	-1.919001	-1.603280
H	6.304762	-1.883583	-1.189303
H	-0.912851	1.359233	-0.144515
S	1.472409	-0.093369	0.075132
C	2.527275	-3.932325	0.591405
C	0.192126	-3.905995	0.474825
N	1.341579	-4.681921	0.621233
O	3.642287	-4.399277	0.695644
O	-0.934819	-4.356243	0.466840
C	1.297224	-6.120710	0.782440
H	2.322487	-6.467834	0.904762
H	0.709788	-6.382588	1.664275
H	0.851724	-6.587453	-0.098340
H	-13.165265	0.429235	-0.455130
C	11.240894	1.154250	-0.582412
H	12.282942	0.950259	-0.823914
H	10.918137	2.035308	-1.152438
H	11.183111	1.397907	0.484021
C	11.031489	-1.098309	-1.663452
H	10.859355	-2.065735	-1.179634
H	10.623622	-1.147458	-2.681629
H	12.107102	-0.942793	-1.730817
C	2.127466	5.965981	-0.328445
H	1.561326	5.502409	-1.147474
H	1.599509	6.863597	-0.009873
H	3.104233	6.270952	-0.719141
C	1.504619	5.322858	2.011890
H	1.052074	6.311315	1.947715
H	0.705262	4.582194	2.147790
H	2.143462	5.301378	2.901477

Table SC-18. Optimized Cartesian Coordinates of the D-ε_3-δ_3-A | [M06-2X/6-31G(d,p) solvent model: CPCM, $\varepsilon_{ethanol}$ =24.55].

C	5.079079	0.359412	-0.122193
C	5.492740	-0.970446	-0.251553
C	6.886687	-1.132636	-0.292490
C	7.545379	0.083581	-0.194645
S	6.418997	1.430023	-0.052419
H	7.390362	-2.085132	-0.389991
C	8.940455	0.391926	-0.191709
C	10.010574	-0.444973	-0.268447
C	11.368786	0.153920	-0.242774
O	12.328538	-0.774584	-0.312059
O	11.586683	1.341725	-0.166997
C	9.898711	-1.864868	-0.368633
N	9.793860	-3.016564	-0.450272
H	9.209696	1.444521	-0.116886
S	4.147318	-2.087636	-0.326267
C	3.033849	-0.748330	-0.180223
C	3.669783	0.483116	-0.081506
S	2.535627	1.783122	0.066500
C	1.194935	0.641455	-0.005950
C	1.623712	-0.663147	-0.138604
C	-0.641316	2.396176	0.231812
C	-2.062570	2.467860	0.318198
C	-0.167150	1.099044	0.080179
C	-2.698116	1.224916	0.235914
C	-4.128646	1.063249	0.192323
H	-4.644104	2.020772	0.197702
C	-4.861210	-0.076662	0.094471
C	-6.939993	1.067232	-0.762746
C	-8.307404	1.113655	-0.967943
C	-9.139145	0.038333	-0.577276
C	-8.514529	-1.073343	0.031083
C	-7.143317	-1.100602	0.225792
C	-6.314473	-0.031767	-0.150398
C	-3.571793	-3.555562	-0.702972
C	-2.975822	-3.951566	0.515921
C	-3.034944	-3.042975	1.595786
C	-3.649783	-1.808189	1.451239
C	-4.229653	-1.413132	0.241271
C	-4.195734	-2.323100	-0.821545
H	-3.550436	-4.213963	-1.562289
H	-2.598529	-3.300424	2.552735
H	-3.670252	-1.124028	2.295877
H	-4.651351	-2.049479	-1.769765
N	-10.494005	0.068636	-0.796274
N	-2.372915	-5.182043	0.649682
H	-6.700585	-1.971271	0.700576
H	-9.104064	-1.921516	0.356429
H	-8.731710	1.984861	-1.451162
H	-6.339320	1.901263	-1.113157
H	0.952392	-1.511280	-0.197624
S	-1.498043	-0.011710	0.051341
N	0.137391	3.519468	0.296893
N	-2.707833	3.665638	0.453492
C	-1.954831	4.728787	0.508570
C	-0.492456	4.653387	0.431618
C	0.317309	5.913844	0.505820
C	-2.617062	6.067599	0.654647
H	-3.697284	5.931921	0.698573
H	-2.282233	6.574655	1.564949
H	-2.372379	6.721158	-0.188505
H	0.135928	6.439852	1.448309
H	1.376543	5.669523	0.430676
H	0.048232	6.599294	-0.303844
H	13.186535	-0.321155	-0.291185
C	-11.114599	1.294498	-1.261557
H	-12.188231	1.136326	-1.352832
H	-10.943477	2.132112	-0.572054
H	-10.732394	1.581153	-2.247152
C	-11.327065	-0.987061	-0.253173
H	-11.046412	-1.960951	-0.668183
H	-11.257114	-1.049272	0.841307
H	-12.364780	-0.794880	-0.522297
C	-2.150748	-5.989813	-0.535062
H	-1.537124	-5.471315	-1.284955
H	-1.641820	-6.908721	-0.246947
H	-3.100431	-6.266908	-1.003732
C	-1.580979	-5.451716	1.835439
H	-1.147766	-6.447743	1.753505
H	-0.766526	-4.725400	1.965161
H	-2.202975	-5.430435	2.735985

Table SC-19. Optimized Cartesian Coordinates of the D-ε_4-δ_3-A | [M06-2X/6-31G(d,p) solvent model: CPCM, $\varepsilon_{ethanol}$ =24.55].

C	6.183785	-0.908404	0.049706
C	6.996365	-2.017351	0.283041
C	8.367858	-1.739073	0.142805
C	8.594688	-0.417260	-0.197722
S	7.097855	0.497123	-0.346036
H	9.169964	-2.454287	0.278663
C	9.906967	0.113585	-0.393011
C	10.310387	1.367510	-0.723021
C	11.768847	1.622574	-0.854058
O	12.029292	2.893270	-1.174543
O	12.620762	0.779839	-0.689559
C	9.408233	2.452119	-0.950855
N	8.669180	3.325927	-1.135040
H	10.715193	-0.602487	-0.254198
S	6.086454	-3.454426	0.685839
C	4.602732	-2.547212	0.534685
C	4.807545	-1.214737	0.193474
S	3.317940	-0.352059	0.045312
C	2.428344	-1.805509	0.444948
C	3.235832	-2.890264	0.679820
C	-1.403559	-2.151752	0.632475
C	0.981972	-1.731856	0.476043
C	-1.005057	-0.870197	0.309191
H	2.868379	-3.875956	0.938938
N	0.325943	-0.626752	0.224136
S	-0.000954	-3.147878	0.846969
N	-2.728725	-2.405333	0.716627
S	-2.408332	0.127792	0.117172
C	-3.405309	-1.301992	0.468634
C	-4.850494	-1.339981	0.361197
H	-5.227005	-2.358907	0.383213
C	-5.719083	-0.315530	0.167312
C	-7.514964	-1.747120	-0.862654
C	-8.837096	-2.005714	-1.176620
C	-9.860333	-1.097608	-0.816633
C	-9.469842	0.089899	-0.156305
C	-8.139840	0.332953	0.142191
C	-7.126017	-0.581030	-0.183599
C	-4.994413	3.324872	-0.612240
C	-4.492024	3.808793	0.618855
C	-4.419557	2.898271	1.697886
C	-4.815352	1.579892	1.539754
C	-5.304714	1.100726	0.319048
C	-5.406875	2.008703	-0.742143
H	-5.067680	3.982335	-1.469335
H	-4.052064	3.221716	2.663624
H	-4.739637	0.897376	2.382426
H	-5.799310	1.667654	-1.696578
N	-11.176310	-1.355283	-1.103991
N	-4.103270	5.116592	0.763965
H	-7.878058	1.253497	0.655712
H	-10.210820	0.827904	0.124731
H	-9.075357	-2.909412	-1.723264
H	-6.758028	-2.455299	-1.187143
H	12.992229	2.995014	-1.244657
C	-11.518970	-2.503259	-1.922334
H	-12.601001	-2.546640	-2.037567
H	-11.064732	-2.450587	-2.920928
H	-11.193503	-3.434911	-1.447853
C	-12.172242	-0.325824	-0.873307
H	-12.219718	-0.055744	0.186894
H	-11.965699	0.585931	-1.449577
H	-13.149725	-0.705878	-1.166640
C	-4.051279	5.981991	-0.398792
H	-3.702199	6.966846	-0.092206
H	-3.370362	5.596983	-1.169511
H	-5.043106	6.101263	-0.847990
C	-3.470868	5.540498	1.998371
H	-4.146752	5.413421	2.851056
H	-2.550340	4.978451	2.205603
H	-3.220243	6.597707	1.924548

Table SC-20. Optimized Cartesian Coordinates of the D-ε_5-δ_3-A | [M06-2X/6-31G(d,p) solvent model: CPCM, $\varepsilon_{ethanol}$ =24.55].

C	6.936238	-0.383981	-0.210614
C	7.229524	-1.681972	-0.635162
C	8.602993	-1.984239	-0.636120
C	9.359990	-0.906967	-0.208089
S	8.360360	0.483758	0.196617
H	9.021095	-2.936510	-0.934448
C	10.776251	-0.764778	-0.052285
C	11.762868	-1.668791	-0.288040
C	13.167217	-1.251981	-0.036287
O	14.036147	-2.233221	-0.297216
O	13.488661	-0.154900	0.358525
C	11.525547	-2.995028	-0.762284
N	11.319363	-4.068354	-1.148154
H	11.137346	0.197766	0.306408
S	5.799232	-2.595118	-1.059605
C	4.806929	-1.213831	-0.662190
C	5.543758	-0.119124	-0.229598
S	4.522369	1.225268	0.142423
C	3.103998	0.302009	-0.318281
C	3.409966	-0.976337	-0.714679
H	2.671348	-1.692976	-1.052703
C	1.796752	0.927991	-0.263573
C	1.498622	2.263067	-0.272194
C	0.097496	2.514883	-0.235310
C	-0.662454	1.343632	-0.198933
S	0.354757	-0.064197	-0.196006
H	2.247674	3.044720	-0.330890
C	-0.627427	3.748501	-0.249134
C	-2.084815	1.363975	-0.177049
C	-2.040713	3.770504	-0.230154
C	-4.211126	2.346591	-0.173264
C	-4.565605	1.021365	-0.122791
S	-3.142123	-0.011745	-0.107543
C	-2.804776	2.559890	-0.193760
N	-2.438144	5.052102	-0.258226
N	-0.188389	5.015188	-0.289426
N	-1.301882	5.720894	-0.298913
C	-1.265587	7.178449	-0.252596
C	-0.766789	7.685820	1.102876
C	-0.751593	9.213150	1.083113
C	-1.627634	7.146276	2.242704
H	-1.605769	6.053056	2.281359
H	-1.269252	7.525771	3.203160
H	-2.669997	7.461486	2.119778
H	-0.359279	9.603795	2.025334
H	-0.129346	9.597205	0.269497
H	-1.765594	9.606184	0.951608
H	0.259603	7.320066	1.228866
H	-0.617266	7.518637	-1.063607
H	-2.288320	7.509953	-0.445077
C	-5.932153	0.536201	-0.211331
C	-6.408397	-0.720287	-0.034757
C	-8.493719	-2.081586	0.270538
C	-9.808252	-2.397215	-0.032676
C	-10.511441	-1.693097	-1.035304
C	-9.810067	-0.678051	-1.724912
C	-8.497129	-0.375887	-1.404109
C	-7.803057	-1.055084	-0.391033
C	-4.547673	-4.001414	0.405756
C	-3.970608	-3.857249	1.688781
C	-4.250301	-2.668542	2.398676
C	-5.026964	-1.670422	1.831106
C	-5.574399	-1.801000	0.549915
C	-5.336901	-2.998454	-0.135159
H	-4.383648	-4.904377	-0.169084
H	-3.861690	-2.523323	3.398881
H	-5.217943	-0.760552	2.394598
H	-5.774333	-3.142387	-1.119796
N	-11.821763	-1.987238	-1.332208
N	-3.170540	-4.839056	2.225569
H	-7.985816	0.388977	-1.981702
H	-10.286678	-0.135570	-2.532049
H	-10.291101	-3.197742	0.514088
H	-7.987862	-2.641353	1.051954
H	-4.942476	3.145552	-0.208578
H	-6.634778	1.313995	-0.503787
H	14.929014	-1.899620	-0.113183
C	-2.756644	-4.736006	3.611840
H	-3.610994	-4.710037	4.302429
H	-2.136591	-5.595752	3.862109
H	-2.159284	-3.833073	3.775483
C	-3.080707	-6.124404	1.559083
H	-4.060296	-6.612044	1.460572
H	-2.651182	-6.017477	0.557682
H	-2.426199	-6.777227	2.135114
C	-12.441389	-1.372774	-2.490767
H	-13.471943	-1.717281	-2.566652
H	-12.459321	-0.282709	-2.391300
H	-11.920228	-1.622483	-3.425394
C	-12.427267	-3.174250	-0.758696
H	-13.448711	-3.264742	-1.125902
H	-11.879765	-4.089381	-1.022803
H	-12.468298	-3.105127	0.333334

Table SC-21. Optimized Cartesian Coordinates of the D-ε_6-δ_3-A | [M06-2X/6-31G(d,p) solvent model: CPCM, $\varepsilon_{ethanol}$ =24.55].

C	9.714879	-0.043306	-0.056499	C	-8.746508	0.839871	0.312116
C	10.421336	1.160234	-0.075269	C	-8.260907	-0.117659	-0.585507
C	11.815301	0.983583	-0.074889	C	-7.911435	0.318131	-1.867383
C	12.169287	-0.355017	-0.056258	H	-7.732904	1.933594	-3.245985
S	10.760153	-1.411973	-0.039569	H	-9.206583	2.883791	0.703154
H	12.550215	1.779648	-0.088109	H	-9.039976	0.530341	1.311966
C	13.527152	-0.792466	-0.052007	H	-7.537114	-0.405752	-2.586805
C	14.051172	-2.046601	-0.036633	N	-13.049178	-4.326965	0.820435
C	15.529356	-2.188273	-0.035679	N	-8.617014	3.943523	-1.694031
O	15.911478	-3.469212	-0.020905	H	-8.572503	-3.709997	1.438127
O	16.299916	-1.255675	-0.047026	H	-10.637473	-4.898516	1.866608
C	13.254501	-3.232530	-0.022078	H	-12.737963	-2.120893	-0.686142
N	12.598983	-4.188631	-0.010710	H	-10.648183	-0.960091	-1.112750
H	14.265577	0.007690	-0.062839	H	-6.997183	-3.283910	-0.011171
S	9.372067	2.559076	-0.092987	C	-1.455734	-3.327777	0.173867
C	7.976652	1.507572	-0.074113	H	-1.254317	-3.968764	-0.686890
C	8.314296	0.160124	-0.054651	H	-2.204463	-3.808843	0.805674
S	6.907443	-0.845139	-0.029858	H	-0.545807	-3.203550	0.761344
C	5.867493	0.569295	-0.068329	C	1.247608	-2.603756	-1.079339
C	6.578400	1.745691	-0.084845	H	2.090967	-2.585391	-1.771803
H	6.117126	2.725113	-0.120937	H	0.332750	-2.711101	-1.662154
C	4.430921	0.386951	-0.073752	H	1.359841	-3.455421	-0.405590
C	3.740026	-0.777797	-0.308701	C	-1.803656	5.018275	0.632502
C	2.343990	-0.566750	-0.192408	C	-2.479565	5.189309	1.995720
C	1.981482	0.738902	0.110598	C	-1.621597	4.598016	3.111743
S	3.371501	1.749658	0.290026	C	-2.759861	6.672941	2.227174
H	4.215697	-1.721114	-0.551658	H	-3.281765	6.820607	3.175976
C	0.568212	0.800952	0.117295	H	-1.822674	7.238838	2.266888
C	0.117388	-0.513584	-0.149543	H	-3.377923	7.093958	1.428710
N	1.214314	-1.336040	-0.360303	H	-2.103656	4.743069	4.082123
C	-0.395089	1.847818	0.226187	H	-1.461522	3.525064	2.969254
C	-1.770197	1.579462	0.044683	H	-0.640821	5.086257	3.143095
C	-2.233219	0.244397	-0.150321	H	-3.432858	4.647936	1.956598
C	-1.286519	-0.805837	-0.177606	H	-2.449294	5.376427	-0.173193
C	-3.506749	-0.368442	-0.220938	H	-0.853261	5.555643	0.596684
C	-3.308767	-1.740372	-0.252986	H	-4.569857	-3.583023	-0.263070
N	-1.959677	-2.018763	-0.221342	H	16.881891	-3.492873	-0.020741
S	-5.192180	0.028375	-0.235815	C	-8.028972	4.385161	-2.944786
C	-5.619677	-1.691810	-0.253853	H	-8.191925	5.456616	-3.055075
C	-4.505515	-2.501552	-0.259474	H	-6.948598	4.188586	-2.991488
N	-2.439947	2.736347	0.143668	H	-8.502635	3.887008	-3.796699
N	-0.246896	3.164589	0.429592	C	-8.883736	4.931820	-0.665741
N	-1.485073	3.623229	0.359835	H	-9.852650	4.749816	-0.190007
C	-6.974422	-2.207111	-0.170027	H	-8.113519	4.938840	0.118406
C	-8.159316	-1.553008	-0.210941	H	-8.920477	5.919234	-1.124441
C	-10.639281	-1.834227	-0.468184	C	-13.085880	-5.340836	1.857699
C	-11.832110	-2.498439	-0.228387	H	-14.085899	-5.771201	1.897613
C	-11.873162	-3.643186	0.596866	H	-12.383167	-6.149926	1.635922
C	-10.658095	-4.054929	1.188058	H	-12.839941	-4.936064	2.849787
C	-9.476062	-3.377923	0.934863	C	-14.300787	-3.725098	0.400045
C	-9.424133	-2.261061	0.087117	H	-15.121638	-4.388277	0.670433
C	-8.019496	1.649739	-2.241170	H	-14.473293	-2.745957	0.868648
C	-8.491677	2.619503	-1.330392	H	-14.323845	-3.591514	-0.686014
C	-8.845972	2.178631	-0.035310				

Table SC-22. Optimized Cartesian Coordinates of the D-δ_1-A@Ti_5O_{10}| [M06-2X/6-31G(d,p) solvent model: CPCM, $\varepsilon_{ethanol}$ =24.55].

Ti	3.539973	-0.105818	0.092226
Ti	6.516670	-1.543096	1.088995
Ti	6.915270	0.825600	-0.461634
O	4.860971	-2.669315	1.357741
O	7.869577	-0.561800	0.492570
O	6.286595	2.149634	0.444618
O	6.045641	-0.943006	2.666918
O	4.947166	4.171207	-1.365473
O	3.305563	-0.403748	1.839935
Ti	4.314658	-1.705714	2.679831
Ti	4.976205	2.618608	-0.929689
O	6.094354	1.447324	-1.923360
O	3.447879	1.561024	-0.290013
O	3.699397	-2.571618	4.147622
O	5.464237	-0.415653	-0.013629
O	3.381003	-1.283290	-1.618830
H	3.679768	-3.523537	4.296784
C	2.109423	-1.340088	-1.479003
O	1.629844	-0.725603	-0.470122
C	-3.523863	-1.195078	-1.031618
C	-2.569665	-0.446560	-0.340192
C	-1.256833	-0.715370	-0.725105
C	-1.152627	-1.678389	-1.732014
S	-2.757161	-2.232474	-2.172781
H	-2.835744	0.260743	0.434371
H	-0.391940	-0.237730	-0.291322
C	-0.074444	-2.236581	-2.464109
C	-4.960249	-1.267222	-0.867683
C	-5.770634	-0.311436	-0.330477
C	-7.172065	-0.635676	-0.010363
C	-8.181939	0.337575	-0.079926
C	-7.562263	-1.931689	0.364451
C	-9.508484	0.036526	0.174839
H	-7.920142	1.354003	-0.358622
C	-8.880805	-2.252208	0.632281
H	-6.805817	-2.702296	0.482024
C	-9.900155	-1.275580	0.529514
H	-10.247173	0.824056	0.093367
H	-9.120342	-3.262598	0.939194
C	-5.309639	1.074904	-0.099395
C	-5.541567	1.732669	1.115479
C	-4.623812	1.782513	-1.095781
C	-5.076114	3.017064	1.348712
H	-6.081254	1.215425	1.904283
C	-4.165280	3.071443	-0.890672
H	-4.447661	1.305031	-2.055898
C	-4.375103	3.726491	0.346253
H	-5.258806	3.471094	2.314499
H	-3.647431	3.576490	-1.696407
N	-11.211440	-1.587311	0.770321
N	-3.926775	5.004787	0.557950
C	-11.563125	-2.918166	1.227318
C	-12.210810	-0.536170	0.779711
C	-4.052453	5.600100	1.874680
C	-3.084725	5.642437	-0.436214
H	-11.995984	0.227764	1.538121
H	-12.273377	-0.040574	-0.195511
H	-13.184106	-0.973160	0.997823
H	-11.099942	-3.157341	2.193612
H	-12.644385	-2.981964	1.338937
H	-11.252218	-3.678095	0.502195
H	-2.813496	6.637250	-0.086293
H	-2.162119	5.075839	-0.619650
H	-3.612183	5.753140	-1.389816
H	-5.103042	5.670926	2.176512
H	-3.514780	5.025947	2.640975
H	-3.642195	6.608503	1.848737
C	1.296966	-2.098907	-2.420258
C	2.054380	-2.812785	-3.407223
N	2.652976	-3.395087	-4.211011
H	-5.419391	-2.197232	-1.192877
H	-0.398552	-2.919718	-3.248436

Table SC-23. Optimized Cartesian Coordinates of the D-ε_3-δ_1-A@Ti_5O_{10}| [M06-2X/6-31G(d,p) solvent model: CPCM, $\varepsilon_{ethanol}$ =24.55].

Ti	6.467990	-0.543891	0.128720
Ti	9.124661	0.572511	-1.796634
Ti	9.144383	1.687836	0.826124
O	7.740017	-0.304829	-2.906998
O	10.119977	1.694739	-0.836524
O	9.544587	0.379718	1.871367
O	9.652313	-1.086577	-1.568733
O	7.955540	0.576933	4.478255
O	7.043158	-1.993021	-0.744639
Ti	8.092934	-1.880453	-2.266203
Ti	7.865440	0.504021	2.868615
O	7.821968	2.158677	1.946018
O	6.705690	-0.682954	1.819500
O	8.345939	-3.083799	-3.597508
O	7.921924	0.677640	-0.337911
O	5.162209	1.003430	-0.385111
H	8.374146	-4.039210	-3.464994
C	4.169973	0.209421	-0.252695
O	4.444915	-1.007097	0.021133
C	-7.370962	-1.046383	0.287108
C	-8.168709	0.028204	0.038872
C	-9.610771	-0.129247	-0.202183
C	-10.499743	0.935056	0.021669
C	-10.169992	-1.336525	-0.656731
C	-11.864879	0.805211	-0.165761
H	-10.108915	1.885712	0.371966
C	-11.530073	-1.486570	-0.853893
H	-9.520632	-2.174943	-0.890780
C	-12.423383	-0.415287	-0.610579
H	-12.502506	1.655734	0.040573
H	-11.902630	-2.436517	-1.216468
C	-7.610597	1.403966	0.032215
C	-7.604981	2.190810	-1.125673
C	-7.063185	1.956275	1.195338
C	-7.036536	3.455174	-1.139675
H	-8.035066	1.793180	-2.041220
C	-6.507766	3.225618	1.207410
H	-7.061903	1.367617	2.109246
C	-6.474701	4.011367	0.032511
H	-7.032744	4.014335	-2.066728
H	-6.096944	3.606415	2.134008
N	-13.770369	-0.553379	-0.810534
N	-5.928613	5.273367	0.032873
C	-14.318079	-1.845952	-1.174653
C	-14.661438	0.547845	-0.500313
C	-5.727384	5.956917	-1.231381
C	-5.183971	5.719667	1.195542
H	-14.617931	0.823082	0.561383
H	-14.414859	1.435895	-1.092920
H	-15.683438	0.256735	-0.737670
H	-14.094268	-2.610629	-0.419977
H	-15.399807	-1.760632	-1.265455
H	-13.923140	-2.190987	-2.137027
H	-4.805509	6.724003	1.010511
H	-5.827381	5.762561	2.080110
H	-4.333192	5.062373	1.422821
H	-5.267220	6.925767	-1.042171
H	-5.078644	5.388928	-1.912378
H	-6.682260	6.133110	-1.736857
C	-2.098294	-0.339059	-0.028066
C	-1.748497	0.965275	-0.384275
C	-0.371833	1.165861	-0.479044
C	0.367569	0.018018	-0.200641
S	-0.691523	-1.321100	0.183899
H	-2.484296	1.740999	-0.561453
H	0.076359	2.115985	-0.740538
C	1.765000	-0.204550	-0.165714
C	2.793885	0.675285	-0.387381
C	2.615770	2.052592	-0.715324
N	2.462114	3.170208	-0.982902
H	2.092729	-1.212929	0.081571
C	-5.935864	-1.105200	0.349389
C	-5.221341	-2.275989	0.650443
C	-3.811245	-2.130552	0.542324
C	-3.421122	-0.851104	0.152982
S	-4.821944	0.151514	-0.060198
H	-7.827070	-2.023421	0.425631
C	-4.971387	-4.447625	1.260501
C	-3.519236	-4.293187	1.163340
N	-5.790782	-3.462166	1.009782
N	-2.961739	-3.165505	0.810907
C	-2.629559	-5.458629	1.476249
H	-2.855554	-6.308863	0.825400
H	-1.588430	-5.168303	1.339206
H	-2.776576	-5.793719	2.507851
C	-5.549840	-5.773854	1.657593
H	-5.183570	-6.085451	2.640747
H	-6.636231	-5.696887	1.689479
H	-5.267159	-6.554753	0.944533

Table SC-24. Optimized Cartesian Coordinates of the D-ε_3-δ_2-A@Ti_5O_{10}| [M06-2X/6-31G(d,p) solvent model: CPCM, $\varepsilon_{ethanol}$ =24.55].

Ti	-7.951351	0.359849	0.376092
Ti	-10.135090	-0.269816	-2.242847
Ti	-10.692759	-1.891116	0.031628
O	-8.529335	0.745602	-2.838146
O	-11.301597	-1.524049	-1.775532
O	-11.322609	-0.819154	1.219995
O	-10.699833	1.345101	-1.829901
O	-10.297877	-1.595620	3.990027
O	-8.320280	1.964239	-0.303251
Ti	-9.021277	2.181558	-2.011883
Ti	-9.875074	-1.171437	2.490704
O	-9.607563	-2.597954	1.271171
O	-8.547506	0.181418	1.973609
O	-8.897270	3.691115	-3.005932
O	-9.277628	-0.687267	-0.618614
O	-6.561007	-1.113068	-0.163255
H	-8.598460	3.745901	-3.920709
C	-5.611558	-0.367754	0.250854
O	-5.942066	0.756427	0.756290
C	0.565815	-0.660402	0.281586
C	0.372845	0.571516	0.914251
C	-0.973479	0.915139	1.071198
C	-1.823808	-0.059914	0.559785
S	-0.930830	-1.419574	-0.123839
H	-1.343853	1.825276	1.528193
C	-3.233088	0.071258	0.583618
C	-4.211813	-0.772142	0.132430
C	-3.960848	-2.039419	-0.476227
N	-3.756657	-3.068326	-0.969922
H	-3.598033	0.996429	1.026039
S	1.886244	1.322880	1.318407
C	2.761957	-0.036866	0.620473
C	1.920341	-1.009446	0.112164
H	2.272149	-1.920969	-0.354984
C	4.197463	-0.065012	0.617595
C	5.093720	0.861645	1.144261
C	6.462893	0.487545	0.994743
C	6.634838	-0.715215	0.301177
S	5.085043	-1.368406	-0.094189
C	9.047961	-0.976337	-0.393752
C	9.290036	0.460023	-0.643223
C	8.403699	1.229764	-1.404105
C	10.544371	2.488789	-0.166290
C	8.552292	2.600859	-1.528915
H	7.570896	0.741218	-1.903252
C	9.606385	3.276125	-0.871618
H	11.395680	2.952541	0.316603
H	7.843798	3.151608	-2.135132
C	10.183158	-1.911720	-0.529825
C	10.263936	-3.084160	0.236846
C	12.277163	-2.563267	-1.595745
C	11.306253	-3.984431	0.096415
H	9.506032	-3.279491	0.990054
C	12.339505	-3.756658	-0.841047
H	13.052872	-2.330127	-2.314419
H	11.326099	-4.860466	0.732565
N	9.718087	4.644662	-0.921626
N	13.365296	-4.655972	-1.007676
C	8.814608	5.409194	-1.757860
C	10.880836	5.289602	-0.345585
C	14.512135	-4.283167	-1.814949
C	13.492059	-5.767215	-0.083808
H	10.955423	5.079251	0.727610
H	11.815474	4.963734	-0.821771
H	10.789046	6.367678	-0.471011
H	7.772494	5.247034	-1.460588
H	9.034998	6.469589	-1.642453
H	8.909694	5.148829	-2.820886
H	14.350018	-6.372370	-0.373387
H	13.634832	-5.433794	0.953415
H	12.604530	-6.406781	-0.117850
H	15.226636	-5.105250	-1.815803
H	14.217132	-4.094306	-2.852242
H	15.014481	-3.383832	-1.433112
C	7.819582	-1.465329	-0.064423
H	7.689243	-2.545235	-0.080479
C	10.383123	1.116409	-0.066706
C	11.227953	-1.673073	-1.435897
H	11.106764	0.540670	0.504482
H	11.210274	-0.769847	-2.038741
N	4.732741	2.024849	1.766293
N	7.464391	1.251748	1.524618
C	7.109915	2.366970	2.096336
C	5.705835	2.770259	2.212796
C	5.360523	4.068676	2.878408
C	8.186191	3.257750	2.645272
H	4.278992	4.200834	2.880907
H	5.728371	4.089252	3.909016
H	5.824838	4.909554	2.353686
H	9.156721	2.798526	2.457335
H	8.161208	4.237506	2.155457
H	8.059240	3.426781	3.719246

Table SC-25. Optimized Cartesian Coordinates of the D-ε_3-δ_3-A@Ti_5O_{10}| [M06-2X/6-31G(d,p) solvent model: CPCM, $\varepsilon_{ethanol}$ =24.55].

Ti	8.676365	0.898609	-0.135196
Ti	9.888690	-1.612160	1.936282
Ti	9.893247	-2.362828	-0.814224
O	9.007106	-0.143059	2.942031
O	10.299593	-3.032904	0.956158
O	11.100802	-1.398775	-1.578331
O	11.266364	-0.524127	2.032442
O	10.199080	-0.563239	-4.369156
O	9.776235	1.747545	0.992482
Ti	10.281808	0.979869	2.595430
Ti	9.825090	-0.557169	-2.800373
O	8.771463	-2.008007	-2.157182
O	9.219243	0.995326	-1.755293
O	10.934072	1.961757	3.966958
O	9.154451	-0.936089	0.319660
O	6.673971	0.280651	-0.105660
H	10.660206	1.919790	4.890277
C	6.299559	1.500146	-0.122056
O	7.216222	2.385771	-0.127736
C	0.094565	0.475867	-0.153724
C	0.352741	1.853837	-0.130716
C	1.714941	2.176308	-0.123960
C	2.512181	1.037024	-0.140240
S	1.546648	-0.437378	-0.163650
H	2.106677	3.184748	-0.105891
C	3.927729	0.901884	-0.135345
C	4.885388	1.877325	-0.131491
C	4.605890	3.277900	-0.137367
N	4.367673	4.412121	-0.141241
H	4.324481	-0.111993	-0.134494
S	-1.112222	2.811737	-0.115349
C	-2.063388	1.345349	-0.139020
C	-1.289388	0.189726	-0.159989
S	-2.267854	-1.239120	-0.197235
C	-3.729345	-0.255699	-0.178295
C	-3.453526	1.096571	-0.147224
C	-5.350202	-2.219731	-0.289479
C	-6.754474	-2.463055	-0.302333
C	-5.029214	-0.871596	-0.191117
C	-7.530485	-1.301832	-0.216633
C	-8.965784	-1.310198	-0.098381
H	-9.361593	-2.321161	-0.036060
C	-9.826775	-0.263083	-0.003216
C	-11.682470	-1.598055	1.059230
C	-13.018573	-1.809091	1.350799
C	-14.010185	-0.896611	0.921332
C	-13.572969	0.247782	0.217148
C	-12.230171	0.442429	-0.061045
C	-11.246058	-0.477800	0.332480
C	-9.006664	3.399864	0.549991
C	-8.500777	3.797683	-0.708623
C	-8.454529	2.822539	-1.729879
C	-8.888599	1.526960	-1.494064
C	-9.381650	1.132381	-0.245821
C	-9.449531	2.103368	0.760326
H	-9.057331	4.107499	1.367916
H	-8.079165	3.076073	-2.713331
H	-8.832190	0.794628	-2.295671
H	-9.841201	1.829462	1.736601
N	-15.341345	-1.111225	1.183488
N	-8.082625	5.089478	-0.934325
H	-11.934446	1.330080	-0.612560
H	-14.286587	0.989762	-0.118471
H	-13.292390	-2.678946	1.934453
H	-10.953639	-2.308128	1.438717
H	-4.218229	1.863806	-0.134523
S	-6.481716	0.073919	-0.125196
N	-4.445474	-3.242280	-0.373664
N	-7.256567	-3.732013	-0.379903
C	-6.384149	-4.698619	-0.454529
C	-4.939463	-4.446371	-0.456662
C	-3.987841	-5.601205	-0.558023
C	-6.886615	-6.110111	-0.541063
H	-7.976150	-6.105197	-0.536643
H	-6.534181	-6.597540	-1.455385
H	-6.528479	-6.707681	0.303154
H	-4.144005	-6.153001	-1.490355
H	-2.963544	-5.230730	-0.529341
H	-4.138594	-6.307419	0.264174
C	-15.728117	-2.203030	2.057061
H	-16.814083	-2.226027	2.137023
H	-15.401425	-3.164510	1.648107
H	-15.306298	-2.099320	3.066157
C	-16.298238	-0.055249	0.910758
H	-16.072883	0.863619	1.468921
H	-16.317952	0.190033	-0.156088
H	-17.293034	-0.396469	1.193777
C	-7.956770	5.996946	0.191136
H	-7.252825	5.627178	0.949630
H	-7.601748	6.961293	-0.169800
H	-8.926111	6.156958	0.673475
C	-7.358218	5.391126	-2.155062
H	-7.081514	6.444630	-2.152442
H	-6.444125	4.789309	-2.255758
H	-7.983128	5.212182	-3.035827

Table SC-26. Optimized Cartesian Coordinates of the D-ε_6-δ_1-A@Ti_5O_{10}| [M06-2X/6-31G(d,p) solvent model: CPCM, $\varepsilon_{ethanol}$ =24.55].

Ti	10.324735	-0.038050	-0.255155	C	-4.128677	7.728539	0.187268
Ti	11.582875	-1.729176	2.456560	C	-6.589091	7.381199	0.618233
Ti	11.903489	-3.243664	0.051524	C	-11.297523	-1.343034	0.441417
O	10.471483	-0.092680	2.840011	C	-10.548461	-2.470196	-0.173038
O	12.219866	-3.307592	1.962053	C	-10.423653	-3.704923	0.470703
O	12.970537	-2.410702	-1.023697	C	-9.927361	-2.327279	-1.418429
O	12.864583	-0.527667	2.387963	C	-9.671558	-4.738193	-0.072042
O	11.997253	-2.579947	-3.874858	H	-10.916329	-3.857295	1.427697
O	11.363955	1.187648	0.532554	C	-9.181093	-3.348412	-1.984062
Ti	11.728546	0.979358	2.339280	H	-10.025598	-1.384468	-1.951
Ti	11.589468	-2.146716	-2.375886	C	-9.012674	-4.580119	-1.310952
O	10.745725	-3.463929	-1.279861	H	-9.599495	-5.672022	0.471383
O	10.846701	-0.405730	-1.844472	H	-8.732976	-3.190649	-2.957300
O	12.126014	2.362139	3.437851	C	-12.705526	-1.585249	0.823667
O	10.987559	-1.615517	0.673779	C	-13.484737	-2.534349	0.145766
O	8.410943	-0.806364	0.091198	C	-13.327928	-0.885098	1.867829
H	11.718381	2.569433	4.286160	C	-14.816037	-2.753642	0.461216
C	7.894902	0.293875	-0.295122	H	-13.035084	-3.110644	-0.657683
O	8.700599	1.219258	-0.643707	C	-14.656714	-1.091674	2.201489
C	2.087117	2.386150	-0.870539	H	-12.748009	-0.181256	2.458204
C	2.775411	3.501368	-1.323920	C	-15.446946	-2.025170	1.493636
C	4.164314	3.320550	-1.312674	H	-15.368014	-3.497810	-0.099326
C	4.561235	2.071259	-0.854767	H	-15.076951	-0.537127	3.031360
S	3.166771	1.105368	-0.431624	N	-8.238169	-5.586845	-1.843732
H	2.285128	4.411797	-1.647339	N	-16.774296	-2.220389	1.801152
H	4.879955	4.071631	-1.627340	C	-7.737467	-5.452032	-3.197972
C	5.915863	1.664169	-0.749498	C	-8.278567	-6.904758	-1.239571
C	6.443591	0.476857	-0.326102	C	-17.480536	-3.337061	1.202213
C	5.658567	-0.636885	0.104393	C	-17.322111	-1.603897	2.994330
N	5.019218	-1.539373	0.451456	H	-7.912110	-6.874657	-0.208142
H	6.646331	2.412772	-1.051946	H	-9.292456	-7.328544	-1.229258
C	0.661747	2.214037	-0.739515	H	-7.630244	-7.573648	-1.804241
C	-0.006965	1.102806	-0.273693	H	-7.089043	-4.574234	-3.287185
C	-1.403841	1.303453	-0.313323	H	-7.143593	-6.330741	-3.446402
C	-1.793993	2.550698	-0.791755	H	-8.544808	-5.356759	-3.937607
S	-0.428466	3.513776	-1.224756	H	-18.375485	-1.868200	3.078574
C	-3.202885	2.618910	-0.712117	H	-16.806104	-1.929492	3.908377
C	-3.627162	1.364497	-0.209851	H	-17.254695	-0.512809	2.935631
N	-2.516527	0.577849	0.050065	H	-18.503921	-3.351553	1.574953
C	-4.177131	3.641669	-0.913847	H	-17.522481	-3.234340	0.112949
C	-5.533898	3.414649	-0.591967	H	-17.010097	-4.302218	1.436112
C	-5.022728	1.090092	-0.035244	C	-10.731219	-0.124621	0.624645
C	-5.975158	2.128548	-0.157852	C	-7.235059	1.541894	0.108278
N	-6.218069	4.539123	-0.842947	C	-7.025568	0.188551	0.336819
N	-4.053679	4.901247	-1.352836	N	-5.682315	-0.098409	0.248622
N	-5.289175	5.369622	-1.285814	C	-5.211799	-1.455597	-0.003375
C	-5.598417	6.752847	-1.631577	C	-8.204193	-0.574387	0.537419
C	-5.525950	7.704170	-0.430427	C	-9.324882	0.217211	0.454829

Table SC-26 (*cont*). Optimized Cartesian Coordinates of the D-ε_6-δ_1-A@Ti_5O_{10}| [M06-2X/6-31G(d,p) solvent model: CPCM, $\varepsilon_{ethanol}$ =24.55].

S	-8.923291	1.913087	0.144512
H	-6.601000	6.746904	-2.063880
H	-4.877268	7.040989	-2.398640
H	-3.884626	6.757604	0.630549
H	-3.363010	7.958810	-0.559601
H	-4.076333	8.482878	0.976992
H	-6.402542	6.402771	1.071431
H	-6.575768	8.131110	1.413880
H	-7.591205	7.362871	0.179519
H	-5.739843	8.696104	-0.848703
H	-11.374256	0.692989	0.944613
H	-8.240246	-1.637302	0.738785
H	0.488956	0.200150	0.064894
C	-2.431689	-0.570887	0.943824
H	-1.541342	-0.460117	1.565159
H	-3.302995	-0.581398	1.598362
H	-2.367748	-1.512966	0.396112
H	-4.946785	-1.977121	0.918520
H	-6.009079	-2.007677	-0.505757
H	-4.349856	-1.422291	-0.669828

Table SC-27. Optimized Cartesian Coordinates of the D-ε_6-δ_2-A@Ti_5O_{10}| [M06-2X/6-31G(d,p) solvent model: CPCM, $\varepsilon_{ethanol}$ =24.55].

Ti	-11.719756	0.252420	-0.002113	C	11.606758	-4.443753	1.279778
Ti	-14.008429	-1.471334	-1.952518	H	10.910200	-3.160844	2.889301
Ti	-14.324276	-2.017329	0.829202	H	12.515971	-5.354723	-0.468557
O	-12.511227	-0.710565	-3.023645	N	18.508651	-0.296964	-1.861277
O	-15.051049	-2.458301	-0.910198	N	11.133402	-5.619154	1.821216
O	-14.917745	-0.551600	1.503056	C	19.501416	-0.857561	-0.963764
O	-14.669623	0.134534	-2.174499	C	18.923737	0.732752	-2.795763
O	-13.754970	-0.049205	4.260218	C	11.565052	-6.881323	1.250872
O	-12.244752	1.437386	-1.233485	C	10.608327	-5.610730	3.173408
Ti	-13.058810	0.915339	-2.808737	H	18.469968	0.574554	-3.779138
Ti	-13.394763	-0.347994	2.716680	H	18.654515	1.741691	-2.453083
O	-13.166156	-2.159753	2.189214	H	20.005164	0.685264	-2.918036
O	-12.193011	0.710409	1.576517	H	19.368913	-1.939339	-0.862874
O	-12.949131	1.940406	-4.295328	H	20.493396	-0.682423	-1.378593
O	-13.005116	-1.171702	-0.365762	H	19.457917	-0.412382	0.040249
O	-10.212204	-1.199669	0.066889	H	10.291599	-6.619148	3.437007
H	-12.676716	1.649982	-5.173114	H	11.350979	-5.274379	3.910539
C	-9.324185	-0.283517	0.058624	H	9.734190	-4.955744	3.247298
O	-9.736447	0.919613	-0.001307	H	11.108960	-7.697425	1.810000
C	-3.199099	1.119505	0.159628	H	11.242102	-6.970203	0.208650
C	-3.358421	-0.269372	0.147650	H	12.656816	-7.003427	1.282016
C	-4.694211	-0.697343	0.133307	C	12.146579	0.329000	-0.685541
C	-5.568882	0.381908	0.132797	C	14.842551	0.179756	-1.920779
S	-4.716017	1.922685	0.151151	C	11.856128	-2.023162	1.356707
H	-5.011584	-1.731767	0.119192	H	14.110021	0.709906	-2.522839
C	-6.991642	0.424965	0.106975	H	11.679964	-1.083951	1.874254
C	-7.893659	-0.600358	0.107472	C	0.458255	0.524721	0.127562
C	-7.540151	-1.983442	0.147078	C	1.333285	-0.496521	-0.162549
N	-7.240306	-3.102524	0.177121	C	2.674562	-0.046874	-0.081927
H	-7.446036	1.413875	0.079472	C	2.809785	1.293890	0.255495
S	-1.816987	-1.070082	0.152146	S	1.274913	2.041099	0.508186
C	-0.986582	0.478066	0.147052	N	3.919065	-0.591002	-0.314301
C	-1.850981	1.548021	0.158181	C	4.185205	1.610942	0.219621
H	-1.528866	2.581765	0.142540	C	4.857450	0.410367	-0.114076
C	12.978612	-0.732168	-0.486823	C	6.288954	0.392702	-0.219826
C	14.407098	-0.629873	-0.861665	C	7.017184	1.605308	-0.190146
C	15.394998	-1.330733	-0.154367	C	6.324567	2.821747	0.081491
C	16.183277	0.306143	-2.246954	C	4.935702	2.817878	0.330983
C	16.741364	-1.214734	-0.461736	N	4.550922	4.074722	0.593708
H	15.100700	-1.968651	0.674008	N	6.768923	4.081058	0.198689
C	17.175548	-0.394780	-1.526265	N	5.675907	4.762583	0.492022
H	16.457985	0.941129	-3.080043	C	5.739074	6.182993	0.809976
H	17.459478	-1.763839	0.134392	C	6.434694	6.431683	2.151033
C	12.523080	-2.005590	0.126967	C	5.748209	5.660838	3.276329
C	12.757624	-3.236775	-0.494011	C	6.454872	7.933569	2.428651
C	11.408109	-3.203439	1.928540	C	8.376283	1.256402	-0.362978
C	12.310746	-4.430021	0.056100	C	8.446602	-0.126642	-0.450637
H	13.304000	-3.261185	-1.435737	N	7.180921	-0.663296	-0.358838

Table SC-27 (*cont*). Optimized Cartesian Coordinates of the D-ε_6-δ_2-A@Ti_5O_{10}| [M06-2X/6-31G(d,p) solvent model: CPCM, $\varepsilon_{ethanol}$ =24.55].

S	9.953132	1.955884	-0.412137
C	10.697938	0.355170	-0.544232
C	9.761206	-0.652397	-0.555936
H	10.014102	-1.700276	-0.651862
H	12.594774	1.257250	-1.010211
C	6.972355	-2.058328	0.009232
C	4.092894	-1.839778	-1.044294
H	7.853513	-2.403913	0.553796
H	6.111772	-2.133363	0.674487
H	6.823071	-2.698016	-0.862940
H	4.208823	-2.694324	-0.375010
H	3.213487	-1.997574	-1.670711
H	4.962413	-1.758860	-1.696833
H	6.243294	5.856524	4.231178
H	4.699781	5.966963	3.367462
H	5.771455	4.581852	3.096637
H	6.948761	8.483616	1.622303
H	5.434607	8.319707	2.529685
H	6.987052	8.143742	3.359849
H	7.466668	6.072738	2.053162
H	6.267043	6.683784	-0.005135
H	4.704093	6.531474	0.835219
H	1.017249	-1.498768	-0.427975

Table SC-28. Optimized Cartesian Coordinates of the D-ε_6-δ_3-A@Ti_5O_{10}| [M06-2X/6-31G(d,p) solvent model: CPCM, $\varepsilon_{ethanol}$=24.55].

Ti	12.696147	0.060155	-0.233435
Ti	14.620406	-1.559533	2.133924
Ti	14.864343	-2.748102	-0.450890
O	13.310544	-0.339201	2.973995
O	15.479726	-2.915755	1.373600
O	15.727210	-1.585518	-1.378001
O	15.564422	-0.083618	2.011962
O	14.678100	-1.482822	-4.239023
O	13.445886	1.371206	0.725957
Ti	14.140176	1.082657	2.413945
Ti	14.277949	-1.367107	-2.679831
O	13.706327	-2.948774	-1.807592
O	13.230687	0.077169	-1.858161
O	14.414766	2.248407	3.772691
O	13.700793	-1.449646	0.477704
O	10.962094	-1.108387	-0.057214
H	14.693333	3.165208	3.660026
C	10.245096	-0.072494	-0.250824
O	10.858372	1.031725	-0.420768
C	4.191899	1.177902	-0.497855
C	4.718796	2.453423	-0.725291
C	6.119319	2.480734	-0.737184
C	6.665997	1.224330	-0.518079
S	5.426293	-0.007948	-0.297085
H	6.729069	3.362551	-0.894661
C	8.068294	1.004191	-0.472207
C	8.781165	-0.141463	-0.267464
C	8.190615	-1.425212	-0.056653
N	7.704730	-2.463832	0.112360
H	8.672681	1.897345	-0.620335
S	3.483570	3.673767	-0.924723
C	2.255675	2.456408	-0.691782
C	2.776690	1.184224	-0.478927
S	1.517291	0.019621	-0.245488
C	0.296659	1.261780	-0.462476
C	0.840747	2.503862	-0.686367
H	0.249616	3.394656	-0.860295
C	-1.108601	0.921023	-0.383343
C	-1.695293	-0.309952	-0.553891
C	-3.101790	-0.222489	-0.387381
C	-3.566525	1.054881	-0.104920
S	-2.271957	2.192424	-0.009849
H	-1.140226	-1.208138	-0.798349
C	-4.976658	0.997447	-0.045826
C	-5.325685	-0.356049	-0.266386
N	-4.168816	-1.088023	-0.495365
C	-6.011619	1.969717	0.079200
C	-7.366015	1.593718	-0.046612
C	-7.726604	0.222921	-0.202899
C	-6.704786	-0.755285	-0.244045
C	-8.952017	-0.481770	-0.221310
C	-8.656903	-1.835922	-0.238149
N	-7.290032	-2.014607	-0.246421
S	-10.658845	-0.202555	-0.186343
C	-10.965155	-1.948249	-0.165917
C	-9.797430	-2.678715	-0.194955
N	-8.119543	2.697444	0.060570
N	-5.956899	3.296743	0.258822
N	-7.228481	3.658367	0.229072
C	-12.278875	-2.551756	-0.030322
C	-13.504988	-1.977008	-0.047071
C	-15.967655	-2.423250	-0.216827
C	-17.108343	-3.151438	0.083690
C	-17.050756	-4.268193	0.945548
C	-15.793389	-4.586300	1.504997
C	-14.664469	-3.847266	1.189736
C	-14.711004	-2.756262	0.309030
C	-13.628870	1.193911	-2.129367
C	-14.115003	2.151290	-1.212944
C	-14.394072	1.712222	0.100846
C	-14.210436	0.385891	0.461397
C	-13.709476	-0.558056	-0.442144
C	-13.434873	-0.124420	-1.742752
H	-13.396829	1.477110	-3.148407
H	-14.761333	2.408550	0.844248
H	-14.446412	0.076998	1.476598
H	-13.049414	-0.837945	-2.466588
N	-18.174263	-5.013223	1.233254
N	-14.325659	3.461635	-1.588026
H	-13.725697	-4.107278	1.670414
H	-15.698869	-5.403586	2.209012
H	-18.050271	-2.845949	-0.354919
H	-16.051219	-1.572515	-0.887163
H	-12.225037	-3.624059	0.150494
C	-6.678245	-3.279118	0.140031
H	-6.438829	-3.902978	-0.723473
H	-7.377600	-3.817668	0.781811
H	-5.773219	-3.082316	0.715197
C	-4.050307	-2.375228	-1.168288
H	-3.218783	-2.320242	-1.872832
H	-4.960620	-2.571868	-1.734626
H	-3.866974	-3.190815	-0.466137
C	-7.643587	5.027749	0.502783
C	-8.292766	5.155993	1.883686
C	-7.365491	4.630166	2.977046
C	-8.669802	6.617015	2.121137
H	-9.178826	6.729448	3.081726
H	-7.773406	7.246454	2.139660
H	-9.333995	6.992906	1.337388
H	-7.830071	4.745897	3.959831
H	-7.135600	3.570209	2.832852
H	-6.420782	5.185645	2.979784
H	-9.206410	4.549153	1.871934
H	-8.335816	5.332147	-0.286211
H	-6.737081	5.633994	0.439326
H	-9.786452	-3.761946	-0.180391

Table SC-28 (*cont*). Optimized Cartesian Coordinates of the D-ε_6-δ_3-A@Ti_5O_{10}| [M06-2X/6-31G(d,p) solvent model: CPCM, $\varepsilon_{ethanol}$ =24.55].

C	-13.810741	3.915357	-2.866391
H	-14.038477	4.974058	-2.985222
H	-12.723305	3.779964	-2.952334
H	-14.287018	3.377587	-3.692262
C	-14.595165	4.450912	-0.561279
H	-15.524517	4.220285	-0.031112
H	-13.786165	4.517810	0.179860
H	-14.715783	5.425990	-1.031666
C	-18.111025	-5.998399	2.296442
H	-19.081085	-6.486140	2.385881
H	-17.369473	-6.770277	2.068251
H	-17.853359	-5.552758	3.267854
C	-19.474492	-4.498405	0.845637
H	-20.244312	-5.194547	1.176496
H	-19.681879	-3.512721	1.285444
H	-19.550578	-4.408738	-0.242544

DSPACE

https://dspace.org/

Computational insights into bis-N,N-dimethylaniline based D--A photosensitizers bearing divergent-type of -linkers for DSSCs

Nalçakan, Harun; Kurtay, Gülbin; Sarkavak, Kübra; en, Nilgün; Sevin, Fatma

2023-07
Elsevier
https://doi.org/10.1016/j.jmgm.2023.108485
Nalçakan H, Kurtay G, Sarkavak K, et al., (2023) Computational insights into bis-N,N-dimethylaniline based D--A photosensitizers bearing divergent-type of -linkers for DSSCs, Journal of Molecular Graphics and Modelling, Volume 122, July 2023, Article number 108485

Downloaded from a DSpace repository. https://dspace.org/